Università degli studi di Roma "Tor Vergata"

Facoltà di Scienze Matematiche, Fisiche e Naturali

Tesi di Dottorato in Scienze Chimiche

XIX CICLO

"Synthesis and Characterization of New Porphyrin-Fullerene Architectures and Their Potential Applications for Photocurrent Generation"

Supervisore:
Prof. Pietro Tagliatesta

Dottorando:
Angelo Lembo

ANNO ACCADEMICO 2005-2006

Acknowledgements

I would like to thank the professor Pietro Tagliatesta, who gave me hospitality in his laboratory during these three years of my Ph.D. thesis and who offered me the possibility to learn a lot about chemical synthesis and also because he believed in all my ideas even if they appeared impossible to realize and above all when such ideas failed he continued to trust in me.

I also would like to thank Mr. Alessandro Leoni, who helped me to solve all the technical problems in the lab and who never failed in giving me good advices to do right my work, he was for me more than a technician. I must not forget to say "thank you" to Mr. Giuseppe D'Arcangelo for GC and FAB Mass analyses and Dott. Marzia Nuccetelli for the MALDI-TOF analyses. I am very grateful to professor Dirk M. Guldi, who gave me the opportunity to study the photophysical properties of my compounds in his laboratories at the "Friedrich-Alexander University" in Erlangen (Germany) where I have started to learn something about the fluorescence studies; in particular I am also very grateful to all of the guys of the research group of prof. Guldi who were very kind with me during my periods in Erlangen, their kindness and helpfulness made me feel at home. A particular thank to Mateusz Wielopolski, who performed the computational studies on the HOMO-LUMO orbitals of the porphyrin-fullerene compounds reported in this thesis and to Vito Sgobba who never said "no" to all my demands for help.

Last, but not least, I would like to thank my family: my mother Luisa, my father Michele and my brother Alessandro. They tolerated all my groundless complaints during these years even that they always supported me in doing everything and they never had doubts about my capabilities. To conclude, as Latins said: "dulcis in fundo" (sweet at the end) I have to be very grateful to my girlfriend Valentina, she gave me the biggest help that I needed, with her constant and not intrusive presence she was always able to find the right words to support me in all the moments of my work, especially in the difficult ones. She was always with me, contributing to make more beautiful this adventure, also making renunciations to share with me every moments and I have only one regret: the impossibility to find the right words to say thank her.

INDEX

Chapter 1

"Natural Photosynthetic Systems"

1.1. Introduction

One of the most studied and appealing cycle of reactions in natural systems is the photosynthetic cycle; because its peculiar and fascinating aspects, involving light harvesting, energy and electron transfer and above all, water splitting and conversion of carbon dioxide into carbohydrates, the photosynthesis is one of the most articulated enzymatic catalyzed reaction path on the Earth. The most relevant aspect of the photosynthesis is the fact that all the energy necessary to the whole process is supplied by the sunlight. All the photosynthetic organisms in fact, are able to convert the sunlight radiation into chemical potential useful for the carbohydrates synthesis[1]. It is possible to understand the importance of this aspect considering that the enormous quantity of energy, coming from the sun, that during the daylight hours reaches the Earth surface is a thousand time higher than that produced by all of electrical power stations and this is true considering even only the ground surface of the U.S.A[2].

More or less 50% of that radiation, roughly in the visible, is of a frequency useful for photosynthetic organisms. Moreover it has not be neglected that the by-product of photosynthetic activity of green plants, algae and cyanobacteria is the molecular oxygen; so the photosynthesis, expelling oxygen as by-product of reaction and assimilating carbon dioxide in organic matter, determines the composition of our atmosphere and sustains almost all life of our planet providing a readily usable carbon source[1].

For these reasons the photosynthesis was one of the most studied phenomena of our times since the isolation and characterization of chloroplasts by Robert Hill in the 1939. Especially during the last decade a lot of scientists have perceived the powerful aspects and potential applications of the photosynthetic processes, in particular, the possibility to use the sunlight as a renewable energy source has produced a very large number of studies concerning the photophysical characterization and X-Ray structure determination of different photosynthetic natural systems. It is important to notice that only if we understand how sunlight is used by nature we will be able to reproduce some aspects of the photosynthesis that help us to obtain energy without using oil or in general fossil fuel, that is a consuming energy source.

The capability to develop processes that use the sunlight to produce energy, hold also a social implication: the possibility to fill the existing economic gap between the northern and southern region of the world[3] as was outlined by Giacomo Ciamician in his lecture "The Photochemistry of the Future" at the VIII International Congress of Pure and Applied Chemistry in New York

in the 1912: *"Solar energy is not evenly distributed over the surface of the earth. There are privileged regions, and others are less favoured by the climate. The former ones would be the prosperous ones if we should become able to utilize the energy of the sun. The tropical countries would be conquered by civilization which would in this manner return to its birth-place"*.[3,4]

The study of a photosynthetic apparatus requires a large effort between different disciplines, such as quantum mechanics, biochemistry, biophysics, molecular and structural biology and so on[1]. One of the most important data that we have to know to elucidate the photosynthesis mechanism is the crystal structure of the system, in order to understand how the different chromophores work and how they can interact with each-other. Starting from this point it is possible to shed light into the physical laws that govern processes like energy and electron transfer and trying to set up a synthetic apparatus able to mimic the photosynthetic reactions. Obviously since nature has an enormous advantage, consisting in million of years of evolution, it will be impossible to reproduce a wholly working photosynthetic system, but what we have to do is to find out the principal rules that will allow us to simulate the meaning aspects of the entire photosynthesis.

In the following chapters the green plant and bacterial photosynthesis will be discussed, including some structural aspects concerning the spatial disposition and energetic interaction of the main chromophores, in order to point out how nature regulates a very complicate process fine tuning every single aspect.

1.2. Natural Photosynthetic Systems

The green plants photosynthesis is accomplished by several reactions occurring in the chloroplasts[1]. These reactions are catalyzed by a series of protein complexes hosted in the lipid membrane bilayer. Beyond the simple aspect of the chemical reaction for the glucose synthesis, depicted in the Scheme 1.2.1, are hidden complex and articulated bio-machines able to produce carbohydrates starting from water and carbon dioxide.

$$6CO_2 + 6H_2O \xrightarrow[h\nu]{} C_6H_{12}O_6 + 6O_2$$

Scheme 1.2. 1 *Chemical reaction for the synthesis of glucose.*

The principal actors of this history are the Photosystem I (PSI) and Photosystem II (PSII) that capture the light energy to funnel it towards the photosynthetic reaction centers (RC) where the resonant energy produces the first step of the electron transfer chain: the expulsion of one electron. In the subsequent steps a series of protein complexes such as cytochrome ($Cytb_6f$ complex), plastocyanine and ferredoxin are involved; all these proteic complexes have the task to bring electrons up to the ferredoxin-NADP reductase for the reduction of NADP to NADPH. The last part of the work, but not less important, is performed by the ATP-Synthase, that produce ATP exploiting the chemical potential of proton gradient, previously formed through the thylakoid membranes, as consequence of the electrons transport along the photoactive subunits (Figure 1.2.1)[1].

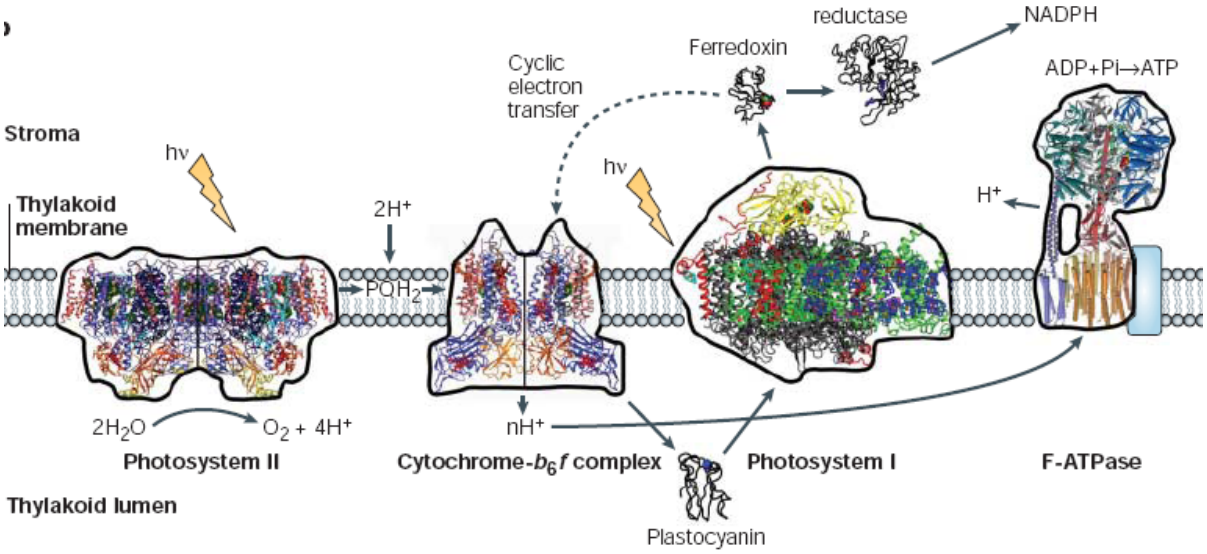

Figure 1.2. 1 *Structures of the membrane- protein complexes that drive oxygenic photosynthesis*[1]

To conclude the photosynthethic cycle the ATP and NADPH produced in the "bright phase" of the process were used in the "dark phase" to fix the CO_2 in sugar. The two photosystems, PSI and PSII, hold a key role in the whole process and they belong to the family of the photosynthetic reaction centers, that is divided in two classes according to the terminal electron acceptor: PSI belongs to the type I that presents iron-sulphur clusters as electron acceptor, while PSII belongs to the type II having a quinone as the final electron acceptor[5]. Both systems share some structural and functional aspects such as the presence of a certain number of chlorophylls as antenna system, the existence of a reaction center containing a special pair of chlorophylls (P_{680} for PSII and P_{700} for PSI) that act as first electron donor. Moreover both reaction centers show a pseudo C_2 symmetry concerning the cofactors involved in the electron transfer reaction.

Furthermore some similarities have been also found in the helical arrangements of the central protein core, that harbours the reaction centers of the two systems and the capability to drive the light energy toward the chlorophyll special pair. All these aspects induce to consider that there was a common ancestor both for PSI and for PSII[6]. Anyway their resemblance is only apparent because, if we focus our attention to the role that they cover in the photosynthesis, it is clear how the nature, through the evolution, has gave them very different works to do. The PSII (P_{680}) can be considered as the strongest oxidant in nature able to oxidize a tyrosine residue, that in turn takes an electron from the manganese ions cluster. After several cycles it generate a high potential (> 1 V) sufficient to split water into oxygen and protons. On the other hand the PSI (P_{700}) carries out the opposite work and could be considered the strongest reductant in natural organisms. The reducing equivalents produced by P_{700} are used by the photosynthethic organisms to reduce the iron-sulphur protein Ferredoxin[1]. Such opposite functions imply also fundamental differences between the two systems, not only under a structural point of view. One macroscopic difference is the number of chlorophylls that constitute the antenna system. In PSI we find a larger number of pigments, not only in the core of the system but also in the extrinsic protein complex called Light Harvesting Complex (LHC) that helps the photosystem to capture the photons[6,7]. This implies different quantum yield: almost 100% for PSI and 85% for PSII. The minor content of chromophores may be also attributed to the destructive oxidant potential produced by P_{680} that can oxidize every pigment in proximity of the special pair. In fact the loss of quanta in P_{680} can cause damages in the surrounding protein and a fact that corroborates this hypothesis is the fast turn over in the synthesis of the subunit D1 (see Figure 1.2.2) of PSII. Because its proximity to the special pair, its synthesis represents the 50% of the total protein synthesis in the chloroplast even if the D1 subunit constitutes only 0.1% of the total protein[1]. To demonstrate that the photosynthesis is fine tuned in all its aspect we have to underline that the nature has supported such type of consideration. In fact when the extraction of water is impaired (for example at low temperature) the P_{680}^{+} can receive electrons from a secondary pathway involving $Cytb_{559}$, a carotenoid and a chlorophyll located at the periphery of the PSII reaction center (Figure 1.2.3); this prevents serious damage to the protein bulk of PSII itself[1,8].

For a better understanding of the functionalities of the two photosystems, we will discuss separately some aspects concerning PSII and PSI, despite the fact that they act in series. Even if there are many differences between a plant and a photosynthethic bacterium, their relative reaction centers and photosystems show a certain degree of similarity, except for some structural and regulating tools, that will be outlined later. At this point of discussion the generic

description of one photosystem could be considered of general validity. The structure of PSII is taken from crystallographic data coming from a study on cyanobacterium *Thermosynecochoccus Elongatus*[8]. The PSII is a dimer with the two monomer subunits almost identical and containing 19 protein subunits. Each monomer also includes one oxygen evolving center (OEC), one heme *b*, one heme *c*, two plastoquinones, two pheophytins, one nonheme Fe and two bicarbonate ions (Figure 1.2.3). After photon excitation, one electron is extracted from the excited state of P_{680} and passing from a second chlorophyll (Chl_{D1}) and a pheophytin ($Pheo_{D1}$), it arrives to the plastoquinone Q_B. After that with the help of the nonheme Fe, the electron is transferred to the plastoquinone Q_A, that after a second reduction accepts two protons and releasing into the membrane matrix the electrons toward the $Cytb_6f$. During the last passage protons are pumped from the stroma in the inner space of the tylakoid lumen. It is possible to see in the Figure 1.2.2 that also the monomer has a pseudo twofold-symmetry that relates the D1, CP47 and PsbI subunits to D2, CP43 and PsbX subunits. The pseudo C_2 element of symmetry is a constant that we can find in all the photosystem subunits and about this aspect there are some discussions regarding the photoactivity of the two branches of the reaction center (Figure 1.2.3). For example in the PSII reaction center only the A branch is active toward the electron transfer while the B branch participates apparently giving only the contribution of quinone Q_B[8]. This evidence comes from the first published crystallographic data of PSII reaction center where only one quinone (Q_A) is present[9]. Other proofs for this argument could be found in the structural data regarding the two branches. Indeed on the B branch there is a larger distance between the chromophores and differences in the nature of local amino-acids: in the A branch more polar amino-acid side chains can stabilize better the charge separate states such as: P^+Chl^-, P^+Pheo^- and finally $P^+Q_A^-$ (where P indicates the generic chlorophyll special pair)[1,8]. Some experiments have

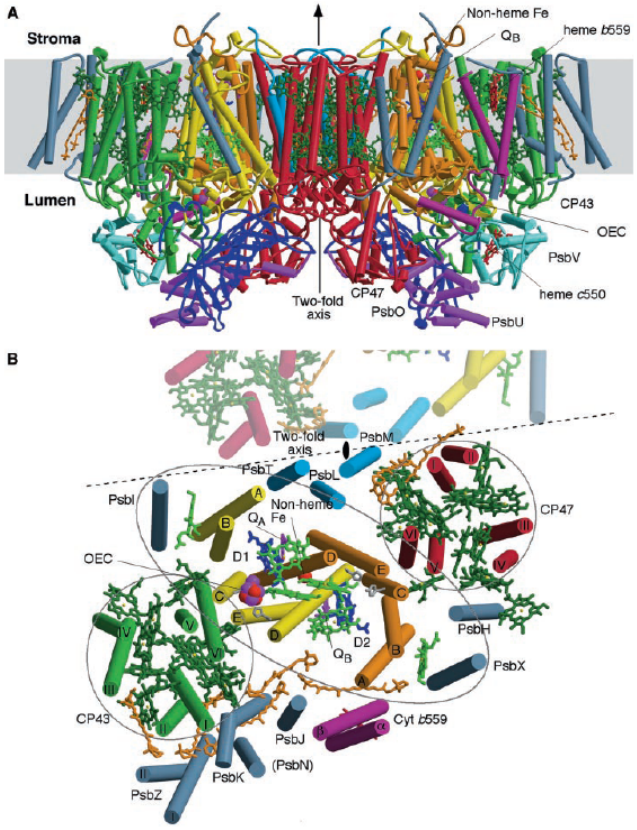

Figure 1.2. 2 *(A) View of PSII dimer perpendicular to the membrane. (B) View of PSII monomer along the membrane normal from the luminal side*[8]

demonstrated that the disposition of the phytyl chains in the chromophores of the A branch are well arranged to get in close contact the cofactors, especially chlorophyll and pheophytin, in order to have a better electronic coupling[10]. Some performed calculations, taking in consideration the structural aspect of PSII reaction center, have shown that even if the B branch is inactive it has a fundamental role in the process. The excitonic states calculated by Nikolay Ivashin and Sven Larsson[10], using time dependent functional theory (DFT) to obtain the Q_y states and an effective Hamiltonian for interactions between them, underline how the trap state is localized on the B side. This is due to the fact that the coplanar orientation of the chlorophyll ring 1 vinyl group with the tetrapyrrole macrocycle, generates a lower excited state, mainly distributed on the B branch. From crystallographic data this group is perpendicular to the chlorophyll ring in the A side. For the same reason it is possible to assume that also the triplet state, coming from the decay of charge separated state, is localized on the B branch. On the other hand having a triplet state on the A branch, where oxygen evolves, could be very destructive because of the possibility to generate singlet oxygen. So the nature has placed the probable source of the singlet oxygen near the oxygen quencher, the carotenes on the B side. Around the PSII reaction center many β-carotene molecules are arranged, mainly on the B side, all of them having a trans conformation. Some of these β-carotene groups have the head group in direct contact with a chlorophyll and this suggests that they can facilitate the long distance electron flow, in particular from Cyt b_{559} in case of risk for self-photooxidation. Another peculiar aspect of the PSII is the presence of the Mn cluster ions, called oxygen-evolving center (OEC)[8], that is capable to carry out the oxidation of water. It works as an electrical accumulator repeatedly oxidized by the P_{680}^+ up to four time through the "S cycle"[2], where S indicates one oxidation state of the cluster, being the S_0 the most reduced state and S_4 the most oxidized one. In the S_4 state the OEC can split the water into dioxygen and protons, coming back to its natural reduced state. The geometrical disposition of the Mn ions in the cluster recalls a cubane like structure[2,8]

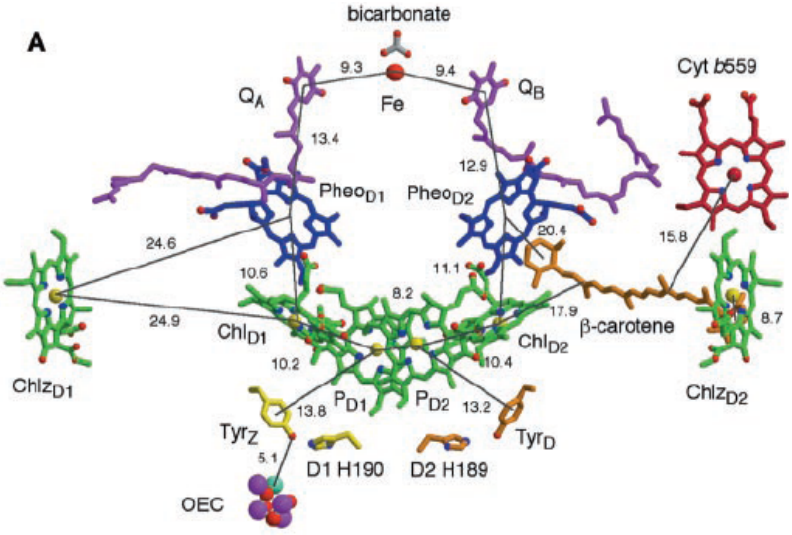

Figure 1.2. 3 *Electron tansfer cofactors of PSII reaction center, with the relative distances between the chromophores given in angstrom*[8]

with 3 μ-oxo bridges connecting three Mn ions in the cluster plus a further μ-oxo bridge binding an external Mn ion that, with the help of the Ca ion present in the cubane like structure, is believed to be the active site for the oxidation of water. The oxidation mechanism of water has still to be clarified, but it is possible to assume that an high electrophilic species, like Mn(V)oxo or Mn(IV)oxyl radical, generated in the active site, can undergo to the attack of a water molecule bound in the active site. Obviously in this description the local amino-acid side-chain plays a key role modulating the distances and interactions between every components and favouring the water binding[8]. To conclude the description of PSII it should be mentioned the presence of an additional extrinsic protein complex harvesting system: Light Harvesting Complex II (LHC-II). As it was pointed out before, the PSII is poor of chlorophylls in the proximity of the reaction center, so the nature has provided an auxiliary apparatus to modulate the energy absorption. The crystal structure of LHC-II was isolated in a trimeric arrangement from *Spinacea oleracea* by Zhenfeng Liu, Kebin Wang and co-workers[7]. Each monomer contains 14 chlorophylls, 8 chlorophylls *a* and 6 chlorophylls *b* located around the interface between each monomer. In the study was outlined how a net of hydrogen bonds brings three chlorophylls *b* in close contact leading a sort of cluster and how this disposition can facilitate the energy transfer. Besides the pseudo circular disposition of pigments, forming an inner ring (6 Chl*a*) and an outer one (8Chl*a* + 8Chl*b*) at the monomer-monomer interface in the trimeric structure, allows a very efficient absorption of incident light from all directions. From the crystallographic data a consistent number of carotene molecules emerges, most of them are in all trans conformation; such molecules not only cover a structural role but together with xanthophyll molecules are involved in a non radiative dissipation of excess energy, that is one of the photoprotective strategies evolved by the plants. LHC-II has another important role: it takes part to the distribution of excitation energy between the two photosystems[7,11]. This aspect depicts the two photosystems as two dynamic machines capable to adapt themselves to the environmental changes in order to optimize the photosynthesis efficiency.

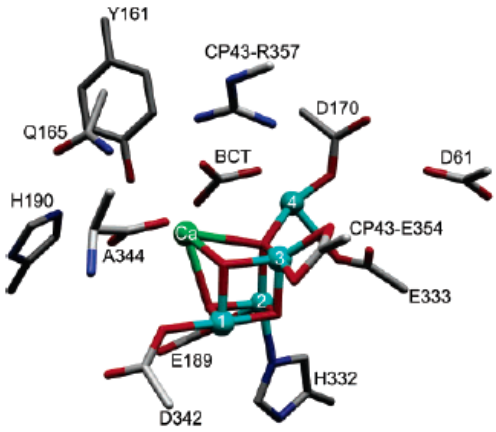

Figure 1.2. 4 *Crystallographic model of OEC. Mn cyan, O red, C grey, N blue, Ca green, BCT denotes bicarbonate. Unless otherwise indicated, amino acids belong to the D1 subunit*[2]

The description of plant PSI will be discussed in a parallel way with that of photosynthetic bacteria because there are many differences that must be outlined. One of the best refined

structure of plant PSI was obtained by Adam Ben-Shem, Felix Frolow and Nathan Nelson from *Pisuvum sativum*[6]. The PSI was crystallized together with Light Harvesting Complex I (LHC-I). The first evidence that emerges from the data is the fact that the plant PSI is monomeric while the PSII is dimeric and furthermore the cyanobacterial PSI is trimeric[5]. While such difference between PSI and PSII can be justified considering the differences previously described, the trimeric structure of PSI in cyanobacteria arises from the different environmental conditions in which bacteria must live. Despite this fact, also in the protein core of PSI, where we find the reaction center, again a pseudo two-fold symmetry can be found. In the Figure 1.2.5 is clearly visible how the LHC-I is loosely bound to PSI and forms a sort of belt surrounding one side of the photosystem. At the same time between them there is a cleft that is filled with chlorophylls that cover an important role for the energy migration. In fact considering the distance between the antenna system and the core of PSI, the energy transfer from the periphery of LHC-I should be very much lower without the so called "gap" chlorophylls (dark pink in the Figure 1.2.5). A similar work is done by the "linker" chlorophylls (red in the Figure 1.2.5) that guarantee a good energy transfer along the dimeric subunit (Lhca1-Lhca4 and Lhca2-Lhca3) of the LHC-I. The main difference in term of absorption between LHC-II and LHC-I is the longer wavelength absorption spectrum, mainly due to the tighter interaction between chromophores in the LHC-I. An interesting study of Robert C. Jennings, Giuseppe Zucchelli and co-workers[12] had shown how the fluorescence decay of the PSI-LHC system is wavelength dependent in the region that goes from 690 to 770 nm. A comparison between fluorescence steady state data and time resolved measurements elaborated with the Arrenius-Eyring theory confirms that the "wavelength dependent" activation energy is due to a different thermal activation energy for energy transfer from the low energy chlorophyll states (red chlorophyll states on the LHC-I) to the bulk chlorophyll state (in the core of PSI). The biological role of this low energy chlorophylls is to supply a better

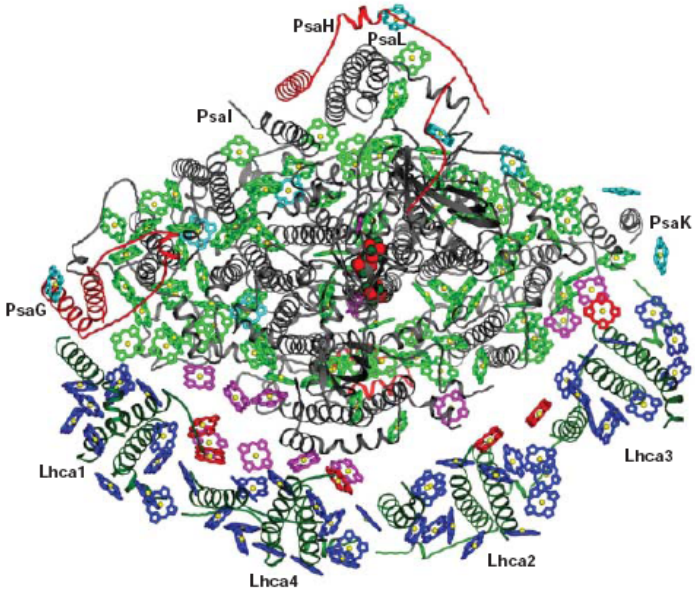

Figure 1.2. 5 *A view from the stroma of the plant PSI. The subunit of LHC-I are indicated as Lhca1, Lhca2, Lhca3, Lhca4 and relative Chls are in blue. "Gap" chlorophylls in dark pink and " linker" chlorophylls in red*[6]

light absorption in dense vegetation where the ambient light is enriched by the wavelength above 690 nm respect to the normal daylight. What we have just described underlines one more time the dynamism of plant photosynthetic apparatus that is able to adapt itself in real time to the fickle environmental conditions, in order to have always the best performance in the photosynthesis. In the plant PSI crystal structure we can find at least other two evidences of this ability: the LHC-I is composed by four monomers bound together giving two dimeric units, but only the subunit Lhca1 is tightly bound to the core of PSI through the proteic subunit indicated in the Figure 1.2.5 as PsaG. This suggests that the Lhca1 could be thought as an anchor point for the LHC-I, while the remaining subunit are bound at varying stoichiometries depending on environmental conditions[6]. In the PSI it has been seen that the protein subunit named PSaH is necessary as docking site for LHC-II, in fact as we have pointed out before, when an excess of light was captured by PSII a small population of LHC-II trimers dissociates from PSII and associates with PSI, in order to redistribute the excitation energy[11]. Finally another evolutive improvement in the plant PSI consists in the presence of a longer amino terminal domain in the PsaF subunit respect to that in cyanobacteria, that allows a better binding of plastocyanin, giving as a result a two order of magnitude faster electron transfer from the copper atom of that protein to P_{700} (Figure 1.2.6). The reaction center of PSI is composed by six chlorophylls, two of them forming the special pair (P_{700}), two philloquinones plus different iron-sulphur clusters, all these cofactors are arranged in a two-fold symmetry like that seen in the PSII reaction center, but in this case both branches are photoactive towards the electron transfer, even if the A side presents higher rate constant values. In the crystal structure of PSI from cyanobacterium *Thermosynecochoccus Elongatus* published by Patrick Jordan, Petra Fromme and co-workers[5] is outlined how this dissymmetry in the electron transfer could be explained taking in consideration the hydrogen bonding net present in the A branch, and absent in the B branch; this net can facilitate the stabilization of the different excited states. Despite the fact that this was seen in a cyanobacterium, we can assume that it is valid also for plants and green algae because the structural organization of chromophores and amino-acids environment is preserved, even if we

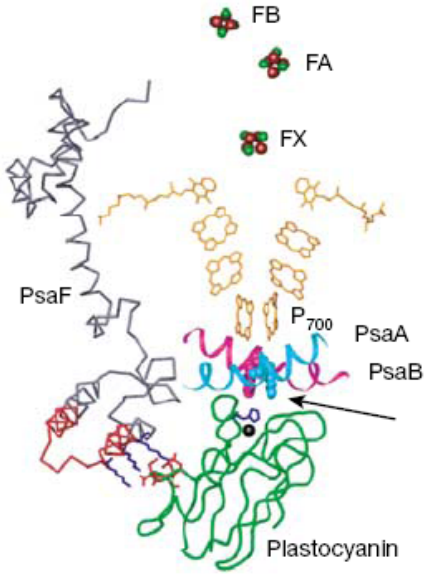

Figure 1.2. 6 *P_{700} of green plants. The arrow indicates the two tryptophan residues necessary for electron transfer from copper ion of Plastocyanin to the oxidized P_{700}. The interaction of PsaF subunit with plastocyanin is also shown*[6]

can find different quaternary structures (e.g. plant PSI monomer versus cyanobacterium PSI trimer). In the Figure 1.2.6 the two tryptophan residues necessary for electron transfer from copper ion of Plastocyanin to the oxidized P_{700} are also shown and the electron flow through the pigments of PSI reaction center is almost similar to that we have seen for PSII reaction center. Excited P_{700} donates one electron to the adjacent chlorophylls that in turn pass the electron to the phylloquinone and the electron arrives to the Ferredoxin, passing through the iron-sulphur clusters. P_{700}^{+} is finally reduced by Plastocyanin with electron coming from PSII. To conclude the description of PSI we should not forget to mention that the PSI can perform also cyclic electron transfer (see Figure 1.2.1), having as a partner the $Cytb_6f$[l]. This path is used only to pump protons within the lumen of tylakoid and most probably is connected to the fact that are necessary more than 12 protons, for plants, to perform the synthesis of 3 ATP molecules and with this alternative path the organism is able to recover the right quantity of protons: in fact the proton number for the ATP synthesis is species dependent. For example the yeast mitochondria need 10 protons to synthesize 3 ATP while plants 14 protons and since with the linear electron flow from PSII to PSI only 12 protons enter in the tylakoid lumen, the remaining 2 recovered with cyclic electron transfer. In principle this can also justify the higher quantum yield of PSI respect to PSII.

We have seen that the entire photosynthesis is fine tuned with a lot of tools such as: hydrogen bonds, protein structures, distances between the chromophores, amino-acids surrounding, electronic coupling between chlorophylls and we have also seen that the plants are able to adjust the stoichiometry of their active systems as answer to the environmental changes. This is true even for the cyanobacteria that under stress conditions (iron deficiency) produce a giant ring chlorophyll-protein complex around the trimeric PSI [13] (Figure 1.2.7). All these aspects point out how it is impossible to reproduce synthetically such type of systems and also understand the physical laws that govern the phenomena it is not so easy when we have to deal with hundred chromophores that interact between them in different way as we can see in the subsequent paragraph.

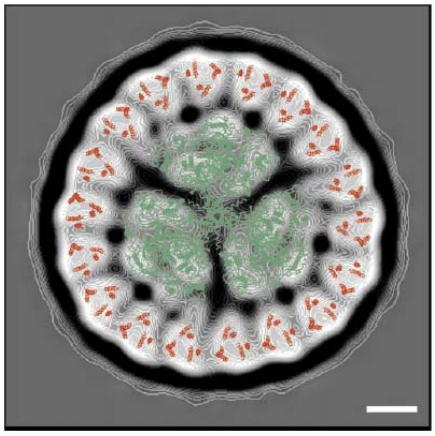

Figure 1.2. *7 PSI trimer structure and giant chlorophylls ring obtained from X-Ray crystallographic data plus electron microscopy*[13b]

1.3. Energetic Aspects of Photosynthesis

In this brief section the coupling of chromophores, the rising transients after reaction center photoexcitation and the electron transfer mechanism will be discussed. Our aim is not to clarify completely all the energetic aspects but to show how much is complicate to find unique theory that can explain in a simple manner the energetic interaction between the single chromophores. For our purpose it is useful to take as example the bacteria reaction center that shows a simpler absorption pattern due to the fact that in the photosynthetic purple bacteria is possible to obtain the crystals of the reaction center separated from the light harvesting complex. This reduces the difficulty in the interpretation of the data that come out from the experiments. In the Figure 1.3.1 the absorption features in the visible and near IR of *Rhodobacter Sphaeroides* reaction center is reported, with relative chromophores colours code[14]. Since the structural analyses have revealed high similarity between the pigment arrangement of PSII and that of bacteria, the bacterial reaction center can serve as a realistic model for PSII. In the reported spectrum the absorption of the special pair bacteriochlorophylls is located at higher wavelength as result of the high level of electronic coupling between the two pigments[14]. This allows to the special pair to act as a sink of energy, that, once it was captured, is transferred to the near chromophore which shows an absorption band at higher energy and so on. One of the first debate, on the electron transfer in the reaction center, was focalized on the existence of the $P^{+}B_A^{-}$ charge separated state (where B_A indicates the bacteriochlorophyll in the A branch); the first ultrafast studies of J. L. Martin and J. Breton[15] showed that the lifetime of special pair excited state (P^{*}) was more or less 2.8 ps and that the rising time for the reduced bacteriopheophytin (H_A) had the same value, so the authors concluded that the first electron transfer step occurs between the special pair and bacteriopheophytin in one step, leaving to the bacteriochlorophyll B_A the only role to increase the electronic coupling in order to design a superexchange electron transfer mechanism. In 1989 Kirmaier and Holten[16], and later (1991) Zinth and Wachtveitl[17] published papers where new transient absorption data, with a time costant of 0.9 ps, were reported around 1020 nm, where the absorption of $BChl^{-}$ (B_A^{-}) is located. This was a proof for a "two steps" electron transfer

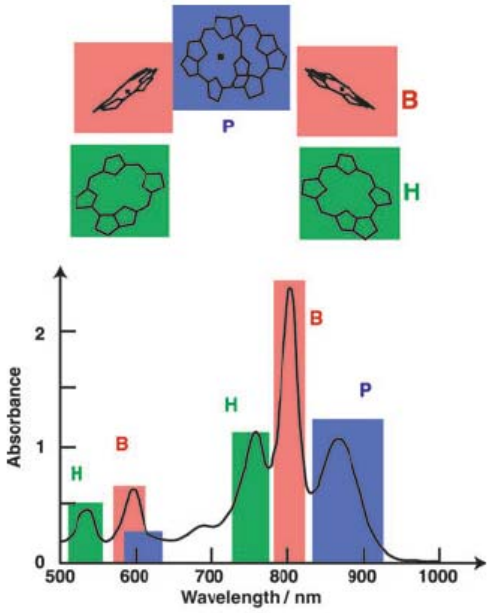

Figure 1.3. 1 *Absorption spectrum of reaction center from Rhodobacter Shpaeroides*

mechanism. Other evidences for the existence of $P^+B_A^-$ come from transient dichroism experiments that reveal an angle between the transition moment dipole of the special pair and that of the subsequent intermediate in electron transfer reaction, of 26°±8°, that corresponds to the angle between Q_y transitions of the special pair P and those of the accessory bacteriochlorophyll B_A[14]. At the moment a more recent investigation performed by A. Dobek, M. Ziolek[18] and co-workers outlines again the presence of a "two-steps" electron transfer mechanism in the primary electron transfer reaction. Recently another study of Kirmaier and Holten[19] was published to evaluate which is the origin of the two different electron transfer rate in the two branches of reaction center. Using the DNA site directed mutagenesis, different *Rhodobacter Capsulatus* reaction centers were prepared, in these centers it is possible to find modified energetic level of the radical pairs in order to evaluate how much the electronic coupling participate to the difference in electron transfer rate constant along the two branches. The results indicate that almost the 30% of the discrepancy in the rate constant has to be attributed to the electronic coupling, the remaining 65%-70% due to other factors such as free energy, reorganization energy and one or two step electron transfer mechanisms in the two sides of reaction center. An interesting study about the energy transfer interaction in the LHC of purple bacteria was published by V. Sundström, T. Pullerits and R. van Grondelle[20]. They have analyzed the nature of energy transfer in purple bacteria LHC-II. They found that the reaction center is arranged in a circular structure composed by 9 subunits, each subunit presents an αβ helices-heterodimer that binds three bacteriochlorophylls *a*, two of them very close to each other, plus carotenoid molecules. In the purple bacteria LHC the looser bound BChls *a* constitute the B800 system, while the tightly bound ones constitute the B850 system, both of these systems presenting a circular arrangement of the pigments. The energy transfer between this two systems and between each pigments within one system, was studied by applying the incoherent hopping transfer, when very weak interactions are present, and exciton theory when the interactions between the chromophores are much stronger. The principal outcome of this study is the difficulty to describe every part of the system with only one theory. When the authors tried to calculate the lowest exciton state of LHC, applying the perfect exciton model, they obtained a lowest excitonic state with very little dipole strength, since all dipoles were considered to be in the plane of the ring. This implies a low-temperature non radiative state. The experimental data showed the contrary, with a dipole strength localized on 2-3 monomer. Moreover the dipole moment of emitting state was more or less temperature independent. Further refinements of calculations, introducing disorder elements, allowed them to obtain a result much more closer to the experimental data; in conclusion this means that the disorder

(such as spectral inhomogeneity) destroys the "delocalized exciton" picture that could be applied to a maximum of 4 monomer. We conclude that in some cases we have to adopt exciton theory, while in other cases the electron hopping theory. Another outcome of the previous investigation was to show a dense interaction between the carotenoid molecules and B850, in fact almost all energy absorbed by these molecule is transferred to the B850 system, the 75% in a direct way, while the remaining 25% passing before through the B800 system. In the work is also showed how carotenoids are able to give ultrafast response to local electrical field generated by excited chlorophylls and how this response is different when the excitation is located on B800 or B850. This feature of the carotenoid molecules is good candidate as probe of local dynamic and structural changes.

In the short picture of photosynthesis given in this paragraph, a very high level of complexity about energetic interaction emerges, but it is possible to get into account some parameters such as: electronic coupling, distance and relative orientation between chromophores and also temperature dependent electron transfer rate, adopting the simpler Marcus theory.

Chapter 2
"Electron Transfer Theory"

2.1. Introduction

In order to simulate the natural electron and energy transfer reactions is necessary to have a theoretical background that allows us to take into considerations many, the principal ones, of the aspects that characterize such type of reaction. We have to be grateful to the work of many scientists such as Libby, Taube, Hush and first of all Marcus if at the moment it is possible to conceive and build up synthetic systems that mimic some of the aspects of natural photosynthesis. In particular the theory developed by Rudolph A. Marcus[21], as consequence of his studies and conclusions on experiments carried out by Libby[22] on isotopic electron transfer in metal complexes, is one of the best full-comprehensive and well organized theory. Such theory is suitable to explain a lot of experimental data and it also foresaw the existence of a particularly interesting region in the electron transfer free energies, the so called "inverted region", before that such region was found in the experimental analyses.
This theory gained to Marcus the Nobel Prize in Chemistry in the 1992[23] and in this chapter some of its features will be summarized.

2.2. General Observations

To point out the main points of the Marcus theory is useful to start from general observation on a bimolecular electron transfer reaction with a donor (D) and an acceptor (A), both the molecules being in the fundamental state or in the respective excited states. In any case the principles are the same and no modifications are necessaries. Usually the Marcus electron-transfer theory is applied for outer sphere electron-transfer. Considering the three steps depicted in the Scheme 2.2.1, to have an electron transfer reaction both donor and acceptor must form a precursor complex[21] (2.2.1a), after that the reorganization of nuclear coordinates and electron energy levels leads the precursor complex in a transition state in which the electron transfer takes place, generating the following complex (2.2.1b) that, for the Franck-Condon principle, has the same nuclear coordinates of precursor complex. The last step is the dissociation in the products (2.2.1c). From a steady state analysis it is possible to obtain the overall rate constant k_{obs} (Expression

Figure 2.2. 1 *Rudolph A. Marcus*

2.2.1), and to make some experimental considerations about the phenomenon: if k_s is much more higher than k_{-ET} the equation for k_{obs} becomes simpler (Expression 2.2.2a) and when the dissociation rate constant (k_d) is much higher than the constant for the forward electron transfer (k_{ET}) the expression of k_{obs} is that reported in the Expression 2.2.2b and we are still able to obtain information on k_{et} from experimental measurements; on the contrary if k_{ET} is much higher than k_d we are in the diffusion-controlled limit and we could not obtain any type of information about the electron transfer rate. Obviously if the donor and acceptor molecules are hold together by covalent bonds the only meaning step reported in the Scheme 2.2.1 is described by the equation 2.2.1b.

$$D + A \underset{k_d}{\overset{k_a}{\rightleftharpoons}} D/A \qquad 1a$$

$$D/A \underset{k_{-ET}}{\overset{k_{ET}}{\rightleftharpoons}} D^+/A^- \qquad 1b$$

$$D^+/A^- \xrightarrow{k_s} D^+ + A^- \qquad 1c$$

Scheme 2.2. 1 *Three steps in a bimolecular electron-transfer reaction*

$$k_{obs} = \frac{k_a}{1 + \frac{k_d}{k_{ET}} + \frac{k_d k_{-ET}}{k_s k_{ET}}} \qquad \text{or} \qquad \frac{1}{k_{obs}} = \frac{1}{k_a} + \frac{k_d}{k_a k_{ET}}\left[1 + \frac{k_{-ET}}{k_s}\right]$$

Expression 2.2. 1 *Electron transfer rate constant for a bimolecular reaction from steady state analysis*

$$\frac{1}{k_{obs}} = \frac{1}{k_a}\left[1 + \frac{k_d}{k_{ET}}\right] \qquad k_{obs} \cong \frac{k_a k_{ET}}{k_d} \qquad k_{obs} \cong k_a$$

2a 2b 2c

Expression 2.2. 2 *Exemplification of k_{obs}: 2a) when $k_s >> k_{-ET}$, 2b) when $k_d >> k_{ET}$ and 2c) when $k_{ET} >> k_d$*

Extremely important it is to know the different state energies respect to the ground state, especially for the photoinduced electron-transfer. In this latter case we should know both the singlet and triplet excited state energies and first of all the free energy of reaction (ΔG°, Expression 2.2.3) that could be obtained from cyclic voltammetry measurements since it is given by the difference between the standard reduction potentials of donor and acceptor; the terms ω^P and ω^R correct for the work of bringing D^+ and A^- and D and A, respectively, together.

$$\Delta G^\circ = e\left(E^\circ_{D^+/D} - E^\circ_{A/A^-} \right) + \omega^P - \omega^R$$

Expression 2.2. 3 *Free energy of electron transfer reaction where P and R indicate products and reagents respectively being e the electronic charge*

2.3. Classical Marcus Theory [21,24,25]

Despite the fact that the Marcus theory presents a quantum mechanical aspect, in a first step it is possible to calculate the electron transfer rate applying a classical method based on the simple transition state theory. To simplify the problem, the multinuclear coordinates dependence of the reactant and product energy potential surfaces could be reduced to a mono-dimensional dependence, introducing the reaction coordinate, that is the path along which the electron transfer takes place. In general if all the nuclear modes, including solvent molecules, are considered, the potential energy surface is not parabolic, but describing this potential surface as a Gibbs free energy, we can still use a parabolic approximation.

In the subsequent discussion the letters R and P will be used to indicate respectively the reactant (D/A) and the products (D^+/A^-). Taking into consideration what we have just reported, the electron transfer rate constant can be expressed as a product of three factors (Expression 2.3.1), k_{el}, that indicates the electronic transmission coefficient usually considered to be unitary in the classical approach, ν_n, the frequency of passage through the transition state and finally an exponential term that takes into account the activation energy (ΔG^*).

$$k_{ET} = k_{el}\nu_n \exp\left[\frac{-\Delta G^*}{k_B T} \right]$$

Expression 2.3. 1 *Electron transfer rate constant from classical approach*

An important quantity in the theory is the reorganization energy λ defined as the change in the Gibbs energy when the reactant state (D/A) are distorted in the equilibrium coordinates of product state (D^+/A^-) without electron transfer (see Figure 2.3.1). When the vibrational modes of both reactant and product states are assumed to be parabolic it is possible to find a correlation between ΔG° and ΔG^* in which is involved also λ (Expression 2.3.2).

$$\Delta G^* = \frac{\left(\lambda + \Delta G^\circ\right)^2}{4\lambda}$$

Expression 2.3. 2 *Relation between activation free energy and free energy of electron transfer reaction*

One of the most relevant consequence of the relation described in the Expression 2.3.2 is the existence of the "inverted region" in electron transfer reaction. In general we expect that an increasing in the free energy ΔG° should favour the formation of the products but in this case is not so obvious. It is possible to analyze the fact considering the four cases depicted in the Figure 2.3.1.

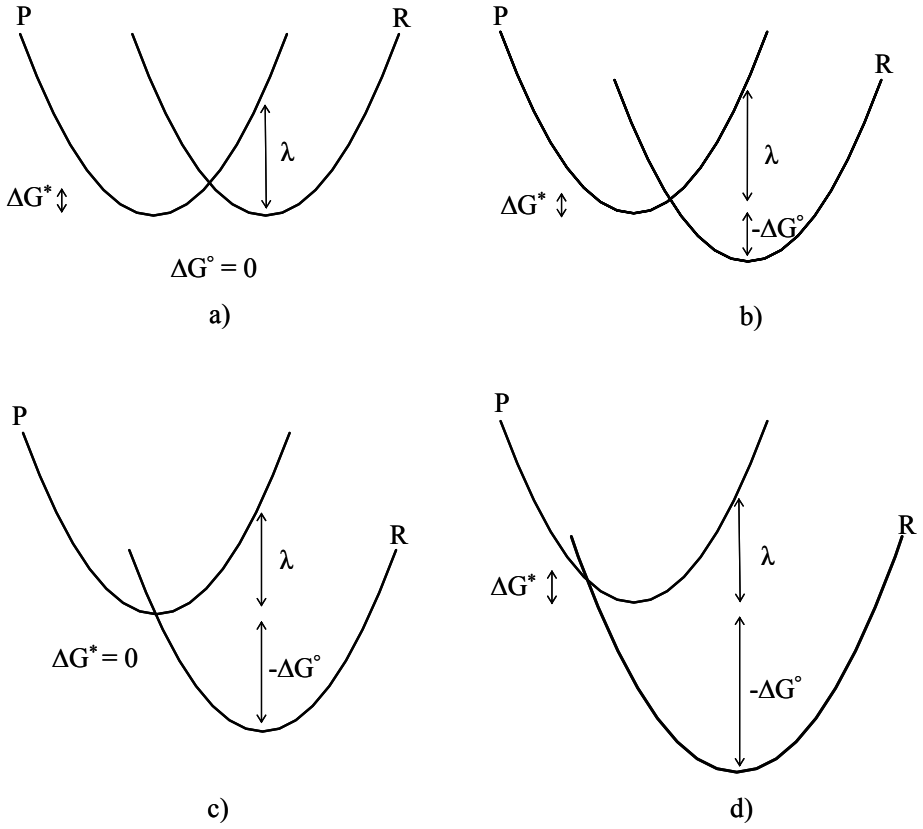

Figure 2.3. 1 *Four cases for electron transfer reactions depending on free energy values related to the reorganization energy. For comments see text.*

In the case a) the reaction is isoergonic ($\Delta G° = 0$) and there is an appreciable value of activation energy (ΔG^*); when there is a gain in the free energy, $\Delta G°$ becomes more negative, b) case. We have an increment in the k_{ET} and in this condition we are in the "normal region" where $0 \leq -\Delta G° \leq \lambda$. The electron transfer rate constant can reach a maximum value when there are no activation energy barriers, c) case, where the activation energy is equal to zero. This happens if $-\Delta G° = \lambda$ and in a such situation $k_{ET} = k_{el}\nu_n$ and since k_{el} is assumed to be unitary in a classical approach, $k_{el} = \nu_n \approx 10^{13}\ s^{-1}$. At this point if the free energy starts to become much more negative ($-\Delta G° > \lambda$) the intersection between the two surfaces is shifted towards left, determining an increasing ΔG^*, that leads to a decrease in k_{ET}. This is the so called "inverted region". By a physical point of view this means that the products are formed in a high-distorted and high-energy state. This was one innovating point of the Marcus theory, even because the first experimental data about the inverted region came out only in the 1984 when Miller, Closs and Calcaterra[26,27] published their contributions on electron transfer reaction in molecules that hold together, through a rigid carbon system, biphenyl donor moiety and different acceptor molecules. Their work shows clearly the pseudo parabolic dependence of k_{ET} from free energy of the reaction (Figure 2.3.2). From such considerations an important role emerges for λ: in fact this energetic parameter could be thought as an arbiter respect to the rate constant of electron transfer reactions. For this reason is necessary to have a model that makes explicit some aspects of such reorganization energy. Remaining in the classical approach, λ may be split in two contributions: the first deriving from the nuclear vibrational modes elaborated with an harmonic potential having a reduced force constant for each vibration. This component is independent from the solvent and is indicated as λ_{in} (Expression 2.3.3). The other component, λ_{out}, is called the solvent reorganization energy since it arises from different orientation and polarization of solvent molecules around the reactant state (D/A) and product state (D^+/A^-). While in most cases the λ_{in} value is quite small, the respective value for λ_{out} presents consistent entity. The solvent reorganization energy could be modelled considering the solvent as a dielectric continuum and in this case λ_{out} is described by the Expression 2.3.4.

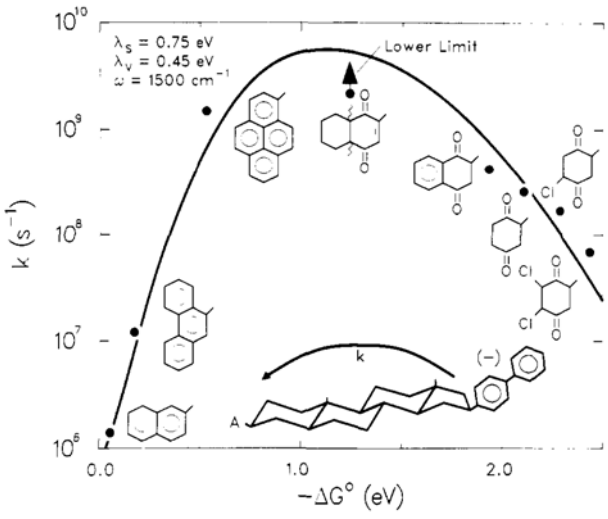

Figure 2.3. 2 *Dependence of k_{ET} from the free energy of electron transfer reaction ($-\Delta G°$). Inverted region is shown*[27]

$$\lambda_{in} = \frac{1}{2}\sum_i \overline{f}_i \left(r_R^{eq} - r_P^{eq}\right)^2$$

Expression 2.3 3 *Equation for inner reorganization energy, being f_i a reduce force constant and r^{eq} the equilibrium bond length of reactant (R) and products (P). The sum is taken over the significant intramolecular vibrations.*

$$\lambda_{out} = \frac{1}{2}\varepsilon_0 \left[\frac{1}{\varepsilon_{op}} - \frac{1}{\varepsilon_s}\right] \int \left(E^R - E^P\right) dV$$

Expression 2.3 4 *Equation for solvent reorganization energy, where ε_s and ε_{op} indicate respectively the static and optical dielectric constant of the medium and ε_0 the permittivity of the vacuum. E^R and E^P are the electric fields generated by reactants and products*

Solving the integral in Expression 2.3.4 means to adopt a more elaborated model for the reactants and products and in this case is possible to consider the reagents as spheres. In such a way the λ_{out} is described by the equation reported in Expression 2.3.5, where the a_D and a_A are the radii of the donor and acceptor molecules, r_{DA} is the center-to-center distance and Δe is the charge transferred in the reaction.

$$\lambda_{out} = \frac{(\Delta e)^2}{4\pi\varepsilon_0}\left[\frac{1}{2a_D} + \frac{1}{2a_A} - \frac{1}{r_{DA}}\right]\left[\frac{1}{\varepsilon_{op}} - \frac{1}{\varepsilon_s}\right]$$

Expression 2.3 5 *Equation for solvent reorganization energy coming from spherical reagent model*

The reorganization of the solvent molecules is a question that has an enormous importance since many electron transfer reactions cannot occur in some solvents and can occur in others. This is mainly true for the photoinduced electron transfer when donor and acceptor are chemically bound together through a "linker". In such a case the starting state may be uncharged while the final products are charged and the choose of the right solvent, for having the longest lifetime for the charge separate state, becomes very important. In fact very polar media can stabilize the charged final products but, due to its polarity, will be affected by high value of λ_{out}, on the contrary very apolar solvent will have low values for λ_{out}, but high

activation energy for electron transfer reaction, due to its inefficiency in solvating the activated complex with a partial charge separation. We should reach a compromise. Another further evidence of the importance of λ is given by the studies carried out by Libby who pointed out how small ions, such as Fe^{2+} or Fe^{3+}, had lower k_{ET} respect higher ions[22,23], such us $[Fe(CN)_6]^{3-}$, $[Fe(CN)_6]^{4-}$ or MnO_4^-, being equal the electron transfer process. Libby explained this fact assuming that the solvent molecules could not rearrange their relative orientation when an almost instantaneous electron transfer occurs, generating an activation energy barrier, that is higher for small ions compared with less solvated complex. In his study Libby also found a sort of exception: the isotopic electron transfer in the pair $[Co(NH_3)_6]^{3+}$ and $[Co(NH_3)_6]^{2+}$ showed small k_{ET} value, even if these ions are big complexes like $[Fe(CN)_6]^{3-}$ or $[Fe(CN)_6]^{4-}$. This discrepancy was justified by Libby adducing a large difference in the Co-N bond length in the two different oxidized complexes[23], but this aspect didn't sound good to Marcus who was moving his first steps towards the electron transfer theory just from this point.

In the classical approach the factor k_{el} in the Expression 2.3.1, is assumed to be equal to one, but this is not even the truth; we can divide the electron transfer reactions in two classes, according to the relative electronic coupling between the reactants and products state: *adiabatic electron transfer reactions* with high electronic coupling that have a $k_{el} \approx 1$, and *non adiabatic electron transfer reactions* with a low value of electronic coupling and in this case k_{el} will be much more less than 1. An exemplification of this difference is given in the Figure 2.3.3: in the *adiabatic* reaction the electronic coupling is enough strong to split in two, at the intersection, the two potential surfaces. In this case the electron transfer remains mainly in the lower surface and the transmission coefficient is more or less equal to one. In *non adiabatic* reaction the system usually stays on the reactant potential surface and only occasionally crosses over the product potential surface. To take into consideration this aspect we need to modify the classical vision of the Marcus theory and introduce the quantum mechanical aspect.

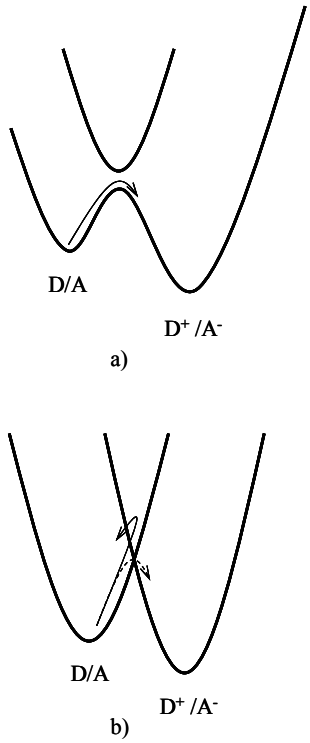

Figure 2.3. 3 *Adiabatic a) and nonadiabatic b) electron transfer*

Before to show the equation for k_{ET} in the *non adiabatic* reactions it is necessary to underline the key role played by the nuclear motions in this circumstance. In particular the vibrational function overlap of both products and reactants is important. In fact the electron transfer can take place when such a overlap is good enough in proximity of the

intersection point, even if the system does not have the right activation energy. This is due to tunnelling effect which can be distinguished in electron and nuclear tunnelling, the latter is more important because of the very little shifts of the nuclei from reactants to products state for generating the effect.

Looking at the Figure 2.3.4 we have three possibilities to see an electron transfer: electron transfer for *electron tunneling at the transition state*, represented by the wave functions in the case 1), where the systems are at the crossing point with the same nuclear configuration (overlap between the vibrational wave functions) and so there is a finite possibility to have electron transfer although the electronic coupling (in general indicated as $\boldsymbol{H}_{RP}$) is very small. Since it is necessary to reach the excited vibrational state the whole reaction will be temperature dependent. In the case 2) is represented the *activated nuclear tunneling* that allows the electron transfer reactions to take place even if the two systems are below the intersection point, also in this case there will be a dependence from the temperature. As last, *temperature independent nuclear tunnelling* is depicted in the case 3), where there is again a finite possibility to have electron transfer even at very low temperature, because there could be very imperceptible overlap between vibrational wave functions and in such a case the reaction is temperature independent.

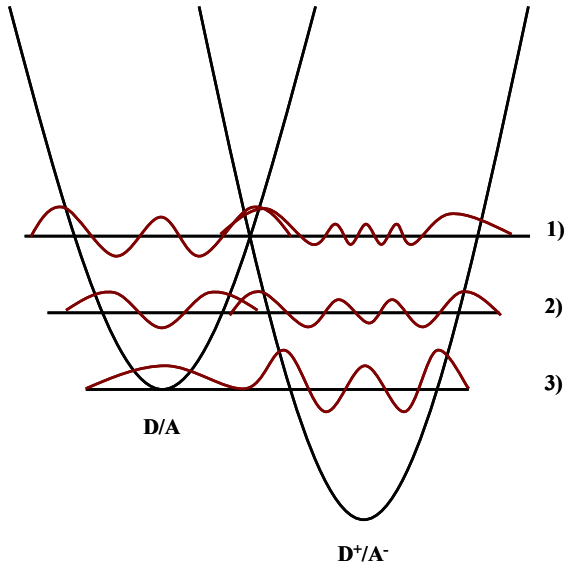

Figure 2.3. 4 *Energy surfaces for quantum mechanical electron transfer theory. The wave functions illustrate symbolically the importance of vibrational overlap.*

To formulate the new expression for the electron transfer rate constant in the non adiabatic condition it is possible to start from the Fermi "Golden Rule" that expresses such a constant as a product between the electronic coupling ($\boldsymbol{H}_{RP}$) and the Franck-Condon factor (F.C.W.D. Franck-Condon weighted density of states) that calculates the overlap of all the vibrational modes, including those of the solvent molecules, each weighted for the relative probability (Expression 2.3.6). To elaborate the general expression it is necessary to solve the Franck-Condon factor and for this purpose there is a semiclassical approach that treats quantum mechanically only the vibrational modes of the systems while those of the solvents are treated with a classical method. Adopting further exemplifications[24] the non-adiabatic k_{ET} can be well defined by the equation in the Expression 2.3.7. Such equation works very well in the normal

region but not in the inverted region. In fact Marcus and Siders had shown[28] that the falloff of k_{ET} in the inverted region is not parabolic but almost linear because the nuclear tunneling is very active, due to a good overlap of the vibrational wave functions.

$$k_{ET} = \left(\frac{2\pi}{\hbar}\right) \cdot H_{RP}^2 \cdot F.C.W.D.$$

$$H_{RP} = \left\langle \Psi_R^\circ \middle| \hat{H}_{el} \middle| \Psi_P^\circ \right\rangle$$

$$F.C.W.D. = \sum_j \sum_i \left\langle \chi_{Pi}^\circ \middle| \chi_{Rj}^\circ \right\rangle^2 P(\varepsilon_{Rj}) \delta(\varepsilon_{Pi} - \varepsilon_{Rj})$$

Expression 2.3 6 *Expression of k_{ET} by a quantum mechanical point of view. Ψ indicates the electronic wave function of reactants (R) and products (P); χ_{Pi} the vibrational wave function of the level i for the product and χ_{Rj} the vibrational wave function of the level j for the reactants.*

$$k_{ET} = \frac{2\pi}{\hbar} H_{RP}^2 (4\pi\lambda k_B T)^{-1/2} \exp\left[-\frac{(\lambda + \Delta G^\circ)^2}{4\lambda k_B T} \right]$$

Expression 2.3 7 *Semiclassical expression for the electron transfer rate constant.*

The inverted region gains a very high importance in the photoinduced electron transfer, as Kakitani and Mataga revealed in their work[29]. Adopting their modifications to the Marcus theory, an uncharged starting state should have a larger value of λ comparing to an ion pairs. In this case they predicted that a charge separation reaction should enter in the inverted region only at high value of $-\Delta G^\circ$, while the charge recombination reaction should present a smaller value of $-\Delta G^\circ$ to enter in the inverted region. This aspect is really useful for obtaining high lifetime of charge separation state.

In this paragraph all the aspects that influence the electron transfer were presented by a theoretical point of view. In the further paragraph the experiments, carried out to shed light into such type of reaction, will be discussed in order to outline in a brief manner how the different factors influencing the electron transfer act.

2.4. Electronic Factor, Solvent and Bridge Effect on Electron Transfer Reactions.

To well understand how the electronic factor changes within different systems, is useful to take in consideration some elementary models and for this aim is also useful to rearrange the expression of k_{ET}, that will be divided into three parts according to the treatment made by Marcus, Sutin and Newton[25,30,31]. The electron transfer rate constant could be expressed as the product of the afore mentioned three factors: electronic transmission coefficient k_{el}, effective nuclear vibration frequency ν_n that tends to destroy the right configuration at the parabolas intersection and the nuclear factor k_n. These three factors are well expressed in the equation reported below[32]:

$$k_{ET} = k_{el}\nu_n k_n \qquad k_{el} = \frac{2\left[1-\exp\frac{-\nu_{el}}{2\nu_n}\right]}{2-\exp\left(\frac{-\nu_{el}}{2\nu_n}\right)}$$

$$\nu_{el} = \frac{H_{RP}^2}{\hbar}\left(\frac{\pi}{\lambda RT}\right)^{1/2} \qquad k_n = \exp\left(\frac{-\Delta G^*}{RT}\right)$$

Expression 2.4. 1 *The different factors taken in consideration in this chapter.*

An important aspect is how the electronic coupling changes with the distance between the redox sites. To simplify the model is possible to assume[30,31,32] that $\boldsymbol{H}_{rp}$ decreases exponentially with the distance, such decrease being measured by the parameter β in the Expression 2.4.2, where r_0 is the van der Waals contact distance between the redox sites and $\boldsymbol{H}_{rp}^0$ is the electronic coupling for such distance.

$$H_{rp} = H_{rp}^0\left[\frac{-\beta(r-r_0)}{2}\right]$$

Expression 2.4. 2 *Distance dependence of electronic coupling*

Obviously the k_{ET} decrease with the distance interposed between the donor and acceptor site, could be different if such distance is simply filled with solvent molecules or with a "molecular

bridge". In this latter case it is possible that the donor and acceptor orbitals can interact with the bridge orbitals. If the bridge is composed by different units is possible to estimate the electronic coupling between the donor and the first unit, the acceptor and the last unit and also between the different units. If such coupling is not high, through the perturbation model[32,33,34,35] , it is possible to write the whole electronic coupling as reported in the Expression 2.4.3.

$$H_{rp} = \frac{H_{D1} H_{nA}}{E_D - E_1} \prod_{i=1}^{n-1} \left(\frac{H_{i,i+1}}{E_d - E_{i+1}} \right)$$

Expression 2.4. 3 *Electronic coupling in a Donor-Bridge-Acceptor unit, where E_D indicates the donor or acceptor energy and E_i the energy of the unit i.*

The last equation reported for the electronic coupling can be used if the interaction with both L.U.M.O. and H.O.M.O. of the bridge is present. In the first case we will have an electron exchange while in the second an hole exchange. An important aspect must be underlined: the electronic behaviour of the molecule that acts as a "bridge" is not an absolute property, but will be dependent upon the donor and acceptor energy levels and also upon the symmetry of the whole system. One of the first study which has furnished data about the "bridge" behaviour, involves metal-to-metal charge transfer, in particular diruthenium complexes where the bridge is formed by polyene subunit[32] (Figure 2.4.1). Such studies were carried out in different solvents[36]. The most important results, considering as solvents nitrobenzene and water, show a value for β equal to 0.2 Å^{-1}, that underlines how the polyene acts as a "molecular wire" due to the extended π conjugation system. Also the behaviour of nuclear and electronic factor were calculated and in general an almost adiabatic reaction ($k_{el} \approx 1$) was found for the polyene bridge even in the presence of a change of metal ions. Due to large value of λ_{out} for such a bridge, the nuclear factor was found to be much more less than one and the distance dependence much more pronounced for the nuclear factor than for the electronic factor. For other bridges such as poly-phenyl bridged ruthenium complex, the β value is higher, most probably due to the lack of coplanarity between the phenyl rings[37]. Changing the nature of the bridge, polyproline instead polyene, has revealed less efficiency in mediating the electron transfer. In fact in the poly-proline bridged system like

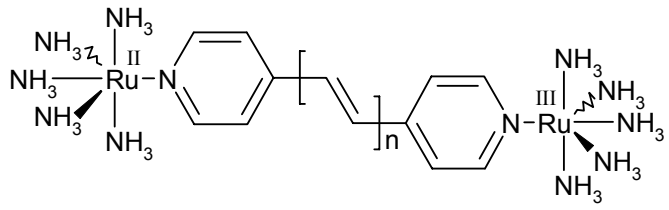

Figure 2.4 1 *Polyene bridged di-ruthenium complex, one of the first bridged system studied for electron transfer.*

Os(II)-Ru(III), both nuclear and electronic factor are less than one[32] with higher value of β (≈ 0.7 $Å^{-1}$); this aspect is probably due to the higher energy of the L.U.M.O. in the polyproline bridge than in the polyene bridge. Differences within the same polyproline systems come out varying the metal, so the couple (bpy-)Ru^{II}-Co^{III} has a value for β twice smaller than the system Os(II)-Ru(III), because the redox potentials of the first system are smaller than those of the second one, allowing a better mixing with the orbitals of the bridge[32].

Another useful study on the parameters that influence the electron transfer is available in the works published by James R. Bolton, John A. Schmidt, Mary D. Archer, Jacquin H. Wilford and coworkers about photoinduced electron transfer in porphyrin-quinone dyad connected with different bridge unit[38]. In these studies particular attention was given to nature of the linkage, solvent and temperature effects. It has been reported that for the molecule depicted in the Figure 2.4.2, a porphyrin linked to a quinone by an amino-acid unit, the electron transfer is faster, in general, in those solvents that present an intermediate value of polarity or more precisely a lower value of ε_s such as 1,2-dibromoethane, chloroform ad chlorobenzene[39]. Moreover it was found that, for the porphyrin-quinone dyad reported in the figure, the electronic coupling between the two moieties is solvent dependent, most probably because conformational effects due to the different dielectric constant of the solvents. Also different bridges were tested, in particular poliaminoacid bridge was found to be very effective because the k_{ET} drops slowly increasing the distance. When an unsaturated bridge is introduced between porphyrin and quinone, the electron transfer goes faster comparing with a saturated ring, but noteworthy a constrained ring such as cyclobutane shows a faster electron transfer than bicyclooctane ring. The strained aliphatic orbitals probably mediate more efficiently the electron transfer reaction.

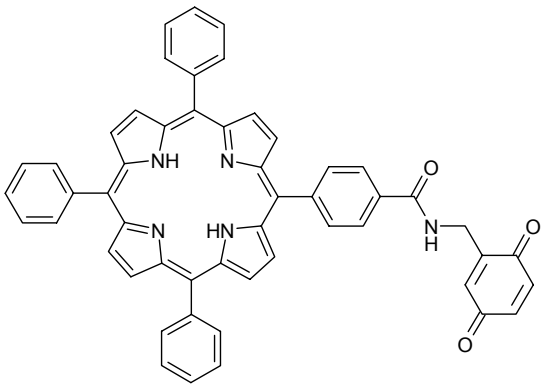

Figure 2.4 2 *Porphyrin-Quinone dyad model, studied for photoinduced electron transfer.*

In these two last examples it has shown how some parameters can influence both the simple electron transfer reaction and photoinduced electron transfer. In the next chapter will be discussed in more details all the systems that are able to reproduce the primary electron transfer reaction which occurs in the natural photosystems, with particular attention to the systems having porphyrin moiety. These chromophores present photochemical properties very similar to those of chlorophylls and bacteriochlorophylls; moreover the chemical synthesis of porphyrin allows to introduce different chemical groups that lead to a very wide type of interactions

between donor and acceptor moiety, useful to obtain long lifetime of the charge separated state. To reach this aim it would be useful to have a very fast forward charge separation and a back-electron transfer deeply inside in the Marcus inverted region.

Chapter 3

"Systems Able to Reproduce Natural Energy and Electron Transfer Reactions"

3.1. Introduction

Once that the Marcus theory became very popular and very useful to understand the influence of different aspects on the electron transfer reactions, the works about systems able to reproduce the primary electron transfer step occurring in the natural photosystems, underwent an enormous increase, especially for those systems that present porphyrin moieties, quinone and carotenoid molecules. Such a systems were deeply studied in order to find a favourable spatial disposition of single chromophores and also a favourable electronic interaction in order to reproduce the longest lifetime of the charge separated state. Many attempts were carried out in such direction and one considerable progress was achieved when Kroto and Smalley discovered the fullerene compounds, in particular the [60]fullerene (C_{60}); for their discovery they were awarded with Nobel prize in the 1996[40]. This molecule shows particular and interesting features and first of all it has been demonstrated its ability to be good electron acceptor[41]. This last characteristic makes the C_{60} suitable for electron transfer reactions. Chemically speaking the C_{60} behaves as an electron poor compound, so it rapidly undergoes to the electrophilic attack; taking into consideration this aspect different functionalizations of C_{60} were developed, in particular the two most famous are the Bingle-Hirsch reaction[42] and the Prato, Maggini and Scorrano reaction[43]. Thank to these studies it was possible to synthesize many porphyrin-fullerene dyads that gave good results in terms of electron transfer.

The use of fullerene has opened a sort of new era for the electron transfer reaction and it made possible to build up also devices for the storage of the solar energy in order to convert it into chemical potential. In the following paragraphs different systems will be discussed, all able to mimic the electron transfer reactions occurring in the natural photosystems, with particular attention to the interaction typology between the chromophores, the nature of the electron transfer, the yield of the reaction and also the lifetime of the charge separated state. Finally some indications will be suggested on how these systems could be used to build organic solar cells, in order to confer also a practical aspect to all the studies carried out on this argument.

3.2. Porphyrin-Quinone Systems

Many efforts were spent to understand the energy and electron transfer phenomena in porphyrin systems especially those containing the same molecules found in the natural photosystems such as carotenoids and quinones. As we have afore mentioned[44] one of the first complete study on porphyrin-quinone system, where different linkers like: amino-acid, phenyl, cyclobutane and bycicloctane were used, was carried out by J. R. Bolton, J. A. Schmidt, M. D. Archer, J. H. Wilford during the 80th. More or less in the same period many authors published many works on simple or articulated porphyrin-quinone systems.

Osuka and coworkers have studied the distance and conformational effect on a porphyrin-naphtoquinone dyad[45] where the quinone moiety is linked to the phenyl group of the porphyrin through an ether linkage in two different positions (Figure 3.2.1), such a disposition leads to discriminate conformational effects. The porphyrin fluorescence was found to be much more quenched when the quinone is bound to the *ortho* position of the phenyl ring than in the *para* position; most probably the *ortho* derivative can interact with the porphyrin ring in such a way to generate a π-π stacking interaction between the two moieties. When the naphtoquinone is substituted in the position number three with a methyl group the authors found out that the fluorescence quantum yield of the porphyrin was higher for the *ortho* derivatives than for the *para* ones and they concluded that the steric hindrance of the substituent prevents the π-π stacking. Moreover the steric hindrance could twist away the *ortho* linked naphtoquinone from an optimal conformation, preventing high fluorescence quenching. There are further studies of Osuka and coworkers[46] on several quinone linked and quinone capped porphyrin systems, where many saturated carbon bonds were placed between the two chromophores. They rationalized the observed fluorescence quenching in terms of a through space energy or electron transfer. Since the falloff of the rate constant in a

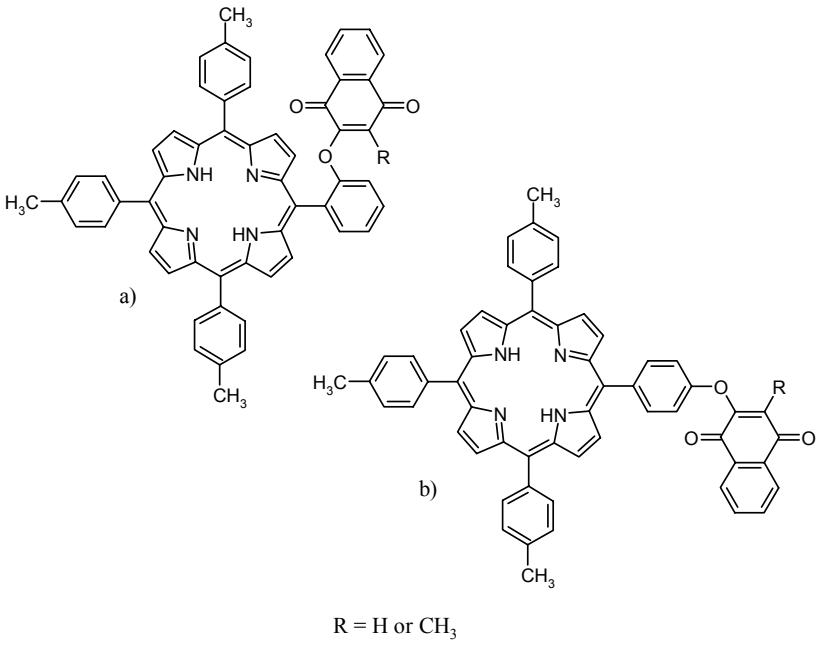

Figure 3.2. 1 *Porphyrin quinone dyads studied by Osuka and coworkers*

through bond mechanism is more or less one order of magnitude per bond, the rate constant of a through bond electron transfer starting from the porphyrin singlet excited state, can not compete kinetically with the rate constant decay of the porphyrin excited state in those compounds where the two photoactive moieties were spaced more than four or five saturated bonds.

Other conformational effect were outlined by the studies of Lindsey and Mauzerall[47,48] published in 1988 and 1990 where a porphyrin-benzoquinone sandwich dyad was reported (Figure 3.2.2). The data suggest the existence of two distinct conformers differing in the interplanar porphyrin-quinone distance: the compound shows a solvent dependent quenching rate of the porphyrin fluorescence, but while in the close conformer the rate constant varies on a little range (4-fold), in the distant conformer the range is greater (10-fold). Furthermore a temperature dependence study was carried out revealing very little or no variation in the rate constant of electron transfer by slowing down the temperature. To explain such data the authors suppose a non adiabatic electron tunneling. This type of mechanism is also supported by other evidence: an electron-nuclear tunneling requires small activation energy and a distance between the donor and acceptor greater than the sum of the van der Waals radii. The complex in the Figure 3.2.2 has both these characteristics. Moreover the authors assume that such electron transfer is through space[47]: the spacer between the two moieties are benzylaniline groups, having high energetic and easily oxidized H.O.M.O.. The addition of acetyl group to the banzylaniline nitrogen atom means increasing the oxidation potential of the amine and the lowering of the H.O.M.O. energy, but the electron transfer rate constant is insensitive to the acetylation reaction, affording a proof that the reaction is not through bond. Other evidence came out from structural considerations, because the bond number is equal in the two conformers, but the electron transfer rate constant is five fold higher in the close conformer (6.5 Å quinone-porphyrin interplanar distance) than in the lose one (8.5 Å quinone-porphyrin

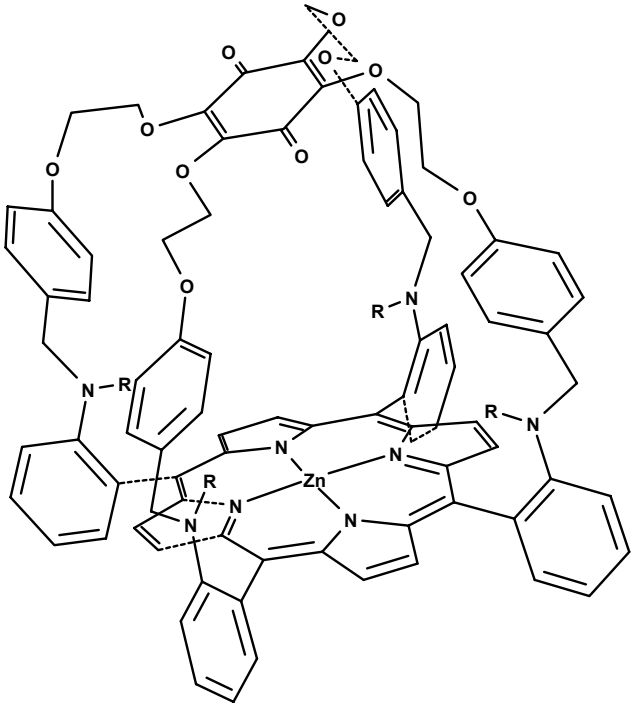

Figure 3.2. 2 *Quinone Capped porphyrin studied by Lindsey and Mauzerall. R = hydrogen or acetyl group*

interplanar distance) only a through space electron nuclear tunneling can account such a data. Mauzerall has continued his study on quinone-capped porphyrin where one or two quinones are stacked up to the two surface of the porphyrin[49] (Figure 3.2.3), the two quinone moieties are linked to the two opposite phenyl rings in a *ortho* position through aliphatic chain composed of four carbon atoms. In both molecules the fluorescence quenching exhibits only weak solvent dependence, but the quenching of the fluorescence emission is different in the monoquinone versus the diquinone molecules and the authors have attributed such difference to the orbital symmetry properties of the system. Besides the fact that a cofacial geometry can increase an electron transfer reaction because of a more favourable interaction between the chromophores, sometimes it is difficult to rationalize the conformational effects in terms of a clear dependence of rate constant from parameters such as distance and relative orientation between the donor and acceptor group, for such a reason several porphyrin-quinone systems were synthesized having rigid geometry in order to link the quinone group to a fixed distance from the porphyrin moiety.

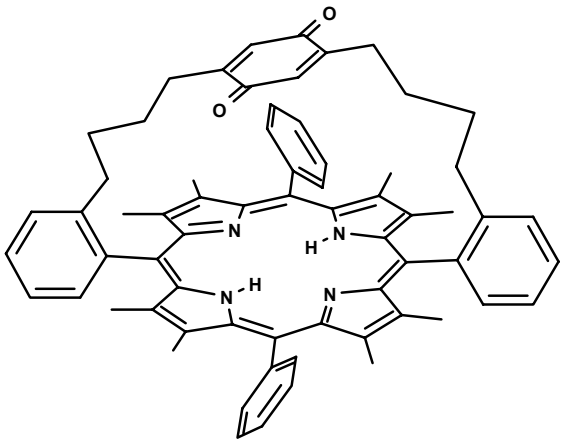

a)

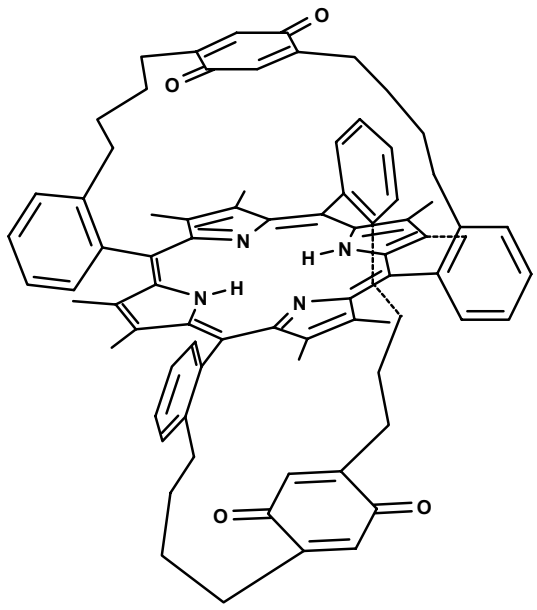

b)

Figure 3.2. 3 *Quinone capped porphyrin systems studied by Mauzerall. Mono quinone capped porphyrin a) and di-quinone capped porphyrin b).*

Sessler and coworkers published in the early 90th a series of works[50,51,52] on rigid quinone substituted porphyrin-dimer systems in order to evaluate the possible superexchange electron transfer mechanism intervening between porphyrin moiety and quinone. Such a study had the aim to verify the hypothesis on the role of the bacteriochorophyll in the natural bacterial photosystems[53]. Two different geometric architectures were synthesized, the first one linear and the second one bent (Figure 3.2.4). Because the fact that the two porphyrins are completely identical, it is not possible to excite selectively only one, unless a zinc atom is introduced, generating two different isomers per

geometry. Proximal and distal zinc derivatives, where the zinc atom is respectively in the quinone bonded porphyrin or in the non quinone bonded porphyrin. The characterization of the complex was quite difficult, but in general some features emerge from UV-vis and cyclic voltammograms. The absorbance data show a little excitonic coupling between porphyrin moiety in the bent system, underlined by the Soret splitting[51]. This was not observed for the linear dimer. The electrochemical studies underline a certain degree of interaction between the two chromophores in the monomer porphyrin-quinone system (Figure 3.2.4 e)). In fact the presence of the quinone increases the oxidation potential of the porphyrin of about 80-90 mV, but in the bent porphyrin-dimer quinone system, it seems that there is not interaction between the different chromophores, while in the linear one a certain degree of communication is outlined. However, despite these differences, both the dimeric systems could be thought as quite good mimicking systems of the natural ones. The fluorescence and subpicoseconds flash photolysis reveal peculiar differences between the proximal (Zn near the quinone) and distal (Zn far away from the quinone) regioisomers[52]: in both the distal regioisomers, linear and bent, it is possible to see a reaction pattern very similar to that seen in the monomer.

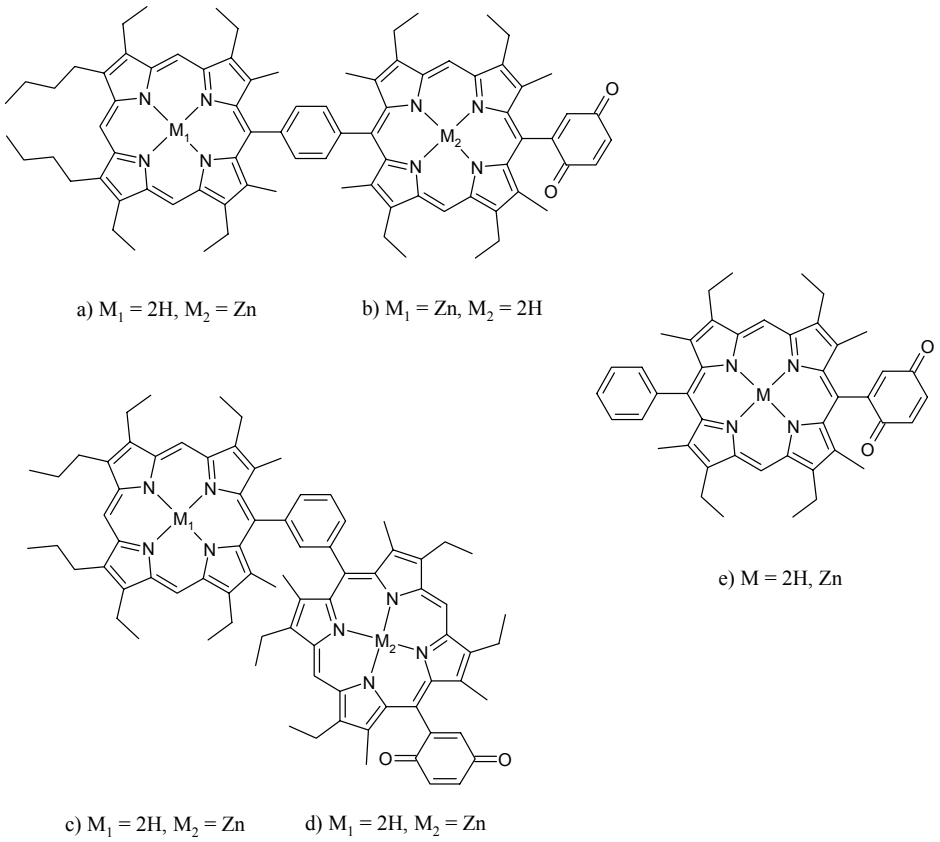

Figure 3.2. 4 *Linear and bent quinone-porphyrin dimer complexes and quinone-porphyrin monomer investigated by Sessler and coworkers.*

After photoexcitation there is a fast charge separation and a subsequent charge recombination within 5 ps, recovering completely the fundamental state. Such data suggest an ultrafast electron transfer due to a favourable energy gradient in the system ZnP-H_2P-Q. In the system H_2P-ZnP-Q the interposed zinc porphyrin constitutes an energy barrier for direct electron transfer from H_2P, in fact the fluorescence studies reveal a fast charge separation-charge recombination within 15 ps plus a second process, within 55-75 ps. This last result is due to the deactivation of the singlet excited state of free base porphyrin induced by the quinone moiety. From such data the authors have assumed the presence of an electron transfer from distal H_2P^* to quinone via mediated ZnP superexchange, an hypothesis proposed also for primary electron transfer step occurring in the reaction center of the photosynthetic bacteria[44].

This study evidences how simply altering the position of a zinc porphyrin it is possible to alter the nature of the electron transfer reaction. The relative orientation between the donor and acceptor group also plays an important role in the electron transfer reaction and this aspect is outlined by the studies of Sakata and coworkers[54,55] who have synthesized porphyrin-quinone dyad where the two photoactive groups are covalently linked by the same number of saturated carbon bonds, but with a different relative orientation (Figure 3.2.5).

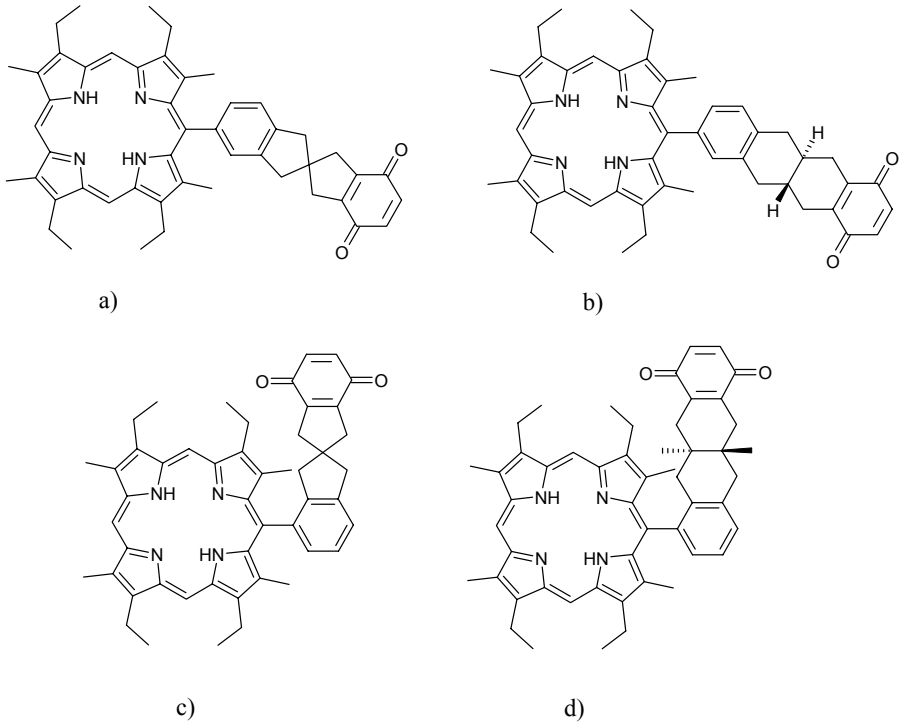

Figure 3.2. 5 *Spiro porphyrin quinone compounds a) and c) and relative bycyclo porphyrin quinone system b) and d) reported in the papers published by Sakata and coworkers*

In both the molecules the donor and acceptor units are separated by 7 carbon bonds giving no interaction in the foundamental state, the only difference is the mutual orientation of the two π-systems: the dihedral angle of the two planes is 150° in the dimer a while in the dimer b the planes are perpendicular each other. Despite this difference the spiro compound a in Figure 3.2.5 undergoes charge separation with a 3.3×10^{8} s^{-1} rate constant while the other compound, with a *trans* configuration of the saturated carbon ring, behaves in the same way with a rate constant of 6.5×10^{7} s^{-1}. Further studies[55] on similar compounds confirm this observation. In fact in the dimer c the electron transfer rate constant is 3.5×10^{9} s^{-1} while in the dimer d is 4.0×10^{8} s^{-1}. Such a difference could be ascribed to a large orientation effect that reveals a through space orbital interaction. Particularly interesting is the work published in 1991 by Antolovich et al.[56] that reports about the electrochemical and photophysical investigation on systems where the quinone moiety is linked to the *beta* position of the porphyrin pyrrole ring affording a lightly modified porphyrin compared with the classical tetraaryl or alkyl octasubstituted porphyrins. This work outlines two important points: how an aliphatic ring such as norbornyl unit can act as a good bridge allowing an outstanding electronic coupling between the two aromatic rings and how the change of the solvent can dramatically affect the value of the energy barrier, limiting the electron transfer reaction due to the lack of a sufficient driving force (ΔG°). Appling the Marcus theory and comparing the electrochemical data, the authors estimated the activation energy and the driving force for the free base and zinc derivatives of both systems depicted in the Figure 3.2.6; such a values are: ΔG° = -0.4 eV and ΔG* = -0.09 eV for the free base derivatives and ΔG° = -0.7 eV and ΔG* = -0.02 eV for the zinc derivatives in polar media. In the free base compound a a rapidly electron transfer, with a rate constant of about 2.5×10^{10} s^{-1}, occurs after excitation in solvent of moderate to high polarity despite the distance that is 11.6 Å. This is possible thanks to the presence of the norbornyl unit, that, as mentioned above, leads to a good electronic coupling between the chromophores. While the absence of an electron transfer in low polar media could be attributed to the lack of driving force, the rate constant is limited by the changes in ΔG*. Because of the fact that the activation energy is dependent by both ΔG° and λ, passing from less polar to more polar solvents, an increase in magnitude of the reorganization energy partially deletes the gain obtainable from the further decrease in ΔG*; these aspects do not allow to the compound a to achieve a complete barrierless electron transfer (ΔG* = λ). The free base derivative of compound b presents very low or no electron transfer rate constant most probably due to the higher intercoming distance between porphyrin and quinone that lows down the electronic coupling. This fact also may be due to the presence of an higher activation energy compared to the similar compound a. The introduction of a zinc atom

in the compound b affords a lowering of the barrier of about further 0.06 eV, leading to an electron transfer reaction with a rate constant of a maximum of 1.4×10^{10} s^{-1} in chloroform. Such results confirm the importance of the solvent effect and also that saturated carbon bonds can mediate electron transfer affording a superexchange mechanism through σ bond interactions. This is also particularly true for the zinc derivatives of compound b, able to give fast electron transfer despite the distance (16.2 Å) between the donor and acceptor sites that is higher than that in the natural photosystems.

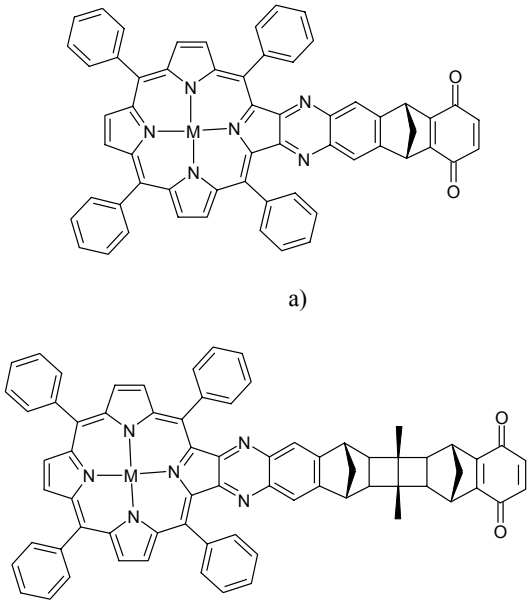

Figure 3.2. 6 *Quinone beta linked porphyrin systems in the Antolovich's work*

The electronic coupling between the chromophores allows a quite fast electron transfer also in other systems that present moderate or little driving force, this aspect could be exemplified by the dyad synthesized and studied by Cormier and coworkers [57] where an antraquinone is directly linked to the position number 5 of a tetraphenylporphyrin, such arrangement allows a so strong electronic coupling, also in the foundamental state, that the absorption spectrum of the porphyrin is perturbed by the presence of the quinone acceptor. Despite of the fairly negative driving force that the system presents, quite high electron-transfer rate constant are reported in polar media. The electronic interaction or more in general the interaction between the chromophores is a key feature of the natural photosystems so that the special pair in PSI and PSII is built with two chlorophylls, or bacteriochlorophylls, which clearly show excitonic interaction[58]. For such reason many porphyrin dimers and oligomers were synthesized in an appropriate geometry to give a good electronic interaction. One of the pioneeristic study on this argument was carried out by Osuka and Maruyama [59] who synthesized different geometrical arranged porphyrin dimers using as linker a naphthalene subunit. This choice allowed them to dispose the two porphyrin either in a edge-to-edge and face-to-face structure, obtaining different electronic coupling degree. The strength of the coupling was

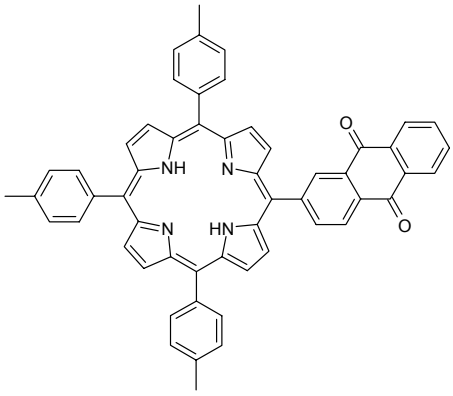

Figure 3.2. 7 *Porphyrin anhraquinone system studied by Cormier et al.*

evaluated applying the dipole-dipole exciton theory and the entity of such an interaction can be seen in the Soret band splitting. It is most important to point out that for all the cofacial geometry, especially for those compounds that have other type of linker like anthracene and biphenylene bridged porphyrin, the exciton coupling is so strong to completly delete the fluorescence emission, a fact that underlines how not only the S_2 state is perturbed (splitting of the Soret band) but also the S_1 state (Q bands)[59]. The study about the excitonic interaction was continued by Nagata with the help of Osuka and Maruyama[60]. They investigated more complex oligomers made up of three or five porphyrins in an edge-to-edge or in a face to face geometry. The principal outcomes show as the changes in the absorption properties are proportional to the number of chromophores in the oligomers and in particular for the linear systems the splittings and the red shifts of the Soret are higher and proportionate to the number of porphyrins. It is possible to reach the same conclusion for the blue shift of the Soret band in the multi stacked systems. These results have led to the birth of more complicated multiporphyrin-quinone systems. In particular those studied by Osuka[61,62] are formed by 2, 3 or 4 porphyrins, two of them in a cofacial arrangement to mimic the special pair in the natural photosystems. The study reveals that after excitation a fast electron transfer occurs between the porphyrin and quinone adjacent to each other and a subsequent more difficult detectable electron transfer from the artificial special pair to the central porphyrin.

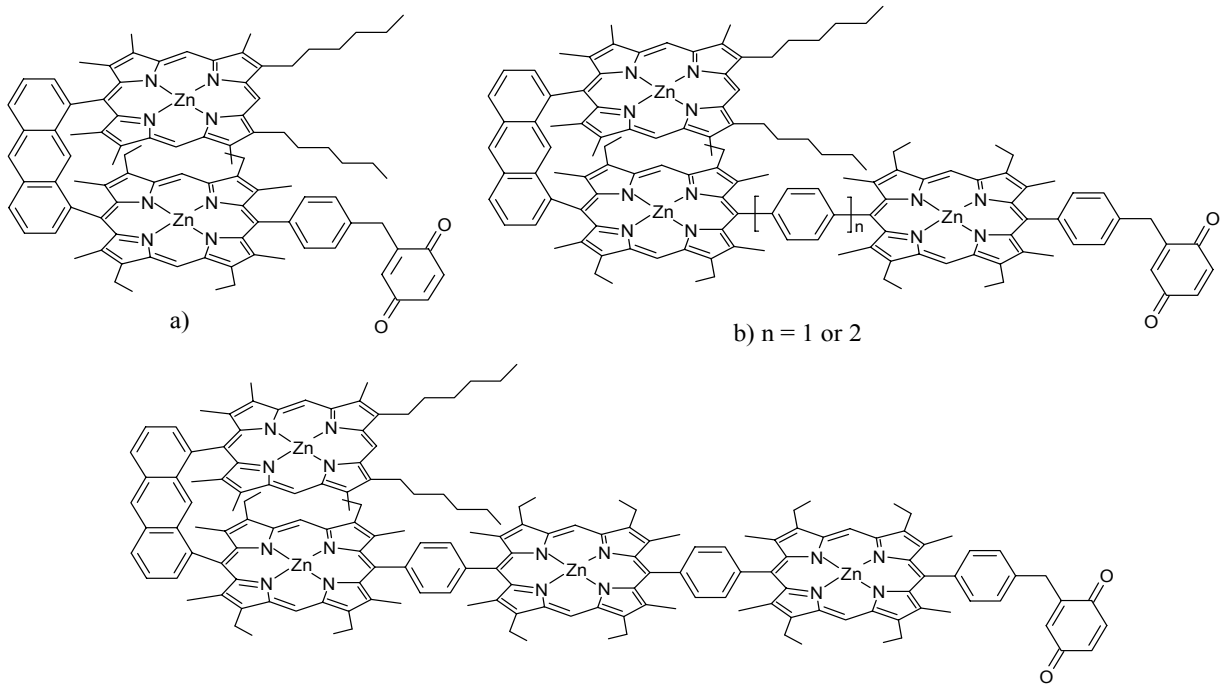

Figure 3.2. 8 *Multiporphyrin quinone systems studied by Osuka showing artificial special pair (cofacial porphyrin dimer). The system b), when n = 2, affords a lifetime for the charge separated state of 500 ps.*

The lifetimes for the charge separated state are 20, 50 ad 70 ps respectively in those system that present only one phenyl ring as spacer between the single chromophores, while the lifetime increases up to 500 ps in the system with a biphenyl spacer (Figure 3.2.8).

The lifetime of the charge separated state in porphyrin-quinone systems discussed up to now lies between picoseconds[51,52,61,62] and few nanoseconds[56]. A particular improvement in the lifetime was achieved when carotenoid molecules started to be used as supplementary electron donor and also as further absorbing chromophores in the near UV and visible region. The papers published by Gust, L. Moore and A. Moore[63,64,65] in this area are particularly interesting. In one of their studies[65b] the interaction typology between carotene and porphyrin was investigated preparing *ortho*, *meta* and *para meso*-phenyl carotene substituted porphyrins. The steady state fluorescence, transient absorption and transient fluorescence emission showed the presence of a triplet-triplet energy transfer from the porphyrin to the carotenoid moiety and singlet-singlet energy transfer from the carotenoid molecules to the porphyrin. The rates of all the process are higher for the *ortho* and *para* isomers than for the *meta* ones and even the analysis of the triplet-triplet energy transfer suggests the presence of a "through bond" interaction mechanism involving the π-electrons of the linkage bonds (amide linkage), rather than a direct "through space" interaction between the two moieties. One of the first triads studied was the carotene-porphyrin-quinone system where the porphyrin and the quinone are separated by many methylene subunits[64a]. The main result of such a study was to underline how the increasing of the methylene subunits up to four, leads the system to adopt many conformations with different quinone orientations relative to the porphyrin moiety, making difficult the interpretation of the electron transfer dependence from the distance between the porphyrin and the quinone. An interesting photophysical study was reported in 1988 on a carotenoid-porphyrin-diquinone system[64b] (Figure 3.2.9). In this paper it was outlined a multistep electron transfer occurring after excitation of the porphyrin moiety. A particular feature is the key disposition of the two terminal quinones, the first having a more negative redox potential was linked directly to the porphyrin, while the second one with the less negative redox potential was at the end. Such disposition promotes sequential electron transfer from naphthoquinone to the benzoquinone. After the first electron transfer step ($C\text{-}P^{\bullet+}\text{-}Q_A^{\bullet-}\text{-}Q_B$) between the porphyrin and the naphthoquinone with a rate constant of 2×10^{10} s^{-1}, the whole process affords a charge separated state ($C^{\bullet+}\text{-}P\text{-}Q_A\text{-}Q_B^{\bullet-}$) with a lifetime of 460 ns in dichloromethane and 4 μs in acetonitrile with an overall quantum yield of 0.23 at room temperature and 0.50 at 240 K. The two different pathways ($C^{\bullet+}\text{-}P\text{-}Q_A^{\bullet-}\text{-}Q_B$ and $C\text{-}P^{\bullet+}\text{-}Q_A\text{-}Q_B^{\bullet-}$), that lead to the final state, compete with the back electron transfer of the first step and guarantee

the high efficiency to the entire process. The subsequent developments of this first study have generated much more complicated systems, but with remarkable improvements in the lifetime of the charge separated state.

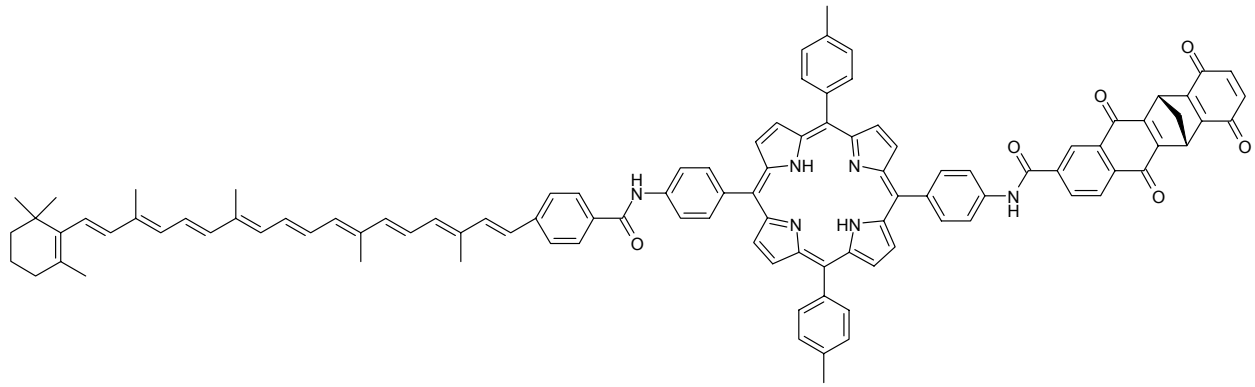

Figure 3.2. 9 *Carotenoid-porphyrin-diquinone tetrade studied by D. Gust, T. A. Moore and A. L. Moore. Such a system produces a long lifetime for charge separate state 4 μs in acetonitrile*

Another tool for inducing multistep electron-transfer even in the absence of a quinone as last acceptor is to vary the electrochemical properties of the porphyrin. It is possible to do that introducing perfluorophenyl groups as in the system represented in the Figure 3.2.10 a where the electron-transfer occurs from the central porphyrin to the perfluorinated one. The studies[65a] demonstrate the presence of inter-porphyrin singlet-singlet energy transfer with rate constants ranging from 8.1×10^{8} s^{-1} to 2.3×10^{10} s^{-1} and electron-transfer starting from the singlet excited state of zinc derivative to the perfluorinated porphyrin with a rate constant of 3.5×10^{9} s^{-1} and a quantum yield of 0.68. After this electron-transfer, the radical cation of the zinc porphyrin oxidizes the carotenoid to give the final state $C^{\bullet+}$-ZnTPP-$TPP_f^{\bullet-}$ with a lifetime of 250 ns and a quantum yield of 0.32. All the efforts from the D. Gust, T. A. Moore and A. L. Moore research group produced also other two systems b and c depicted in the Figure 3.2.10. Both the tetrads present good lifetime for the charge separated state due to the multistep electron transfer strategy: the first one b shows a lifetime of 2.9 μs in anisole with a quantum yield equal to 0.25[64d], while the second one c has a lifetime of 55 μs and the corresponding quantum yield is 0.83. In this last case it was shown that removing the zinc atom from the porphyrin produces a longer lifetime equal to 340 μs but the quantum yield drops down dramatically to 0.15[66].

The systems reported in this paragraph were synthesized and studied contemporary with the first studies on the primary electron transfer reaction in the natural photosystem and also contemporary with the first well defined crystallographic data on these systems. It is natural

that in all of them the principal efforts are dedicated to reproduce the architecture of the natural reaction centers, putting particular attention to the geometrical disposition of the covalently linked porphyrin quinone couple. Just a little bit later the key role of the natural photosynthetic antenna systems became more clear and also the nature of the interaction, mainly energy transfer, between the chlorophylls that constitute the antenna began to acquire importance. An increasing number of studies were published on several multiporphyrin arrays and on how it was possible to modulate the energy transfer processes in these artificial antenna systems. In the next paragraph some examples of these arrays will be given and other strategies adopted to recreate the properties of the natural antenna systems will be reported, such as the use of self-assembling system, or the synthesis of dendrimeric unit.

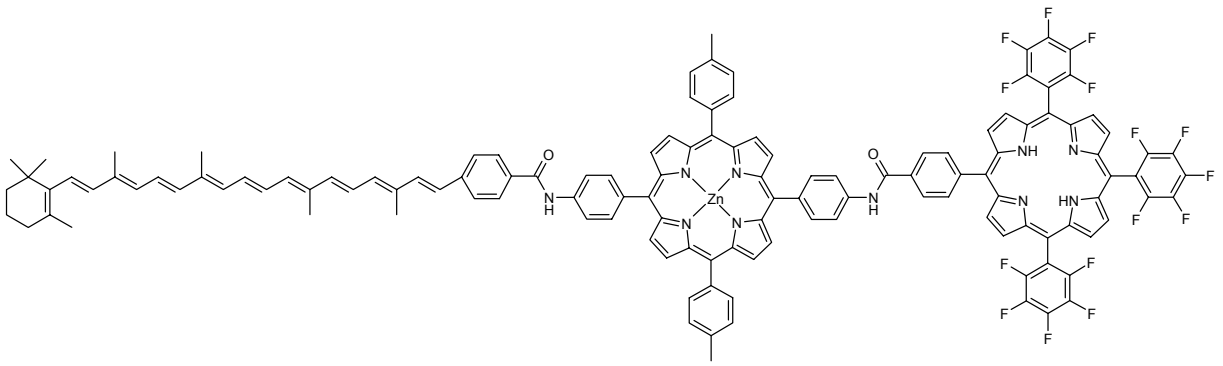

a)

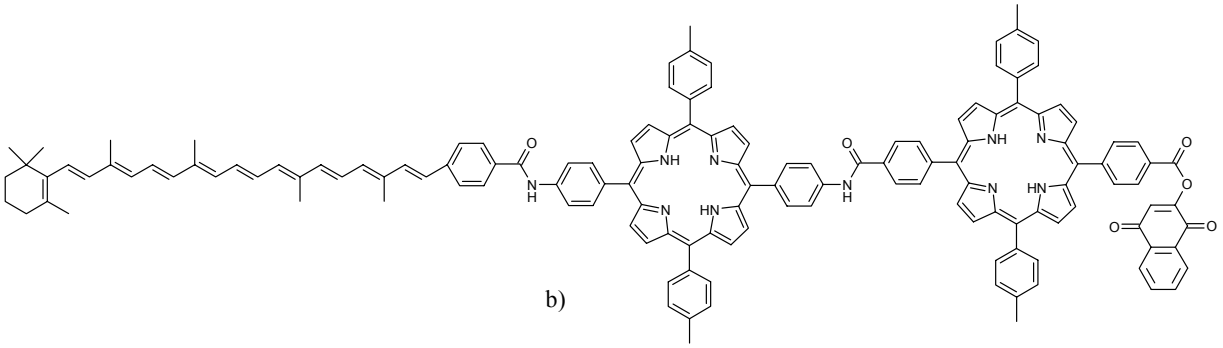

b)

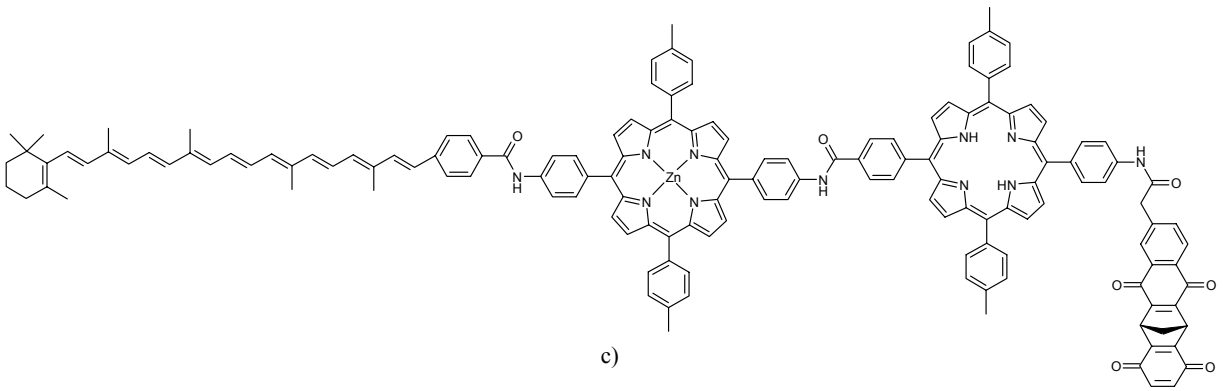

c)

Figure 3.2. 10 *Carotenoid-porphyrin-quinone complexes reported by Deven Gust, Thomas A. Moore and Ana L. Moore and coworkers in their works*

3.3. Porphyrin Light Harvesting Systems

As we have seen in the chapter one, the photosynthesis is based on two main structures: a reaction center where the charge separation occurs and a highly efficient light harvesting system made up of several chromophores, the carotenoid molecules and chlorophylls being the most abundant. It was shown the crucial importance of these systems in funnelling the harvested solar energy towards the reaction center, mainly through energy transfer processes. It appears clear that to reproduce the whole photosynthetic process it is necessary to synthesize "artificial harvesting systems". For such a purpose the porphyrins seem to be the more suitable compounds because of their resemblance with natural chromophores and also for their synthetic versatility, which allows to modulate the electronic interaction and build up several architectures. In this direction a particular contribution was given by the works of Lindsey, Holten and Bocian. Their principal efforts were dedicated to synthesize multicomponent macromolecular architecture with different geometries in order to fine tuning the electronic communications among the single components. First studies were carried out on dimeric and trimeric porphyrin arrays where the linker is a diphenylacetylene moiety[67]. In the dimeric array with one zinc porphyrin and one free base porphyrin (Figure 3.3.1 a) the energy transfer is highly efficient up to 95-99% and charge transfer reaction is not observed in almost all the used solvent. An interesting aspect is the fact that energy transfer seems to take place with a "through bond" mechanism, because the introduction of steric groups on the linker, preventing a pseudo coplanarity between the two systems, slows down the rate constants of energy transfer up to 4-fold. Moreover the rate constants range from 1×10^{10} s^{-1} to 4×10^{10} s^{-1}, values which are higher than those predicted by Förster mechanism (through space). Despite that, the electronic communication is weak because each prophyrin retains its intrinsic radiative and non radiative rates upon incorporation into the array. The fluorescence analyses of the trimeric linear array furnish an energy transfer rate constant of 1.9×10^{10} s^{-1} in toluene at room temperature from the two isoenergetic zinc porphyrins to the free base one (Figure 3.3.1 b), confirming that the inclusion of multiple isoenergetic pigments into linear or two dimensional arrays permits efficient overall energy transfer. The medium effects, like variation in solvent polarity, and axial coordination, are not very important and induce only very little changes in the rate constants. The subsequent development of this work [68] was to verify how, altering the geometrical disposition of the porphyrin, the energy transfer process could change and to analyze in a deeper way the electronic communication between the pigments. Raman spectroscopy has been used to investigate this last point. From the data it is possible to observe large resonance Raman intensity enhancements for aryl-ring and ethyne-bridge stretching

modes, in the unconstrained array. These findings were attributed to an excited state conformational change that enhances the conjugation between the π-electron system of the porphyrin and the bridge group. The intensity of the vibrational modes decreases as the torsional constrain increases and all the data reinforce the "through bond" mechanism for the energy transfer. On the other hand the alteration of the geometry into the array does not affect the energy transfer process. In fact in the right-angle trimeric array (Figure 3.3.2) all the photophysical properties seem to recall those in the linear array.

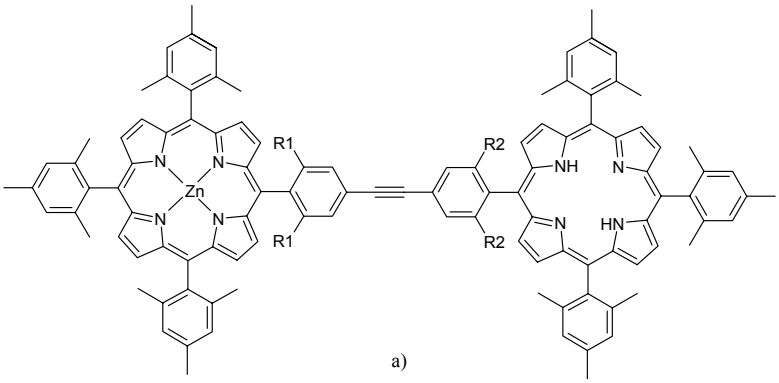

$R_1 = R_2$ = H unhindered dimer
$R_1 = CH_3$ R_2 = H or R_1 = H $R_2 = CH_3$ monohindered dimer
$R_1 = R_2 = CH_3$ bis hindered dimer

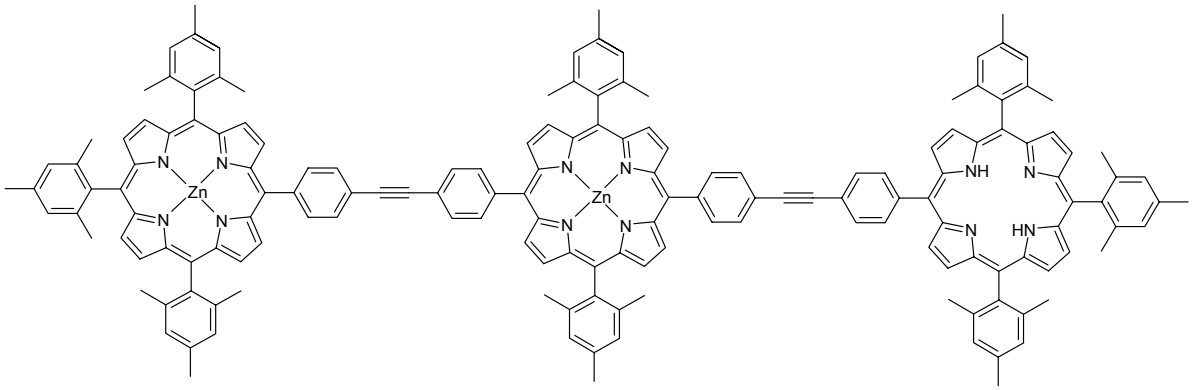

Figure 3.3. 1 *Linear dimeric and trimeric array with aryl-ethyne bridge investigated by Lindsey, Bocian and Holten*

Further development regards the effects of restricted porphyrin-porphyrin rotation on the energy transfer. For this reason Lindsey and coworkers synthesized a square macrocyclic array of four porphyrins that locks the pigments in a mutually coplanar architecture[69]. Transient absorption data in toluene at room temperature, indicate that energy transfer from zinc porphyrin to the neighbouring free base porphyrin occurs with a rate constant equal to 3.8×10^{10} s^{-1}. From resonance Raman spectroscopy and further fluorescence analysis, comparing the

planar tetramer with a dimer, no evidences emerge that the geometric constraints, imposed by the closure of the structure, can alter the through bond electronic communication among the porphyrins. One of the most remarkable result obtained by Lindsey, Bocian and Holten on the structural control of photoinduced energy transfer is reported in a work[70] published on 2000 where a family of diphenylethyne-linked porphyrin dimer and trimer were reported. The peculiar aspect of these compounds is the typology of the linker attachment, in particular *meso-para*/*para-meso*, *meso-meta*/*para-meso*, β-*para*/*para-meso* and β-*meta*/*para-meso* substituted dimers and also trimers were prepared (Figure 3.3.3). Thanks to all these compounds it was possible to discriminate the effect due the different linker position on the energy transfer. Empirically it was found that in the dimer the energy transfer rate constant, from the zinc porphyrin to the magnesium porphyrin, decreases according to the following order: *meso-para*/*para-meso* > β-*para*/*para-meso* > *meso-meta*/*para-meso* > β-*meta*/*para-meso*. In the trimer, a zinc porphyrin is interposed between a magnesium porphyrin and a free base porphyrin in a linear geometry. Such disposition allows a slow energy transfer directly from the magnesium porphyrin to the free-base porphyrin with a rate constants of a magnitude order equal to that previous reported for the dimer. This energy transfer is not affected by temperature changes so it is possible to assume that it occurs via superexchange mechanism utilizing the orbital or excited state of the intervening zinc porphyrin. Another important tool to modulate the energy transfer in the porphyrin array is to alter the symmetry of the H.O.M.O. varying the meso substituents: in general when the phenyl group brings electron-withdrawing substituents, such as fluorine, the H.O.M.O. of the porphyrin is the a_{1u}, which present electron density on the β-pirrole carbon atom and a node corresponding to the *meso* position of the tetrapyrrole ring. On the contrary when we have electron releasing groups like methyl group, the a_{2u} orbital becomes the H.O.M.O. of the porphyrin and this latter symmetry presents electron density on the *meso*

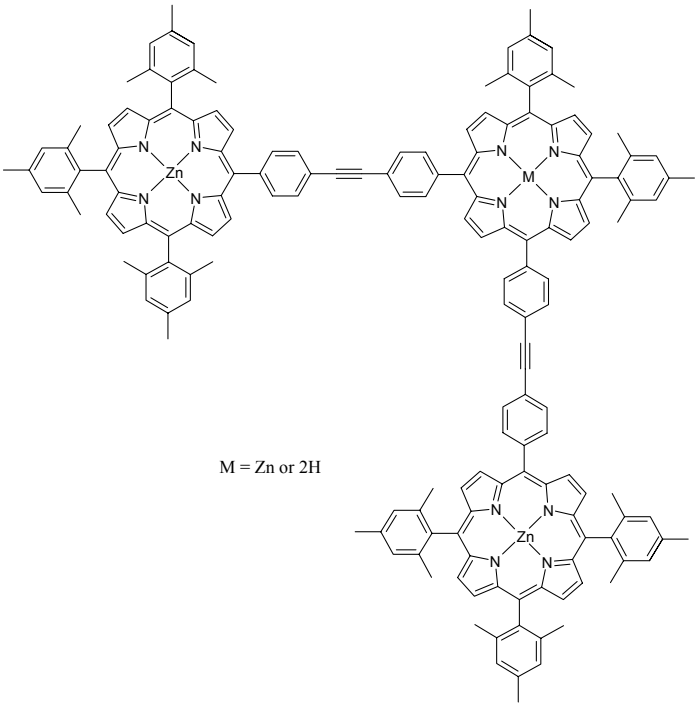

Figure 3.3. 2 *Right-angle trimer reported in the work published by J. Lindsey and D. Bocian. See text.*

carbon atom of the porphyrin ring. It is possible to modulate the energy transfer flow simply changing the substitution pattern at the periphery of the porphyrin as it is demonstrated in a review published by Holten, Bocian and Lindsey[71].

Obviously, since the dimer, trimer and tetramer synthesized by the authors show "through bond" energy transfer, attaching the linker to the electron-reach carbon atom means to increase the energy transfer rate, while in the opposite case the rate of the process will be slowed down. In the aforementioned review are summarized all the results of the previous works and in particular is outlined how all the synthesized architectures present weak electronic communication in the fundamental state. The overall characteristic properties of the array could be thought as the sum of those of the individual pigments, nevertheless such electronic coupling is sufficient enough to guarantee good energy transfer and hole/electron hopping. Particularly interesting is the star shaped harvesting system (Figure 3.3.4), with a central free base porphyrin, and the linear porphyrin tetramer that acts as a logic gate (Figure 3.3.5). In the former it was demonstrated, through EPR measurements, that the ground state hole hopping is a facile process and the hole resides over the four peripheral zinc porphyrins due to their lower oxidation potential comparing with the free base. In the linear array when a boron dipyrrine unit is used as photonic input, the absorbed energy flows through the neutral molecular wire and is emitted from the free base porphyrin. In this situation the molecular gate is on. When the magnesium porphyrin is oxidized, the excited state of the free-base porphyrin is completely quenched and there is no emission subsequent the excitation of the boron dipyrrine

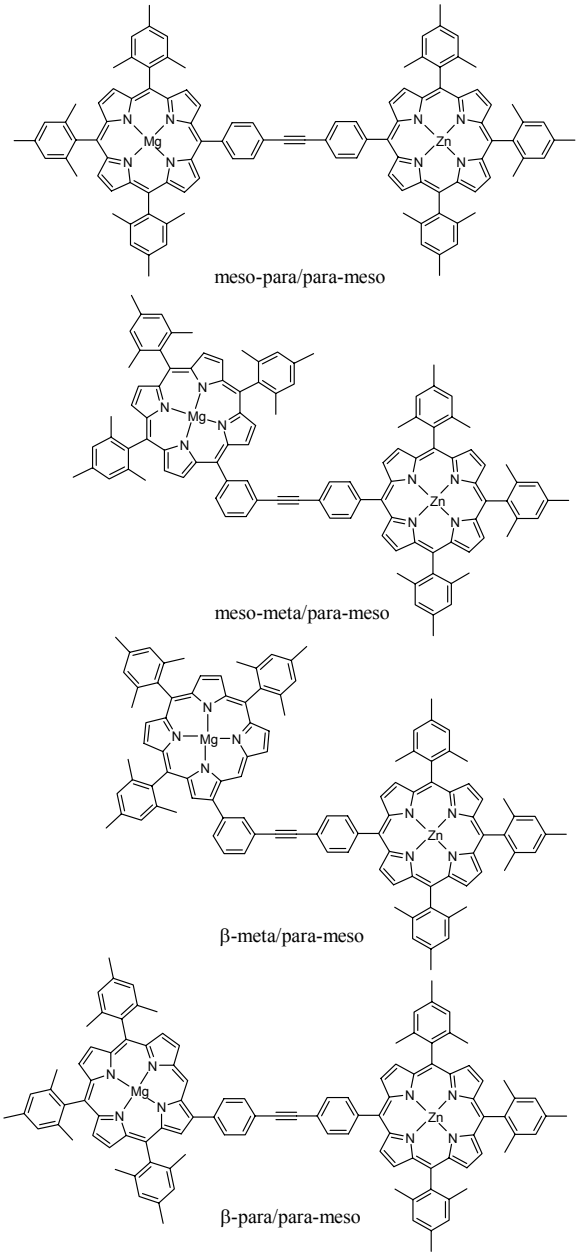

Figure 3.3. 3 *Porphyrin dimers with different site of connection and respective nomenclature, synthesized by Lindsey*

moiety. In such case the gate is off. All the examples reported up to now, concerning the works published by Lindsey and coworkers, are a good evidence on how it is possible to modulate the energy transfer using several arrangements and knowing which mechanism is at the base of the phenomenum, in this particular case through bond mechanism.

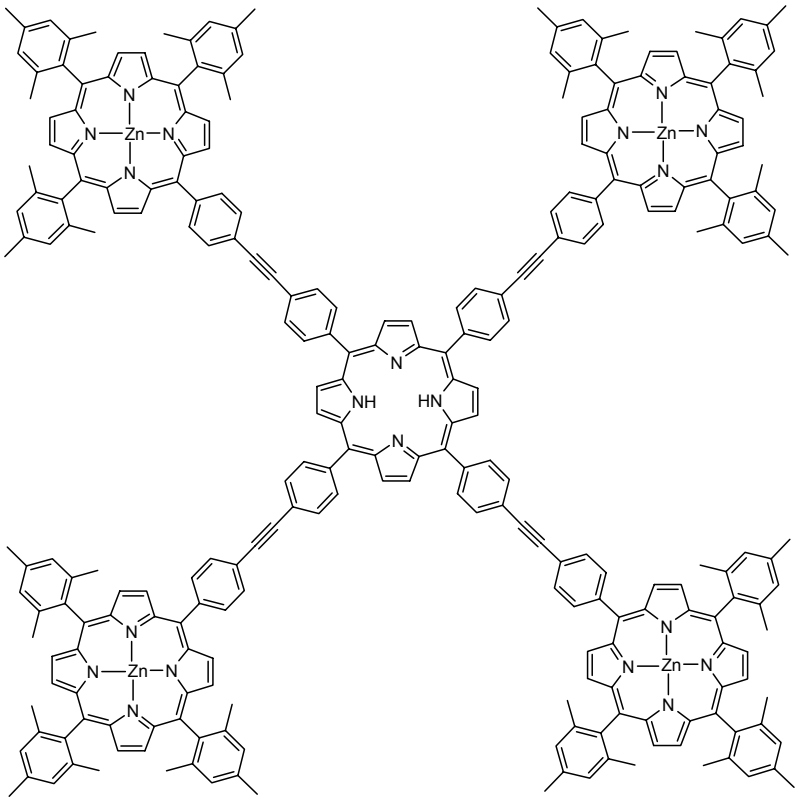

Figure 3.3. 4 *Star shaped antenna system developed by Lindsey, Bocian and Holten. Upon oxidation the hole is completely delocalized over the four peripheral zinc porphyrins.*

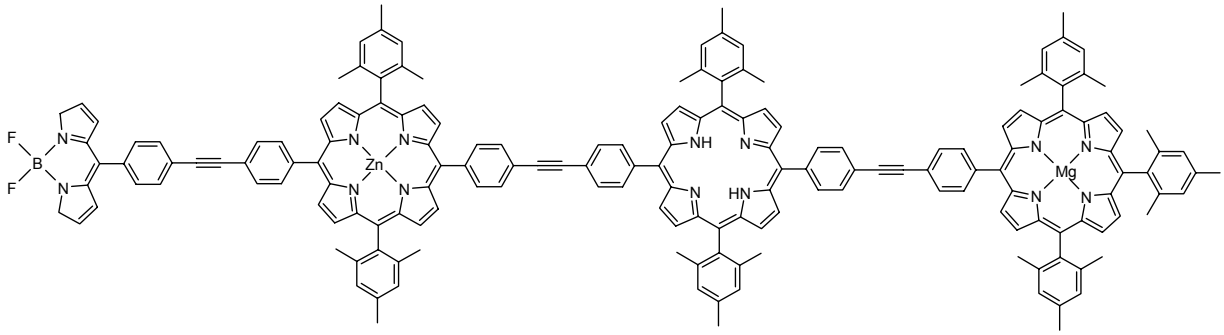

Figure 3.3. 5 *Linear tetramer that acts as a logic gate: in neutral condition the energy absorbed by the boron dipyrrine moiety is emitted as fluorescence by the free base porphyrin thanks to a good energy transfer along the wire. When the magnesium porphyrin is oxidized, the singlet excited state of the free base porphyrin is quenched and the gate is off.*

As we have seen, in the previous examples the energy transfer process has a "through bond" electronic interaction, but in many cases it is difficult to say exactly how many of a whole energy transfer process is a Förster mechanism (through space coulombic interaction) or a Dexter mechanism (through bond interaction). The Förster mechanism is considered to be operative on a long distance[72] in a non covalently linked donor-acceptor pairs while the Dexter mechanism can act at a short distance[73]. The possibility to know when these two mechanisms play a key role into chromophoric array can be very useful to build up antenna system. An elegant study of A. Osuka, D. Kim and coworkers discriminates between these two different mechanisms into several porphyrin dimers, having linker of different lenght[74]. Keeping in mind the results produced by Lindsey et al., about the effect of the orbital symmetry on energy transfer, the authors have reported a family of porphyrin dimers with phenylene, diphenylene and bis(phenylethynyl)phenylene spacers with different substitution pattern and also porphyrin dimer directly linked through the *meso* position without using any spacer. They found that the energy transfer rates increase becoming shorter the center-to-center separation, reaching a maximum value (1.8×10^{12} s^{-1}) in the directly *meso-meso* linked dimer (Figure 3.3.6). In this last case they also observed a lack of influence of the *meso* substituents (pentafluorophenyl or 3,5-bis(octyloxy)phenyl) on the process, so they suggested a predominant Coulombic interaction for the energy transfer in this close proximity porphyrin dimers. In another work of A. Osuka and J. M. Warman[75], the through bond excitonic interactions are taken into account and also in this case different porphyrin dimers were synthesized. It was found that in the dimer linked by only one σ bond and by 1,4-phenylene unit there is mainly Coulombic interaction, while in those cases where diethynylthiophene, butadiyne or diethynylanthracene were used as bridge (Figure 3.3.7), the electronic coupling is higher and presents through bond mechanism. In particular cumulenic and cumulenic quinoidal resonance structures are supposed to be responsible for the strong electronic coupling in the excited state for those compounds that have ethynyl units. So in general the results provide an inverse distance effect so that the electronic interaction between porphyrin moieties increases with the increasing length of the intervening spacer. Once that the interaction typology in the base subunit, preferentially dimer, is known, it becomes possible to synthesize antenna structures with higher

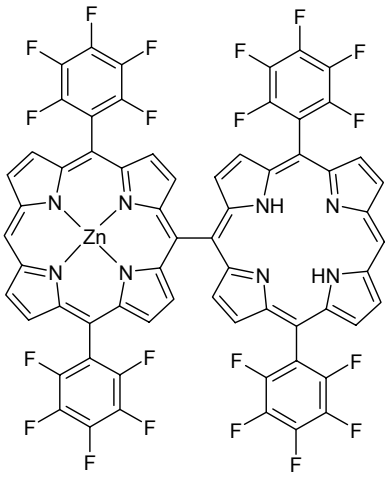

Figure 3.3. 6 *Meso-meso linked porphyrin dimer, presenting through space energy transfer in the work published by Osuka and Kim*

complexity degree assuming that the energy transfer within such a systems remains equal to that seen in the dimer. Taken into consideration this starting point a lot of linear, bi-dimensional and tri-dimensional arrays were synthesized, sometimes with a geometry which recalls that observed in the natural photosystems. Essentially two approaches are used to build up such a systems: covalent and self-assembling strategy. The self-assembly is more suitable to generate systems of high complexity starting from subunits that present a quite low synthetic difficulties. On the other hand, one of the best candidate to reproduce natural light harvesting properties is the dendrimeric structure obtainable by several synthetic routes. Starting from the dimer reported in Figure 3.3.6 A. Osuka, D. Kim and coworkers have extensively developed rod like porphyrin arrays. In one of their paper [76] the synthesis of several molecular wires which include up to 128 zinc porphyrin units is reported. Such a wire seems to be a good candidate as light harvesting photonic wire also because the mutual perpendicular orientation of the monomer prevents any stacking. This observation is indirectly confirmed by the absorption spectra of the different molecular wires, the excitonic interaction between pigments splits the Soret band into two contributions: the low energy Soret band (bathochromic shift B_x) and the high energy Soret band (ipsochromic shift B_y). The first one undergoes to an increasing red shift as the number of pigments increases, while the second one essentially remains fixed at 413 nm. This means that only one of the two mutual perpendicular components (B_x and B_y) of the Soret band couples in a right way within the wire, and such a component is B_x, which is disposed along the *meso-meso* bond so that all the B_x components are parallel, while the B_y is cancelled out because of the perpendicular conformation of neighbouring porphyrins. In conclusion the unperturbed Soret band at 413 nm for all the arrays suggests the averaged perpendicular conformation (Figure 3.3.8). The fluorescence study has further confirmed that the exciton is delocalized over a maximum of 6 or 8 porphyrin units, affording a rapidly transmission of singlet excitation energy.

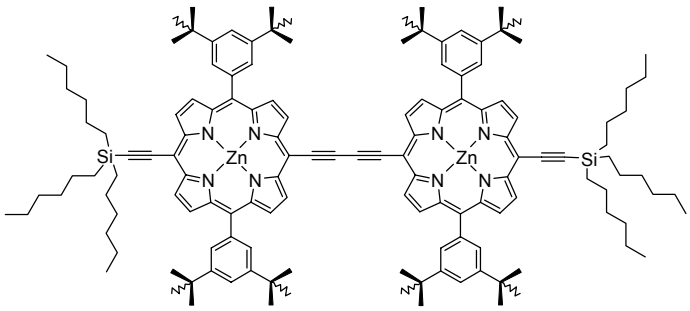

Figure 3.3 7 *One of the zinc porphyrin dimers studied by Warman and Osuka, in this case is represented a butadiyne linker*

In a further work the efforts of the same authors produced probably the longest porphyrin wire ever seen, containing the incredible number of 1024 porphyrin units[77] with a length of 0.84 μm. The fluorescence studies outlined some critical features: the fluorescence quantum yield

increases in the wire when a maximum value of 16 porphyrins are included. When the number of pigments becomes bigger than 16 both the fluorescence quantum yield and the fluorescence lifetime start to decrease consistently up to 512 subunits. Moreover in the array with a number of chromophores less than 16 the fluorescence decay is monoexponential while when the arrays becomes longer than 16 units the decay is biexponential and the fast decay component increases as the array's length increases. Finally in the arrays with 256 and 512 subunits the fluorescence decay is wavelength dependent, in particular the decay profile becomes slower as the wavelength moves towards red. All these features outline that the energy transfer occurs from the initially excited shorter porphyrin oligomer to the longer ones, there is a sort of energy migration behaviour. In spite of the low synthetic yield (between 2 and 15%) of the longer wire it is possible to transform the less long array into a completely fully π-conjugated system passing from photonic wire to electronic wire[78] (Figure 3.3.9). These new systems show drastically altered absorption spectra, in particular the Soret band is splitted in two parts with a conspicuous red shift and the Q bands gain intensity, reaching the IR region. Moreover the first oxidation potential of the metal derivatives is consistently reduced. All these topics are attributed to an extremely strong electronic interaction, due to the completely planar structure. For these characteristics the "porphyrin-tapes" can be not only good antenna systems, but could find application also as molecular electronic devices. Anyway a deeper insight into the interporphyrinic electronic interactions reveals a more complicated picture: it was pointed out[79] that for the *meso-meso* linked arrays the interporphyrinic charge transfer excited state can strongly couples with the B_x state via transition dipole moment, producing anomalies in the absorption spectra. Furthermore such type of interaction is dependent from the dihedral angle between neighbouring porphyrin planes and obviously the porphyrin tapes present a more articulated exciton interaction due to the strong electronic coupling[78c,d]. This outlines one more time how passing from single monomer or dimer to system of high complexity the situation becomes more complicated and more difficult to elucidate. Osuka, Kim and Sumi verified also

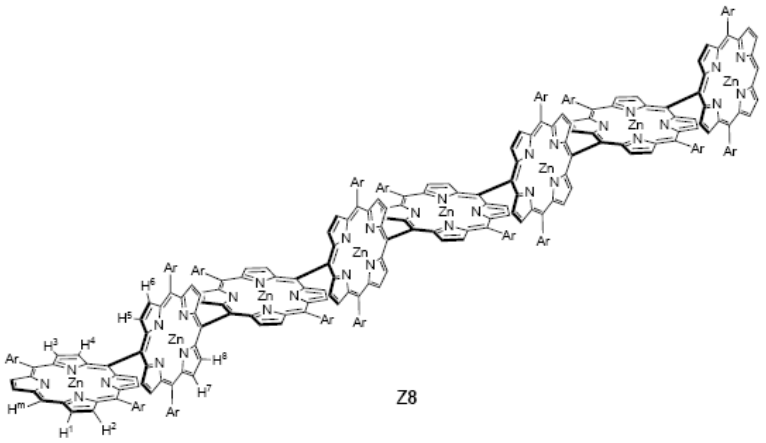

Figure 3.3 8 *Wire like antenna system synthesized and studied by A. Osuka, D. Kim and coworkers. It is represented the octameric system*

the efficiency of their wire synthesizing linear array with a terminal acceptor 5,15-bis-phenylethynylated zinc porphyrin[80]. They proved that near quantitative excitation energy transfer occurs from the wire to the acceptor with the only exception of the longer array (24 subunit), that presents residual fluorescence coming from other pigments in the array and not exclusively from the terminal acceptor. The energy transfer rate constant range from 4×10^{12} s^{-1} for the dimer to 9×10^{9} s^{-1} for the longest array (24 pigments).

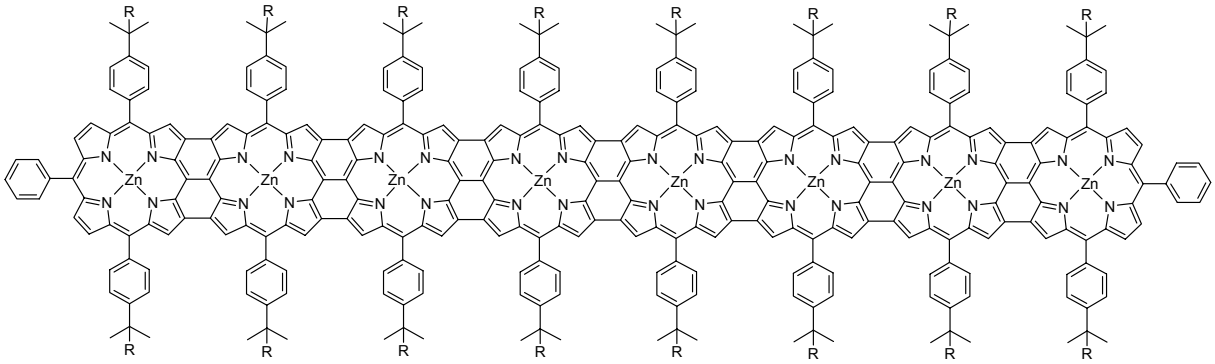

Figure 3.3 9 *Porphyrinic Tapes formed by eight pigments, it presents enourmous red shift of the absorption bands up to 1500-2000 nm, confirming the large π conjugation*[78c]

The most recent effort of the Osuka group in synthesizing artificial light harvesting system is the production of giant porphyrin wheels[81]. This work was inspired by the fact that the purple photosynthetic bacteria have two different light harvesting systems (LHCI and LHCII) with a pseudo circular arrangement of the chromophores[82]. The biggest wheel reported in the work is composed by 24 porphyrins and has a diameter of 7 nm. The time resolved fluorescence studies together with transient absorption anisotropy decay measurements have confirmed an efficient excitation energy hopping with a rate of 2.85×10^{10} s^{-1}. A second but much more little porphyrin wheel is also reported in a previous work[83]and even in this case good excitation energy hopping rates have been observed (Figure 3.3.10).

The synthetic difficult procedures to obtain antenna systems can be exceeded using the self assembling strategy, through which it is possible to generate ordered structures with a well defined geometry starting from simple molecule. An example is reported by L. J. Wan et al.[84] who observed the self-assembly of Zn(II) *meso*-4-tetrapyridylporphyrin that produces well organized hollow hexagonal monodimensional nanoprism (Figure 3.3.11). Furthermore with the aid of a surfactant the authors demonstrated to be able to produce tridimensional arrays with the possibility to tailor the nanoprism size controlling the experimental procedures. The paper underlines the great potentiality of the self-assembling strategy. Using ligands that bind the

metal in the metallo porphyrin, it is possible to obtain architectures with different geometry, using pyridine and imidazole as the preferred ligands for such purpose.

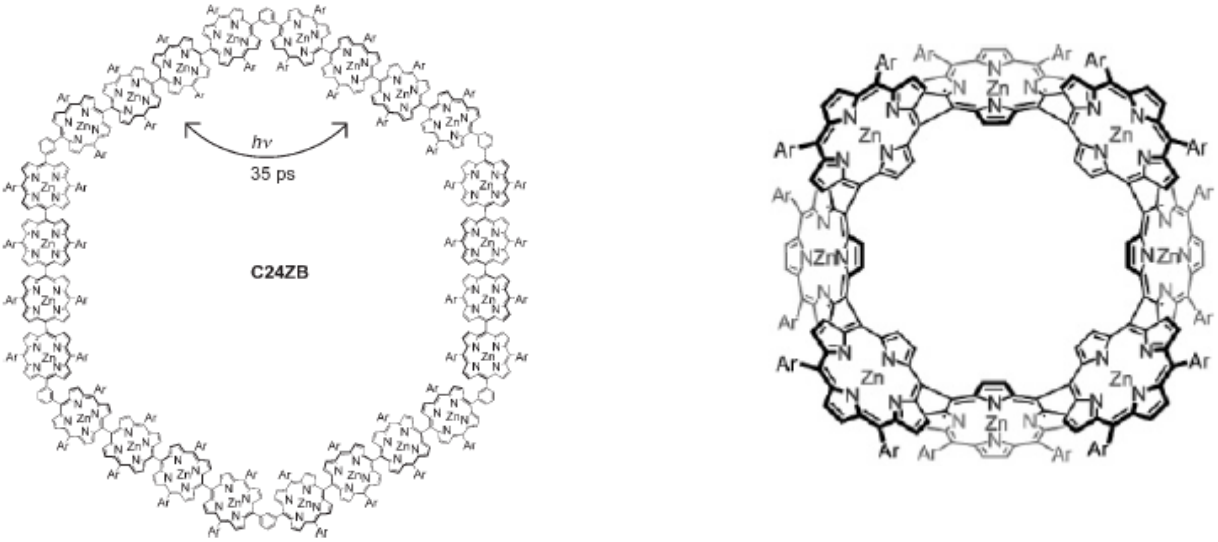

Figure 3.3 10 *On the left: giant wheel reported by Osuka's group as good antenna system because of its ability to undergoes an energy transfer reaction between the chromophores[81]. On the right: a second circular antenna system with a different geometry respect the first one[83].*

The complexation of ruthenium porphyrin by tetrapyridyl porphyrin was reported by several research group[85], the forming side-to-face assembly (Figure 3.3.12) shows a strongly perturbed singlet excited state of the ruthenium porphyrin, due to the heavy metal effect and this induces a highly intersystem crossing to the triplet state, almost 100%. After excitation at 532 nm efficient triplet-triplet energy transfer from ruthenium to free base porphyrin occurs with a rate value in the range of 10^8-10^9 s^{-1}. An elegant study of pentameric self assembling light harvesting system was reported by Hunter et al.[86]; a dimer of porphyrins was synthesized to be perfectly complementary to a zinc porphyrin (Figure 3.3.12). Furthermore the intramolecular hydrogen bonds constrain the molecules to adopt essentially one conformation, minimizing the loss of rotational entropy upon binding. After the formation of the complex the free-base porphyrin is encapsulated in a spherical array of four zinc porphyrins. Simultaneous excitation of both the porphyrin moieties at 560 nm has shown that the emission fluorescence of the central free base

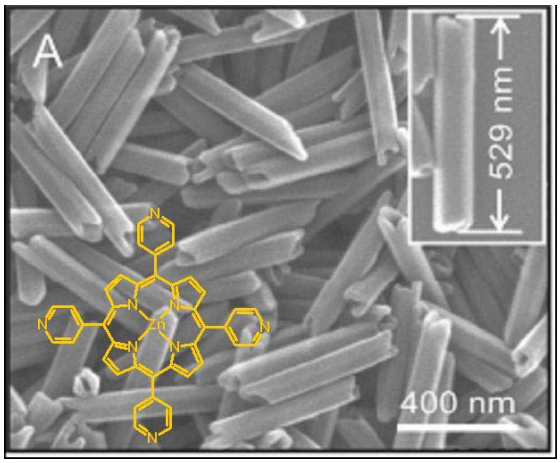

Figure 3.3 11 *SEM image of the nanoprism formed by the self assemling of Zn-tetrapyridylporphyrin*

increases up until two equivalent of the zinc dimer was added, while the fluorescence titration confirms a quenching of the zinc porphyirn emission equal to 70%. The rate constant for the energy transfer was exstimated to be 2×10^9 s^{-1}.

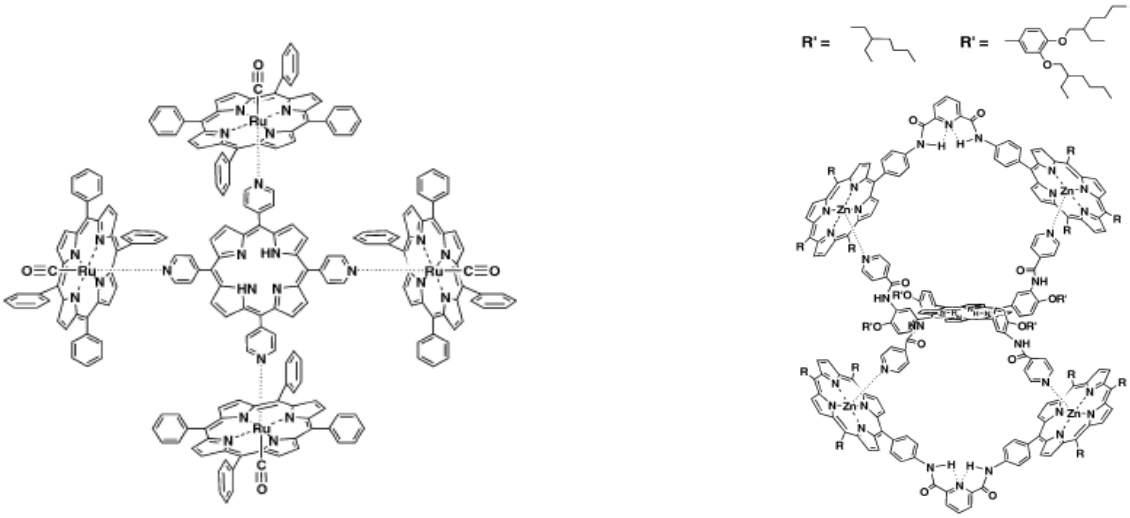

Figure 3.3 12 *On the left: side-to-face self assembled antenna system studied by many authors[85]. On the right pentameric self assembled antenna system reported by Hunter et al., the free base porphyrin is completely surrounded by four zinc porphyrin*

Using the high affinity of the phenanthroline-strapped porphyrin derivatives for the imidazole J. A. Witko, A. M. Albrecht Gary, J. Weiss and coworkers synthesized a self-assembly photonic wire[87]. The peculiar aspect resides in the stepwise energy transfer, obtained using boron dipyrrine as first energy donor, zinc porphyrin as intervening acceptor and free base porphyrin as the last energy acceptor (Figure 3.3.13). Förster mechanism is supposed to take place due to the overlapping emission spectra of the donor with absorption spectra of the acceptor. The global energy transfer efficiency among the wire is 80%. Balaban[88] and coworkers have demonstrated that through the synthesis of appropriate zinc porphyrins, modified with the same functionality groups found in the chlorophylls, mainly hydroxyl, acetyl and formyl groups, it is possible to obtain, in non polar solvents, large self assembled systems that mimic the chlorosomal chlorophylls' architecture. They found that the interaction of the different substituents on the tetrapyrrole ring with the zinc atom of the porphyrin is responsible for the observed highly ordered stacked systems, although strictly anhydrous conditions are required to avoid competitive interaction with solvent or water with the oxygen atoms of the functional groups. The assembly is further outlined by the broadened and red shifted absorption spectrum of the system, that disappears after the addition of stoichiometric amount of methanol, underling the destructive interaction of polar and coordinating solvents with functional groups

of the pigments. Kobuke and coworkers developed efficient self-assembly systems based on the interaction of imidazolyl-zinc porphyrin monomer and dimer. The introduction of a N-methyl-imidazole in the *meso* positions of the porphyrin leads to a formation of a slipped cofacial dimer that resembles the geometry of the special pair in the natural photosynthetic reaction center. The synthesis of several special pair-electron acceptor systems, consisting of a complementary slipped cofacial dimer of imidazolyl-substituted zinc porphyrins, bearing a piromellitdiimmide as electron acceptor[89] has allowed to demonstrate the great improvements gained in the charge separate state, formed upon excitation. The electrochemical study shows a split of the oxidation potentials from two peaks in the monomer, to four peaks in the self-assembled dimer. Furthermore the shift values of the first oxidation potentials, obtained changing the solvent polarity, for the dimer are almost half of those obtained for the monomer. This is the proof that the radical cation is fully delocalized over the whole π system of the dimer. The systems present also small reorganization energy respect to the monomer, aspect that implies the increase of the rate constant for the charge separate state and the diminishing of the rate constant for the charge recombination. Adopting the imidazolyl-zinc porphyrin subunits, Kobuke et al. extensively developed cyclic self-assembling antenna system[90], very similar to those sinthesized by Osuka and coworkers, but just a little bit smaller. Kobuke and coworkers studied the self-assembling reaction of an imidazolyl-porphyrinato zinc(II) dimer, where the two porphyrins are connected through a phenylene ring with an angle of 120°. They found two stable macrorings composed by 5 and 6 subunits (dimer), that, in analogy with the aforementioned Balaban work, are stable in solid phase and in solution unless coordinating solvent is added[90a]. The largest one of the two rings obtained has an intermolecular diameter equal to 41 Å (Figure 3.3.14). Some developments were later reported about the photophysical study of these new self-assembling antenna systems[90b]. Time-resolved fluorescence anisotropy analyses together with transient absorption decay measurements confirmed an efficient exciton energy hopping within such a ring, that could be well explained

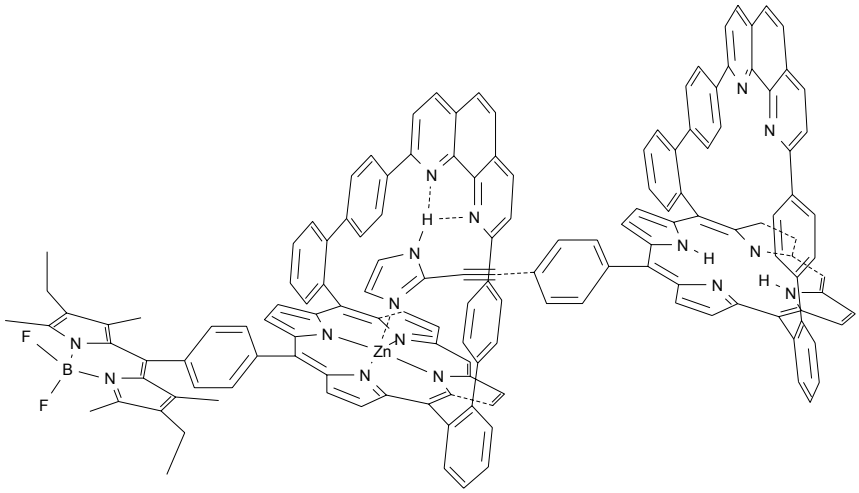

Figure 3.3 13 *Self assembling photonic wirecomposed by Boron dipyrrine moiety as donor, zinc porphyrin and free base porphyrin as last acceptor*

adopting Förster energy hopping theory, based on dipole-dipole interaction[90c]. In particular the five member ring presents higher exciton energy hopping time between two neighbouring dimer units than the six member ring (21 ps vs 13 ps respectively). This difference could be attributed to a small difference in the orientation factor (k) which is of crucial importance in the dipole-dipole interaction. A larger value of k in the hexagonal ring induces a larger transition dipole coupling energy as compared to the pentagonal structure.

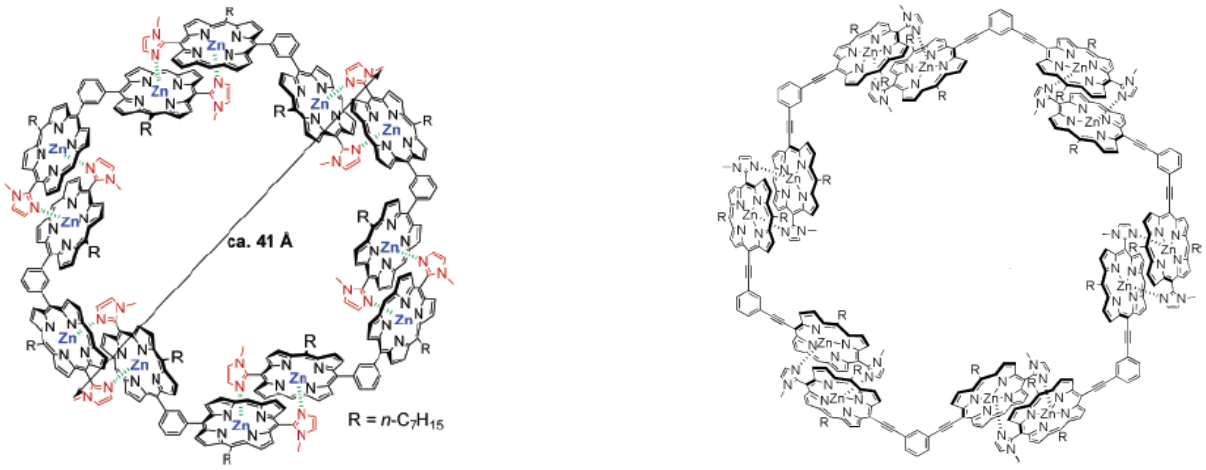

Figure 3.3 14 *Two different circular self assembly antenna systems on the left the first one published by Kobuke and coworkers[90a], on the right the following developed systems[90c]*

Not only circular assemblies were studied by Kobuke and his research group but also potential applications of linear self assembling array were evaluated, in particular the imidazolyl porphyrin derivatives were demonstrated to be good charge separating system for photocurrent generation[91]. Both simply linear porphyrin arrays or porphyrin-electron acceptor hetero dimer system were self-assembled on Au electrode surface or over an ITO electrode. The first published works demonstrated a photocurrent quantum efficiency ranging from 0.10% to 0.26% for linear oligomer of porphyrins assembled on Au electrod[91a], such a values are not so good but in the linear self assembled array were used only porphyrins without any other acceptor, in fact the introduction of a piromellitimmide electron acceptor in the imidazolylporphyrinatozinc(II) special pair leads to an increased photocurrent quantum efficiency, obtaining a 230 nA/cm^2 after excitation with a Xenon lamp[91b]. Anyway the best results are reported for the synthetic imidazolylporphyrinato zinc(II) special pair assembled on a modified indium-tin oxide (ITO) electrode (Figure 3.3.15), immersed in a solution containing a quinone as an electron sacrificer[91c].

In such assembly fast charge injection occurs from the S_2 excited state of the porphyrin before that internal conversion to S_1 excited state takes place, moreover the nature of the binding molecule used to block the dimer onto ITO modified surface alter the band gap of the electrode modifying the quantum efficiency; the best result are obtained with a phosphonyl anchor group. The quantum efficiency reaches a value of 15% although the irradiance light must be monochromatic, because the excitation wavelength corresponds to the Soret band absorption. The possibilities to generate several architecture employing different subunits are virtually infinite as it is possible to see in the Figure 3.3.16 where the self assembled porphyrin boxes, obtainable tailoring the length of the pyridyl ligand and also the length of the porphyrin wire, are reported, Osuka and Kim have studied these systems, demonstrating the presence of an efficient exciton energy migration, so that also the porphyrin boxes could be considered as promising artificial antenna systems[92].

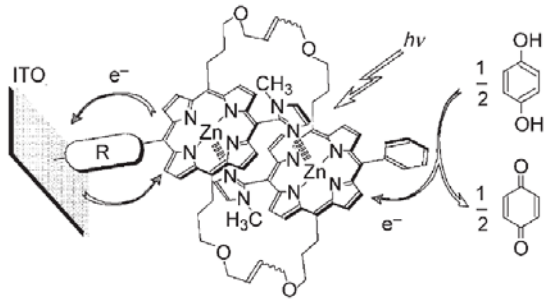

Figure 3.3 15 *Photocurrent generation at ITO surface modified through self assembled synthetic special pair*

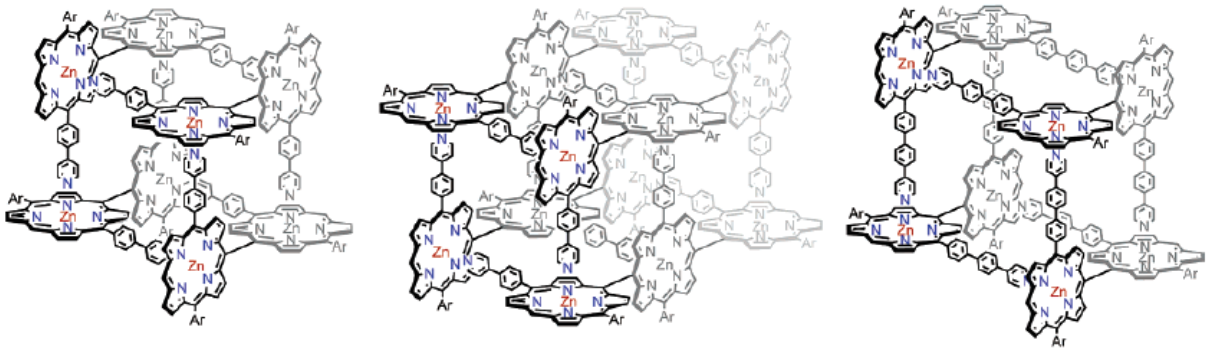

Figure 3.3 16 *Self assembling porphyrin boxes as artificial light harvesting systems*

The X-ray data of the natural photosystems show that the antenna systems are composed by a large number of chromophores disposed with a defined three dimensional geometry. The great number of pigments is the secret for a very high light harvesting capacity. Dendrimers are hyperbranched, three dimensional molecules with a regular treelike arrays of branch units, hence this structure offers the possibility to hold together a great number of pigments in order to mimic the natural light harvesting systems.

There is an important aspect that must be outlined: despite the geometrical resemblance with natural systems, the units within a dendrimeric structure have to present a cooperative

behaviour, otherwise the acquired light energy is scattered and the excited states are lost before the energy is channelled toward an electron active site that can start the electron transfer reaction [93]. Many dendrimer were developed and studied and their electrochemical or photoactive units were used as active sites[94], containing porphyrins for the reasons before mentioned. Few examples will be taken into consideration to show their potentiality. In the first part of this paragraph the critical studies of Lindsey, Holten and Bocian on dimer, trimer and tetramer of porphyrins linked by a diarylethyne residues are reported. Their outcomes find terminal application in the synthesis of a dendrimeric unit made of 21 porphyrins, to be more precise 20 zinc porphyrins that surround one free base porphyrin[95]. This dendrimer (Figure 3.3.17) shows a broadened and red shifted Soret band due to the inter porphyrin exciton coupling while the Q bands do not undergo in any changes. Nevertheless the first oxidation potential maintains more or less the same value increasing the size of the dendrimer. These findings point out a relatively weak, but significant, electronic coupling between ground and excited state of the chromophores. Fluorescence study has revealed an efficient energy transfer (92%) from the zinc porphyrins to the central free base porphyrin within 220 ps. Moreover bulk electrolysis measurements have shown how it is possible to remove from the dendrimer up to 21 electrons yielding a stable "super-charged" π-cation radical. All these features are favourable properties for harvesting solar energy.

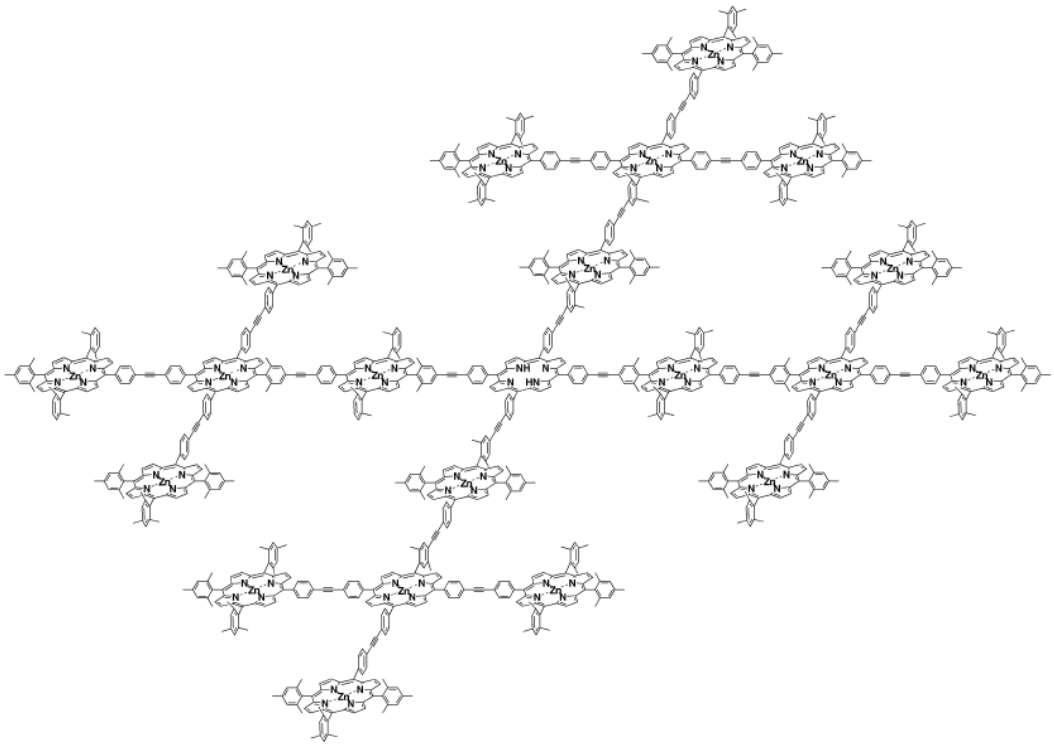

Figure 3.3 17 *Porphyrin dendrimer developed by Lindsey, Holten and Bocian*

Dendrimeric antenna systems have shown also to have a morphology dependent properties, in a work of Aida et al.[96]. Such paper clearly shows different energy transfer efficiency between star shaped dendrimer and conical dendrimer. The biggest dendrimer contains 28 zinc porphyrins divided into four branches and a central free base porphyrin core (Figure 3.3.18), while the conical dendrimer is only one branch of the biggest one. Both systems have very small red shift of the Soret band (1.3 nm) compared with the monomer and this indicates that there is very weak ground state interaction between the zinc porphyrins. After excitation at 554 nm the emission spectrum of the star shaped dendrimer presents only emission from the free base porphyrin, while the conical one have a residual emission coming from the zinc porphyrin branch. The overall energy transfer efficiency is 71% for the star shaped dendrimer and only 19% for the conical one. These results point out an evident morphological effect present in the dendrimer structures. A different type of porphyrin dendrimer was reported by K. P. Ghigghino, M. J. Crossley; E. W. Meijer and coworkers [97] : the dendritic structure is formed by poly(propylene)immine dendron and porphyrins are linked to the periphery of the system (Figure 3.3.19). The first, third and fifth generation bearing respectively 4, 16 and 64 porphyrins, were investigated through time resolved anisotropy fluorescence measurements (TRAMS) that have permitted to evidence structural effect on the energy transfer process. In particular in the first generation dendrimer, the efficient energy transfer can be interpreted through Förster type, while in the third generation dendrimer the energy transfer seems to be confined only to the porphyrins contained within a dendron, probably due to segregation effect induced by the dendron structure. The fifth generation need a more complicated theoretical base to be described because the data suggest the presence of independent and simultaneous energy transfer. One fast component between the porphyrins contained on the surface of the dendrons

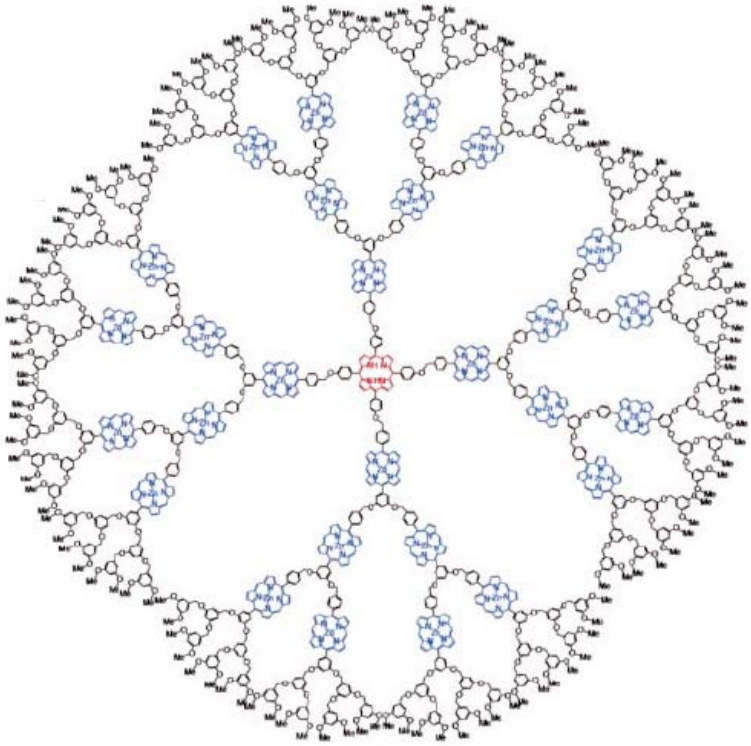

Figure 3.3 18 *Star shaped dendrimer reported by T. Aida and coworkes. Efficient energy transfer from zinc porphyrins to free base porphyrin occurs*

and another one, more slow than the first, between porphyrins in adventitious dendrons. Even in this last case it is possible to discern the morphological effect of the structure, that recovers an important role in the dendritic antenna system and it is discernable also how the growth of the system can lead to a more complicated interactions between the pigments. Particularly in those systems that present a same degree of conformational changes like those studied by Aida and Ghigghino, while the rigid structure showed in the dendrimer synthesized by Lindsey and coworkers does not allow any conformational or structural influence on the energy transfer process. Moreover the tree-like structure of dendrimer offers a wide potential tool to generate three dimensional and highly efficient light harvesting system.

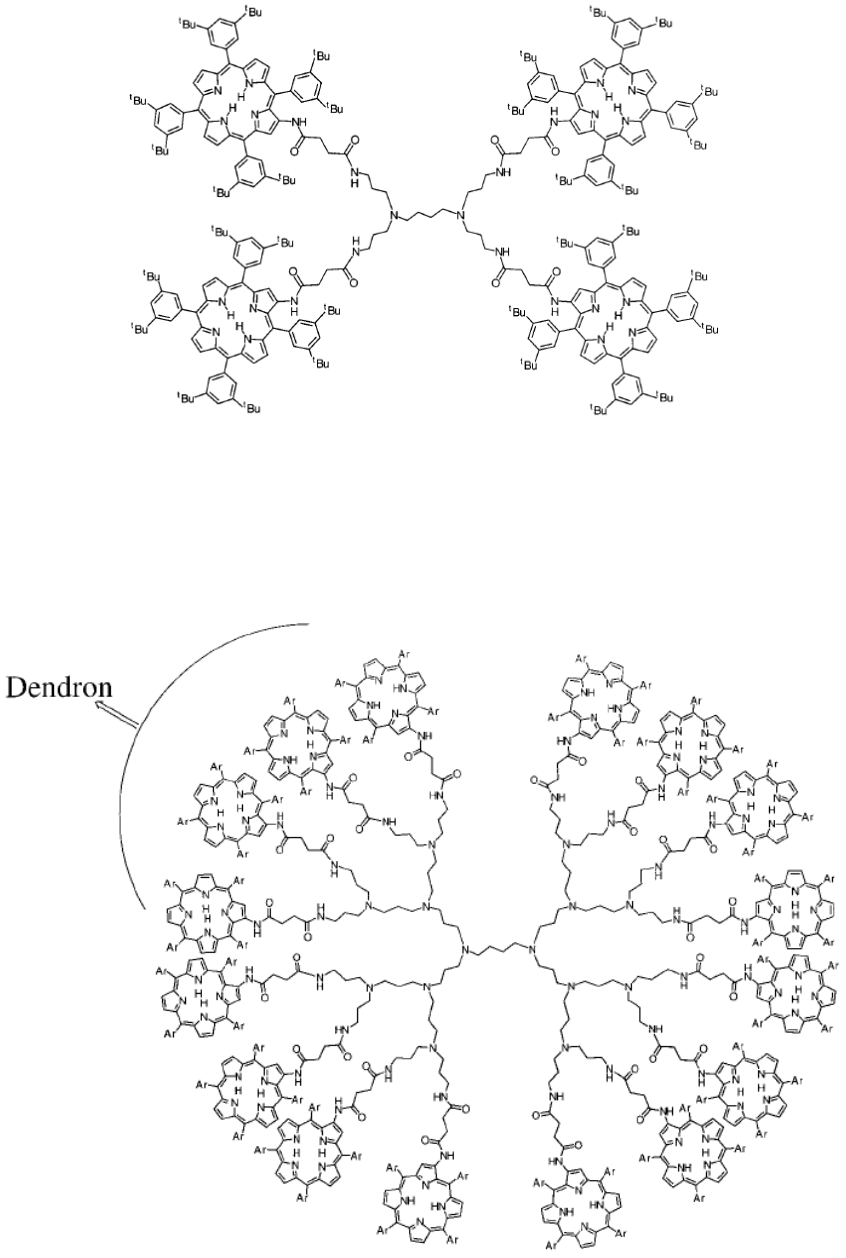

Figure 3.3 19 *First generation (top) and third generation (bottom) of dendrimer studied by Ghigghino et al.*

3.4. Porphyrin-[60]Fullerene Systems

As we have pointed out in the introduction of this chapter, the discovery of [60]fullerene have brought the scientific community into a new fervid and productive period. The characteristics of the new molecule were investigated and the peculiar properties pointed out. They showed that the C_{60} could be considered a powerful building block for material science, in particular the three-dimensional π conjugated system gives to the molecule attractive electron acceptor capability. The first electrochemical studies[41] have demonstrated that C_{60} can accept in a reversible manner up to five electrons (Figure 3.4.1), being the first reduction potential equal to -0.36 in benzene and -0.44 in CH_2Cl_2, a peculiar aspect that make fullerene as a good candidate for donor-acceptor system in the electron transfer reactions. The photophysical properties of C_{60} were also deeply investigated: the excitation in the UV-visible region implies the filling of the singlet excited state, that lives for few nanoseconds, before converts into the longer lived triplet excited state through a spin-forbidden intersystem crossing, due to an efficient spin-orbit coupling [98] . Both excited states present characteristic transient absorptions in the near IR region at 920 nm for the transition $S_1 \rightarrow S_2$ and at 750 nm for the transition $T_1 \rightarrow T_2$ in toluene solution[98c,d]. When the [60]fullerene is functionalized, obtaining methanofullerene and N-methylfulleropyrrolidine, the loss of a double bond perturbs the π-system and it is possible to notice such a perturbation in the respective UV-visible absorption and transient absorption spectra, these latter showing an appreciable blue shift[98a]. An important aspect to underline is the fact that between the longest absorption wavelength and the shortest emission wavelength there is only very small Stokes shift, which underlines just a little solvent reorganization around the C_{60} molecule, an aspect that is compatible with the highly and symmetric rigid structure of the fullerene (Figure 3.4.2). The most important photophysical aspect of the fullerene is the well visible radical anion around 1080 nm. After functionalization, this band is shifted at 1040 nm for methanofullerene derivatives and at 1010 nm for the N-methylfulleropyrrolidine derivatives[98a]. It appears clearly how these features make appealing those systems which present natural like donor molecules such as porphyrins and very good

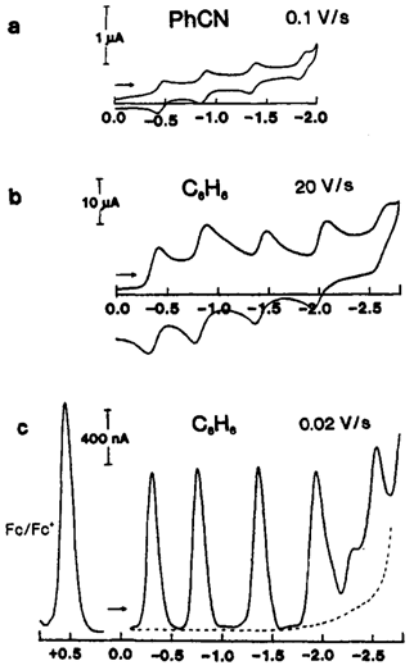

Figure 3.4. 1 *Cyclic voltammetry in benzonitrile a) and benzene b) of C_{60} and differential pulse voltammetry of C_{60} in benzene c). All the reduction potentials are referred to a SCE*[41b]

electron acceptor like the [60]fullerene; following some examples concerning several interaction typologies between fullerene and porphyrins will be reported, starting from simple covalent systems and arriving to self assembling porphyrin-fullerene systems. Noticeably all the strategies previously described, adopted to generate good electron-transfer porphyrin-quinone systems, self-assembling porphyrin light harvesting systems and porphyrin dendritic systems, are revised introducing the fullerene moiety, generating a well defined architectures. The great improvements obtained introducing the fullerene will be outlined, especially in the section dedicated to the application of several systems for photocurrent generation, that is the terminal aim for which all these systems were synthesized and studied.

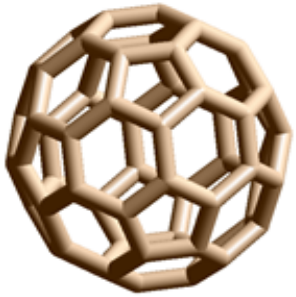

Figure 3.4. 2 *Ribbon-like three dimensional structure of [60]fullerene*

3.4.1. Covalently Linked Porphyrin-Fullerene Systems

One of the most predominant effect of the introduction of fullerene in the donor acceptor system is the increase of the excited charge separated state lifetime which is possible to see comparing different systems with the same porphyrin electron donor. The porphyrin quinone dyad synthesized by Antolovich et al.[56] (Figure 3.2.6 b) was modified substituting the benzoquinone with the fullerene (Figure 3.4.1.1) and the studies immediately revealed the differences in terms of electron transfer and charge recombination rate constants[99]. After excitation, photoinduced electron transfer in the porphyrin-fullerene dyad occurs with a rate constant of 1.0×10^{10} s^{-1}, that is one order of magnitude bigger than that observed in dyad of Antolovich. The main difference resides in the charge recombination reaction, in fact in the porphyrin-fullerene derivative such a rate constant is about one thousand times slower than that found in the porphyrin-quinone dyad (2.4×10^{6} s^{-1} vs 2.0×10^{8} s^{-1} respectively). An analogous porphyrin-fullerene dyad, where the C_{60} is linked to the porphyrin *meso*-phenyl ring through an amide bridge, synthesized by H. Imahori and coworkers[100], shows a forward electron transfer rate equal to 9.0×10^{9} s^{-1} and a back electron transfer rate of 2.0×10^{9} s^{-1}. The faster rate for the forward electron transfer in the C_{60} containing dyad is attributed to the curved surface of the fullerene, that can couple with the bridge by means of many more atoms than a planar component. This fact implies that the fullerene H.O.M.O. shows a delocalization into the bridge. The large difference between the charge recombination rate of the porphyrin-quinone dyad and compound reported in the Figure 3.4.1.1 is ascribed to the symmetry reason. The aforementioned compound belongs to the C_s point group, therefore the charge recombination

process is forbidden because the charge separated state has A″ symmetry while the ground state has A′ symmetry[101]. The presence of a flexible bridge in the dyad studied by Imahori and coworkers allows to remove the symmetry restriction and the process is faster. However it must be pointed out that the rate of the electron transfer process involving fullerene compounds can be strongly influenced by the very small reorganization energy of this kind of molecules. A simpler porphyrin fullerene dyad was reported by Reed, Boyd and Drovetskaya [102]. Adopting the Prato reaction they condensed a 2-formyl-5,10,15,20- tetraphenylporphyrin with the fullerene, obtaining a dyad where the distance between the two chromophore is very short because the fullerene is directly linked to the β position of the tetrapyrrole ring (Fidure 3.4.1.2). From UV-visible analyses it has been shown that the Soret band is red shifted of about 6-7 nm, and such a shift is solvent independent. The authors justify that as a through space interaction between the chromophores. The subsequent fluorescence and electrochemical studies carried out on free base and zinc porphyrin-fullerene dyads were useful to determine the energetic levels for the energy and electron transfer process[103]. In particular the charge separated state lies at 1.58 eV and 1.38 eV above the ground state of the free base and zinc derivatives respectively. All the fluorescence studies have confirmed a solvent dependent reaction pathway; in fact in toluene the singlet-singlet energy transfer process is the unique process and occurs with a rate constant of 4.5×10^{10} s^{-1} for the free base dyad and 4.9×10^{10} s^{-1} for the zinc analogue. Using the more polar solvent benzonitrile the reaction is shifted towards the electron-transfer and to be more precisely photoinduced electron-transfer compete with the energy-transfer, the first with a rate of 1.8×10^{11} s^{-1} while for the second with a rate constant of 7.1×10^{10} s^{-1} both referred to the free base derivative. However in benzonitrile the singlet-singlet energy-transfer from the porphyrin to the C_{60} is followed by generation of the charge separated state. In this case it is possible to conclude that excited radical pair is formed with a unit quantum yield either directly after excitation or via C_{60} singlet excited state. The lifetime of the charge separated state is 290 ps for the free base derivative and 50 ps for the zinc derivative. Even if these times are not so long it is important to observe that a simple porphyrin-fullerene dyad obtained easily from one single reaction affords lifetime value for the radical pair higher, sometimes comparable, to those observed in the complicated multiporphyrin-quinone

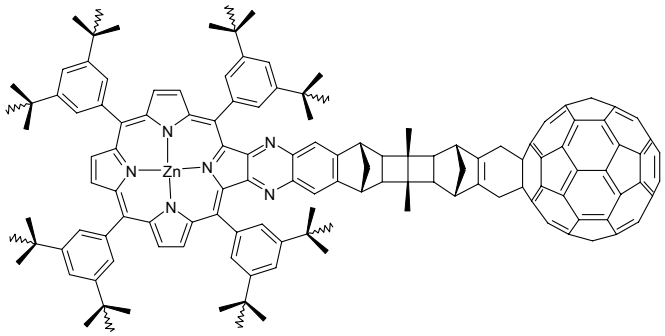

Figure 3.4.1. 1 *Porphyrin-fullerene dyad studied by K. P. Ghigghino, M. N. Paddon-Row and coworkers*

architecture proposed by Osuka et al.[61,62] and depicted in Figure 3.2.8 of the paragraph 3.2. From these two examples it is clear how much bigger is the advantage to use fullerene instead a quinone as the last electron acceptor. The substitution of the zinc atom with another metal can also influence tremendously the energy and electron transfer process as reported in the work of Guldi, Schuster and coworkers[104]. In this case a copper porphyrin-styrene-C_{60} hybrid was synthesized and fully chracterized (Figure 3.4.1.2).

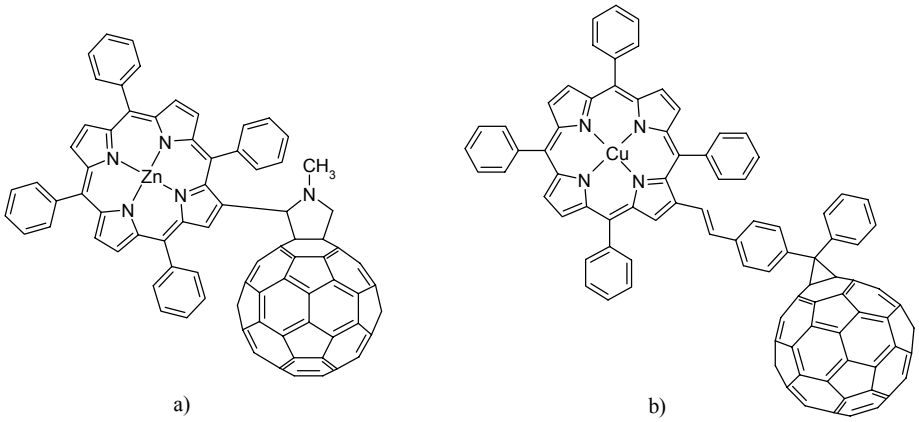

Figure 3.4.1. 2 *Directly beta linked porphyrin-fullerene dyad studied by C. A. Reed et al. a) and copper porphyrin-styrene-fullerene hybrid developed by Guldi, Schuster and coworkers*

The introduction of a copper atom into the porphyrin moiety changes radically the excited state levels. Due to its paramagnetism the excited states of the copper porphyrin are doublet and quartet, while the zinc porphyrin presents singlet and triplet excited state. A further difference is the presence of a linker unit that should guarantee an extension of conjugation from the tetrapyrrole ring to the fullerene moiety. However these are little changes compared with the deep differences that we will see in the lifetime of the charge separated state. The photophysical pathway in the copper porphyrin-fullerene dyad strongly depends from the solvent polarity; in particular in toluene, the energy transfer takes place from the termally equilibrated triplet-doublet/triplet-quartet excited state of the copper porphyrin to the triplet excited state of the fullerene (transient absorption maxima at 720 nm) with a rate constant of 1.7×10^{9} s^{-1}. The solvent dependence clearly emerges studying the photophysical properties in solvent of different polarity such as chloroform, dichloromethane and benzonitrile. In benzonitrile is clearly visible after excitation, a transient at 1040 nm rising with a rate constant of 3.5×10^{9} s^{-1}, that can be doubtless attributed to the C_{60} radical anion. The charge separated state lives 140 ns, but the best result is obtained in chloroform where the charge recombination has a rate constant of 2.4×10^{6} s^{-1} and this implies a lifetime of the charge separated state of 415 ns. The authors

exclude that a so long lifetime for the excited radical pair could arise from a second electron transfer from Cu(II) to give Cu(III) because of the unfavourable free energy changes associated with the process. A so consistent increase in the lifetime of charge separated state, subsequent to the small differences introduced in the dyad outlines how powerful is the strategy to associate porphyrin and fullerene moieties in several architectures. The architectures presented up to now prevents a π-π stacking between the flat aromatic system of the porphyrin and the curved surface of the C_{60}, but there are reports that discussed a so strict interaction, synthesizing appropriate porphyrin-fullerene dyad[105] (Figure 3.4.1.3).

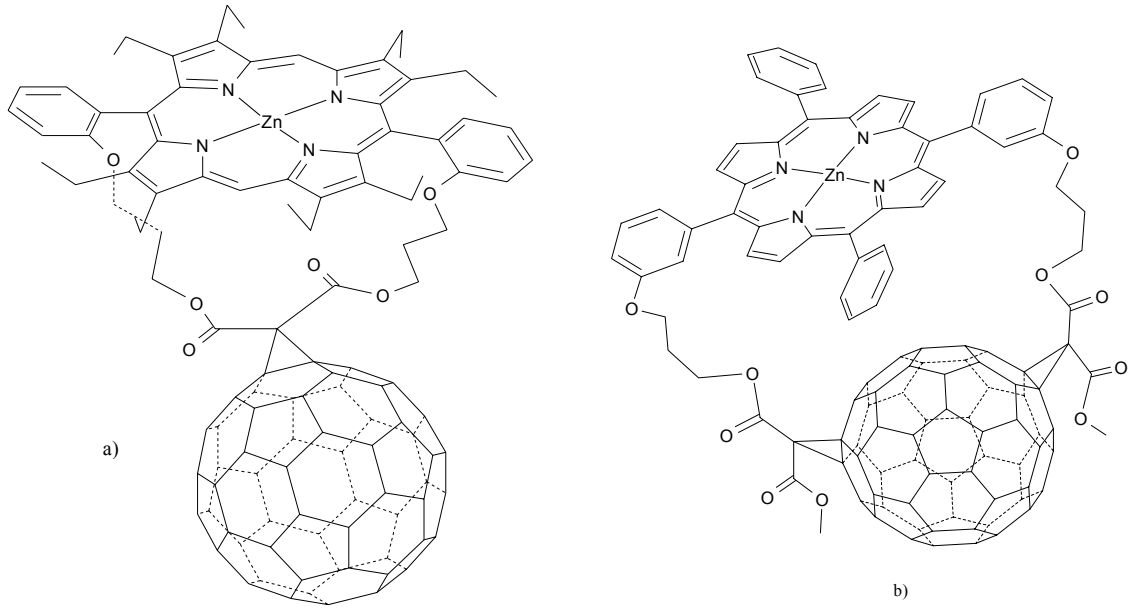

Figure 3.4.1. 3 *Two different porphyrin-fullerene systems that allow the π-π stacking between the two moieties. System b shows the formation of a new transient in nonpolar solvent, called exciplex.*

In those systems where it is possible a strict interaction between porphyrin and fullerene, explicated through the π-system, it is also possible to discern new absorption and emission features, arising from such interaction. In a work of Chukharev, Guldi and Lemmetyinen several porphyrin double-linked fullerene systems (Figure 3.4.1.3 b) were synthesized to evaluate the ground and excited state interchromophore interactions[105b]. A deep study has led the authors to evaluate all the parameters that govern the Marcus theory, such as free energy (ΔG°) of the electron transfer reaction, the reorganization energy (λ) and the electronic coupling (V), in particular it has been outlined the existence of a new state when the π-electronic interaction between the two moieties is very strong. The new systems present a conspicuous perturbation of the absorption spectra in non polar solvent. The broadened and red shifted Soret band, together with the decrease of its intensity give evidence of a close interaction between the

two moieties, an interaction that is further outlined by the presence of a new broad absorption band in the near-IR region, dominant in the 600-850 nm. Furthermore, beside a residual porphyrin fluorescence emission, the fluorescence spectra of both free base and zinc derivatives are dominated by an emission maximum at 730 and 810 nm respectively. All these features are typical of an exciplex state and it is important to notice that the absorption characteristics disappear passing from less polar to more polar solvent and also the exciplex intensity emission tends to decrease, probably because its low formation quantum yield. The exciplex state is commonly defined as a new excited state of the system that shows a partially charge transfer character. From a quantum mechanical point of view it could be defined as a linear combination of the excited wave functions of the porphyrin, fullerene and excited charge transfer state[105b]. The authors estimated that the quantum yield of the exciplex state emission in non polar solvent such as toluene is 1%, indicating that the non radiative emission is not the principal deactivation pathway, so they have supposed, taking into consideration the experimental data, that in non polar solvent the exciplex excited state is deactivated passing through a lower energetic charge separated state, which undergoes to the fundamental state faster than when it is formed. On the other hand in polar solvents like benzonitrile it is possible to see the charge separated state evolving from the exciplex state with rate constants of the order of 10^{11} s^{-1}. The meaning result of the work consists in the possibility of tuning the electronic coupling using several double linker having different length and in particular the strongest coupling (450 cm^{-1}) has been observed employing a dioxyethyl linker. A similar compound (Figure 3.4.1.3 a) was deeply investigated through time resolved electron paramagnetic resonance spectroscopy[105c]. Despite the structural analogies with the previous described dyad, the reaction pathway found is quite different. The studies were also carried out in frozen media and it was possible to determine the exact reaction pathway. The close proximity of porphyrin and C_{60} implies a fast electron transfer both in non polar and polar solvents. It was demonstrated by the authors, that the nature of the radical ion pair is characterized by an equilibrium between its singlet and triplet radical pair excited state. Moreover the dyad presents a peculiar deactivation pattern. Since the free energy of the back electron transfer to the ground state locates this deactivation pathway in the Marcus inverted region, the radical pair before decays into the excited triplet state of the zinc porphyrin, which subsequently, through triplet-triplet energy transfer, brings to the formation of the triplet excited state of the C_{60}; this is a particular deactivation pathway for the porphyrin fullerene dyad. Moreover the study has pointed out the possibility to generate charge separated state with different energy depending on the temperature values, using the peculiar properties of the liquid crystals, that can behave as non polar solvent at low

temperature and as polar solvent at room temperature or higher. In conclusion the radical pair in toluene, below 178 K, decays within 900 ns, a value extremely high respect to those seen up to now. One of the best strategy to obtain long living charge separated state is to reproduce multistep electron transfer, generating an energy gradient through the use of many different chromophores in order to bring the positive and negative charges far away. Imahori, Fukuzumi, Ito and Guldi have developed very efficient systems able to produce multistep electron transfer[106]. In these cases the last electron donor is not the porphyrin, but a ferrocene unit, that thanks to its redox properties allows to increase the lifetime of the charge separated state. One of these systems, composed by a ferrocene moiety, a porphyrin (either zinc or free base derivative) and C_{60}, was investigated in three different polar solvents, THF, benzonitrile and DMF[106a]. The system shows two different pathways that lead to the final radical ion pair ($Fc^{\bullet+}$-Zn/H_2P-$C_{60}^{\bullet-}$). A linear stepwise pathway, starting from porphyrin singlet excited state, that decays into the first charge separated state (Fc-Zn/$H_2P^{\bullet+}$-$C_{60}^{\bullet-}$) and a subsequent hole transfer from the porphyrin to the ferrocene unit to generate the last radical ion pair. A second pathway that from the singlet excited state of the porphyrin passes through a first electron transfer from ferrocene to porphyrin to give $Fc^{\bullet+}$-Zn/$H_2P^{\bullet-}$-C_{60} and a second electron transfer step that brings the electron on the fullerene. It has been pointed out that increasing the solvent polarity the lifetime of the charge separated state increases, in particular τ = 3.7 (THF), 7.5 (benzonitrile) 16 μs (DMF) for $Fc^{\bullet+}$-ZnP-$C_{60}^{\bullet-}$ and τ = 8.3 (benzonitrile) 19 μs (DMF) for $Fc^{\bullet+}$-H_2P-$C_{60}^{\bullet-}$, indicating that these charge recombination rates are in the normal region of the Marcus curve, so as the driving force for the charge recombination increases, the rate constants also increase. The electronic coupling (V) for the triads is estimated to be equal to 0.019 cm^{-1}, while the reorganization energy equal to 1.09 eV, while in the light of the Marcus theory, the dependence of V from the distance is deduced to depend primarily on the nature of the bridging molecule. Furthermore in both the triads the long lived charge separated state is generated with a quantum yield close to unity. An incredible improvement in the lifetime of the radical ion pair is achieved adding a further porphyrin unit and obtaining a tetrade[106b] (Figure 3.4.1.4). In such a system the lifetime of the charge separated state reaches an incredible value of 0.38 s in a frozen benzonitrile matrix (193 K) and 0.34 s in DMF at 178 K, values that, as it has been outlined by the authors, are comparable to those seen for the bacterial photosynthetic reaction centers. This was due to the presence of a cascade of energy transfer processes coupled to a multistep electron transfer. From the singlet excited state of the zinc porphyrin a singlet-singlet energy transfer generates the singlet excited state of the free base porphyrin, from which the first electron transfer step occurs, giving the radical anion on the C_{60} and the radical cation

localized on the free base porphyrin. Through two subsequent charge shifts the hole is transported on the zinc porphyrin and then on the ferrocene moiety to generate the final long lived radical ion pair (Scheme 3.4.1.1). The only drawback is the low quantum yield of the entire process 0.20 in THF, 0.24 in benzonitrile and 0.17 in DMF. The authors attribute this aspect to the competition of the charge shift passages versus the decay of the first excited charge separated state (Fc-ZnP-$H_2P^{\bullet+}$-$C_{60}^{\bullet-}$) towards the triplet excited state of the porphyrin and C_{60}.

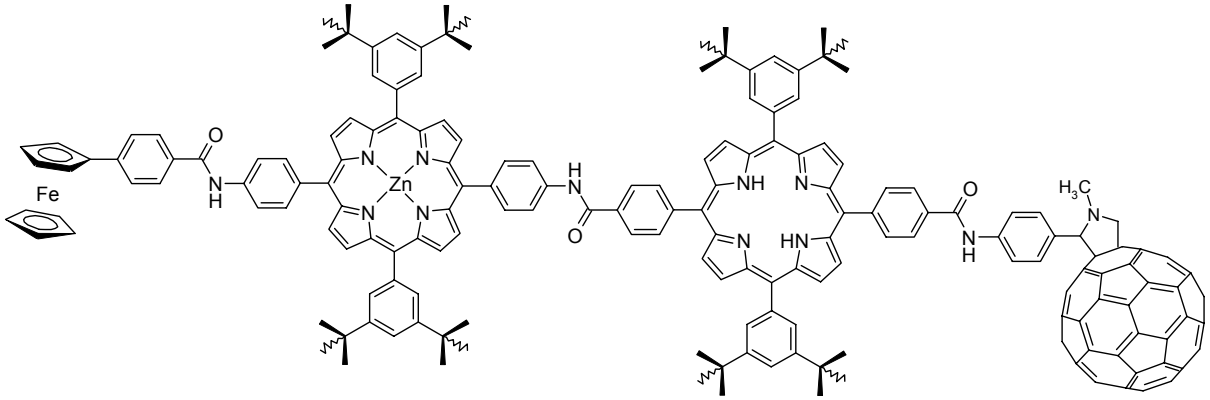

Figure 3.4.1. 4 *Tetrade developed by Imahori and coworkers able to produce an incredible long lived radical pair (0.38 s in frozen benzonitrile matrix) after excitation of the zinc porphyrin*

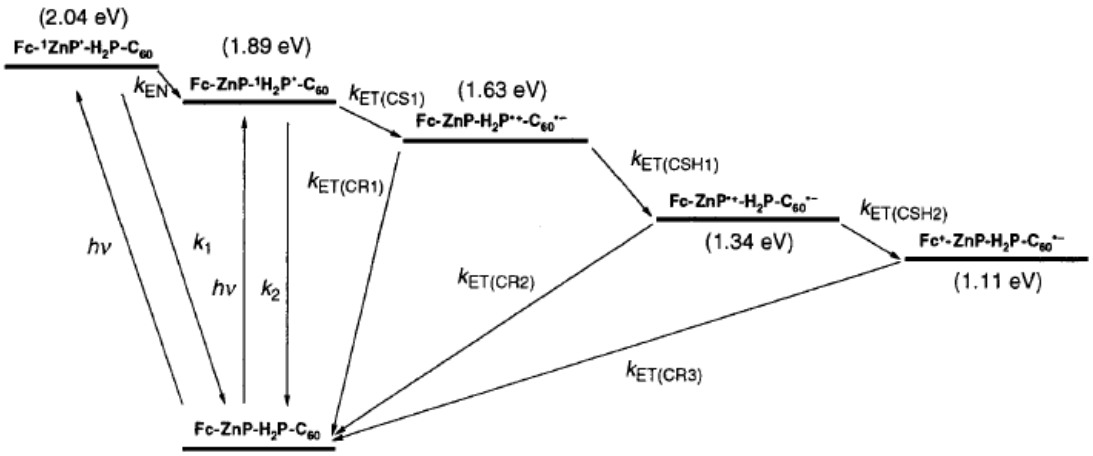

Scheme 3.4.1. 1 *Energy level diagram that represents the energy transfer cascade coupled to multistep electron transfer for the tetrade depicted in the figure 3.4.1.4*[106b]

The introduction of a zinc atom in the free base porphyrin adjacent to the fullerene greatly increases the lifetime of the final radical ion pair[106c], passing from 0.38 s of the previous system to 1.6 s at 163 K in DMF of this last one, however the main problem is the low quantum yield of the entire process, 0.34 in DMF, although there is an improvement respect to the system with one zinc porphyrin and one free base porphyrin. It was possible to increase the overall quantum

yield altering the intervening porphyrins, Imahori and coworkers have synthesized and studied a pentade, where a three *meso-meso* directly linked zinc porphyrins acted as light harvesting system (Figure 3.4.1.5)[106d]. The photoirradiation of the Fc-$(ZnP)_3$-C_{60} results in photoinduced electron transfer from both porphyrin singlet and triplet excited states to fullerene moiety to produce radical cation trimer-C_{60} radical anion pair Fc-$(ZnP)_3^{\bullet+}$-$C_{60}^{\bullet-}$. Transient absorption studies confirm the subsequent formation of the final charge separated state $Fc^{\bullet+}$-$(ZnP)_3$-$C_{60}^{\bullet-}$. The final radical ion pair decays obeying to a first order kinetics with a lifetime of 0.53 s at 163 K in DMF, but it is more important to untline that the overall quantum yield remains high (0.83 in benzonitrile) in spite of the long distance between the donor and acceptor moieties. The authors suggest that such a high quantum yield arises from efficient charge separation along the porphyrin trimer while slow charge recombination is associated with localized porphyrin radical cation on the porphyrin trimer. The increased light harvesting efficiency is ascribed to the exciton coupling in the porphyrin trimer and also to the increased number of harvesting pigments.

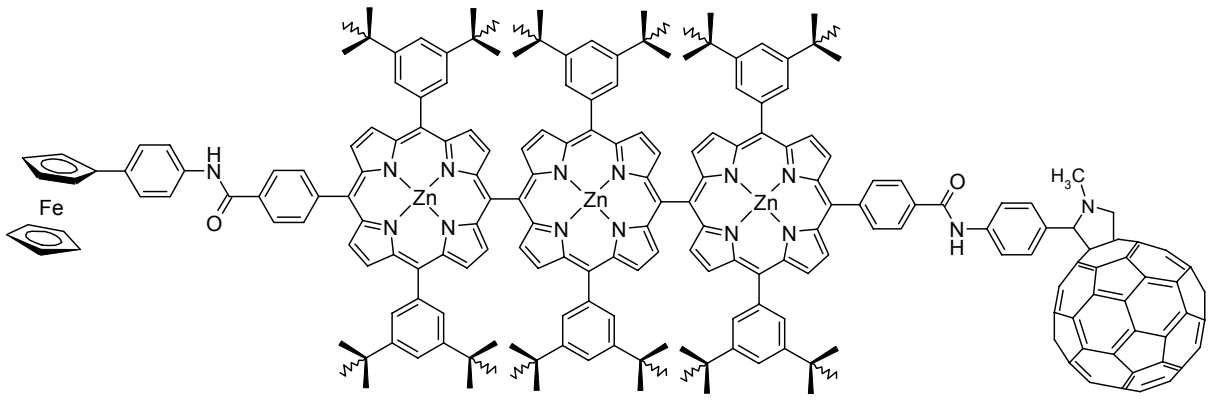

Figure 3.4.1. 5 *Pentade reported by Imahori et al. that shows good lifetime for the charge separated state and good quantum yield for the formation of the radical ion pair*

An analogous strategy was adopted by Lindsey, A. Moore, L. Moore and Gust to synthesize an hexade made up of five porphyrins and C_{60} as last electron acceptor[107], but the geometry of the compound is completely different respect to the linear one previously reported. The hexade has a star shaped geometry equal to that depicted in the figure 3.3.4, but in this case we have three peripheral zinc porphyrins, one central zinc porphyrin and one peripheral free base porphyrin directly linked to the fullerene moiety (Figure 3.4.1.6). The authors have varied the nature of this last porphyrin demonstrating how the different nature of the frontier orbitals and oxidation potential values can influence the electron transfer process. The zinc porphyrins could be considered as an antenna system that funnels the solar energy towards the synthetic free base

porphyrin-fullerene reaction center. In the hexade 2, in 2-methyl-THF at room temperature, the excitation of the peripheral zinc porphyrins is followed by singlet-singlet energy transfer to the central zinc porphyrin with a time constant of 50 ps. The excitation is passed on the free base porphyrin in 32 ps to produce the relative singlet excited state, from which the first electron transfer step takes place to generate the first free base porphyrin-C_{60} radical ion pair within 25 ps and with a quantum yield close to unity (0.98). Due to thermodynamically favourable migration of the hole on the zinc porphyrin array, a long charge separated state is formed, with a lifetime of 240 ns and an overall quantum yield of 0.90. In benzonitrile the lifetime reaches the value of 25 μs. Changing the nature of the free base porphyrin dramatically influences the overall process, in fact passing from the tetraaryl porphyrin to octaalkylporphyrin (hexad 1) the quantum yield for the charge separated state is lowered to 0.69 and the respective lifetime is much more lower, 1.3 ns. The authors attribute these effects to the difference in electronic composition of the free base porphyrin: in the tetraarylporphyrin the H.O.M.O. has a_{2u} symmetry while in the octaalkylporphyrin the symmetry is $a_{1u.}$ Moreover the oxidation potential has shifted from 1.05 V for the tetraarylporphyrin to 0.84 V for the octaalkylporphyrin. These results could be understood on the basis of the factors that influence through bond energy and electron transfer processes described in the works of Lindsey and coworkers and reported in the previous section (Paragraph 3.3). Other systems able to give multistep electron transfer were reported by L. Moore, A. Moore and Gust; in one of their system with an additional electron donor such as carotene, the lifetime of the charge separated state is equal to 5 μs. In such a system the presence of the carotene molecule allows to increase the aforementioned lifetime up to 50% by the application of a magnetic field of 41mT at 77 K, thanks to a Zeeman effect, that restricts the decay of the charge separated state only from one triplet state of the carotene moiety[108a]. In one more recent work[108b] the same authors have developed a gable system composed by a zinc porphyrin, a free base porphyrin, a fullerene acceptor and a tetraphenylbenzene core, located between the two porphyrins, acting as an ultraviolet antenna system. The study reveals that, after excitation, singlet-singlet energy transfer occurs between the two porphyrins in 59 ps; subsequently an electron transfer from the first singlet excited state of the free base porphyrin takes place within 25 ps, yielding the first charge separated state. Finally a further charge shift produces the final radical ion pair ($ZnP^{\bullet+}$-H_2P-$C_{60}^{\bullet-}$) with an overall quantum yield higher than 90%. The charge separated state lives 50 ns in 2-methyl-THF and 220 ns in benzonitrile, then it undergoes in a deactivation pathway that leads to an excited triplet state of the chromophores in 2-methyl-THF, while in benzonirile it leads directly to the ground state. The reported multistep electron transfer process seems to be the most efficient

way to produce long living charge separated state, but it is necessary a strong synthetic effort to obtain so articulated systems and under a theoretical point of view at each step a fraction of the excitation energy is lost[109], lowering the final quantum yield.

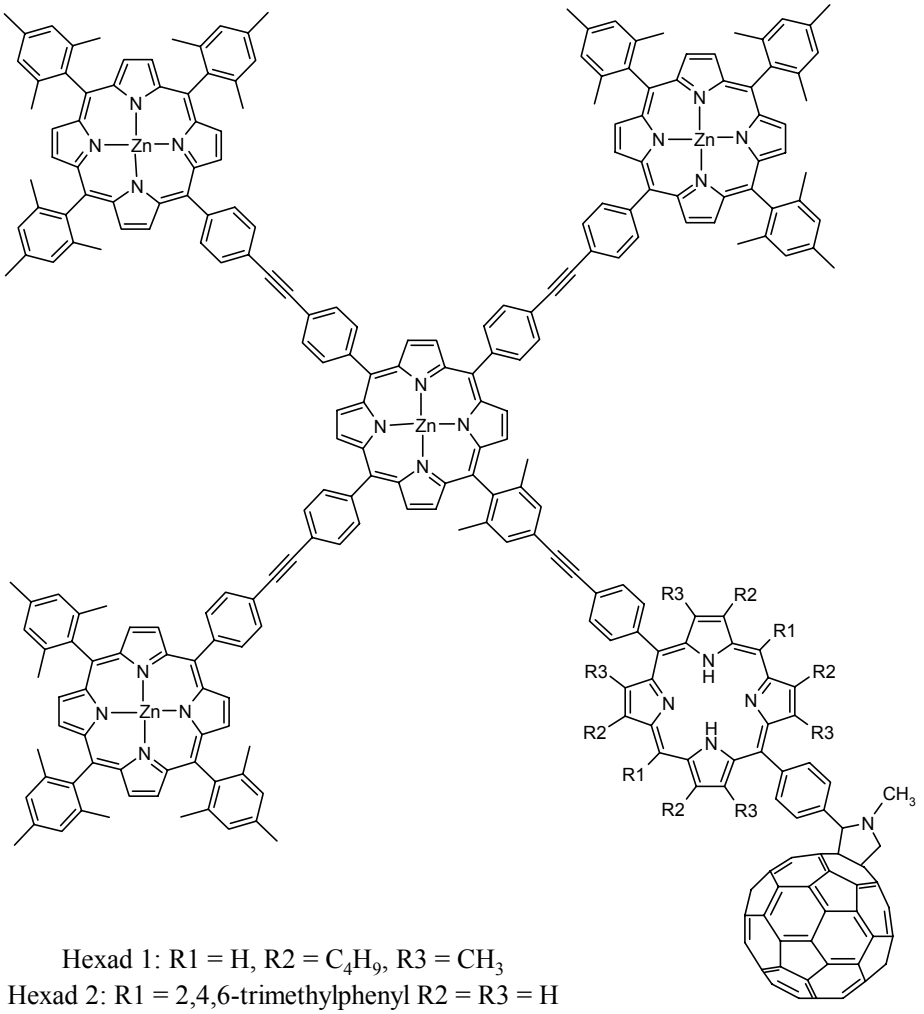

Hexad 1: R1 = H, R2 = C_4H_9, R3 = CH_3
Hexad 2: R1 = 2,4,6-trimethylphenyl R2 = R3 = H

Figure 3.4.1. 6 *Star shaped porphyrin-fullerene hexad developed by Lindsey and coworkers*

Important developments were achieved by Fukuzumi and his research group in synthesizing donor-acceptor dyad with low synthetic effort, but having high charge separated state lifetime. In such a system the porphyrin donor was replaced by a chlorophyll derivative and in one of the synthesized system, reported in the Figure 3.4.1.7 the charge separated state lives for 230 μs in benzonitrile at 25 °C, an extremely long lifetime for a simple dyad[110]. It seems that a so long lifetime should be due to an inactivated nuclear tunnelling, that in general promotes the charge recombination reaction when this step is located in the Marcus inverted region, but this is not the case. Several chlorophyll-fullerene dyads were synthesized and in general all of them present value of the lifetime for the charge separated state in the range of hundreds microseconds, confirming the peculiar characteristic of chlorine or bacteriochlorine-fullerene

dyads[111]. However the best result in such direction was obtained using a tetraarylporphyrin, bearing an imidazole ring fused on the β-pyrrole positions (Figure 3.4.1.8). The zinc derivative after excitation gives a charge separated state with the incredible lifetime of 310 μs at room temperature in benzonitrile[112], a value that is extremely long for a simple porphyrin-fullerene dyad; interestingly the respective free base derivative does not show charge separation state upon excitation, but the porphyrin singlet excited state is rapidly converted into the respective triplet excited state before the compound comes back to its fundamental state. All the systems reported in this paragraph are a clear example of how it is possible to obtain long lifetime for the charge separated state, using porphyrin and fullerene chromophore and how such systems show better characteristics respect to those with quinone acceptor. Furthermore all these systems are covalently linked and if on one side this approach allows to create very different architectures, on the other hand it implies a noteworthy synthetic effort. In the next section some self assembled systems will be briefly taken in consideration to underline some of their advantages respect to those systems which are just described here.

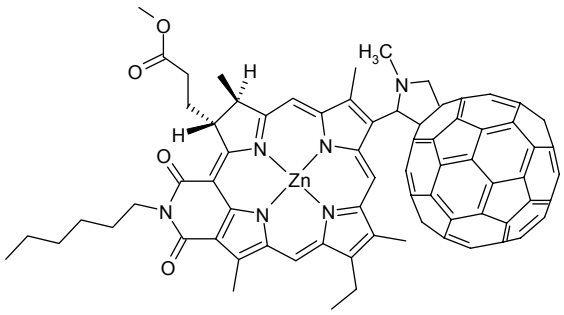

Figure 3.4.1. 7 *Zinc chlorin fullerene derivative with long radical ion pair lifetime (230 μs)*

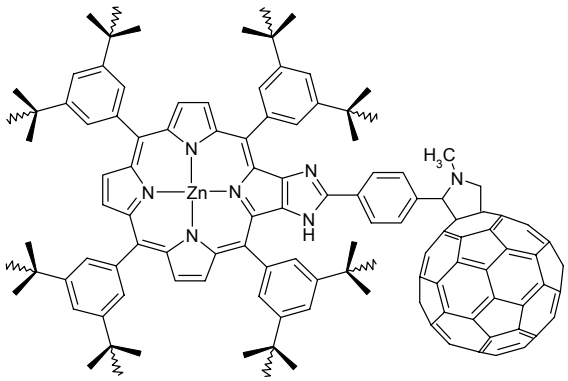

Figure 3.4.1. 8 *Porphyrin-fullerene dyad with a charge separated state lifetime of 310 μs*

3.4.2. Self Assembling Porphyrin-Fullerene Systems

The principal advantage in using a self-assembly strategy is to avoid difficult synthetic route for obtaining the desired porphyrin-fullerene adduct. Obviously the formation of the adduct is governed by the equilibrium condition, so to have a good quantity of the self-assembled donor acceptor photoactive unit it is necessary that the value of the binding constant is as higher as possible, otherwise the formation of the complex will be only in a few percentage[113]. There are many properties that could be used to generate a self-assembling system, for example in the particular case of the porphyrin and fullerene it is possible to exploit the π-π interaction between the tetrapyrrole aromatic ring and the curved surface of the C_{60}. As pointed out by Boyd and Reed such spontaneous interaction is useful to generate ordered porphyrin-fullerene arrays or to construct host-guest complexes [114]. Sometimes it is necessary to synthesize some geometrical preorganized host (Figure 3.4.2.1) to obtain a tight binding as reported in a work of Sanders and coworkers[115]. However due to the so close proximity between the two systems it is impossible to modulate in some way the electron and energy transfer reaction between the two moieties, so the meaning interaction that is often used in porphyrin-fullerene self-assembling systems is the capability of nitrogen compound to bind axially several metal porphyrin derivatives. Depending on the nature of the metal and the nitrogen ligand it is possible to obtain self-assembling system under equilibrium condition or also stable assembled porphyrin-fullerene complex. This last expedient is reported by Prato, Valli, Paolucci and Guldi to obtain metal coordinated fullerene-porphyrin dyad for Langmuir-Blodgett deposition[116]. In the report a pyridyl derivative of fulleropyrrolidine is self assembled with a ruthenium porphyrin and the high affinity of the pyridine ligand towards the metal atom guarantees an irreversible reaction (Figure 3.4.2.2 a). After a deep electrochemical study with reference compounds, the authors presented the photophysical study of the dyad both in solution and in the solid state. In the first case a fast electron transfer from the triplet state of the porphyrin occurs in polar media, while in non polar media like toluene, it is observable triplet-triplet energy transfer between the ruthenium porphyrin and fullerene moiety. In the solid phase a film composed of 40 or 60 monolayers of the stacked dyads shows as the only deactivation pathway of the excited state a

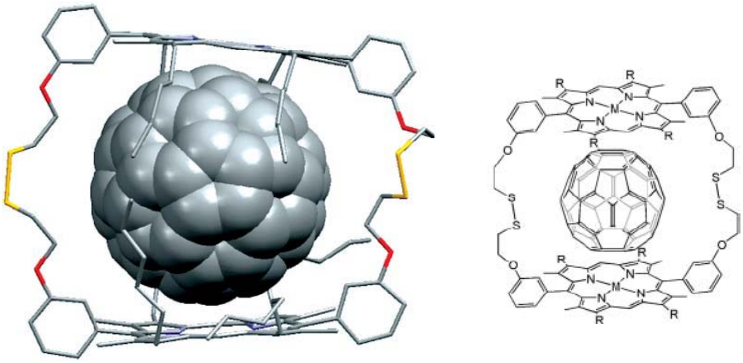

Figure 3.4.2. 1 *Host guest porphyrin-fullerene complex studied by Sanders and coworkers. M = Zn or 2H and R = C_6H_{13}*

triplet-triplet annihilation. To circumvent this problem the dyad has been deposed in a mixture of 1:20 ratio with arachidic acid and in such condition it has been observed a charge separated state with a lifetime of 2.2 μs. A great contribution to the study of self assembling system was given by D'Souza and his research group. In a paper published in 2002 together with Ito they reported on the self assembling of several fulleropyrrolidine derivatives with zinc tetraphenylporphyrin[117]. Different N-pyridyl substituted fulleropyrrolidine derivatives, plus N-phenylimidazole fulleropyrrolidine (Figure 3.4.2.2 b) compound were studied using cyclic voltammetry, UV-vis spectroscopy and fluorescence techniques. In particular it has been shown that the binding constants follow the order *ortho*-pyridyl << *metha*-pyrydil ≈ *para*-pyridyl << N-phenylimidazole with values ranging from 7×10^3 to 1.1×10^4 M^{-1}. The UV-vis absorption spectrum of ZnTPP shows substantial changes upon addiction of different fulleropyrrolidine ligands. A red shift both for the Soret and Q bands is mainly observable together with the appearance of many isosbestic points, with the only exception for the *ortho*-pyridyl derivative, that presents low binding capability. Through cyclic voltammetry studies accompanied with computational studies it has been demonstrated that the H.O.M.O. orbital is located on the porphyrin, while the L.U.M.O. on the C_{60}. Further fluorescence steady state and time resolved measurements clarified the reaction pattern that takes place after excitation of the zinc porphyrin. In *ortho*-dichlorobenzene an *intra*molecular electron transfer occurs from the singlet excited state of the porphyrin to give a charge separated state with different rate depending upon the axial ligand. These rate constants range from 10^7 to 10^{10}, being the highest one that corresponding to the imidazole ligand. In coordinating solvent such as benzonitrile, an *inter*molecular electron transfer takes place starting from the triplet excited state of the porphyrin. The meaning result of this work is the possibility to tailor the electron transfer rate changing the nature of the axial ligand. An analogue study[118] was carried out with a magnesium porphyrin and imidazole fulleropyrrolidine derivative. In this case the authors

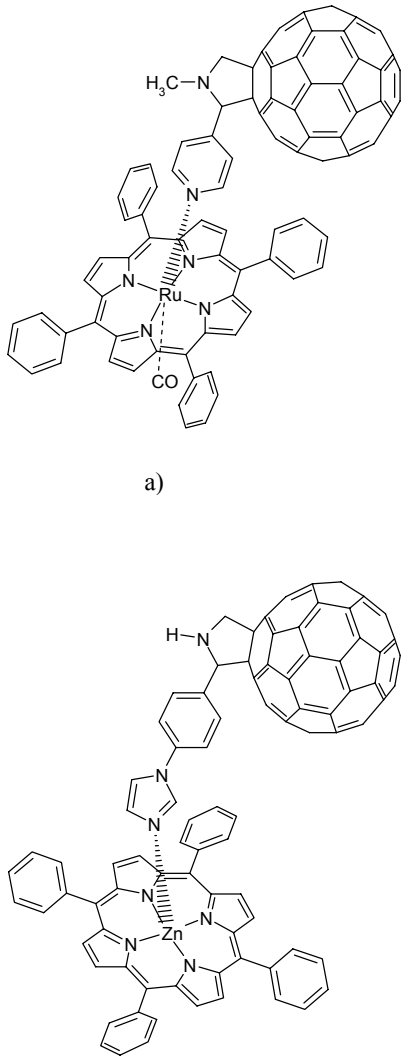

Figure 3.4.2. 2 *Self assembled dyad for Langmuir-Blodgett deposition a)*[116] *and ZnTPP-Imidazolyl fulleropyrrolidine self assembling system b)*[117]

failed in finding a double axial coordination between two molecules of imidazole fulleropyrrolidine and one of magnesium porphyrin, but they demonstrated the presence of an electron transfer occurring in *ortho*-dichlorobenzene solution with a rate constant equal to 1.1×10^{10} s^{-1} giving a charge separated state that lives for 12 ns before to decay in the fundamental state. The substitution of zinc atom with magnesium does not give appreciable variations, in fact the binding constant remains more or less equal (1.5×10^{4} M^{-1}) to that previous reported. An improvement in the self assembling systems was apported by further study of D'Souza and Ito and their respective research groups, adopting a "two point" binding strategy[119]. They have synthesized an appropriate zinc porphyrin crown ether able to bind a complementary fullerene derivative through axial coordination and cation crown ether complexation (Figure 3.4.2.3). The first advantage of the two points binding strategy is the possibility to obtain assembled complex also in coordinating solvent such as benzonitrile. The binding constant was found to be 4.4×10^{4} M^{-1}, a very high value if we consider the fact that it has been obtained in coordinating and polar solvent. The photophysical behaviour upon irradiation of the porphyrin moiety testifies an efficient electron transfer with a rate constant of 3.1×10^{9} s^{-1} and a quantum yield of 0.89. The charge recombination has been estimated to occur within 47 ns that is a quite long lifetime for a charge separated state coming from a self assembled system. Keeping in mind the results coming from the "two points" binding strategy, D'Souza et al. have developed new systems where it is possible to modulate the axial ligand interaction or π-π interaction between porphyrin and fullerene[120]. Two porphyrins bearing one or four [18]crown-6 ether moieties were synthesized together with hexyl ammonium derivative of fulleropyrrolidine bearing a pyridyl group or a non coordinating phenyl group. The study reveals high stability of all supramolecular complexes, even in polar media, and a geometry dependence from the position of the crown ether in the porphyrin moiety, but also from the typology of interaction (axial coordination or π-π interaction). Hence it has been possible to tailor the interchromophore interactions, by using the axial ligating pyridine entity on the fullerene or phenyl entity it is possible to achieve control on axial coordination or π-π interaction. Although axial ligation plus cation-crown ether complexation give a more stable complex than that furnished by π-π interaction plus cation-crown ether complexation, the

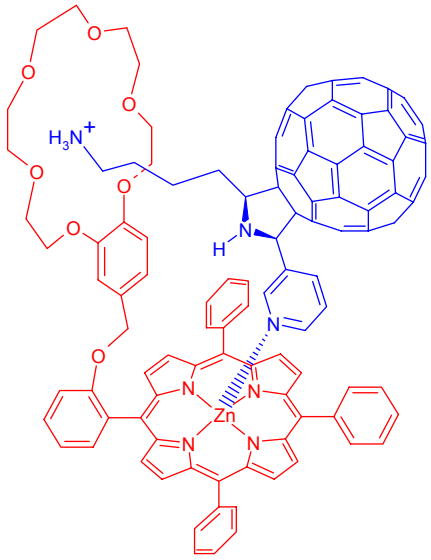

Figure 3.4.2. 3 *"Two point" binding porphyrin fullerene dyad*[119]

fluorescence study revealed light induced electron transfer from the singlet excited state porphyrin to the fullerene as the principal fluorescence quenching mechanism, irrespective of the type of binding modes. Both the interactions give quite good lifetime for the charge separated state in the range that goes from 50 to 500 ns. Moreover it has been shown the possibility to increase the lifetime of the radical ion pair modulating the axial coordination and π-π interaction by adding pyridine to the solution containing the dyads. In this last case a little increase in the forward electron transfer rate and a conspicuous decrease in the back electron transfer rates were observed. The lowering in the back electron transfer rate was attributed to an higher distance between the two moieties upon the addiction of pyridine. This work outlines the potentialities of a self assembling system compared to the possibility to tailor and modulate the electron transfer reaction, a feature impossible to find in the covalently linked systems. Another example in such direction is the use of potassium to switch between inter and intra molecular electron transfer in crown ether appended free-base porphyrin-fullerene complex[121]. Porphyrins with a different number of appended crown ether moieties were studied to evaluate the binding properties towards the pristine C_{60} (Figure 3.4.2.4). Electrochemical measurements and the free energy values (ΔG°) estimated by electrochemical data, suggest a possible *intra*molecular electron transfer from the singlet excited state of the porphyrin, subsequently observed through steady state, time resolved fluorescence and transient absorption study. The rate constants for the forward electron transfer are of the order of 10^9 s^{-1} and the observed lifetimes for the radical ion pairs are of the order of ten ns. The binding constants show a sort of cooperative binding increasing the number of crown ether moieties. The nature of the binding process resides into π-π interaction between the two chromophores, supported by local interactions between the crown ether entities and the fullerene core. The same analyses carried out in a solution containing potassium cation showed an *inter*molecular electron transfer with rates that are slightly higher than those in a diffusional control. Such

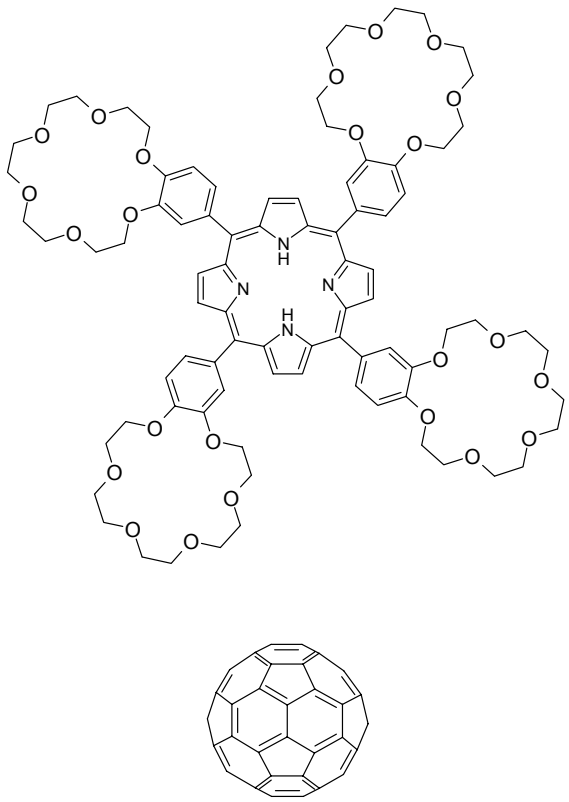

Figure 3.4.2. 4 *One of the crown ether appended porphyrin used to bind the pristine C_{60} in the work of D'Souza and Ito[121]*

*inter*molecular process is also confirmed by the recovering of the fluorescence emission of the porphyrin in the presence of potassium cation and furthermore by the fact that the rate of the C_{60} radical anion growth increases upon further addiction of pristine fullerene, indicating a bimolecular kinetic. The authors also showed the possibility to switch again the *inter*molecular electron transfer into *intra*molecular one adding an excess of [18]-crown-6 ether to the solution, which sequesters the potassium cation. Employing the self-assembling strategy D'Souza, Ito and coworkers synthesized a supramolecular triads composed by boron dipyrrin, zinc porphyrin and fullerene (Figure 3.4.2.5) as a model for the photosynthetic antenna reaction center complex [122]. In the complex the dypirrin moiety acts as antenna system and a selective excitation results in an efficient energy transfer that creates singlet excited state of the zinc porphyrin with a quantum yield of 0.83 and a rate of 9.2×10^{9} s^{-1}. Upon formation of the supramolecular triad (K_b = 1.6×10^{4} M^{-1}), an electron transfer evolves from the singlet excited state of the porphyrin, leading to a charge separated state with a rate constant of 4.7×10^{9} s^{-1}. The radical ion pair decays to the ground state with a rate constant equal to 2.0×10^{8} s^{-1} in *ortho*-dichlorobenzene solution. The studies reported by D'Souza and Ito on self assembling porphyrin-fullerene systems clearly show the opportunity to tailor the energy and electron transfer reactions throughout different strategies. These systems are evidently much more pliable than the covalently linked system, even if they do not show the longest lifetime for the radical ion pair seen in the whole covalent systems. A noteworthy work on self assembling systems was published by Hirsch, Guldi and Jux[123] and the innovative aspect of this work is the use of electrostatic interaction, mainly Coulumbic interactions, to generate a strong assembled system. For this aim dendritic fullerene and eight-positive charged zinc porphyrin were synthesized (Figure 3.2.4.6). The basic idea was to have many charges in order to obtain a binding constant as higher as possible and indirectly this aspect implies a non negligible advantage: the possibility to work in aqueous solution, a more friendly solvent. Uv-vis and fluorescence studies led to evaluate the association constant, which resulted to be 1.1×10^{8} M^{-1},

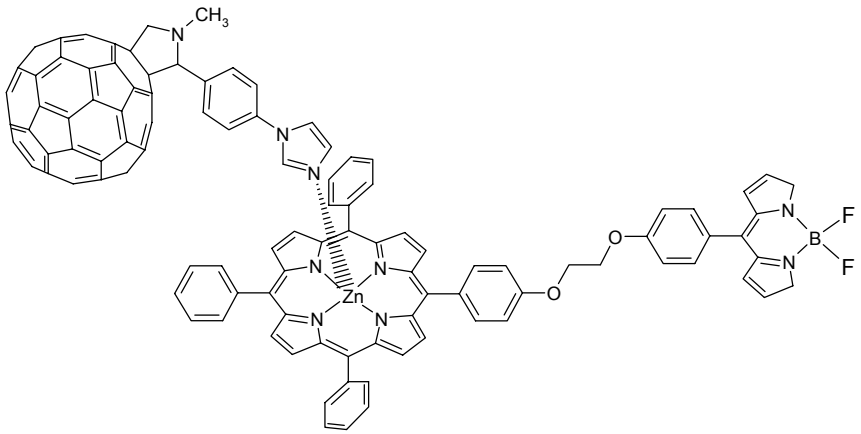

Figure 3.4.2. 5 *Self assembling boron dipyrrine-zinc porphyrin-fullerene triad mimics the photosynthetic antenna reaction center complex*[122]

a value extremely high and much more higher than one thousand time than those observed in the "two point" binding strategy[119,120]; the authors also demonstrated that the value of the association constant tends to decrease when the ionic strength increases. The addition of the dendritic fullerene to an aqueous solution of the porphyrin induces the quenching of the fluorescence porphyrin emission. Further transient absorption studies revealed electron transfer as deactivation pathway of the excited porphyrin, with the charge separated state living for 1.1 μs, a very long value for self assembled system.

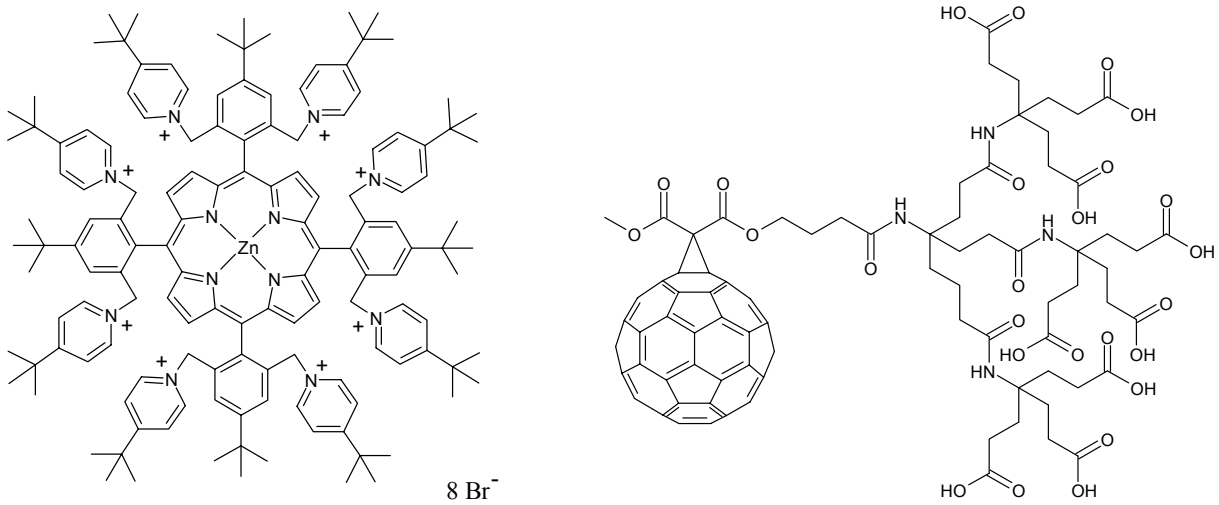

Figure 3.4.2. 6 *Zinc porphyrin and dendritic fullerene compounds used for electrostatic self assembling in the work published by A. Hirsch; D. M. Guldi, N. Jux and coworkers*[123]

In this section many examples of self assembling system have been taken into account to show the potentiality of this strategy in building donor-acceptor photoactive units. In the next section another synthetic strategy will be considered, the possibility to introduce between the porphyrin and fullerene a linker that can exhibit "wire like" behaviour in order to facilitate electron transfer between the donor and acceptor moieties.

3.4.3. Porphyrin-"Wire"-Fullerene Systems

In this section only few examples will be given about the "wire like" behaviour of some intervening spacers between the porphyrin and fullerene site. The aim is to give further demonstration on how many strategies can be used to tailor the porphyrin-fullerene interaction in order to obtain high efficient electron transfer reactions. The mainly used molecules to build up a molecular wire are conjugated oligomer or polimer. Due to their electron density they should be able to offer good "through bond" communication between the redox active sites, offering a low damping factor (β) for electron transfer reaction, so that the distance dependence of such reaction could be attenuated. As the Marcus theory predicts the distance dependence of the electron transfer reaction is principally due to electronic coupling between the donor and acceptor moieties (see Chapter 2) and the damping factor β is a measure of such a dependence when a medium, either solvent molecules or a covalently linked spacer, is interposed. Rearranging the expression of electron transfer rate constant, within the semiclassical approximation of the Marcus theory, it is possible to estimate from experimental data both the electronic coupling (V) and damping factor (β) when a spacer divides the porphyrin and fullerene moieties and hence evaluate its "wire" behaviour. By a theoretical point of view the required condition to have a good "wire behaviour" is that the energy level of the orbitals of the molecular bridge is intermediate between initial and final states of the electron transfer reaction, otherwise it is plausible to suppose that an electron transfer through "superexchange mechanism" takes place[124]. One example of efficient "wire behaviour" was reported by Ito, Otsubo and coworkers [125] in porphyrin-oligothiophene-fullerene triads, where several oligothiophene bridges with different length were tested (Figure 3.4.3.1).

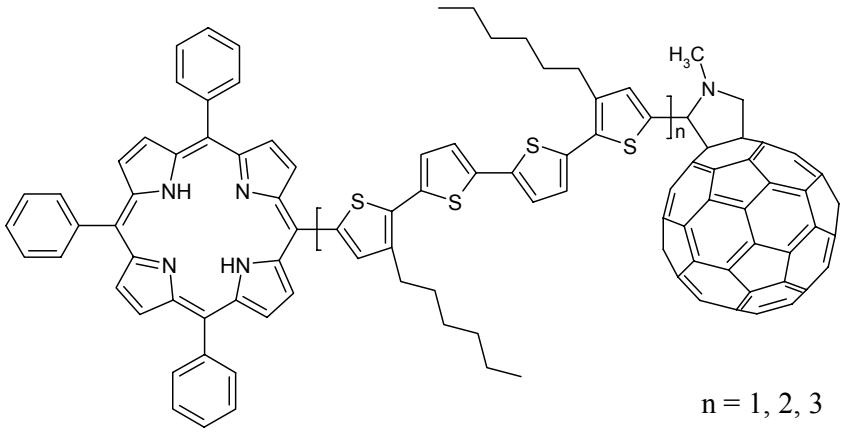

Figure 3.4.3. 1 *Porphyrin-oligothiophene-fullerene triads with a wire like bahaviour of the bridge*[125]

The study revealed a multifunctional role of the bridge: in toluene the bridge acts simply as a spacer confirming singlet-singlet energy transfer process between porphyrin and C_{60}, such a energy transfer is a Förster type since the dependence of the rate constant from the quantity $(1/R_{DA})^6$ was confirmed. In benzonitrile and *ortho*-dichlorobenzene the presence of electron transfer has revealed and the bridge acts in a first time as a good wire and then as an hole acceptor, hosting the radical cation coming from the porphyrin. The pathway reaction for the electron transfer has been elucidated by transient absorption measurements: upon excitation of the porphyrin an electron transfer occurs giving the first radical ion pair, where the negative charge is located on the C_{60} and the positive one on the porphyrin. Due to the energetic motivations a more stable radical pair is formed by the hole shift from the porphyrin to the oligothiophene bridge and finally the charge recombination, located in the Marcus inverted region, leads the systems in the fundamental state. The lifetime for the charge separated state varies depending on the linker length and on the solvent: in benzonitrile it is equal to 2.4, 1.9 and 1.5 μs while in *ortho*-dichlorobenzene is equal to 14, 27 and 20 μs, respectively for n = 1, 2, 3. Since the damping factor is 0.03 $Å^{-1}$ in benzonitrile and 0.11 $Å^{-1}$, in *ortho*-dichlorobenzene a solvent dependence of the wire like behaviour was outlined, moreover the electronic coupling between the different moieties was revealed to be very weak for the back electron transfer (ranging from 0.11 to 1.20 cm^{-1} in benzonitrile and from 0.02 to 0.14 in *ortho*-dichlorobenzene). All these features contribute to make the oligothiophene spacer a good bridge for electron transfer reaction over a long distance.

An other good example of molecular wire was showed in a work of Martin, Guldi et al.[126] where *para*-phenylenevinylene oligomers were used. The synthesized triads show a distance between the porphyrin and fullerene of 26.1 Å and 39 Å respectively when n is equal to 1 and 2 (Figure 3.4.3.2). The fluorescence study pointed out a good interaction between the bridge and the two redox active sites and such interaction is mainly based on energy transfer process and no electron transfer was showed to occur between the bridge and C_{60} or between the bridge and porphyrin in the synthesized reference compounds. However after excitation of the porphyrin in the triads, fast electron transfer occurs with rate constants varying from 3.2×10^9 s^{-1} to 4.5×10^9 s^{-1} both in THF and benzonitrile solution and slow charge recombination rates were found, from 9.3×10^5 s^{-1} to 4.4×10^6 s^{-1}. Fast electron transfer over a so long distance is feasible only postulating a very good "wire like" behaviour of the bridge, while on the other hand temperature dependence electron transfer studies, together with electrochemical data, suggest to exclude stepwise mechaism as charge recombination pathway and leave the superexchange mechanism as the operative mode. At least in the low temperature domain found in the analyses

carried out by the authors. However the estimated dumping factor is equal to 0.03 $Å^{-1}$ and the electronic coupling for the forward electron transfer is 2.0 cm^{-1} and in this last case the same dumping factor of that found in the work of Otsubo and Ito was obtained, although the bridge is chemically different.

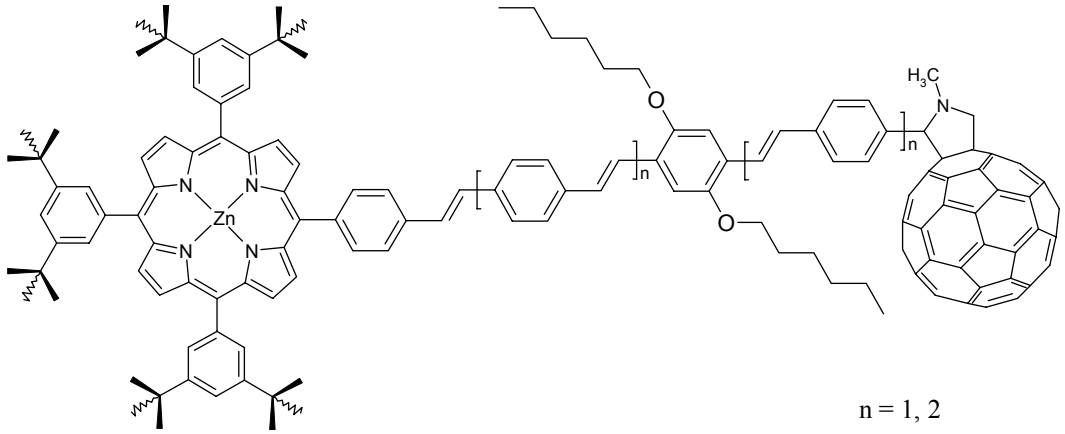

Figure 3.4.3. 2 *Porphyrin-oPPV-Fullerene triads developed by N. Martin, D. M. Guldi and coworkers*[126]

In previous reports the systems are not completely fully conjugated due to the presence of a sp^3 carbon of the pyrrolidine ring. To avoid this little drawback in order to obtain a really full conjugated system Schuster et al. synthesized porphyrin-polyalkynyl-fullerene systems of different length (Figure 3.4.3.3), functionalizing the C_{60} through nucleophilic addiction of litiumacetylide[127]. The cyclic and differential pulse voltammetry studies lead to suppose the presence of porphyrin-fullerene electronic coupling due to the shift of some reduction waves, passing from the data concerning the porphyrin and fullerene reference compounds, to those about the porphyrin-polyethynyl-fullerene systems. However the fluorescence studies reveal energy transfer in toluene solution and electron transfer in THF and benzonitrile. Both the processes maintain high rate constants despite the different distances that separate the donor and acceptor groups. In toluene after singlet-singlet energy transfer, the C_{60} singlet excited state decays into the C_{60} triplet excited state, before that the system comes back to the ground state, while the radical ion pair decays monoexponentially directly to the ground state. The lifetimes of the charge separated state are longer in THF, ranging from 555 to 714 ns, than in benzonitrile, from 322 to 526 ns. Finally the authors, plotting the rates for the back electron transfer versus the porphyrin-fullerene distance, estimated a dumping factor equal to 0.06 $Å^{-1}$.
Similar studies were carried out on a porphyrin-linker-fullerene systems, which present the peculiarity to have an alkynyl bridge directly linked to the β position of the pyrrole ring[128]. This guarantees an extension of conjugation that involves directly the aromatic system of the

porphyrin (Figure 3.4.3.4). Such compounds show ultrafast deactivation of the porphyrin singlet excited state (rate constants around 10^{10}) but, while in toluene this deactivation arises from intramolecular energy transfer, which generate as last product the C_{60} triplet excited state, in THF and benzonitrile transient absorption measurements clearly show the formation of a radical ion pair.

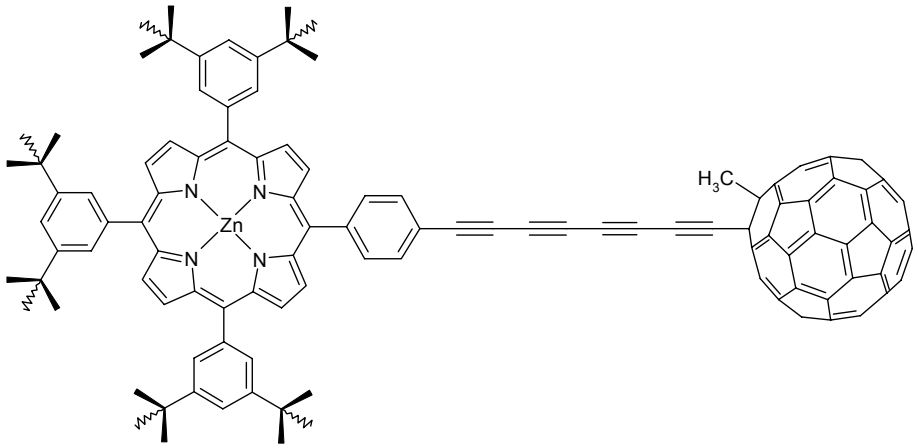

Figure 3.4.3. 3 *The longest porphyrin-polyethynyl-fullerene system reported in the work of D.I. Schuster et al.*[127]

The systems present an increase of the rate constant for the forward electron transfer as the polarity of the solvent increases, while the back electron transfer decreases in less polar solvent. Such results evidence that the charge recombination process is located in the Marcus inverted region while the charge separation ones in the normal region. However the extention of conjugation from the tetrapyrrole ring up to the fullerene surface is responsible for a quite low ratio between the forward and back electron transfer rate constants ($k_{ET}/k_{BET} \approx 7$), hence the lifetime of the charge separated state is quite low and resides in the picosecond time domain. The important outcome of this study is to have outlined the importance of the substitution pattern, in fact when the same linker is attached to the *para* position of the meso phenyl ring of the porphyrin (previous work described) the $k_{ET}/k_{BET} \approx 7400$. So dramatic effect underlines one more time how many tools is possible to use to tailor the electron transfer processes.

Much published papers were presented above to underline the many interaction typologies between porphyrin and fullerene which were developed during the past years. However all the examples regard compounds studied in solution. The application of such compounds to build up working solar cells requires some modifications under a synthetically point of view. It is possible to obtain vectorial multistep electron transfer on a electrode surface modifying this surface with right porphyrin-fullerene systems, bearing self assembling group such thiol groups that have high affinity towards gold electrode[129], or carboxyl groups towards tin electrode[130].

Moreover it is possible to generate an organic solar cell employing layer-by-layer deposition, based on Coulumbic interaction between the single chromophores used[131] or using a self assembling plus supramolecular approach that yield quaternary structures (clusters) of porphyrin and fullerene, subsequently deposited on the electrode surface[132].

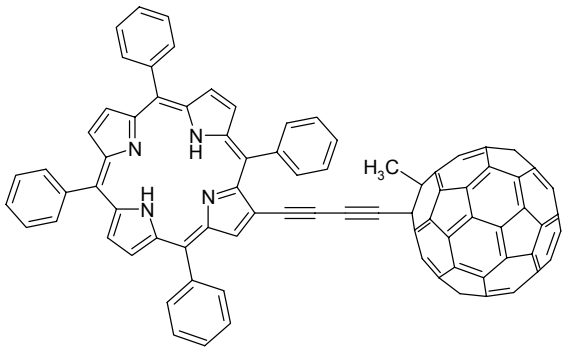

Figure 3.4.3. 4 *Completely conjugated porphyrin-fullerene system studied by D. I. Schuster et al.*[128]

Obviously passing from the solution to the solid state the systems requires further studies to verify if the adopted strategy shows the best obtainable conditions to maximize the yield of photocurrent generation, this implies that a lot of other parameters have to be optimized in order to produce a well working device. Undoubtedly if the system used to build the solar cell have intrinsic good characteristics the result will be better. This last research field is in continuous growth, because of the possibility to obtain energy storing of the solar radiation throughout organic devices. This is an appealing perspective to solve energetic and pollution problems.

Chapter 4

"New Porphyrin-Fullerene Compounds"

4.1. Introduction

As it was possible to see in the previous chapter, during the last 10 years porphyrins and fullerene were widely used to build different molecular networks able to mimic the natural photosynthetic processes. The main goal of such studies was to understand the structural parameters that govern these phenomena in order to achieve the storing of solar energy and its conversion into chemical potential. It has been pointed out that several interaction typologies between porphyrin and fullerene exist: interaction through covalent bonds[102-112], through axial self assembling[116-119], through π-π stacking and also coulombic interactions[120,121,123]. Moreover the possibility to modulate these type of interactions emerged. In most cases the production of a long living charge separated state is achieved through multistep electron transfer along different subunits, including ferrocenyl moiety as last electron donor[133]; in other cases simple systems such as porphyrin-β-linked fullerene dyad [134] and much more often chlorophyll or bacteriochlorophyll-fullerene dyads[135] demonstrated to be able to produce long lived charge separated state, despite their structural simplicity. Especially in this last case the use of natural compound as starting material is often required, therefore the application of simple synthetic pathways, able to afford new functionalized porphyrin derivatives emerged as an important aspect of such studies. The introduction of substituents in the β-positions of the pyrrole rings can deeply modify the photophysical properties of the porphyrin, so such a strategy could be a good candidate to further tailor the porphyrin-fullerene interaction. The purpose of the thesis is to synthesize and characterize new covalently linked porphyrin-fullerene compounds adopting β-modified porphyrins as starting material and arriving to a well defined architecture bearing a molecular wire directly attached to the pyrrole ring. For such compounds a synthetic strategy for introducing appropriate groups, in order to make possible application for organic solar cells, will be also shown.

4.2. Synthetic Strategy

In this section all the synthetic routes adopted to obtain the desired compounds will be described, highlighting the meaning passages and the results obtained. The first aspect that has to be presented is the choice of the linker; in doing that, we have focused our attention on ethynylenephenylene oligomers because of their synthetic versatility and their physico-chemical properties. It has been shown that these molecules, due to their high electron density and extended π-system are quite good electron carrier[136]. In particular once that they are self-assembled on a metal surface (i.e. gold surface) these systems are able to transport and storage negative charge via the localized molecular orbitals[136c,d]; due to the extended π conjugation the oligo-ethynylenephenylene compounds have the characteristic to maintain in contact, over an intermediate or long distance, one electron donor and one electron acceptor group, both covalently linked to the two extremities of the oligomer; as revealed by the "push-pull" effect[136e] a typical property for these compounds. From a synthetic point of view it is possible to obtain these compounds in good yields through the well known Sonogashira coupling[137]. For our purposes it was necessary that the molecular "wire" bore a formyl group at one end, to give the Prato reaction with C_{60}. To synthesize the oligomers a stepwise iterative procedure was adopted, using as terminal subunits 4-ethynylbenzaldehyde and 1-iodo-4-(trimethylsilylethynyl)benzene, this latter synthesized modifying the literature procedure[138] in order to improve the yield. The cited reactions are reported in the following scheme (Scheme 4.2.1).

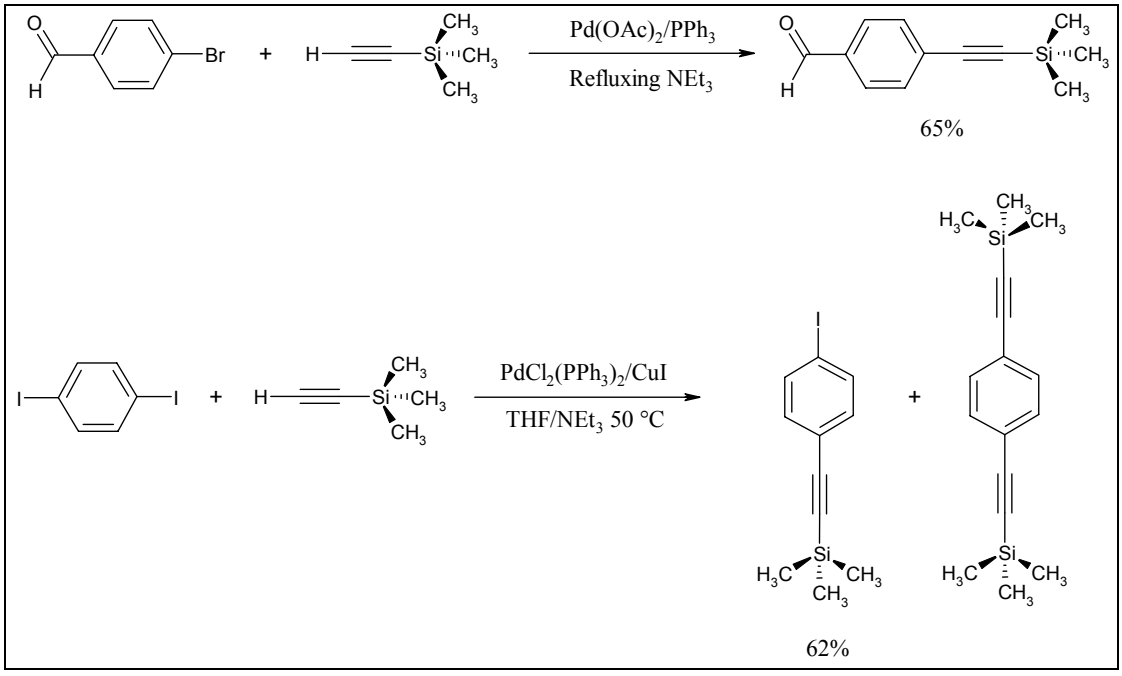

Scheme 4.2. 1 *Synthetic routes to 4-(trimethylsilylethynyl)benzaldehyde and 1-iodo-4-(trimethylsilylethynyl)benzene*

The relative quite low yield for the aldehyde comparing with those reported in literature[137a] is probably due to the non completely anhydrous conditions, while the improved yield for 1-iodo-4-(trimethylsilylethynyl)benzene relative to that reported in literature[138a] has been achieved using a slight excess of diiodobenzene (1.5:1) and adding dropwise a trimethylsilylacetylene solution to the reaction. The desired product is purified from the bis addiction by-product through a silica gel chromatography eluting with petroleum ether.

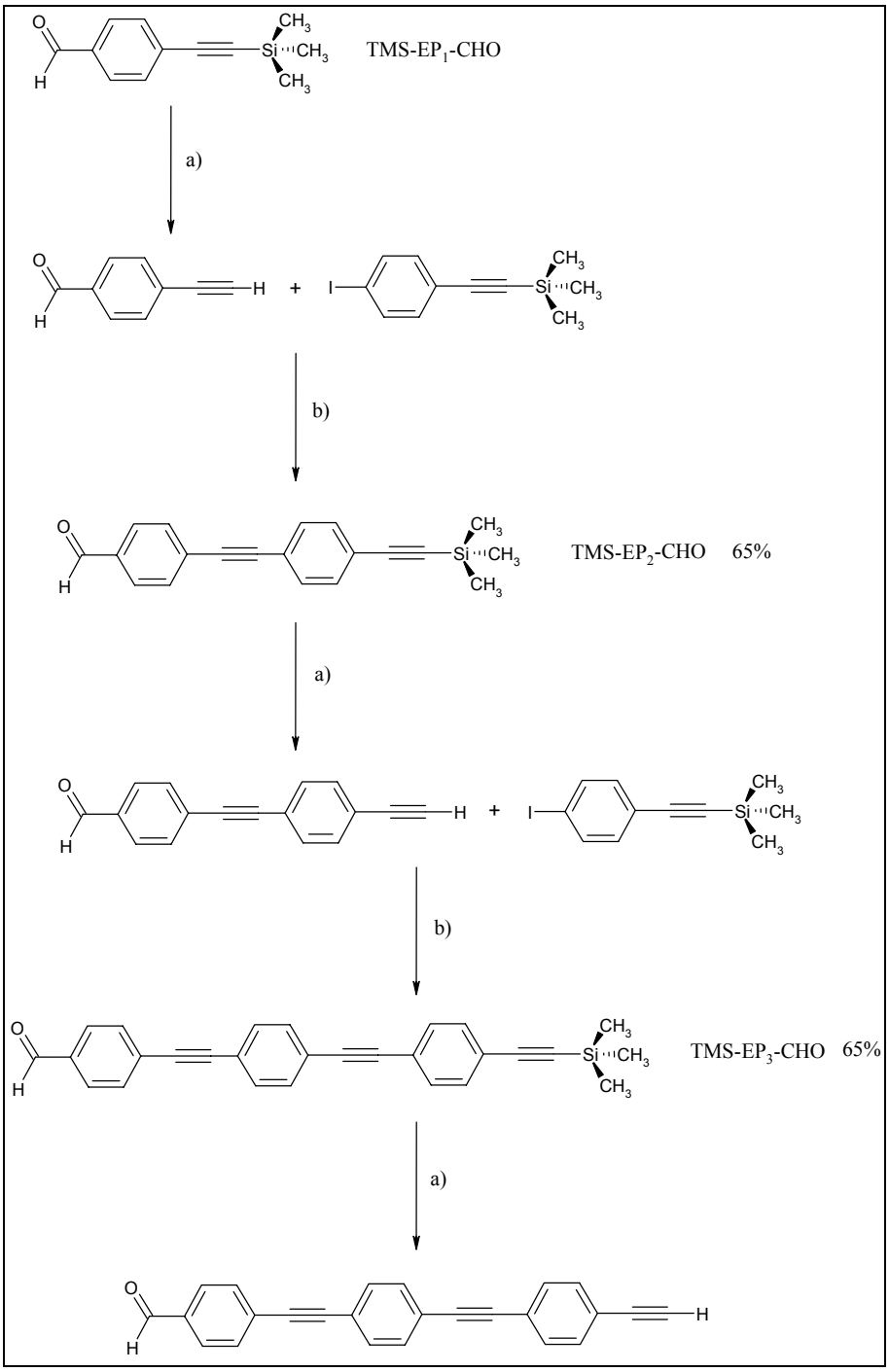

Scheme 4.2. 2 *Synthesis of "molecular wire" a) K_2CO_3 in $CH_3OH/CHCl_3$ solution b) $PdCl_2(PPh_3)_2$/CuI in THF/NEt_3 at 50 °C*

Through quantitatively deprotection of terminal ethynyl group, carried out in K_2CO_3 in $CH_3OH/CHCl_3$ solution and condensation reactions, the different oligomers with two and three ethynylenphenylene subunits were synthesized (See previous Scheme 4.2.2). The same identical yield for the two wires leads to suppose that a certain percentage of the starting terminal alkynes undergoes to omocoupling reaction due to the presence of copper iodide as cocatalyst and much more important to the presence of oxygen in solution, although the reaction apparatus was carefully deoxygenated with a stream of argon and maintained under inert atmosphere (Nitrogen) for all the reaction time. The molecular wires are subsequently used to synthesize the fullerene reference compounds (Scheme 4.2.3 and 4.2.4), necessary for the photophysical and cyclic voltammetry studies. As it has been aforementioned the formyl group at one terminal of the oligomer was used in the Maggini, Scorrano and Prato reaction[139] to functionalize the fullerene moiety. The ^{1}H-NMR analyses reveal characteristic proton pattern of N-methylfulleropyrrolidine in all the fullerene derivatives as it is shown in the inset reported in the Figure 4.2.1: one singlet at 2.86 ppm due to the methyl substituent on the nitrogen atom, one singlet at 4.89 ppm due to the hydrogen in position 2 of the pyrrolidine ring and two doublets at 4.22 and 4.96 due to the methylene protons. The values reported are those related to the N-methyl-2-[4'-ethynylphenyl]-3,4-fulleropyrrolidine, while for the other compounds the signals undergo to a very little shifts, remaining substantially in the same range.

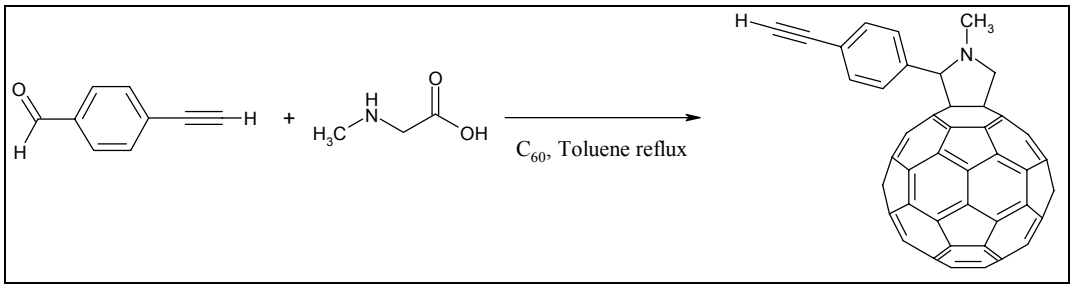

Scheme 4.2. 3 *Synthesis of N-methyl-2-[4'-ethynylphenyl]-3,4-fulleropyrrolidine*

In the wires with two and three subunits, the trimethylsilyl group linked to the terminal triple bond was left in order to confer a mayor solubility to the respective fullerene derivatives in the solvents such as dichloromethane, chloroform and toluene. The oligoethynylenephenylene-fullerene systems will be indicated with the names TMS-EP_2-C_{60} and TMS-EP_3-C_{60}, where TMS = trimethylsilyl and EP = ethynylenephenylene, except for the compound reported in the Scheme 4.2.3 for which the full name will be used.

The ^{1}H-NMR analysis of all the three fullerene derivatives has showed unresolved proton signals between 7.00 and 8.00 ppm most probably due to the steric hindrance of the phenyl ring

directly linked to the pyrrolidine ring; such hindrance could not allow the free rotation around the single bond that links the oligo-ethynylenephenylenes to the position number 2 of the pyrrolidine ring as drawn in the Figure 4.2.2.

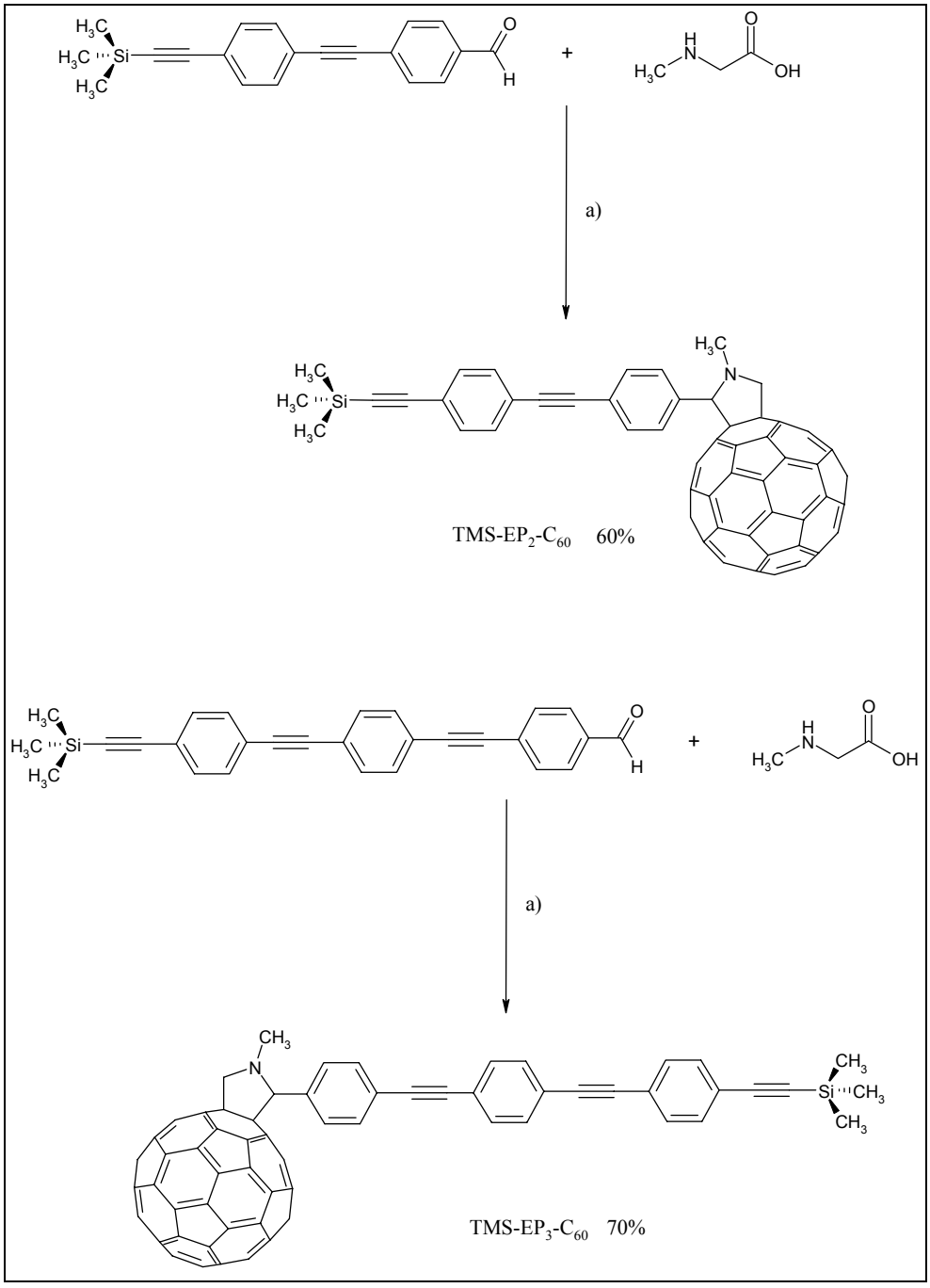

Scheme 4.2. 4 *Syntheses of TMS-EP$_n$-C$_{60}$ derivatives a) C$_{60}$, Toluene refluxing under inert atmosphere*

This decreased free rotational degree can lead to the unresolved proton signals seen in the NMR analyses, due to the possible contact of the *ortho* hydrogens Van der Waals radium with the fullerene curved surface.

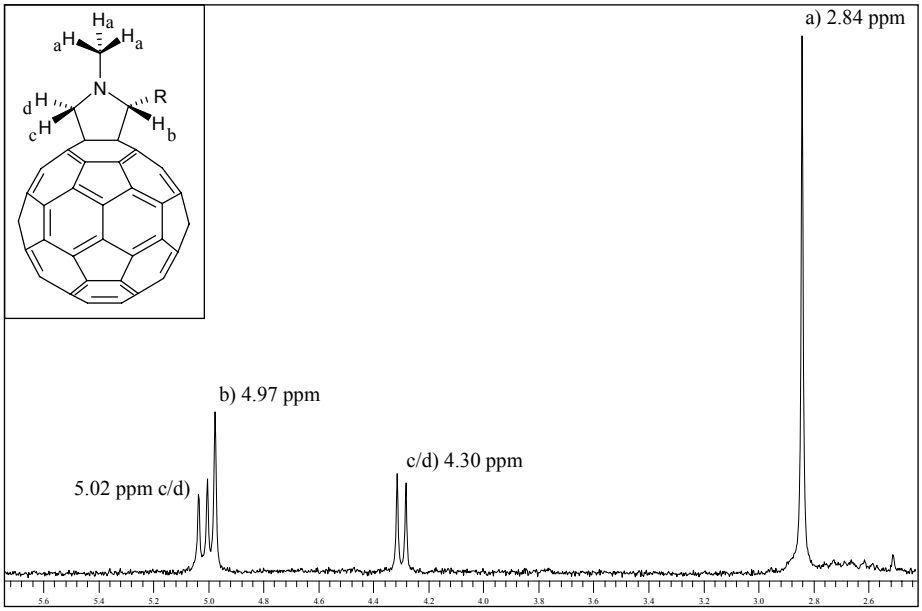

Figure 4.2. 1 *Characteristic proton pattern of N-methyl-2-substituted pyrrolidine ring, being R = TMS-EP$_2$ substituent in this particular case*

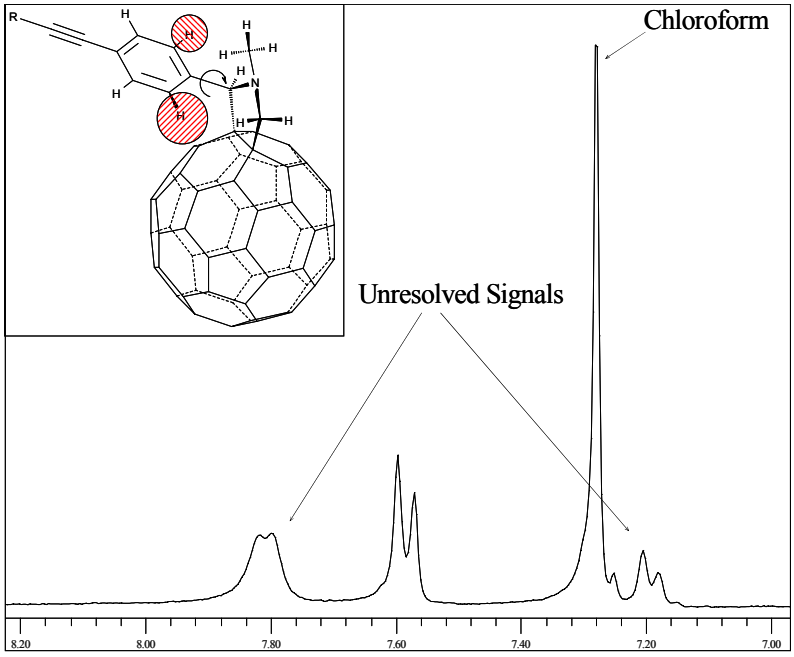

Figure 4.2. 2 *Unresolved ^{1}H-NMR proton pattern in the aromatic region of the fullerene derivatives, most probably due to the contact of the ortho hydrogens of the phenyl ring with the curved surface of the C_{60} (inset). The rapresented ^{1}H-NMR signals are those related to the N-methyl-2-[4'-ethynylphenyl]-3,4-fulleropyrrolidine*

All the fullerene derivatives were also characterized through mass spectrometry analyses, using MALDI-TOF technique that gave as result spectra showing peaks with a charge/mass ratio equal to the respective molecular weights of tested compounds. The subsequent passage was to synthesize an appropriate β-modified porphyrin to use for Sonogashira coupling with the

terminal alkyne deprotected monomer and oligomers. For this aim a radical bromination reaction of the common free base tetraphenylporphyrin (H_2-TPP) was used. H_2-TPP was synthesized with the well known Adler-Longo synthetic method, modified by Gonsalves et al.[140]. The bromination reaction was carried out following the literature procedure[141]using the N-bromosuccinimide (NBS) as the brominating agent. The monosubstituted product was separated from the disubstituted products through silica gel chromatography, eluting with xilene/petroleum ether (40°-70°), 3:2 (Scheme 4.2.5).

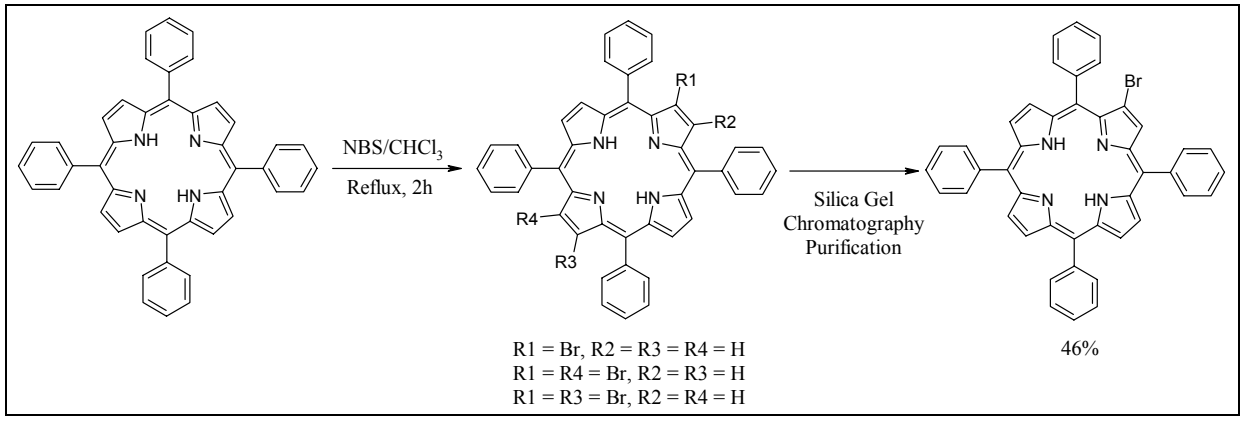

Scheme 4.2. 5 *Synthetic pathway to obtain the H_2-2Br-TPP*

The subsequent coupling reaction with the terminal alkyne products recovers a particular important role, because the synthesized starting materials could not be lost throughout side reactions. To avoid this drawback, the formation of the carbon-carbon bond between the bromo-porphyrin and the previously shown ethynylenephenylene linkers was carried out using the catalytic system $Pd(dba)_2/AsPh_3$ developed by Lindsey and coworkers[142], paying particular attention to the deoxygenation and dilution conditions and first of all avoiding the use of copper iodide as cocatalyst. In this way the homocoupling side reaction between terminal alkynes was suppressed and high yields of the desired compounds were obtained. In order to evaluate the effect of the substitution on the chemical-physical properties of the porphyrin, a fourth β-modified porphyrin was also synthesized using the same approach. This last porphyrin bears the same ethynylenephenylene subunit of the compound **1** depicted in the scheme 4.2.6, but with a methyl group, instead of a formyl grup, on the *para* position of the phenyl ring substituent (Figure 4.2.3). All the new porphyrin compounds were characterized through ^{1}H-NMR analysis and mass spectrometry, adopting the FAB technique for the lower molecular weight compounds (**1** and **4**) and MALDI-TOF for the higher ones (**2** and **3** in the Scheme 4.2.6). In the ^{1}H-NMR analysis, recorded in chloroform solution, diagnostic signals due to the aldehydic proton and to

the typical β-pyrrole proton pattern of porphyrin moiety are clearly visible, while the aromatic protons of the linker are superimposed to the aromatic protons of the porphyrin *meso*-phenyl rings, generating a series of multiplets signals difficult to attribute.

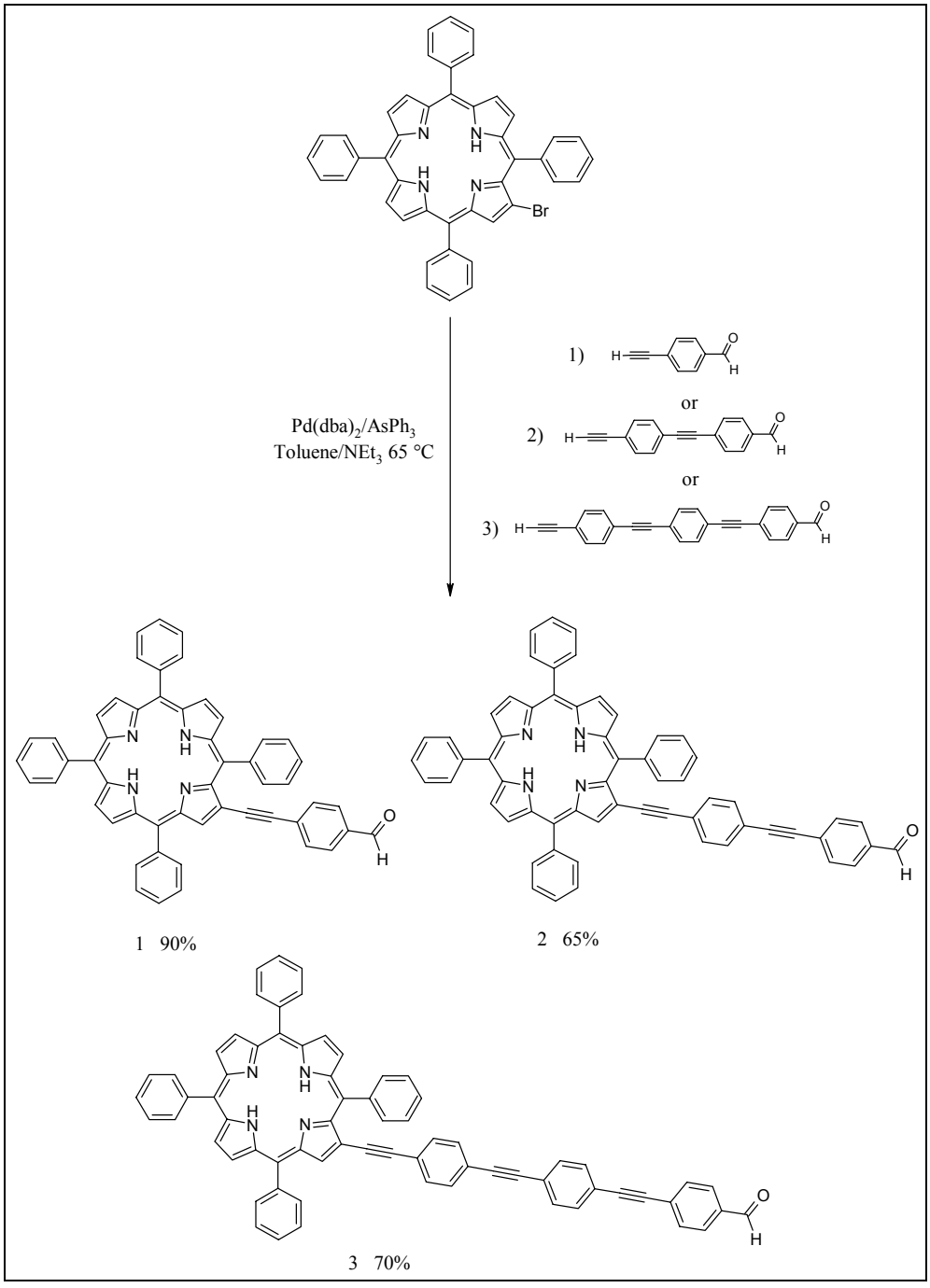

Scheme 4.2. 6 *Synthetic path to the β-modified porphyrins 1, 2 and 3*

The new porphyrins were used to synthesize the desired porphyrin-fullerene systems using the Prato reaction[139], but in this case particular attention was dedicated to carry out the reactions in anhydrous conditions, distilling toluene from sodium prior to use, since it has been reported by

H. Imahori, S. Fukuzumi et al.[143], that in such condition there is the possibility to improve the yield of reaction using an excess of pristine C_{60} respect to the aldehydic compounds. After several experiments it has been noted that for our compounds a large excess of pristine C_{60} does not give an effective improved yield, so we decided to operate in the same conditions reported in literature[143], but using a slightly excess of fullerene respect to the aldehyde (1.5:1). The desired porphyrin-fullerene systems were purified over a silica gel column eluting with toluene, recovering also the unreacted porphyrin and C_{60}, obtaining yields of 60% for the compound **5**, 57% for the compound **6** and 52% for the compound number **7**. The solubility of such compounds is quite good in most of the common solvents: toluene, chloroform, THF and benzonitrile and it tends to decrease as the length of the linker increases. The synthesized porphyrin-fullerene systems are depicted in the Figure 4.2.4.

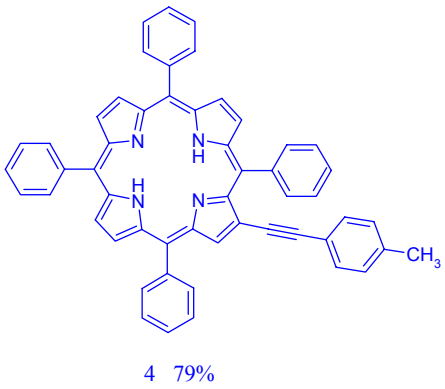

Figure 4.2. 3 *Porphyrin 4 synthesized adopting the same methodology used for the other ones*

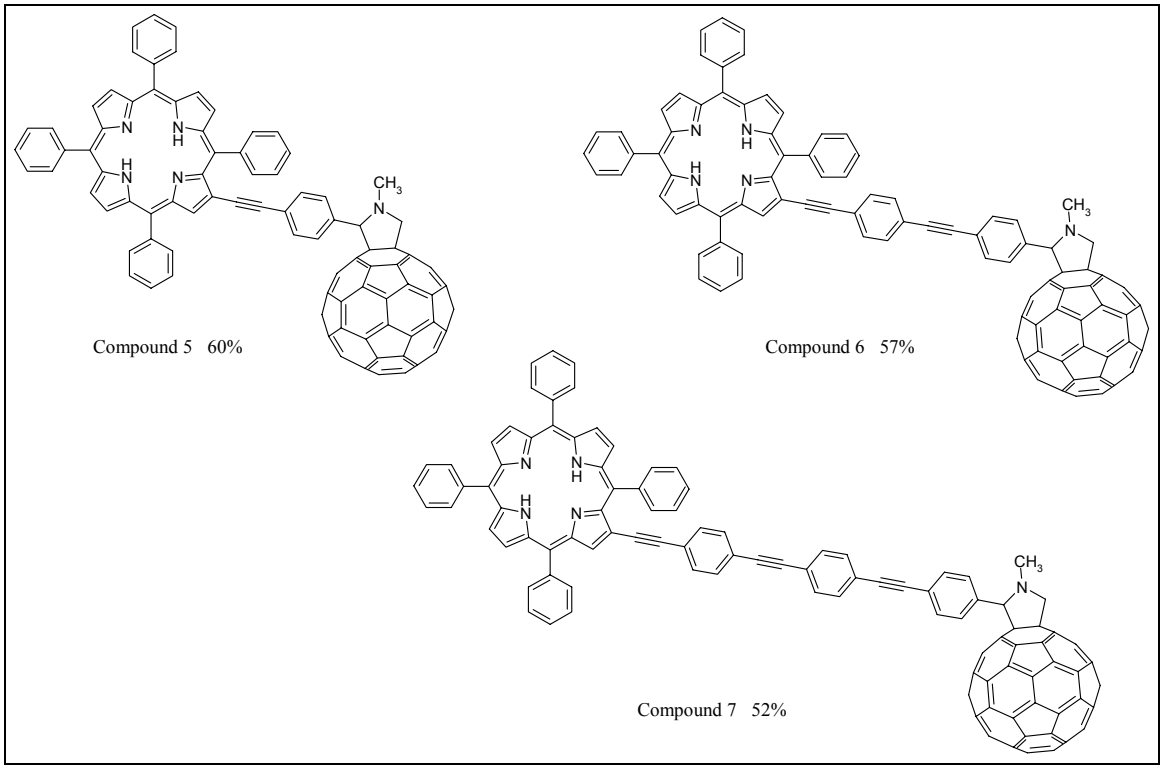

Figure 4.2. 4 *Porphyrin-wire-systems synthesized adopting a slightly modified Prato reaction: a pristine C_{60}/porphyrin ratio equal to 1.5 and anhydrous conditions, using toluene distilled over sodium*

All the free base porphyrins and free base porphyrin-fullerene derivatives were converted into their zinc derivatives dissolving the compounds in chloroform and adding a slightly excess of a

saturated $Zn(OAc)_2$ methanol solution. The reaction was left under argon at room temperature for three hours and then was filtered through a plug of silica gel to remove the excess of salt. The yield is quantitative. The porphyrin-wire-fullerene systems were subsequently investigated through several fluorescence and cyclic voltammetry measurements and also through ^{1}H-NMR and ^{13}C-NMR analyses. The results will be reported in a detailed way in the following sections. The strategy adopted for the introduction of a coordinating group into compound number **5** (see Figure 4.2.4) will be discussed later. The further derivatization of porphyrin-fullerene compound with an appropriate functional group able to generate ordered supramolecular systems lets us to study much more complicated architectures, whose subunits maintain the own chemical-physical properties. Our choice was directed on a pyridyl group, that, as reported in the previous chapter 3 (see paragraph number 4.2), is able to give an axial coordination binding the zinc metal inserted into the tetrapyrrole ring. To avoid the free rotation, that could allow several conformations in the self assembled porphyrin-fullerene oligomers, it is necessary to introduce the pyridyl group in a constrained geometry. Recently P. A. Troshin et al.[144] have reported a new efficient [3+2] cycloaddiction reaction on fullerene, in which primary and secondary amines together with an aldehydic compound are used as substrate to generate the azomethine ylide that later reacts with the fullerene, this new reaction pathway shows also a good stereoselectivity and we have decided to test this route to achieve our aims. The porphyrin compound **1** was left to react with 4-aminomethyl-pyridine and C_{60}, under acidic condition (CH_3CO_2H) in *ortho*-dichlorobenzene solution as reported in the Troshin's work[144] (Scheme 4.2.7).

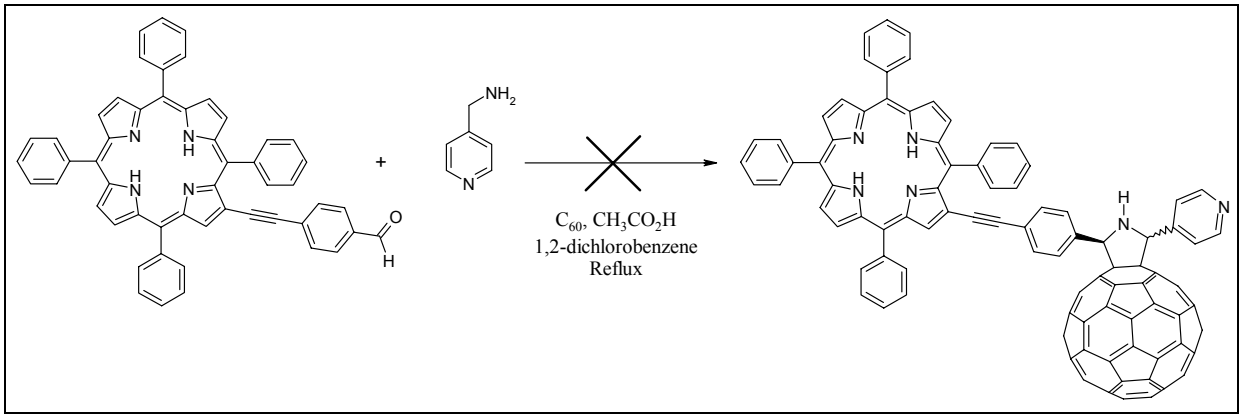

Scheme 4.2. 7 *First synthetic pathway to introduce pyridyl moiety into porphyrin-fullerene dyad*

As it is possible to see in the Scheme 4.2.7 the reaction does not yield the desired porphyrin-fullerene-pyridyl triad, but we are able to isolate one product of the reaction which was

characterized through ^{1}H-NMR and MS-FAB analysis. In the NMR analysis of the isolated compound, the characteristic pyrrolidine signals do not appear and the aldehydic proton is not present. Moreover the aromatic protons pattern is slightly different if compared with that of the compound **1**. The doublet signal due to the protons in the relative *ortho* position respect to aldehydic group (at 7.87 ppm in the ^{1}H-NMR spectrum of compound 1) disappears (See Figure 4.2.5), but the mass spectrometry gives a mass/charge ratio corresponding to the molecular mass of compound 1, so, from these data, we have concluded that the isolated product could correspond to the porphyrin iminoderivative (Figure 4.2.5), that under mass spectrometry experimental conditions (the matrix adopted is a mixture of nitro-benzylalcohol plus trifluoroacetic acid) undergoes to a fragmentation-oxidation that gives back the starting product **1**.

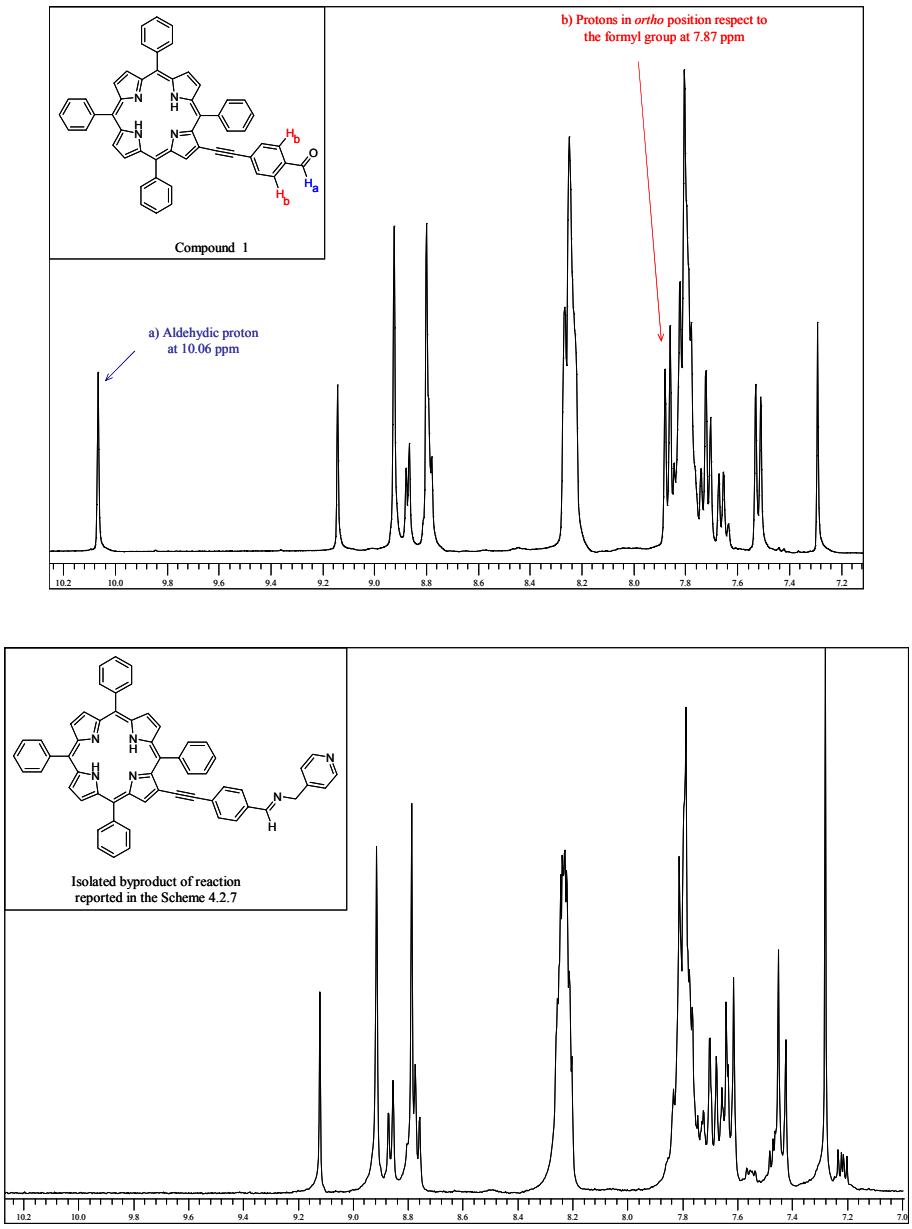

Figure 4.2. 5 *^{1}H-NMR signals of compound 1 (upper part) and byproduct iminoporphyrin derivative (lower part)*

Adopting also the basic conditions reported in the paper[144] and varying the temperature and reaction time not improves were noted and we concluded that most probably the porphyrin iminoderivative requires much more drastic condition to generate the corresponding ylide compound, necessary to the fullerene functionalization. Before to leave definitively this synthetic pathway, some experiments were carried out with 4-(trimethylsilylethynyl)-benzaldehyde and fullerene to verify the reaction conditions. As reported in the inset of the Figure 4.2.6, the reaction carried out using acetic acid as catalyst, in the same condition tested for the porphyrin **1**, gives the desired product with a yield of 17%, but after purification the ^{1}H-NMR analysis reveals the presence of some impurities (See Figure 4.2.6). In conclusion, considering the purification difficulties, the low yield obtained and the much less reactivity of the porphyrin **1**, it has been decided to change synthetic approach, trying to synthesize the N-(4'-pyridylmethyl)-glicine.

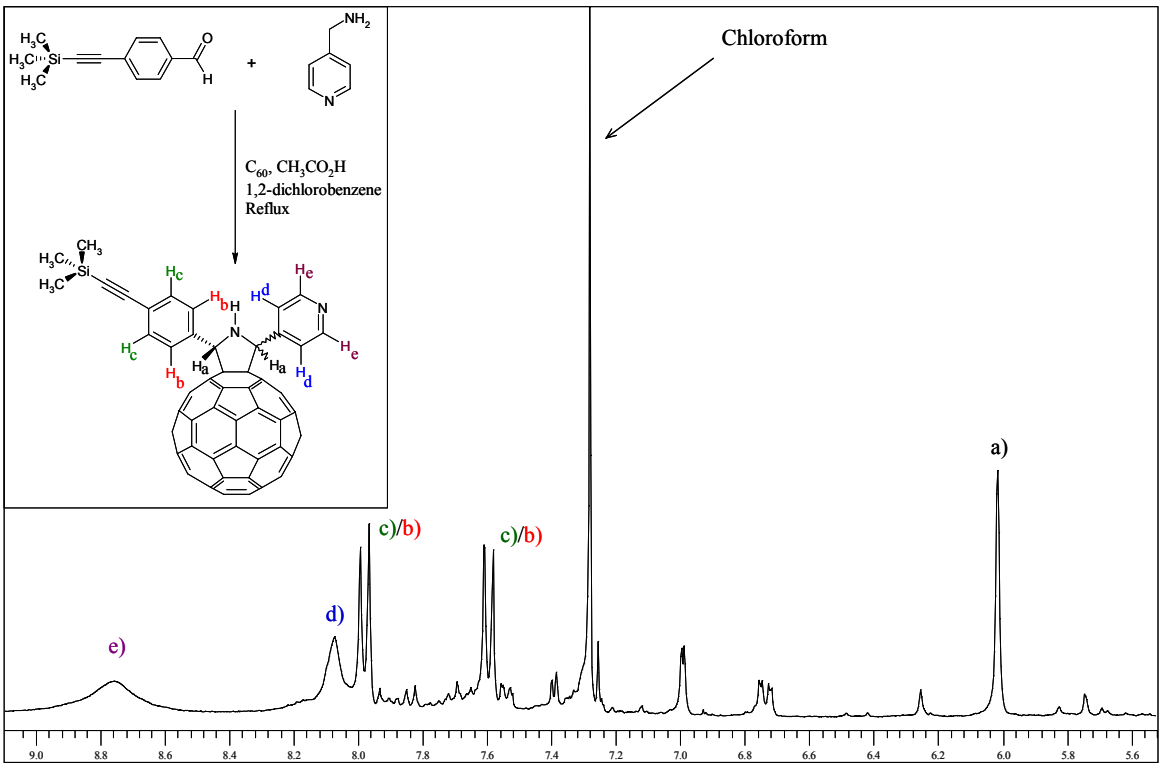

Figure 4.2. 6 *^{1}H-NMR spectrum of pyridyl-fullerene derivatives, impurities are clearly visible in the spectrum, even after purification and unresolved pyridyl signals (d and e) due to diminished rotational degrees. Inset: reaction pathway to synthesize the 2-[4'-pyridyl]-5-[4'-(trimethylsilyl)ethynyl]phenyl-3,4-fulleropyrrolidine.*

The synthesis of N-(4'-pyridylmethyl)-glicine was carried out following the pathway depicted in the Scheme 4.2.8. After a nucleophylic attack of the primary amine to the ethyl-iodo-acetate, the hydrolysis of the ethyl esther affords the desired compound as a very hygroscopic pale yellow powder, that in the presence of moisture starts to become a sticky oil, insoluble in

chloroform, but soluble in methanol. Both the final product and the respective ethyl ester were characterized through ^{1}H-NMR analysis, while only for the ester it was possible to carry out a GC-MS analysis, which shows the peak corresponding to the molecular weight with a mass/charge ratio of 194. The final product was obtained with an overall yield of 77% relative to the ethyl-iodo-acetate. The new glicine derivative was first used for the synthesis of N-(4'-pyridylmethyl)-2-[4'-(trimethylsilyl)ethynyl]phenyl-3,4-fulleropyrrolidine, carried out in anhydrous toluene, under an inert atmosphere (Scheme 4.2.9). Even in this case the protecting group trimethylsilyl was not removed in order to confer a mayor solubility to the compound. After purification on silica gel column, eluting with $CHCl_3$/toluene, 1:1 ratio, the desired product was recovered with 32% yield. The decreased yield comparing to the other functionalizations of C_{60} could be ascribed to the formation of fullerene bis adducts or to other by-products in general.

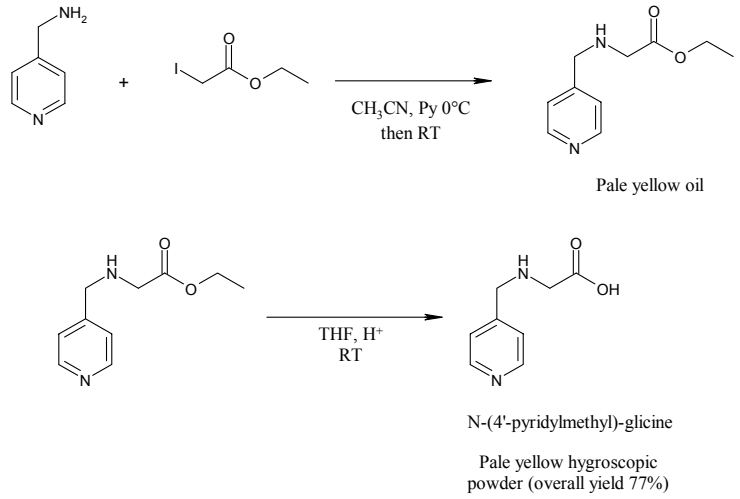

Scheme 4.2. 8 *Reaction pathway to N-(4'-pyridylmethyl)-glicine*

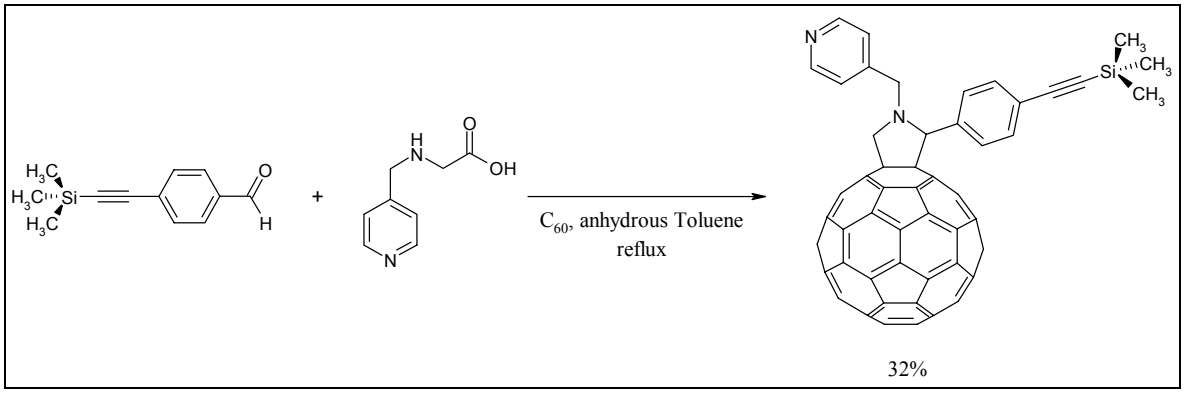

Scheme 4.2. 9 *Condensation reaction to obtain the N-(4'-pyridylmethyl)-2-[4'-(trimethylsilyl)ethynyl]phenyl-3,4-fulleropyrrolidine*

The same identical reaction conditions were used to synthesize the desired porphyrin-fullerene compound with a pyridyl moiety as anchor unit, usinig the porphyrin **1**. This time, after purification, the desired product was recovered in a 50% yield. The triad and respective fullerene reference compound were characterized through MALDI-TOF and ^{1}H-NMR analyses.

The fullerene reference compound shows very good solubility in solvents like chloroform and toluene whilst the porphyrin-fullerene-pyridyl triad is quite reluctant to dissolve in toluene, while its solubility in chloroform is good enough to allow NMR analysis. This study reveals a constrained geometry of the pyridyl group outlined by the presence of two doublet ascribed to the methylene protons in both compounds. The congested geometry denies the free rotation around the nitrogen-methylene bond in the pyrrolidine ring (Figure 4.2.7).

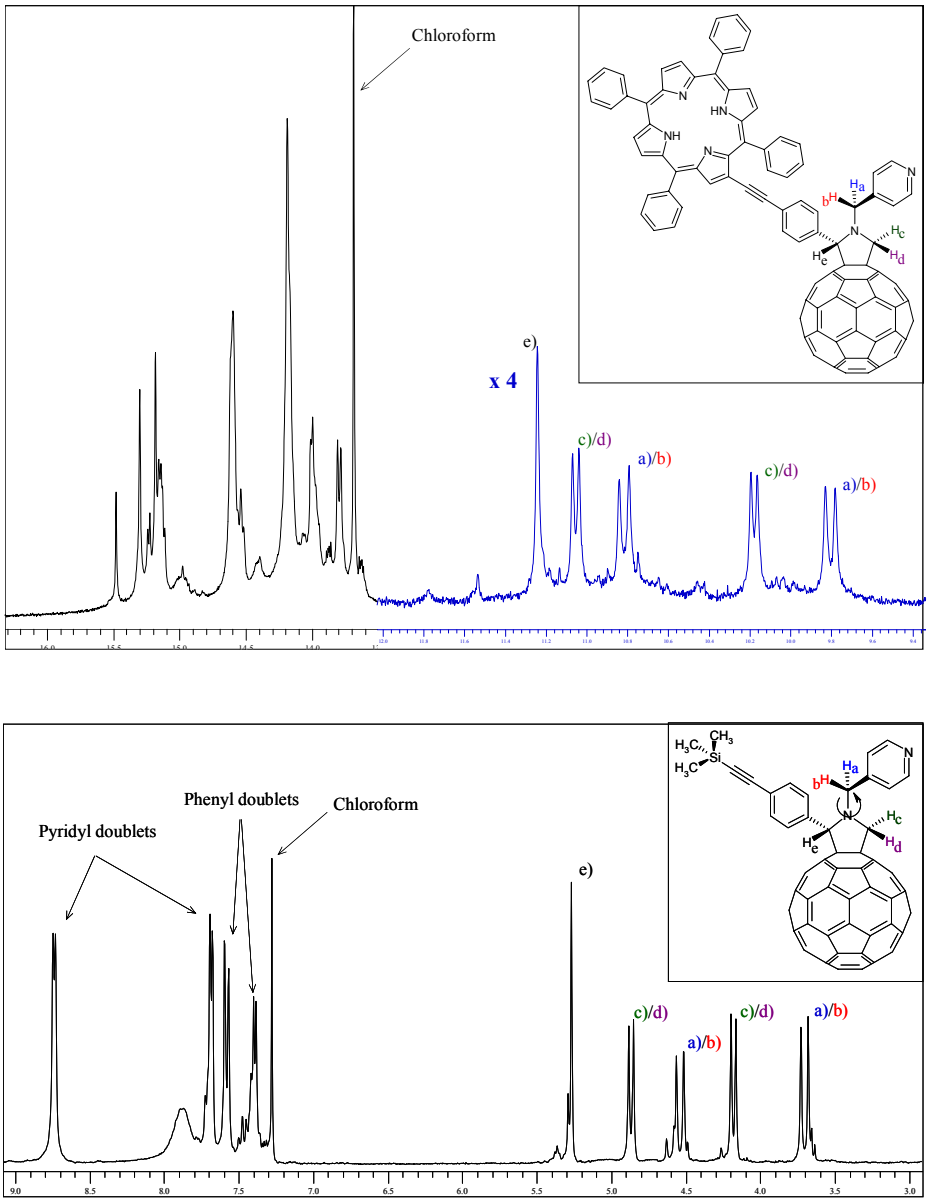

Figure 4.2. 7 *^{1}H-NMR of porphyrin-fullerene-pyridyl triad (upper part) and N-(4'-pyridylmethyl)-2-[4'-(trimethylsilyl)ethynyl]phenyl-3,4-fulleropyrrolidine (lower part)*

Taking in consideration the NMR data, it is possible to conclude that despite the presence of a methylene subunit between the pyrrolidine nitrogen and the pyridyl ring, there are not sufficient

free conformational degrees so that the porphyrin-fullerene-pyridyl triad (H_2P-C_{60}-Py) could be considered as a rigid subunit, which, after the zinc insertion, can self assembly into low flexible molecular wire as reported in the following Scheme 4.2.10.

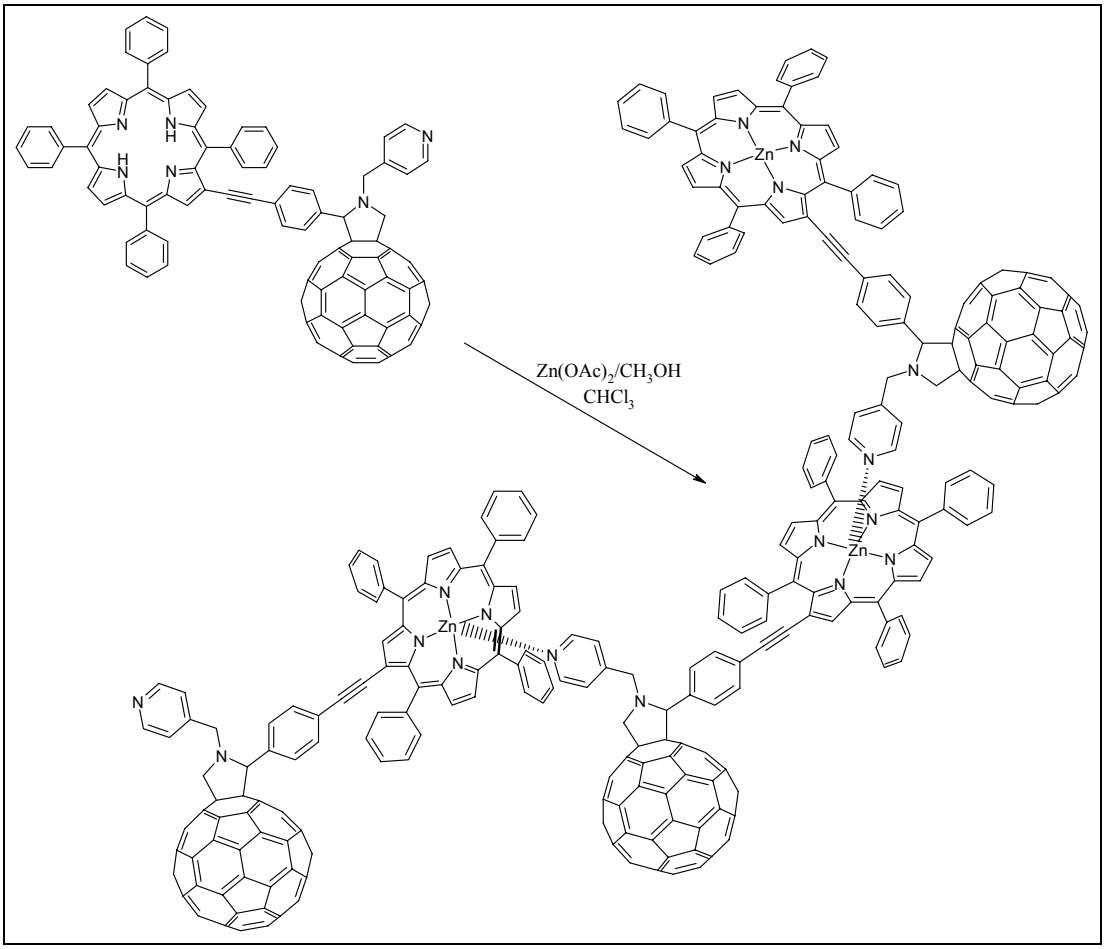

Scheme 4.2. 10 *Zinc insertion into porphyrin-fullerene-pyridyl triad leads to the formation of self assembled oligomer. In the scheme is represented a three subunits wire.*

The self-assembling reaction is immediately evident: during the zinc insertion reaction the chloroform solution turns gradually into a green suspension, where the precipitate is made of insoluble oligomers. The respective porphyrin-fullerene dyad without pyridyl pendant (Compound **5**) after the zinc insertion shows a red-violet colour in chloroform solution but in coordinating solvent such as benzonitrile the colour changes in green, highlighting the axial ligation of a solvent molecule. The same change happens for all the zinc porphyrin derivatives (Compound n° **1**, **2**, **3** and **4**). The extremely reduced solubility of ZnP-C_{60}-Py triad did not allow the characterization through ^{1}H-NMR analysis in chloroform solution to corroborate the self-assembly, observing the upfield shift for the chemical shifts of the protons belonging to the pyridine moiety[145]. The pyridine group offers another advantage; the further derivatization of

the heterocyclic ring into the corresponding methylpyridinium salt. The presence of a net positive charge near the fullerene moiety could, in principle, influence the charge separated state because of its proximity to the C_{60} excited radical anion, generated as product of the photoinduced electron transfer. However the meaning advantage of the methylpiridinium salt is the possibility to use the positive charge to order the triad into self assembled monolayer, using the coulombic interaction and this should offer the opportunity to build organic solar cell for photocurrent generation. The methylation of the ZnP-C_{60}-Py system was carried out using a small quantity of the product to test the experimental condition. The reaction was carried out following the literature procedure[146] but changing the solvent due to the low solubility of the compound (Scheme 4.2.11).

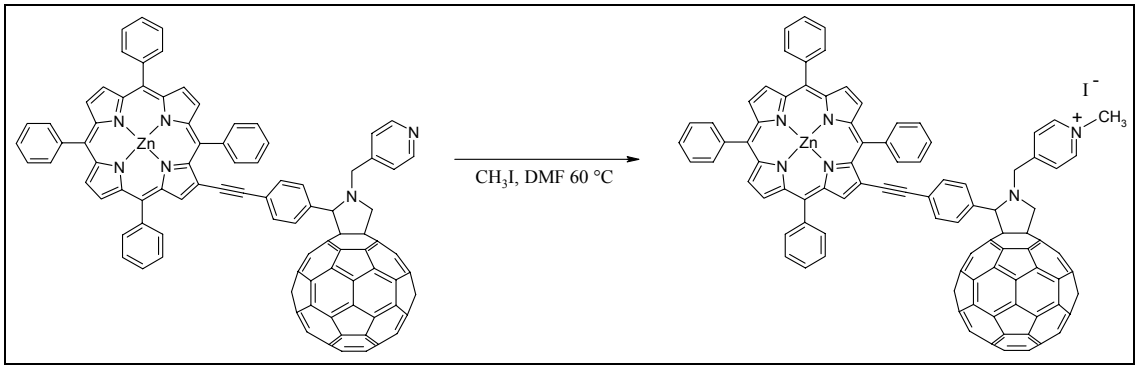

Scheme 4.2. 11 *Methylation reaction of ZnP-C_{60}-Py system carried out in DMF solution*

The conversion is almost quantitative, but the obtained product is in quantity too low to be adequately characterized. Taking into consideration the fact that ferrocene compounds were often used to further increase the lifetime of charge separated state, acting as last electron donor in porphyrin-fullerene systems[133], a ferrocene ligand, bearing pyridine moiety, was synthesized as further piece to be used in potential application for organic solar cells. The starting compound, the ferrocenyl carboxylic acid, was converted into the respective acyl chloride and then the 4-aminomethylpyridine was used to give nucleophylic substitution in order to obtain the final product. Because of the low stability of the ferrocenyl acyl chloride, it is moisture sensitive and goes back to the carboxylic acid compound, the final product was synthesized adopting one pot strategy, without the isolation and the purification of the acyl chloride. To an anhydrous dichloromehane solution of ferrocenylcarboxilic acid PCl_5 was added, in the presence of pyridine. Once that the acid was completely converted into the respective acyl chloride a second dichloromethane solution of 4-aminomethylpyridine was added dropwise. The product was purified over a silica gel plug eluting with diethylether, to remove the

remaining carboxylic acid and then with ethyl ether/methanol, 1:1 to recover the reaction product as dark orange powder in a 55% yield (Scheme 4.2.12).

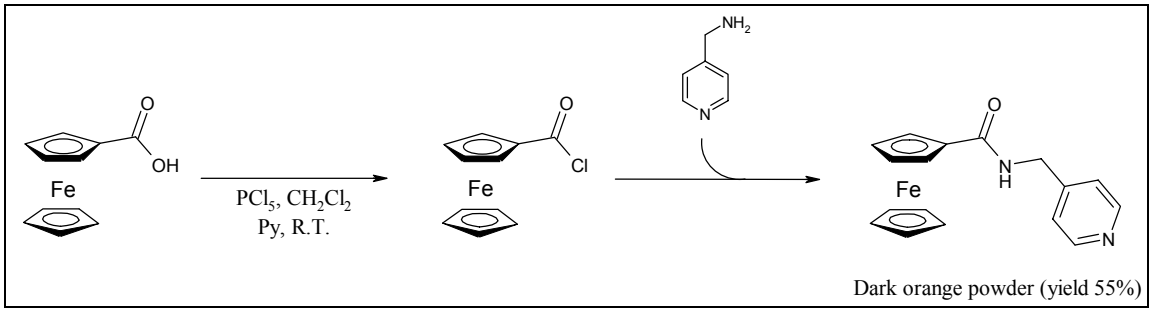

Scheme 4.2. 12 *One pot synthesis of [(4'-pyridylmethyl) aminocarbonyl]Ferrocene*

As outlined before, this coordinating ferrocene moiety can be used as potential last electron donor in all the zinc derivatives of the porphyrin-fullerene systems presented up to now, with the aim to further increase the lifetime of the excited charge separated state.

As reported elsewhere[147] (See Chapter 3 paragraph 3.4.1), some simple porphyrin or chlorine-fullerene compounds show very long lifetime of charge separated state, even if there is only one electron transfer step from the electron donor side to the acceptor donor side, so long values are interpreted on the basis of a lack of activated nuclear tunnelling for back electron transfer due to the constrained geometry of the dyad[147a]. Keeping this in mind it was decided to synthesize a sort of new chelating β-modified porphyrin that, after condensation with C_{60} affords a completely frozen porphyrin-fullerene dyad. To do that it was necessary to introduce two aldehydic functions on the tetrapyrrole ring and to pursue our aim we have synthesized the 2,3-dibromo-5,10,15,20-tetraphenylporphyrin (2,3-dibromo-H_2-TPP). It was not possible to adopt the simple radical bromination reaction of tetraphenylporphyrin because of the impossibility to direct the bromination exclusively on one pyrrole ring, so we chose to follow the well known protocol which introduces a nitro group on a β-pyrrole position, to direct the following bromination in an exhaustive manner only on the opposite pyrrole ring. After the bromination reaction, the nitro group was removed through selective reduction and subsequent oxidative elimination reaction. The reaction conditions are equal to those reported in literature[148] and the complete pathway that leads to the 2,3-dibromo-H_2-TPP is reported in the Scheme 4.2.13. Five steps are necessary to obtain the desired product, and any step gives yields ranging from 70% to 95%, assuring a good quantity of the final product.

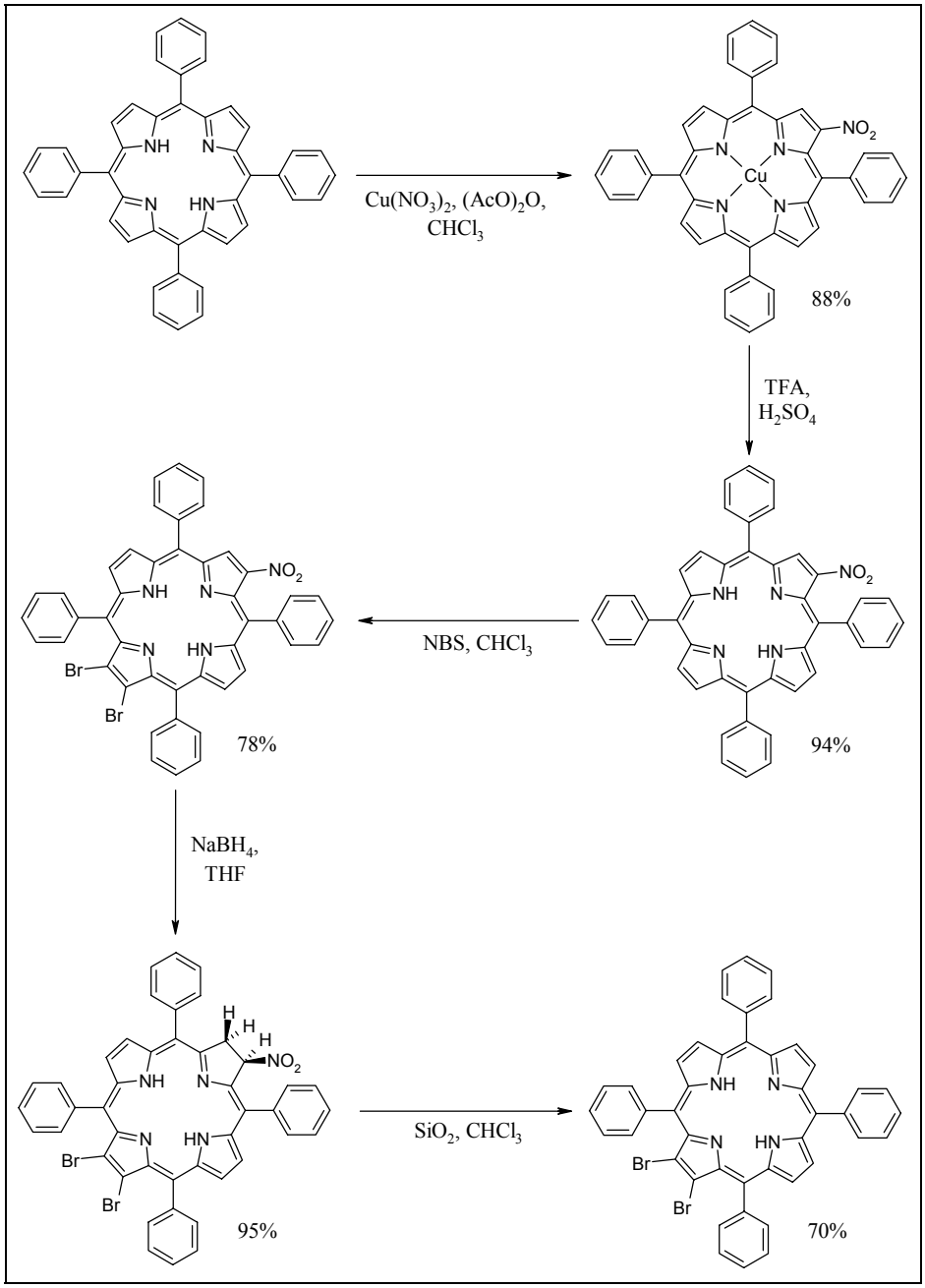

Scheme 4.2. 13 *Synthetic path to obtain the 2,3-dibromo-H_2-TPP*

As for the synthesis of the compound number **1** also in this case the $Pd(dba)_2/AsPh_3$ catalytic system[142] was chosen to carry out the coupling reaction with 4-ethynylbenzaldehyde in the same reaction condition (Scheme 4.2.14). After chromatographic separation, the product was isolated in a 21% yield and characterized through FAB-MS analysis, which shows a clearly peak at a mass/charge ratio equal to 870 corresponding to the porphyrin molecular weight and through ^{1}H-NMR measurements. In the nuclear magnetic resonance spectrum the two

symmetric doublet (8.83 and 8.88 ppm) and one singlet signal (8.73 ppm) of the β-pyrrole proton pattern evidence the C_2 symmetry of porphyrin.

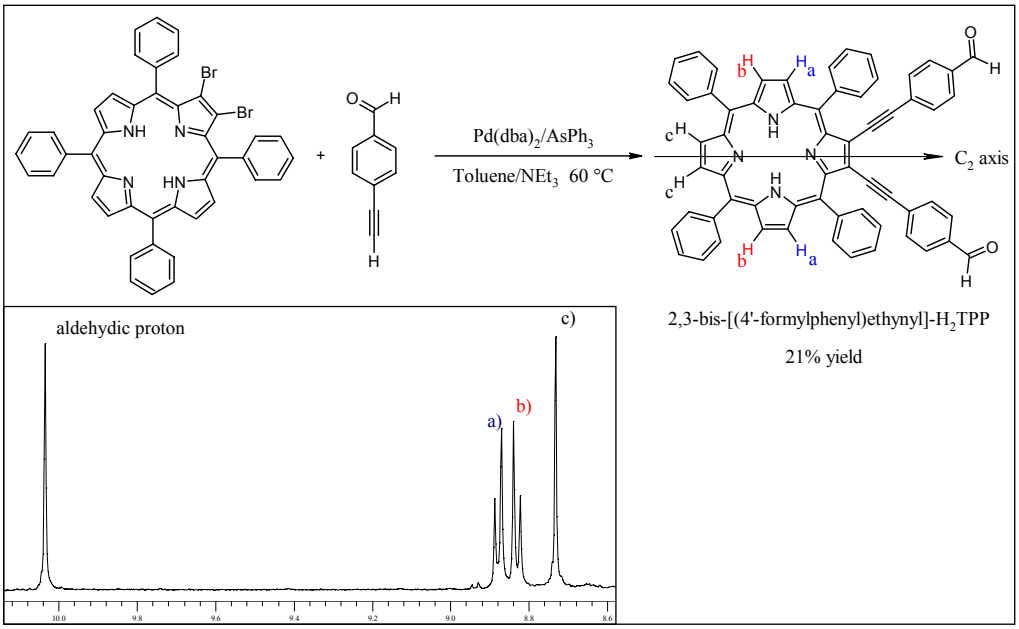

Scheme 4.2. 14 *Synthesis of 2,3-bis-[(4'-formylphenyl)ethynyl]-H_2TPP. Inset: β-pyrrole proton pattern of porphyrin, reflecting the C_2 symmetry*

A so low yield respect to the analogue monosubstituted porphyrin **1** is a not so negligible problem, so we have tried to understand for which reason a series of by-products are produced in an apparently so simple coupling reaction. The first aspect to understand is if the by-products come from a parallel reactions or from a degradation of the desired porphyrin under reaction condition. A little quantity of 2,3-bis[(4'-formylphenyl)ethynyl]-H_2TPP porphyrin was left to react together with $Pd(dba)_2/AsPh_3$ system, in the same identical condition reported in the Scheme 4.2.14. After 24 hours no reaction products were identified and the porphyrin remained unchanged. However one of the by-product formed in the synthesis of the 2,3-bis[(4'-formylphenyl)ethynyl]-H_2TPP was isolated as blue-purple needles (Figure 4.2.8). The MALDI-TOF spectrum of this compound gives a very sharp peak at 870, a molecular weight that could be considered identical to that of the desired product, moreover the NMR spectrum outlines the presence of two different aldehydic proton signals, a β-pyrrole pattern similar to that of the 2,3-bis[(4'-formylphenyl)ethynyl]-H_2TPP, but with two additional doublets at 8.47 and 9.18 ppm. Moreover a much more interesting aspect is the UV-vis spectrum of isolated by-

Figure 4.2. 8 *Blue-purple needles of isolated by-product*

product, that has an extremely shifted and broadened Soret band, indicating an extension of conjugation or most probably a not planar and very distorted tetrapyrrole ring. All these data lead us to suppose that the hypothetical by-product could be the porphyrin depicted in the Figure 4.2.9, together with the aforementioned analyses.

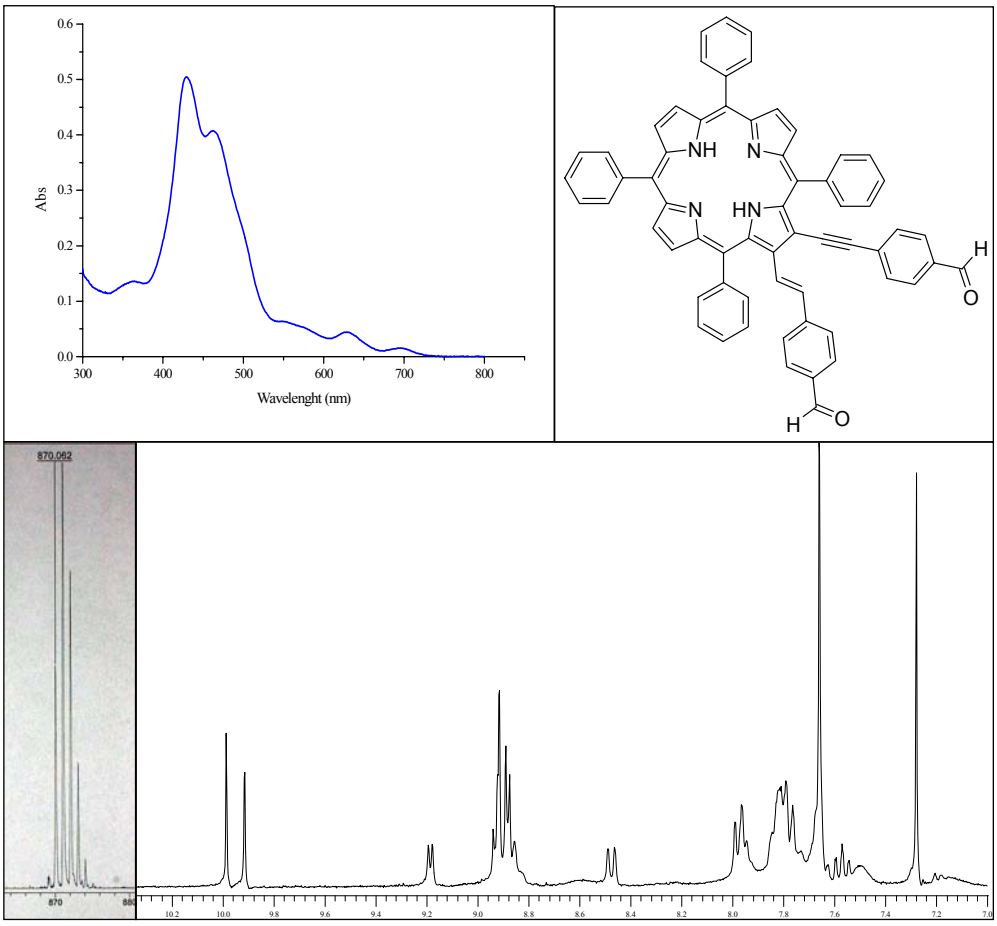

Figure 4.2. 9 *Hypothetical by-product of reaction depicted in the Scheme 4.2.14 and relative UV-visible, ^{1}H-NMR and MALDI-TOF analyses*

Taking into account these results it could be supposed that the presence of two adjacent bromines induce parallel reactions, that afford by-products with very similar structures. Further studies are necessary to clarify all the problems involving this coupling reaction.

The double substituted porphyrin was used for condensation reaction with fullerene and N-methylglicine, in order to verify the possibility to have a sort of cyclic porphyrin-fullerene bis-adduct or a system bearing one β-disubstitute porphyrin, covalently linked to two fullerene moieties. On the basis of energetic and entropic considerations we would expect the fact that after a first condensation of one branch of the substituted porphyrin, the intramolecular reaction should be favourite respect to an intermolecular reaction, so it should happen that the cyclic bis-adduct could be the only reaction product. As reported in the literature, the fullerene can show

several addition patterns for the bis-adduct products[149]. Despite the branches rigidity in the porphyrin compound it is plausible to obtain more than one products (Scheme 4.2.15).

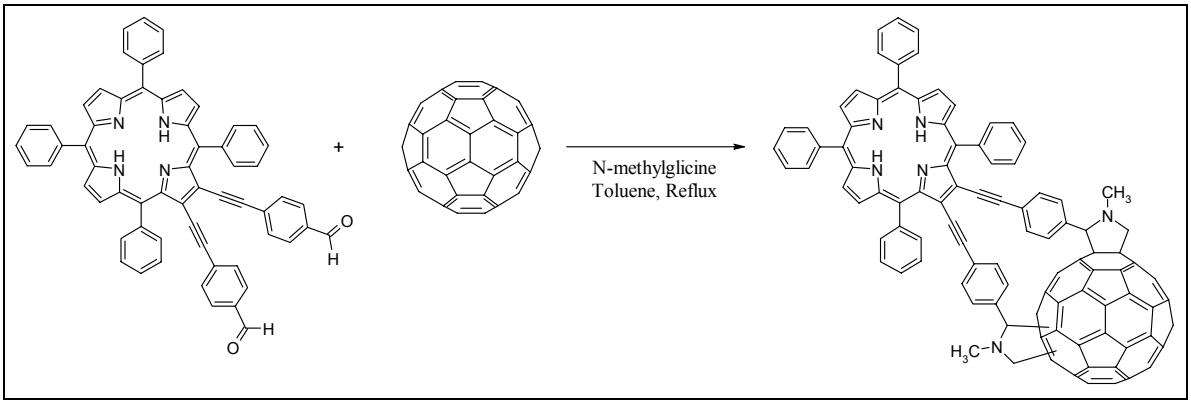

Scheme 4.2. 15 *Synthesis of cyclic porphyrin-fullerene bis-adduct through Prato reaction*[139]

The porphyrin starting product disappears almost completely within 18 hours and after purification on a silica gel column eluting with toluene, three different products were isolated. A first preliminary UV-visible analysis in toluene solution shows that all the three products present a blue-shifted Soret band (438 nm) comparing to that of the starting porphyrin compound (448 nm) in toluene solution. Furthermore it is clearly visible the fullerene moiety absorption between 350 and 300 nm (Figure 4.2.10). On the basis of the experimental data that will be discussed later, some hypothesis will be done about the nature of the three porphyrin-fullerene compounds. First of all it is important to outline that the introduction of two 4'-formylphenylethynyl groups on the same pyrrole ring, deeply affects the UV-visible spectrum of the new porphyrin: the Soret band at 448 nm in toluene solution is consistently red shifted and broadened comparing to the Soret band of H_2TPP (418 nm). Such effect is partially due to the extension of conjugation along the two branches and partially to a possible distortion from planarity of the tetrapyrrole ring. In the UV-visible spectra of isolated reaction products is evident a different absorption shape of the fullerene moiety: the compounds 1 and 3 show an increasing absorption trend starting from 350 nm and arriving at 300 nm, while the compound 2 presents a plateau around 320 nm. These differences could arise from a different addition pattern as reported in the literature in an analogue work, where bisaldehyde tether compounds have been used to synthesize fullerene bis-adduct derivatives[150]. In that work is outlined how different absorption spectrum corresponds to a different addition pattern on the fullerene surface. These differences are clearly visible between 550 and 400 nm, but in our case this spectral window is not useful because it is dominated by the porphyrin absorptions. NMR measurements are obviously necessary for a fully characterization of compounds.

Unfortunately only the compound number 2 is enough soluble in chloroform to afford a good resolution, revealing a particular proton pattern of pyrrolidine ring as depicted in Figure 4.2.11: two magnetically different etherocyclic rings are present as reported in the aforementioned work for a trans-3 bis-adduct[150]. Further solvents must be tested to find the right solution condition to carry out NMR measurements for compound 1 and 3.

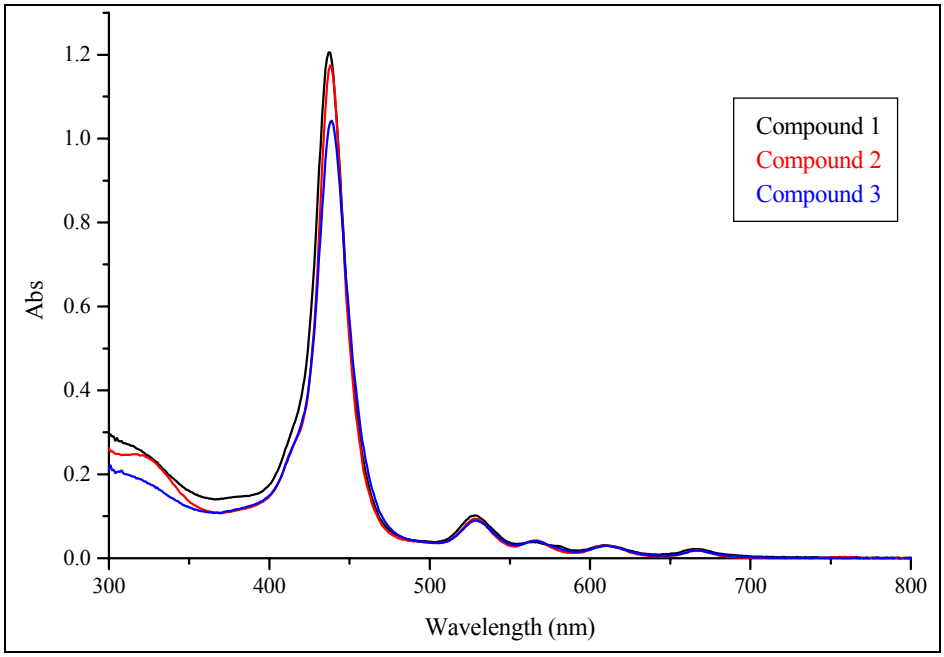

Figure 4.2. 10 *UV-visible spectra in toluene solution of porphyrin-fullerene compounds coming from reaction reported in the scheme 4.2.15*

The MALDI-TOF analyses of these three porphyrin-fullerene adducts show signals with a mass/charge ratio corresponding to a 1644 for sample number 1 and 2 (Figure 4.2.11), undoubtedly equal to the molecular weight of the cyclic porphyrin-fullerene bis-adduct.

For sample 3 is visible only the ions corresponding to a characteristic fragmentation with a molecular base peak equal to 924 due to the loss of the entire fullerene sphere and the following losses of methyl and methylene groups. All the results discussed up to now lead to formulate the hypothesis that the cyclic porphyrin-fullerene bis-adducts could be trans-3 or trans-4 isomers. Because the rigidity of the porphyrin branches it is possible to exclude the formation of cis or equatorial isomers. Although only two hypothetical isomers are possible we have to remember that one generic fullerene 2-substituted pyrrolidine bis-adduct can exist with three different diasteromeric configurations: *R*,*R*, *S*,*S* or *R*,*S* due to the presence of the chiral carbon atom number 2 in the pyrrolidine ring. Further studies are necessary to confirm without any doubts, that cyclic porphyrin-fullerene bis-adduct have been obtained. However a computational study supports our hypothesis, in fact the geometry optimization of trans-3 and

trans-4 cyclic porphyrin-fullerene bis-adducts, carried out adopting the MM+ force field in the HyperChem software, does not evidence a constrained geometry for these isomers and neither a particular distortion of the tetrapyrrole ring (Figure 4.2.12).

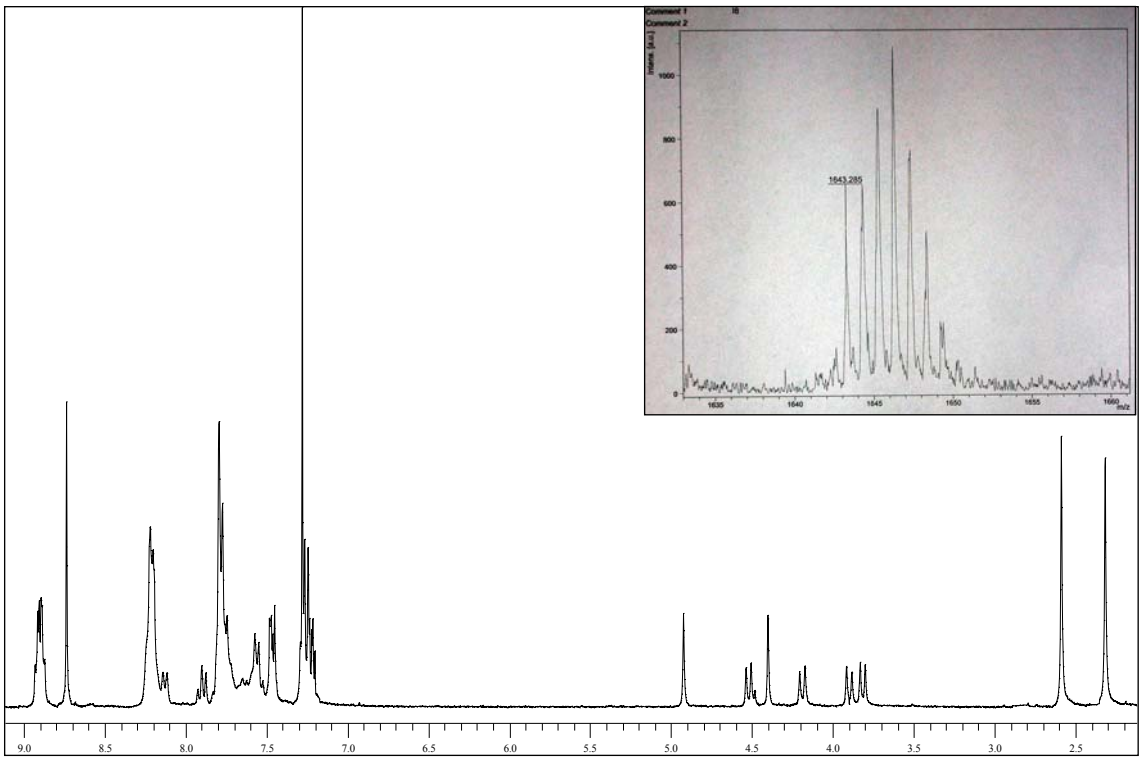

Figure 4.2. 11 *^{1}H-NMR and MALDI-TOF spectra of cyclic porphyrin-fullerene bis-adduct number 2*

The structures depicted in the Figure 4.2.12 have a *R,S* diastereomeric configuration but this is an our arbitrary choice because there are not experimental evidences in this direction. It has been decided to optimize these two configurations only to verify if any structural constrain or geometry distortion are present. A particular aspect that must be discussed is the blue shift of the porphyrin Soret band upon functionalization with fullerene. The distance between the two moieties is large enough to exclude a strong interaction between porphyrin and fullerene, moreover in a directly β-linked porphyrin dyad the perturbation of the porphyrin absorption determines a Soret red shift of the spectrum of 6-7 nm[151]. In our case we suppose that a so strong shift arises from the conformation of the two porphyrin branches: while in the porphyrin these two substituents are tilted but not completely perpendicular to the porphyrin plane, in the trans-4 and trans-3 bis-adduct they are clearly perpendicular to the tetrapyrrole ring (See optimization geometry in Figure 4.2.13 and 4.2.14). So in the first case the porphyrin aromatic ring could undergoes to a deviation from planarity and probably it is also present a little bit longer extended π-conjugation along the branches. These last two aspects could induce in the

porphyrin a much more red shifted and broadened Soret band respect to those observed in the respective porphyrin-fullerene bis-adducts, as depicted in the UV-visible spectrum of Figure 4.2.15.

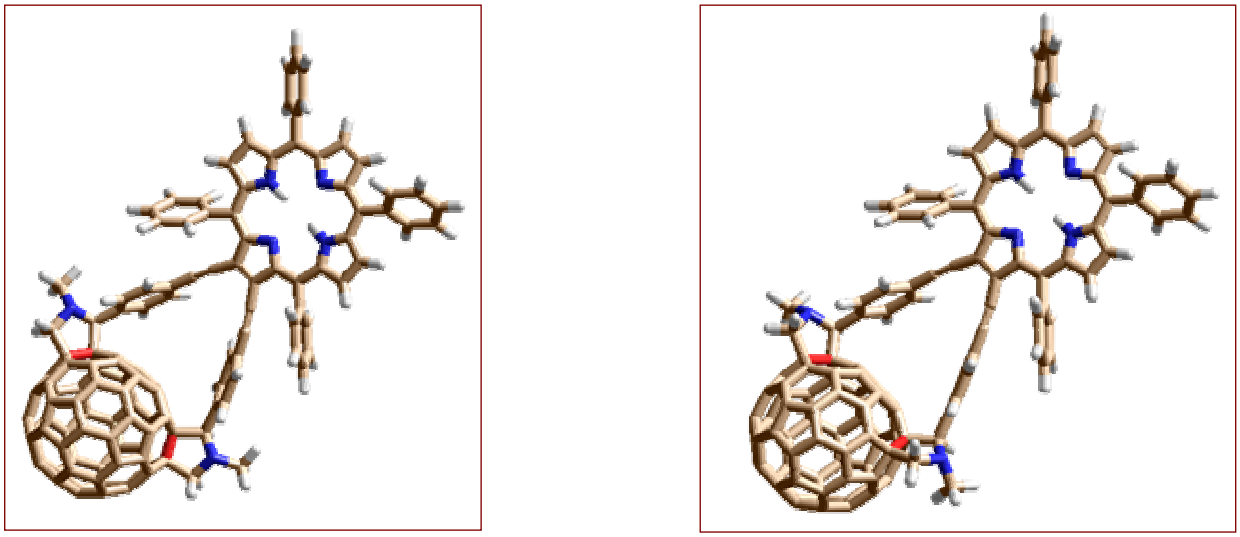

Figure 4.2. 12 *Optimized geometry structures of trans-3 (on the left) and trans-4 (on the right) cyclic porphyrin-fullerene bis-adducts, the addition pattern is highlighted in red*

Although it is necessary to resolve the low yield drawback that affects the coupling reaction for the porphyrin synthesis, these cyclic bis-adducts represent new porphyrin-fullerene compounds with a frozen geometry. In fact there are not rotational free degrees between porphyrin and fullerene moieties and in principal this aspect could allow to evaluate how conformational effects and constrained geometry can influence the electron transfer process as suggested by A. Harriman[147a].

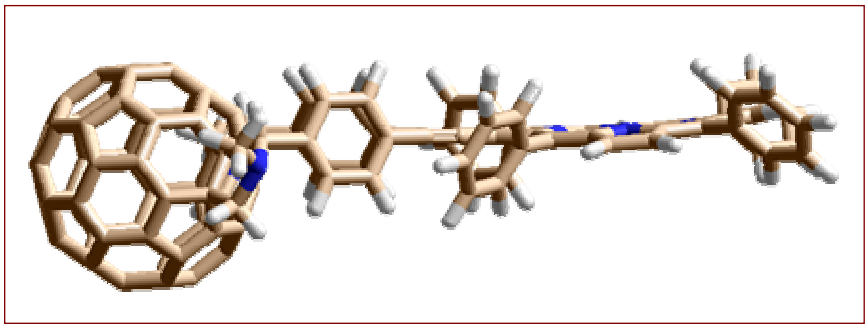

Figure 4.2. 13 *Side view of trans-4 porphyrin-fullerene cyclic bis-adduct. The phenyl rings of two β-substituents are clearly perpendicular to the porphyrin plane that does not show particular deviation from the planarity*

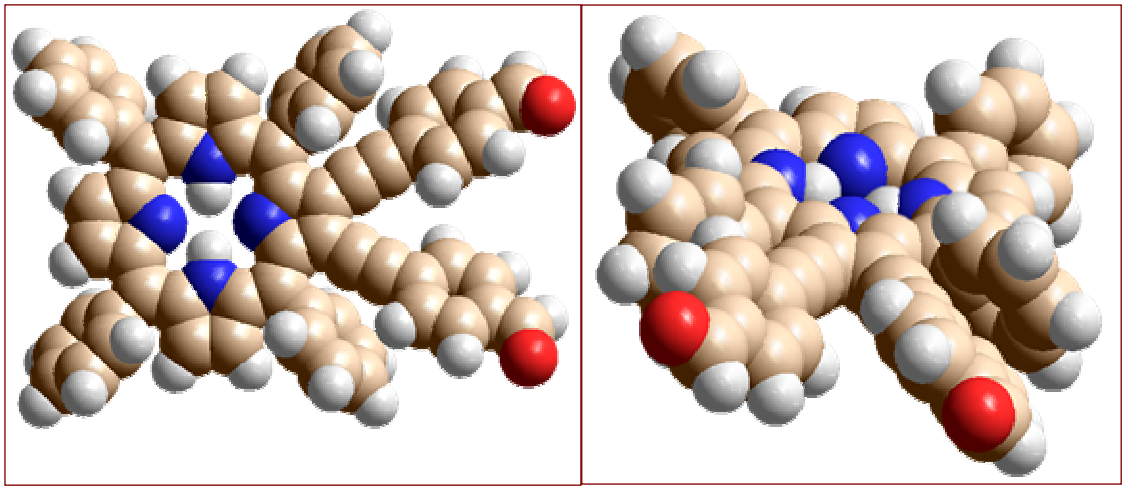

Figure 4.2. 14 *Optimezed structure, with a PM3 method, of 2,3-bis-[(4'-formylphenyl)ethynyl]-H_2TPP top view (on the left) and side view (on the right). It is visible in the side view (on the right part) how the substituent phenyl rings are slighty tilted and not perpendicular to the porphyrin plane.*

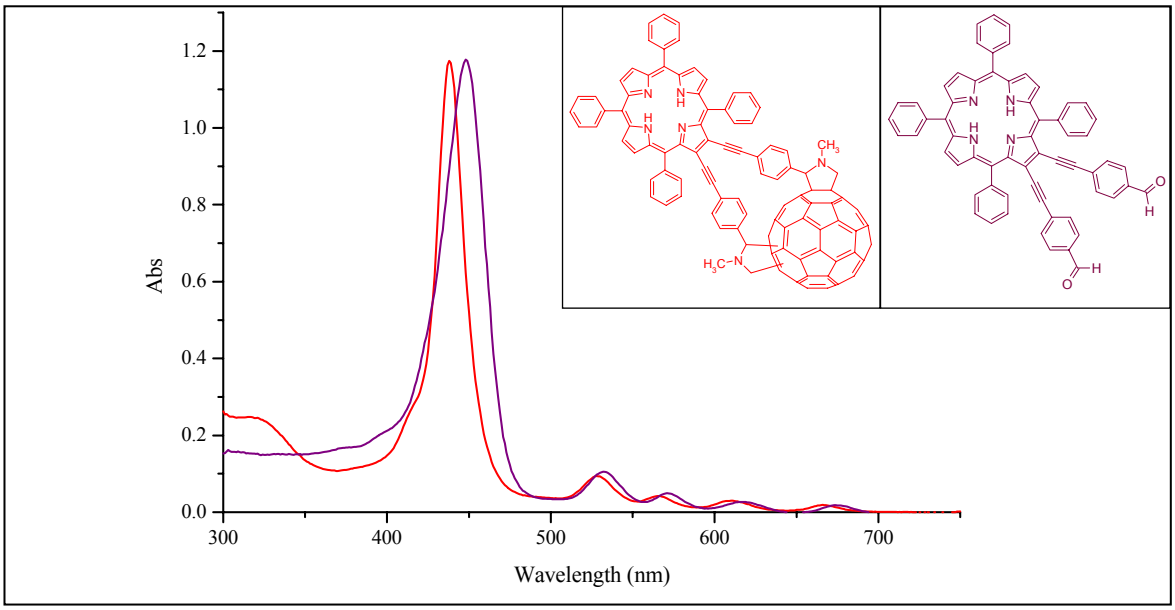

Figure 4.2. 15 *UV-visible spectra in toluene solution of β-di-substituted porphyrin and porphyrin-fullerene cyclic bis-adduct number 2*

In the next paragraph a complete characterization of porphyrin-fullerene dyad number **5**, together with reference compounds, will be reported. ^{1}H-NMR and ^{13}C-NMR spectra, fluorescence measurements, cyclic voltammetry and UV-visible studies will be discussed in details in order to point out the peculiar aspects of new porphyrin-fullerene structure, while in other sections the preliminary studies regarding both the porphyrin-wire-fullerene systems

(Compounds number **6** and **7**) and the self-assembling porphyrin-fullerene dyad will be taken into consideration.

4.3. Complete Study of a New β-Ethynyl Linked Porphyrin-Fullerene Dyad

The new β-modified porphyrins and corresponding porphyrin-fullerene compounds were deeply investigated through NMR studies, cyclic voltammetry, fluorescence and UV-visible measurements[152] the structure of the systems discussed in this paragraph are reported in Figure 4.3.1. With the aim to simplify the discussion each compound will be indicated with the names reported in the aforementioned figure. It is useful to start the discussion taking into consideration the UV-visible absorption spectra in toluene solution of the reported compounds. These spectra show interesting characteristics concerning the porphyrin systems. In Table 4.3.1 the spectral features of all the new compounds are reported, both in toluene and THF. The spectra of systems A and B in toluene solution present a broad Soret band, shifted to higher wavelengths compared with the Soret band of H_2-TPP (418 nm) as it is possible to see in the Figure 4.3.2. The Soret band of system B is located at 428 nm, while that of system A at 432 nm, with values of the molar extinction coefficient of 2.25×10^5 and 2.09×10^5 $M^{-1}cm^{-1}$ respectively, while H_2P-C_{60} shows the Soret band located at 429 nm with a molar extinction coefficient of 2.16×10^5 $M^{-1}cm^{-1}$. Furthermore in this last spectrum, a broad band, located between 300 and 350 nm, due to the C_{60} moiety is present (Figure 4.3.2).

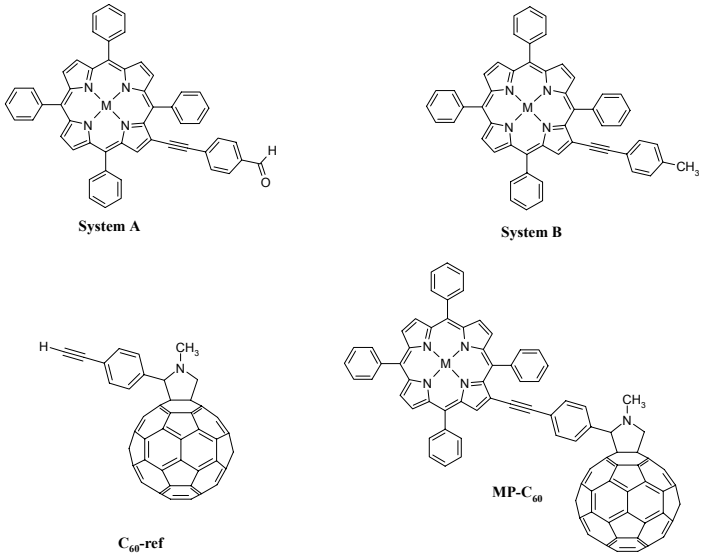

Figure 4.3. 1 *Compounds discussed in the present paragraph. M = 2H, Zn*

In our opinion, the position of the Soret bands and the ε values of such absorptions, compared with those of H_2-TPP, are influenced by the electronic conjugation of the substituent in the β-pyrrole position. The smaller value of ε in system A derives from the electron-withdrawing effect of the aldehydic group. The extension of conjugation based on the resonance effect also justifies the shift of the Soret band to higher wavelengths, if compared with the shift of the band of system B. This observation can be justified by the presence of an electron-donating effect of the porphyrin toward the electron-withdrawing aldehydic group of system A, generating a "push-pull" effect that is transmitted through the carbon-carbon skeleton of the ethynylenephenylene subunit. This effect lowers the electron density of the tetrapyrrole ring, in turn lowering the ε value of system A. On the contrary, in H_2P-C_{60}, only an overall electron-

withdrawing effect due to the presence of the C_{60} moiety can be observed. Furthermore, the Q-bands of all the examined compounds are slightly shifted.

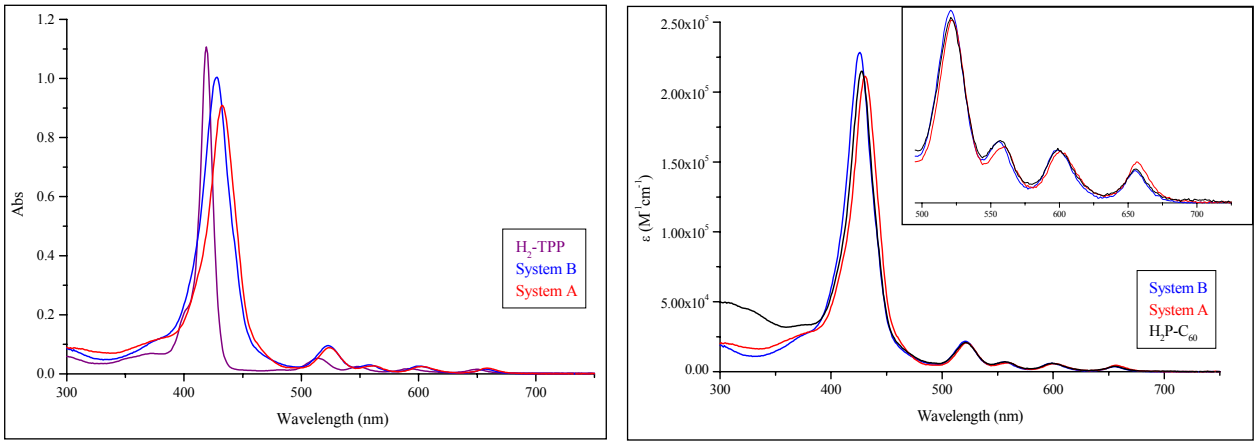

Figure 4.3. 2 *UV-visible absorption spectra in toluene solution of H_2-TPP, System A and System B on the left. A comparison of System A, System B and H_2P-C_{60} on the right part, in the inset the Q-bands absorption is reported.*

The introduction of zinc into the macrocycles produces an increase in the electron density of the rings, giving very similar values of molar extinction coefficients in both porphyrins, 2.38×10^5 and 2.39×10^5 $M^{-1}cm^{-1}$ for systems A and B, respectively, despite the 4 nm difference in the Soret band, 434 nm for system B and 438 nm for system A. The spectra of the free bases and zinc complexes of system B and porphyrin-fullerene dyad are virtually superimposable as illustrated in the Figure 4.3.2 (right part) and in the Figure 4.3.3. From this last figure it is also discernible that the ZnP-C_{60} spectrum is the sum of the Zn-system B spectrum and of the N-methyl-2-(4'-ethynyl)phenyl-3,4-fulleropyrrolidine compound (C_{60}-ref) spectrum . From such data it is possible to make the first conclusions: as it has been expected the new porphyrin compounds show an extension of conjugation along the β-substituent, but much more surprisingly the data suggest that the extension seems to arrive up to the aldehydic group through the carbon skeleton, further studies were necessary to confirm that and they will be reported below. Taking as reference compound the porphyrin system B, it is important to note that the porphyrin and fullerene moieties in the dyad can be considered as non interacting cromophores,

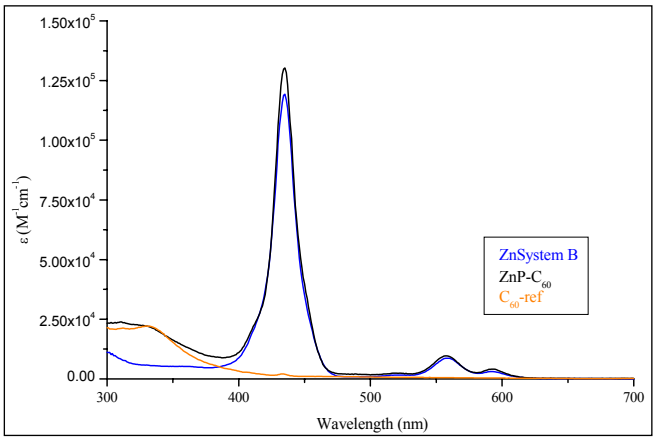

Figure 4.3. 3 *Comparison of the UV-visible spectra in toluene solution of ZnP-C_{60}, C_{60}-ref and Zn-System B*

since no significant shifts were noted in the absorption spectrum of the porphyrin part upon addiction of the fullerene moiety, an aspect that will be pointed out also in the other following studies.

	λ_{max} ($\varepsilon \times 10^{-4}$)	
Compound	Toluene	THF
System A	311(2.17), 432(20.9), 525(2.03), 560(0.62), 602(0.58), 659(0.46)	428(20.2), 522(1.92), 558(0.59), 601(0.54), 658(0.40)
System B	428(22.5), 523(2.15), 558(0.60), 600(0.59), 657(0.36)	424(20.1), 521(1.89), 556(0.62), 599(0.52), 656(0.32)
H_2P-C_{60}	300(4.88), 429(21.6), 523(2.1), 558(0.71), 601(0.62), 657(0.38)	300(4.6), 425(19.1), 521(1.85), 556(0.65), 600(0.54), 656(0.34)
Zn-System A	311(2.17), 438(23.8), 559(1.86), 596(0.96)	437(22.6), 566(1.72), 603(0.87)
Zn-System B	434(23.9), 558(1.75), 592(0.63)	434(24.7), 564(1.67), 600(0.60)
ZnP-C_{60}	311(4.8), 434(26.1), 558(1.94), 593(0.82)	311(4.5), 435(21.6), 565(1.46), 601(0.62)

Table 4.3. 1 *Spectral features in toluene and THF solution of all the compounds reported in this paragraph*

The cyclic voltammetry studies are useful to confirm the interaction between the porphyrin and the fullerene part and also to further test the effect of substituent. The reduction and oxidation potentials are measured in *ortho*-dichlorobenzene solution. This solvent was purified with several washings with concentrated H_2SO_4 and distilled over P_2O_5 under vacuum prior to use, adopting tetra-*n*-butylammonium hexafluorophosphate, recrystallized from ethyl acetate and dried under vacuum at 40 °C for at least one week. For the measurements a three electrode system was used and consisted of a platinum button working electrode, a platinum wire counter electrode and a saturated calomel reference electrode (SCE). This reference electrode was separated from the bulk of the solution by a fritted-glass bridge filled with a solvent/supporting electrolyte mixture. All the potential reported below are referenced to the SCE. As first results the measurements carried out on the free base porphyrins confirm the influence of the β-substituent on the oxidation potentials. In fact the free base porphyrins of system A and B are characterized by two reversible oxidation processes centered at 1.10, 1.43, and 1.08, 1.44 V, respectively, while in general H_2-TPP shows two reversible oxidations at 1.05 and 1.48 V[153]. The two systems also present two reversible reductions centered at -1.10 and -1.34 V for system A and -1.16 and -1.44 V for system B (H_2-TPP at -1.24 and -1.55 V). The difference of 60 and

100 mV, respectively, for the first and second reduction between the two systems reflects the electron-withdrawing effect[154] of the aldehydic group of system A (See Figure 4.3.4). In general it is possible to discern that the electron-withdrawing aldehydic group tends to lower the reduction potential and to increase the oxidation one, an effect in line with the diminished electron density on the tetrapyrrole ring caused by the aforementioned "push-pull" effect where the porphyrin of system A acts as a donor. The zinc derivatives of both systems shows two reversible oxidations at 0.95 and 1.21 V for system A and 0.93 and 1.17 V for system B, while it is possible to detect only one reversible reduction for both of the compounds at 1.28 and 1.33 V, respectively. The zinc derivatives seem to be quite reluctant to undergo to a second reversible reduction, as it is possible to see in the Figure 4.3.5 (left part). In the reduction wave a shoulder appears around 1.50 V that underlines the difficulty to obtain a second perfect reversible reduction and this behaviour is maintained also in the ZnP-C_{60} dyad. Figure 4.3.5 also illustrates the room temperature cyclic voltammograms of system B, H_2P-C_{60} and C_{60}-ref in DCB, 0.05 M $TBAPF_6$. The free base porphyrin-fullerene dyad undergoes three reversible one electron and one reversible two electron reductions plus two one-reversible oxidations between -2.00 and 1.50 V. The reductions of the H_2P-C_{60} occur at $E_{1/2}$ = -0.66, -1.11, -1.44 and -1.67 V; the $E_{1/2}$ values for the second and third reduction are very close to the $E_{1/2}$ values for the first and second reduction of system B, while the $E_{1/2}$ values for the first and fourth reduction of H_2P-C_{60} are almost identical to those for the first and third reduction of C_{60}-ref. The two-electrons process centered at -1.11 V derives from the overlapping of two reductions, one from system B and one from C_{60}-ref. As

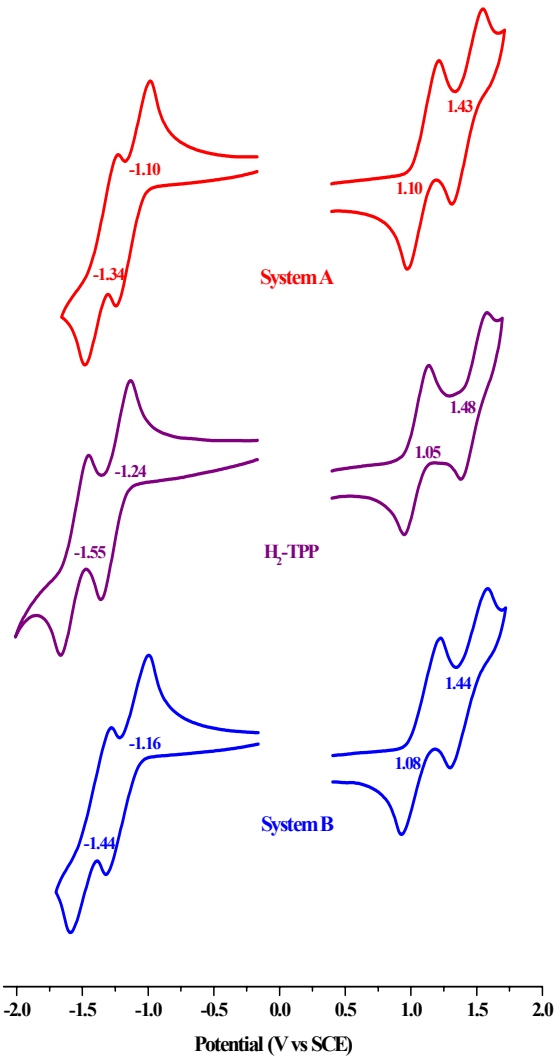

Figure 4.3. 4 *Cyclic voltammograms of free base new porphyrins and H_2-TPP in DCB solution containing 0.05 M $TBAPF_6$*

shown in Figure 4.3.5 the $E_{1/2}$ values for the first and second oxidation of H_2P-C_{60} ($E_{1/2}$ = 1.08 and 1.43 V) occur at virtually identical potential for the first and second oxidation of system B ($E_{1/2}$ = 1.08 and 1.44 V). Such data suggest that the porphyrin and fullerene act as two different and non-interacting chromophores, retaining their own electronic and physical properties. From the reported data, it is evident that the highest occupied molecular orbital (H.O.M.O.)-lowest unoccupied molecular orbital (L.U.M.O.) gap of the porphyrin systems is lowered going from H_2-TPP, 2,29 V to system B and A, 2.24 and 2.20 V, respectively. Furthermore this observation can be justified by postulating the extension of conjugation along the linker. As outlined in the Chapter 2, where the Marcus theory was exposed, the cyclic voltammetry measurements are useful to determine the free energy for charge recombination reaction, so by adding the corresponding reduction and oxidation potentials of the electron-accepting C_{60} and electron-donating porphyrins (System B), respectively, we estimate the following radical ion pair energies: H_2P-C_{60}, 1.74 eV; ZnP-C_{60}, 1.6 eV.

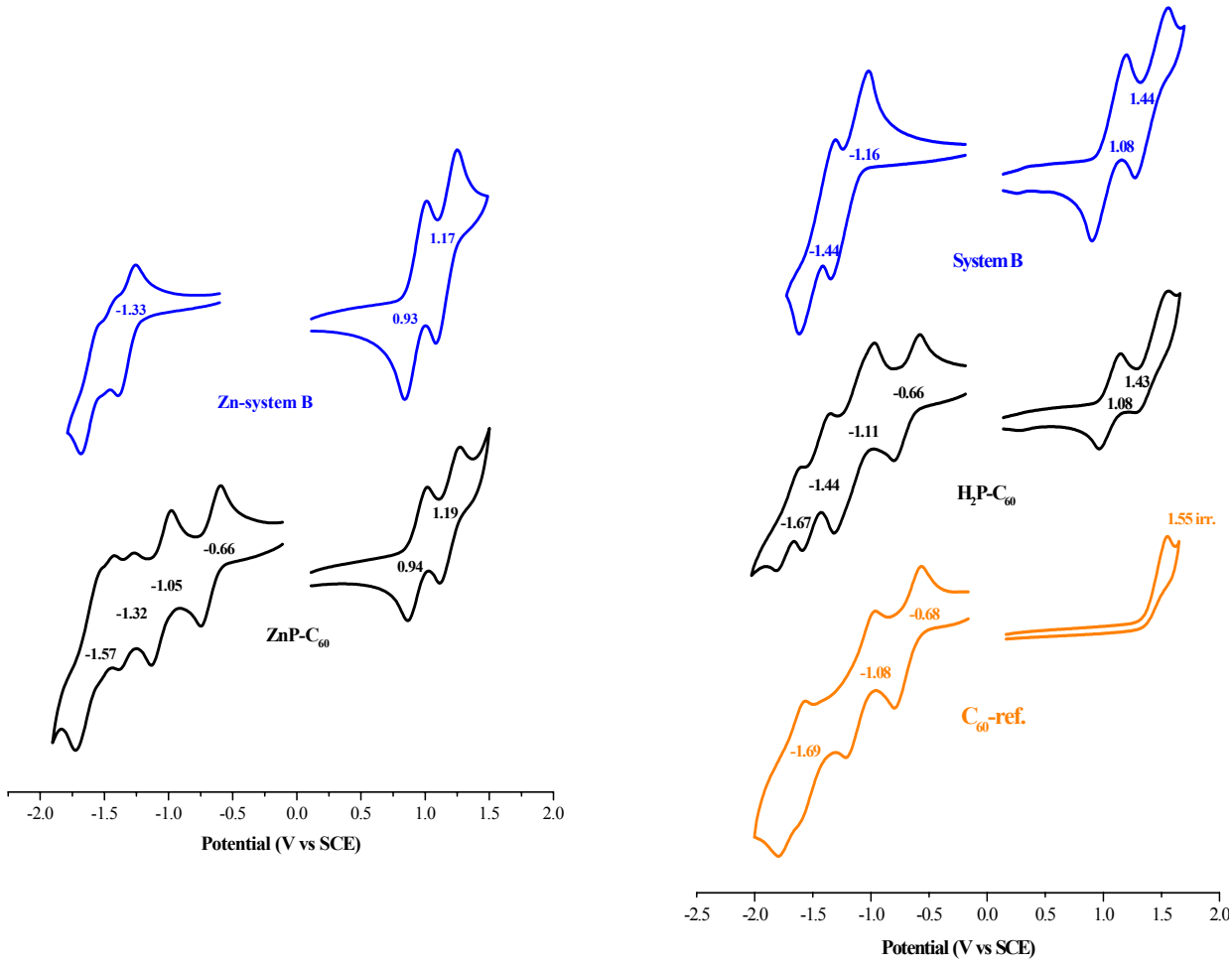

Figure 4.3. 5 *Cyclic voltammograms at 200mV/s in DCB with 0.05 M $TBAPF_6$ as the supporting electrolyte of Zn-system B and ZnP-C_{60} (left part), and system B, H_2P-C_{60} and C_{60}-ref (right part)*

Important data come from NMR bidimensional study of both system A and system B, these data further confirm the "push-pull" effect in the new porphyrin systems. Both porphyrin systems were investigated by ^{1}H-NMR spectroscopy. In addition, system A was probed with two different NMR methodologies, that is, HSQC and HMBC. HSQC allows mapping of the direct coupling of each proton with its relative bonded carbon atom, and HMBC sheds light onto J^2 and J^3 ^{1}H-^{13}C couplings[155]. These methodologies allowed us to assign the NMR signals concerning the (4'-formylphenyl)ethynyl substituent on the pyrrolic ring (Figure 4.3.6). From the inspection of the HMBC spectrum of system A, it is possible to see different signals arising from J^2 and J^3 hydrogen carbon couplings. The two couplings at 135.5 ppm and 129.0 ppm of the aldehydic proton at 10.06 correspond to carbon atoms 2 and 3, respectively. The most diagnostic signals are those that relate to the ethynylene carbons, which are coupled with protons 4 and 3. Their relative resonance frequencies at 9.14 ppm for proton 4 and 7.52 ppm for proton 3 correspond to the resonance frequency of carbon 7 at 91.0 ppm and carbon 6 at 98.3 ppm.

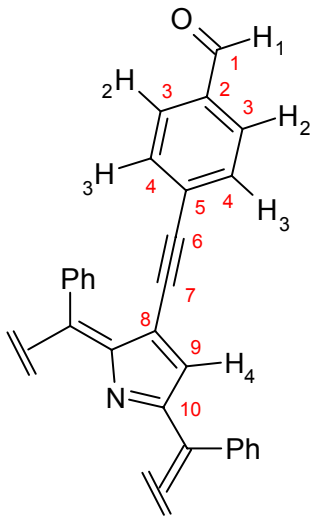

Figure 4.3. 6 *(4'-formyl)phenylethynyl substituent of system A*

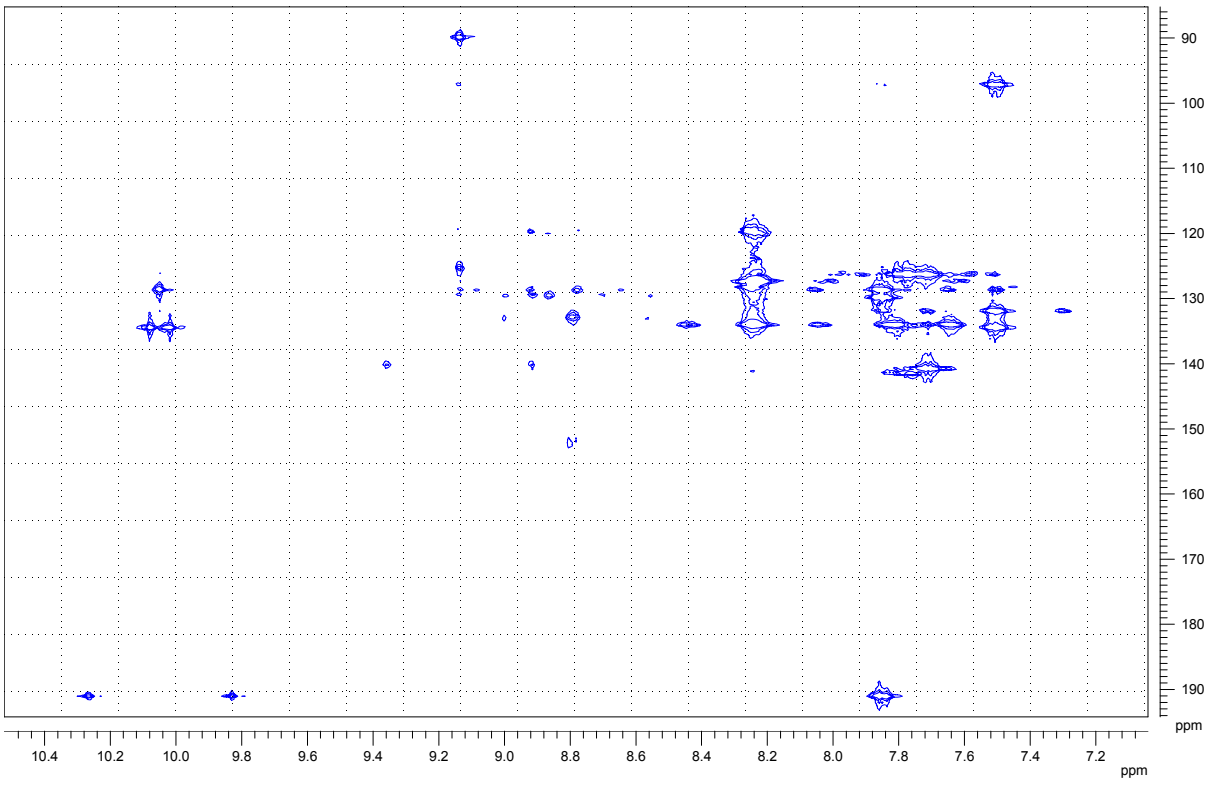

Figure 4.3. 7 *HMBC spectrum of system A in chloroform solution*

In the HSQC spectrum, it is possible to see five different pyrrolic proton signals coupled with four magnetically different carbon atoms: the first one at 9.14 ppm coupled with the carbon signal at 141.0 ppm, the second one the singlet at 8.92 ppm, which corresponds to two different carbon signals at 129.2 and 130.4 ppm, the third one a doublet at 8.87 ppm coupled with a carbon signal at 129.2 ppm, then a singlet at 8.80 ppm coupled with a carbon signal at 133.6 ppm, and finally a doublet at 8.80 ppm coupled with the carbon signal at 130.4 ppm (For elucidations see Figure 4.3.8).

Comparing the ^{1}H-NMR of system A and system B, it is clear that between 8 and 9 ppm different patterns concerning the pyrrole protons are present (See Figure 4.3.9). In system B, a doublet at 8.75 ppm is clearly visible, while, in system A, this is superimposed with the singlet at 8.80 ppm. Changing the substituent on the phenyl ring linked to the β-position, a shift toward lower frequencies is evident when going from a methyl to an aldehydic group. Moreover, the NMR shifts do not all have the same magnitude and so the peak at 9.14 ppm in system A (H_1 in Figure 4.3.10) is shifted in system B at 9.07 ppm (Δppm = 0.07), while all other peaks are shifted by about 0.04 ppm, except the singlet at 8.80 ppm in system A. It is possible to understand all these aspects by postulating an extension of conjugation from the tetrapyrrole ring along the substituent. Figure 4.3.10 depicts the three fundamental resonance structures of porphyrin system A, in which it is clear how only three of the four pyrrolic rings are subjected to the extension of conjugation. On the other hand the two protons on the ring C (H_4) are not affected by this charge delocalization and in this case it is possible to attribute these two protons to the singlet at 8.80 ppm in both systems. The β-pyrrole carbon atoms of rings B and D are magnetically equivalent, and we can attribute the carbon signal at 130.4 ppm to the carbon with the positive charge, while the other one corresponds to the signal at 129.2 ppm. Since the resonance effect depends on the distance relative to the aldehydic group, it is possible to visualize the proton H_2 (8.87 ppm) and proton H_3 (8.80) as a doublets. Notably, such an impact is not discernible for the proton H_5 (8.92 ppm), also because the symmetry of porphyrin is lost.

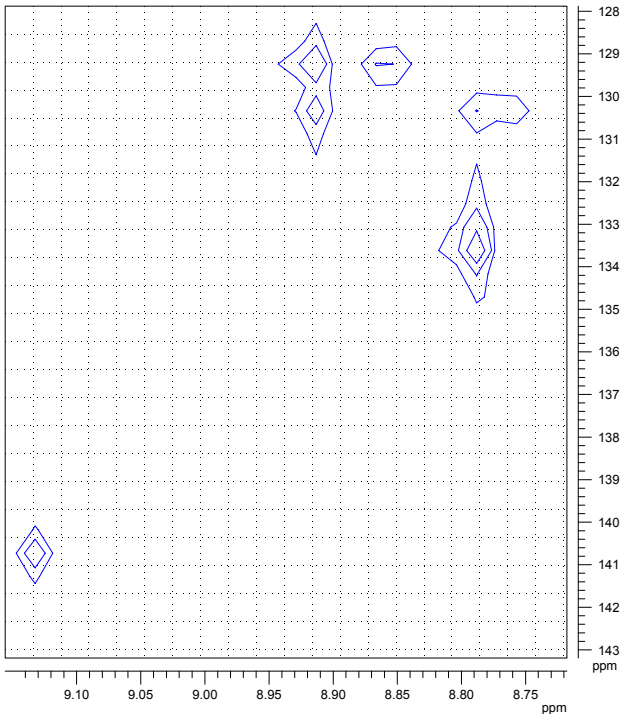

Figure 4.3. 8 *Particular of the HSQC spectrum of system A*

The signal at 133.6 ppm is due to the β-pyrrolic carbon atoms of ring C. These results are in good agreement with the effect of the electron-withdrawing substituents on the β-positions of the tetrapyrrole ring[156] and with the fact that the free base porphyrins tend to retain their aromaticity, excluding, however, the two external double bonds. In our case, only one double bond is excluded from the delocalization. Still, in the HSQC spectrum of system B, five different pyrrolic proton signals seem to couple with four magnetically different carbon atoms, but all of the carbon signals are shifted toward higher fields. In particular, while in system A the carbon with the positive charge in the ring A resonances at 141.0 ppm, in system B, such signal is shifted at 138.0 ppm. This constitutes further evidence of the electron-withdrawing effect of the aldehydic group. Finally, it should be noted that the β-pyrrole proton pattern in the ^{1}H-NMR spectrum of the free base dyad is completely similar to that of system B.

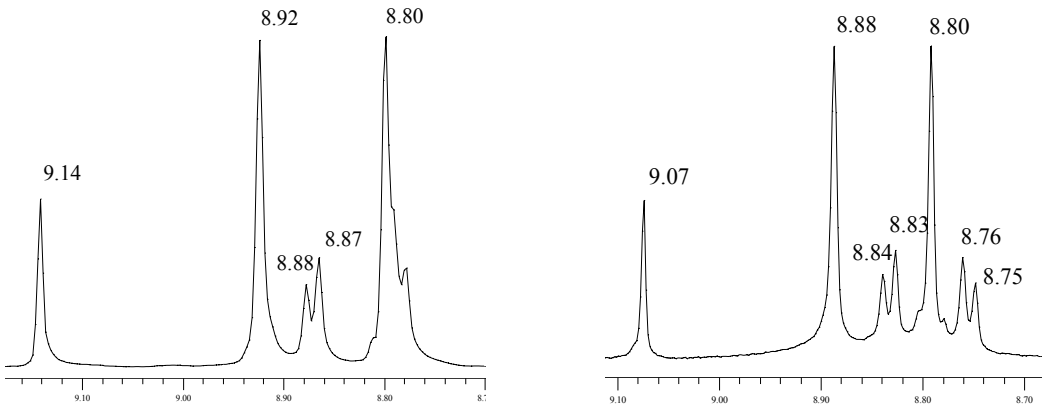

Figure 4.3. 9 *^{1}H-NMR signals pattern of pyrrolic protons of system A (on the left) and system B (on the right)*

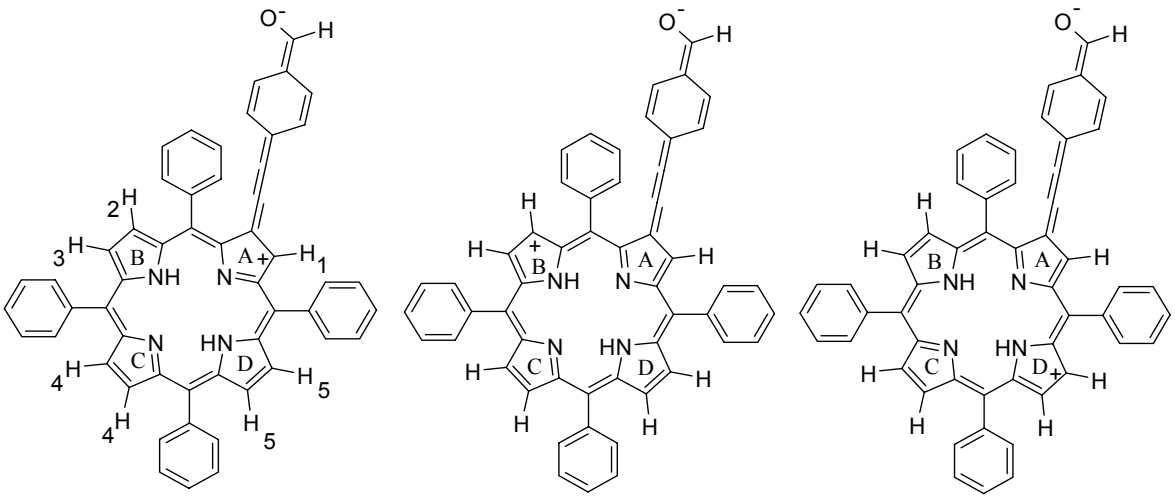

Figure 4.3. 10 *Three fundamental resonance structures of system A*

The ^{1}H-NMR spectra of all the corresponding zinc derivatives present an identical β-pyrrolic proton pattern. In particular the singlet found at 8.80 ppm for the free base is largely shifted to lower field and this fact is due to the coordination of the zinc atom to the nitrogen atom of the pyrrole ring C (Figure 4.3.11). This causes a decrease in electron density on the aforementioned pyrrole ring, and in addition, the average Δppm between pyrrole proton signals of system A and system B is less pronounced in the zinc derivatives relative to the free base porphyrins.

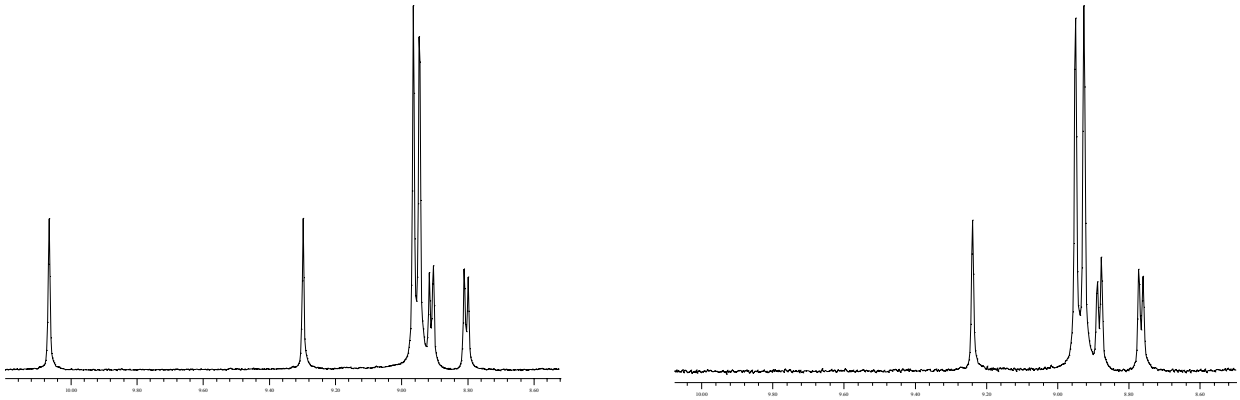

Figure 4.3. 11 *^{1}H-NMR spectra in $CDCl_3$ of Zn-system A (on the left) and ZnP-C_{60} (on the right)*

All of the aspects discussed above suggest the presence of an extension of conjugation from the porphyrin ring along the β-substituent; especially when an aldehydic group is present on the phenyl ring of the substituent, a push-pull effect takes place from the porphyrin to the aldehyde. Moreover, since Zn-system A and Zn-system B have more or less the same extinction molar coefficient, it is possible that the zinc atom turns off this phenomenon, because the metal insertion in the tetrapyrrolic ring makes all of the β-pyrrole positions, in term of resonance structures, equivalent. Therefore the new porphyrin compounds have been deeply studied through UV-visible, cyclic voltammetry and NMR techniques. All the results outline the presence of an extended conjugation along the linker, but even if these results are good enough we were interested to test the behaviour of the new porphyrin-fullerene dyad toward the energy and electron transfer reactions and a detailed fluorescence study has been carried out in this direction, following the meaning results will be summarized.

Steady state fluorescence spectra were recorded to analyze the photophysical properties of new porphyrins and dyads. Four different solvents of increasing polarity have been used to carry out steady state fluorescence measurements: toluene, chloroform, tetrahydrofuran (THF), and benzonitrile. The excitation wavelength was 525 nm for the free base derivatives and 560 nm for the zinc derivatives. In toluene, system A presents two emission bands at 666 and 734 nm, while system B at 663 and 731 nm. Such a difference of 3 nm remains also in other solvents. In

the corresponding zinc derivatives, the emission maxima are located at 607 and 661 nm for Zn-system A, while they are at 605 and 658 nm for Zn-system B. Steady state fluorescence spectra of zinc derivatives in THF and benzonitrile show a substantial red shift due to the coordinating effect of the solvents. In fact, in THF, the first emission maximum of Zn-system A is at 620 nm and, in benzonitrile, it is at 628 nm. Moreover also the emission band shape changes passing from less polar to more polar solvent as it is possible to see in the Figure 4.3.12. The same results were obtained for Zn-system B. In toluene solution, the fluorescence of the porphyrin part in H_2P-C_{60} is quenced for 93% by the C_{60} moiety, the fluorescence quenching is calculated taking system B as a reference. On the other hand, for ZnP-C_{60} the quenching is 99%. In addition to the higher quenching of the porphyrin fluorescence, in the spectra of the ZnP-C_{60} a third emission band appears at 715 nm (Figure 4.3.13). An excitation spectrum collected at 715 nm (i.e., exciting from 400 to 650 nm) confirms the origin of that emission band: the porphyrin moiety. Further analysis on the reference compound N-methyl-2-(4'-ethynyl)phenyl-3,4-fulleropyrrolidine identifies this band as the singlet excited state emission of C_{60} (Figure 4.3.14). The same behaviour has also been observed in chloroform. Such data demonstrate that in toluene solution the principal deactivation pathway of the porphyrin fluorescence is a near quantitative energy transfer from the singlet excited state of the zinc porphyrin to the singlet excited state of C_{60}. In THF and benzonitrile, the porphyrin fluorescence quenching in H_2P-C_{60} is much stronger compared to that seen in toluene and chloroform. In ZnP-C_{60} fluorescence spectra, on the other hand, we do not observe the fluorescence emission of $^{1*}C_{60}$ at 715 nm.

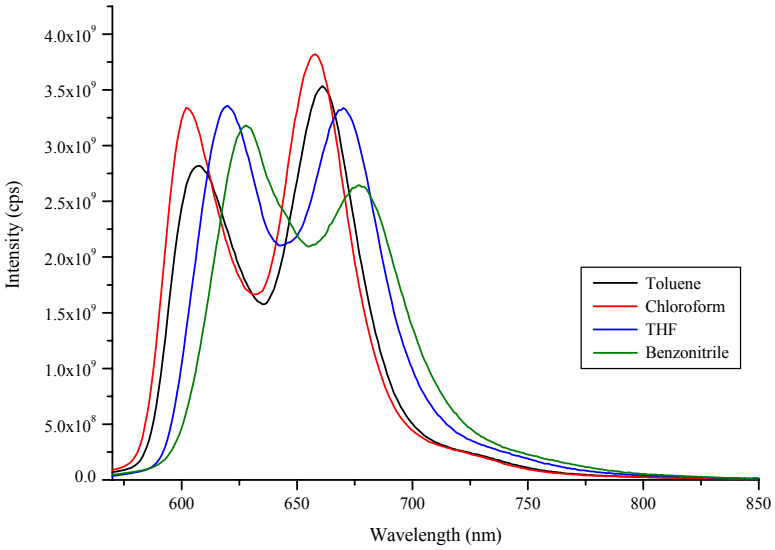

Figure 4.3. 12 *Steady state fluorescence spectra of Zn-system A in different solvents upon excitation at 560 nm. Absorbance values match at the excitation wavelength*

In general, we observe a solvent effect on the fluorescence quenching; in particular the porphyrin fluorescence in H_2P-C_{60} tends to decrease passing from less polar to more polar solvents (Figure 4.3.15). To gather a deeper evaluation of the photophysical phenomena, time

resolved fluorescence spectra were carried out in the nanosecond time domain with a 337 nm nitrogen laser. Unfortunately, for both the free base and the zinc derivatives, the deactivation pathway of the singlet excited state of porphyrin in the dyads is faster than the time resolution. Only the C_{60} singlet excited state deactivation in the ZnP-C_{60}, following the energy transfer reaction in toluene, was recorded. The measured lifetime is 1.30±0.01 ns, a result that is consistent with the singlet excited state lifetime of fulleropyrrolidine derivatives[157].

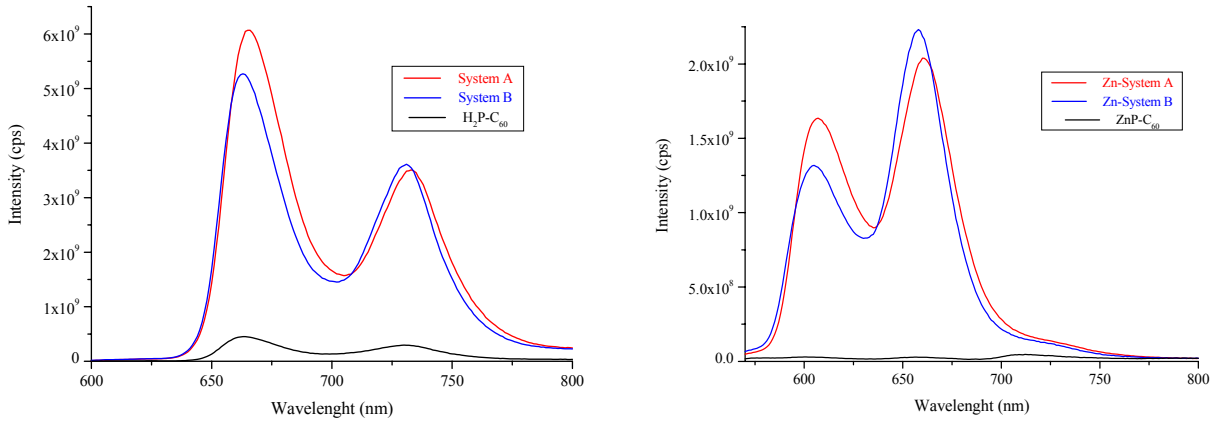

Figure 4.3. 13 *Steady state fluorescence spectra of system A, system B, and H_2P-C_{60} (on the left) and corresponding zinc derivatives (on the right) in toluene solution, upon excitation at 525 and 560 nm respectively.*

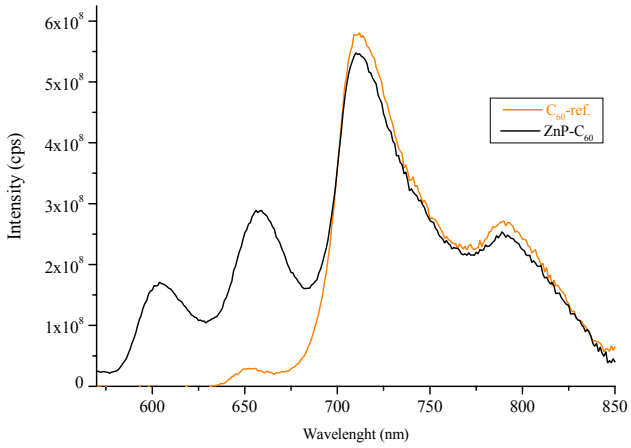

Figure 4.3. 14 *Steady state fluorescence spectra of C_{60}-ref. and ZnP-C_{60} in toluene solution upon excitation at 400 nm. The relative absorbance match (0.05 au) at excitation wavelength.*

From the steady state fluorescence spectra of ZnP-C_{60} in toluene and THF, it was possible to estimate the lifetimes of the zinc porphyrin singlet excited state. In fact, it is possible to correlate the fluorescence quantum yield and the lifetime with the equation reported below, where $\Phi_{Zn\text{-system B}}$ is the zinc porphyrin quantum yield, while $\Phi_{ZnP\text{-}C60}$ is the zinc porphyrin

quantum yield in the ZnP-C_{60} and k_{deact} is the rate of the porphyrin singlet excited state deactivation process:

$$\frac{\Phi_{Zn-SystemB} - \Phi_{ZnP-C_{60}}}{\Phi_{ZnP-C_{60}} \tau_{ZnP-SystemB}} = k_{deact}$$

From these analyses, we succeded in estimate k_{deact} value in toluene as 1.0×10^{11} s^{-1} which corresponds to a lifetime of 10 ps, while in THF a k_{deact} value of 2×10^{11} s^{-1} yields a lifetime of 5 ps. Such results are in a good agreement with the singlet excited state lifetimes measured by transient absorption spectroscopy, (vide infra). Similar results were gathered for the corresponding H_2P-C_{60}.

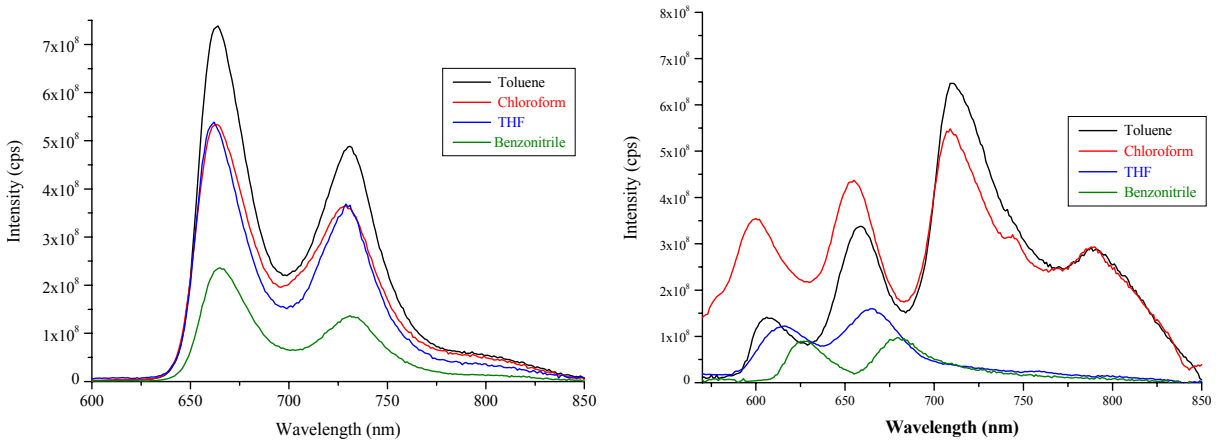

Figure 4.3. 15 *Fluorescence emission spectra of H_2P-C_{60} (on the left) and ZnP-C_{60} (on the right) in different solvents, upon excitation at 525 and 560 nm respectively. The absorbance values match at excitation wavelength for both the free base and zinc derivatives.*

Femtosecond transient absorption spectroscopy was used to complement the aforementioned fluorescence experiments. In particular, the references (i.e., Zn-System B and System B) and the electron donor-acceptor dyads (i.e., ZnP-C_{60} and H_2P-C_{60}) were probed upon 387 nm excitation. This guarantees the predominant photoexcitation of the Zn porphyrin and free base porphyrin chromophores. For the first experiments our attention should be directed to the references. For System B, for example, we saw the nearly instantaneous formation of the singlet excited state – only a fast internal conversion (i.e., ~ 2 ps) from an higher lying excited state precedes the singlet excited state formation – for which we obtained the following spectral characteristics: minima at 521, 557, 600 and 660 nm and a maximum in the near infrared at 700 nm. The minima correspond to the maxima seen in the System B ground state absorption

spectrum. Similar ground state bleachings (i.e., 555 and 595 nm) and new maxima in the near infrared (i.e., 710 nm) were noted for Zn-System B. In contrast, the singlet excited state lifetimes of System B (i.e., 10.5 ns) and Zn-System B (i.e., 2.3 ns) differ fundamentally.

Mainly, the same singlet excited state formations of Zn-System B and System B were recorded in ZnP-C_{60} and H_2P-C_{60}, respectively, despite the presence of the electron accepting C_{60}. This affirms in toluene and THF the successful photoexcitation of the chromophores in the electron donor-acceptor dyads. At longer delay times, however, the electron donor-acceptor dyads revealed a behavior that is vastly different from the reference systems. In particular, ultrafast deactivations of the singlet excited state are derived from kinetic analyses of the ZnP-C_{60} (i.e., toluene: 15.9 ps; THF: 5.8 ps) and H_2P-C_{60} (i.e., toluene: 20.5 ps; THF: 50.7 ps) transient species in the different solvents – see Figures 4.3.16-18.

Spectral characteristics, which are taken immediately at the conclusion of the Zn-Sytem B and System B singlet excited state decays, bear no resemblance with the singlet or triplet features of either chromophore. On the contrary in toluene the distinct absorption of the C_{60} singlet excited state evolve around 900 nm – see Figure 4.3.16 – within the first 100 ps – with kinetics (i.e., ZnP-C_{60}: 17.4 ps; H_2P-C_{60}: 23 ps) that resemble the Zn-System B or System B singlet deactivations. Therefore, we postulate that in toluene a transduction of singlet excited state energy is responsible for the kinetic and spectral observations. On the longer time scale, namely, up to 1500 ns the C_{60} singlet / C_{60} triplet intersystem crossing takes place, which leads ultimately to the quantitative triplet formation, which is spectroscopically confirmed by the growth of a new transient that maximizes at 700 nm. In THF, on the other hand, it is not the C_{60} singlet feature in the near infrared that is seen for both electron donor-acceptor dyads, but the C_{60} radical anion bands, as reported in Figure 4.3.17 and 4.3.18, with maxima at 1000 nm.

The C_{60} radical anion band in the near infrared is complemented by the Zn-System B and System B radical cation absorptions in the visible with transient maxima at 635 and 690 nm, respectively. Both, the radical cation and the radical anion features are formed with the same kinetics, which leads us to conclude that in THF an intramolecular electron transfer converts the initial excited state into a radical ion pair state. Moreover, the radical cation and radical anion transitions also decay with the same kinetics. From the corresponding decay dynamics we derived the lifetimes of the radical ion pair states of 398 and 1175 ps for the ZnP-C_{60} and H_2P-C_{60}, respectively. The different charge recombination dynamics (i.e., 2.5×10^9 s^{-1} versus 8.5×10^8 s^{-1}) are well in line with kinetics that are located in the inverted region of the parabolic dependence of electron transfer rate on the thermodynamic driving force. Below the transient absorption spectra discussed previously are reported.

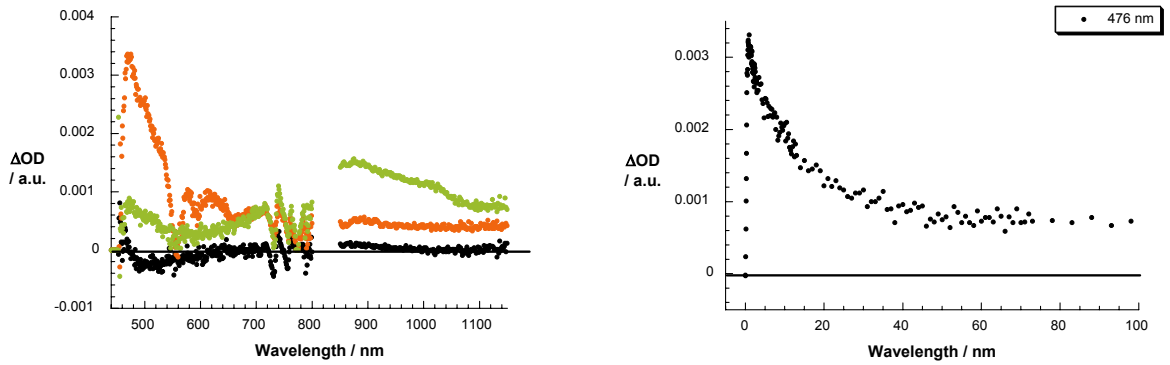

Figure 4.3. 16 *On the left – differential absorption spectra (visible and near infrared) obtained upon femtosecond flash photolysis (387 nm) of ZnP-C_{60} (ca. 1.0 × 10^{-6} M) in toluene with 0.05, 1.4 and 50 ps time delays at room temperature. On the right – time-absorption profile of the spectra shown above at 476 nm, reflecting the intramolecular energy transfer dynamics.*

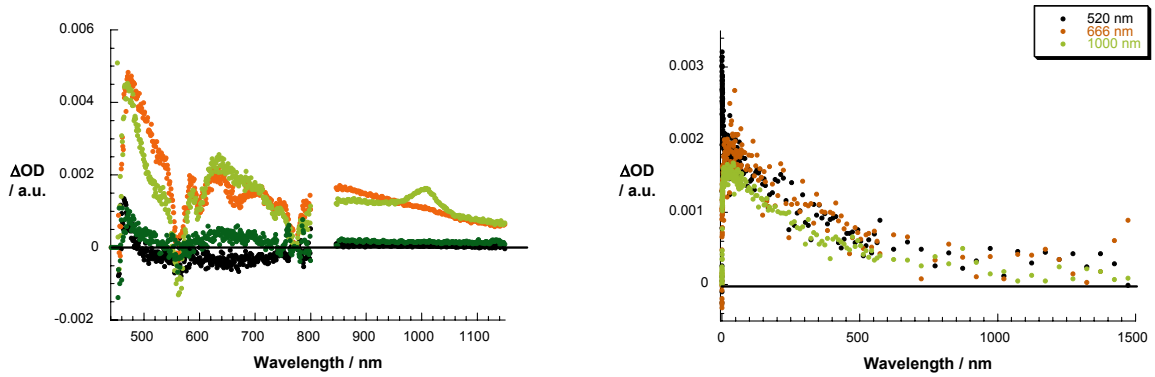

Figure 4.3. 17 *On the left – differential absorption spectra (visible and near infrared) obtained upon femtosecond flash photolysis (387 nm) of ZnP-C_{60} (ca. 1.0 × 10^{-6} M) in THF with 0.05, 1.4, 50 and 1525 ps time delays at room temperature. On the right – time-absorption profile of the spectra shown above at 520, 666 and 1000 nm, reflecting the intramolecular charge separation and charge recombination dynamics.*

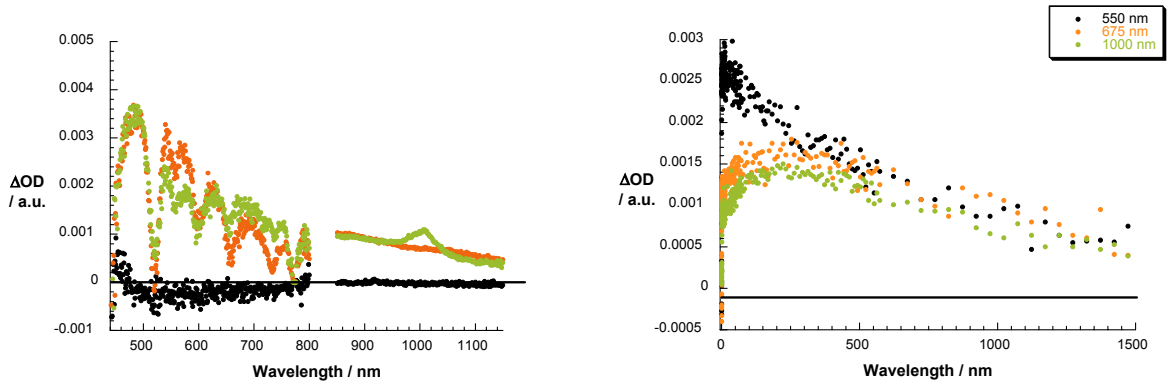

Figure 4.3. 18 *On the left– differential absorption spectra (visible and near infrared) obtained upon femtosecond flash photolysis (387 nm) of H_2P-C_{60} (ca. 1.0 × 10^{-6} M) in THF with 0.05, 1.4 and 200 ps time delays at room temperature. On the right – time-absorption profile of the spectra shown above at 550, 675 and 1000 nm, reflecting the intramolecular charge separation and charge recombination dynamics.*

In conclusion, the new porphyrin-fullerene dyads were deeply investigated and the results contribute to shed light on the porphyrin-fullerene interaction. Taking in consideration the extension of conjugation along the linker in the β position of the porphyrin moiety, and the ultrafast rate constants for energy and electron transfer, it is possible to make the hypothesis that the ethynylenephenylene subunit is a quite good linker to favour the electron transfer processes, even if other studies are necessary to confirm this first result. Furthermore to support our hypothesis the rate constant reported for our porphyrin fullerene dyad are, more or less, of the same order of those reported in the work of Schuster in an analogous compound where the porphyrin is directly linked to the fullerene moiety through a diethynyl linker that assures a complete conjugation between the tetrapyrrole ring and fullerene [158] (see also Chapter 3 paragraph 4.3). Computational study on the porphyrin-fullerene dyad and relative zinc complex to verify where the HOMO and LUMO orbital reside, contributes to further clarify the situation. As it is possible to see in the Figure 4.3.19 both in the free base and zinc dyad the HOMO orbital is on the porphyrin moiety (orange orbital) while the LUMO is located on the fullerene (blue orbital), but while in the free base the HOMO seems to be confined only on the tetrapyrrole ring in the zinc dyad it seems to be enlarged on the linker, that in turn, seems to be coplanar with the porphyrin moiety.

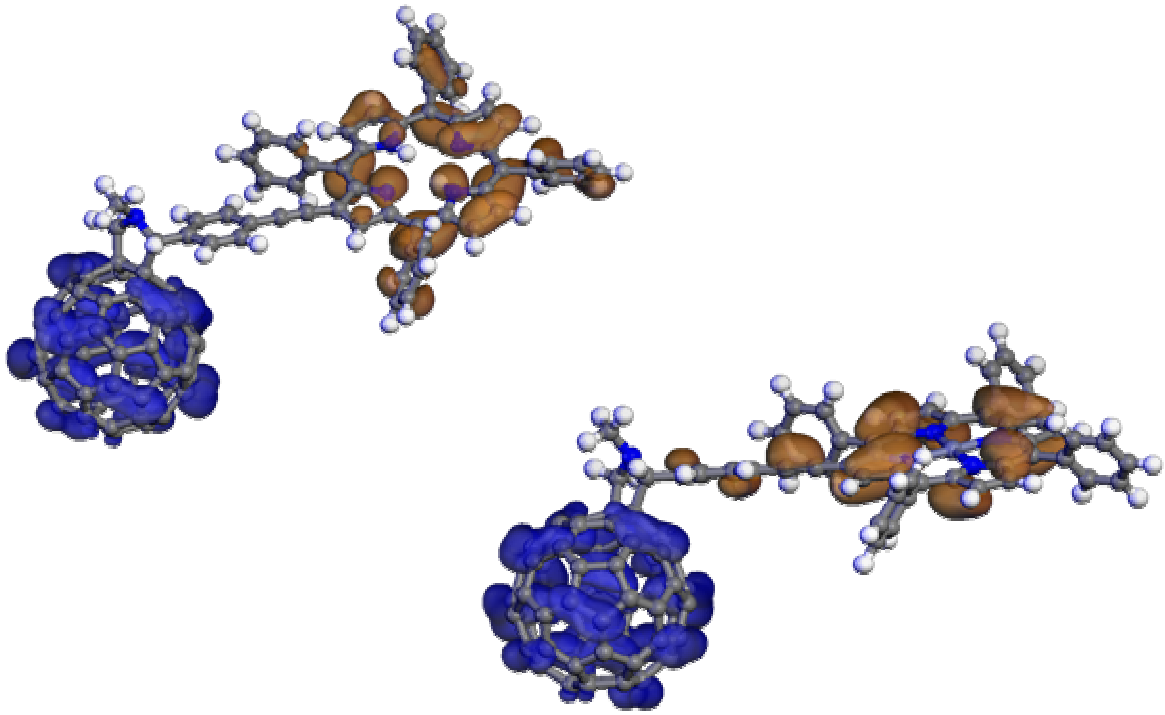

Figure 4.3. 19 *Computational studies carried out at AM1 level on the free base porphyrin-fullerene dyad (on the left) and its zinc complex (on the right)*

Further studies on porphyrin-fullerene system with an increasing porphyrin-fullerene distance and oligoethynylenephenylene spacer are in progress to test the wire like behaviour of this linker, in the next paragraph the first preliminary results will be reported.

4.4. Preliminary Studies on New Porphyrin-"Wire"-Fullerene Systems

As reported in the first paragraph of this chapter new porphyrin-"wire"-fullerene systems were synthesized in order to evaluate the wire behaviour of *para*-oligo-ethynylenephenylene (*p*-OEP) linker. Moreover this type of spacer was directly attached to the β-position of the porphyrin ring, so that it could be possible to estimate eventually direct interaction between the π-system of tetrapyrrole ring and that of the linker. In order to make easier the compound identification during the discussion, the names reported in the Figure 4.4.1 will be adopted, such names summarize the structural characteristic of compounds, being TMS = trimethylsilyle and EP = ethynylenephenylene. Moreover, the results obtained for the porphyrin-fullerene dyads reported in the previous paragraph will be used in this section to have a larger view on the chemical-physical characteristics of new compounds.

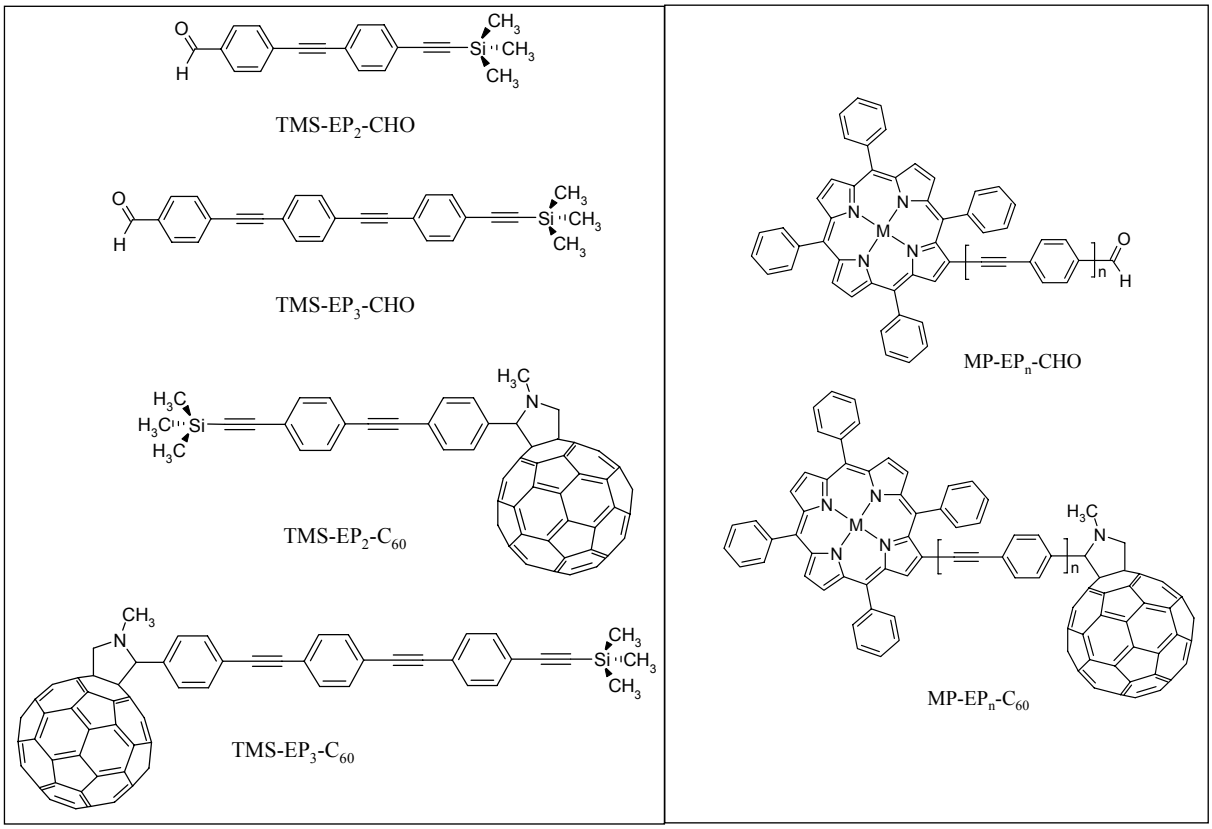

Figure 4.4. 1 *Compounds studied in this section, where M = 2H or Zn and, in the porphyrin compounds (on the right part), n = 1, 2, 3. TMS = trimethylsilyle and EP = ethynylenephenylene*

The new compounds were investigated through UV-visible, cyclic voltammetry and steady state and time resolved fluorescence measurements; all the results will be shown below starting from the UV-visible data obtained in toluene solution. The linker units have absorption in the UV window going from 400 to 300 nm, as it is possible to see in the Figure 4.4.2. Such figure also

shows that increasing the conjugation leads to a red shift of the maximum absorption bands and further, the band shape changes becoming more broad and less defined. In fact, while TMS-EP_2-CHO compound presents two absorption respectively at 325 and 347 nm, the TMS-EP_3-CHO compound has only one maximum at 345 nm. Comparing the UV spectra of the linker with those of the respective "wire"-fullerene systems it is noticeable the blue shift of the absorption bands in these last compounds. Most probably this effect is due to the loss of aldehydic group upon functionalization of the linker with C_{60}; this fact should implies a reduction in extension of conjugation due to the introduction of sp^3 carbon atom at one terminal of the wire. In addiction Figure 4.4.3 shows that in the fullerene derivatives it is present a tail of the absorption band which enters in the visible region, that is typical of the fullerene compounds. Because not deep changes are visible in the "wire"-fullerene systems UV-visible spectra, excluding the aforementioned blue shift justified as a consequence of the removal of the aldehydic group, we can suppose that there is not a deep interaction between the fullerene and the linkers in the fundamental state.

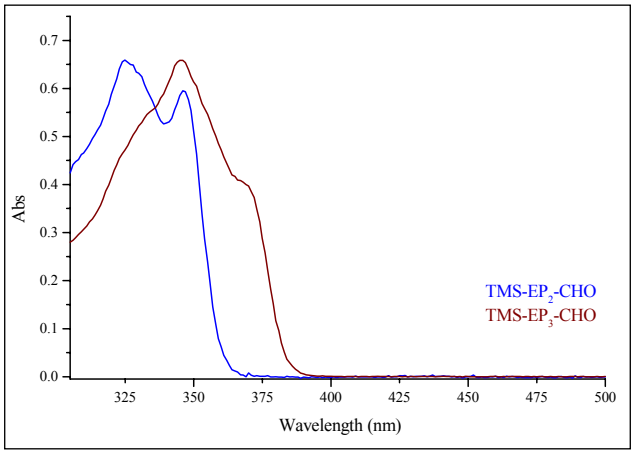

Figure 4.4. 2 *UV-visible absorption spectra of TMS-EP_n-CHO compounds in toluene solution. The absorbance value matches at the respective maxima.*

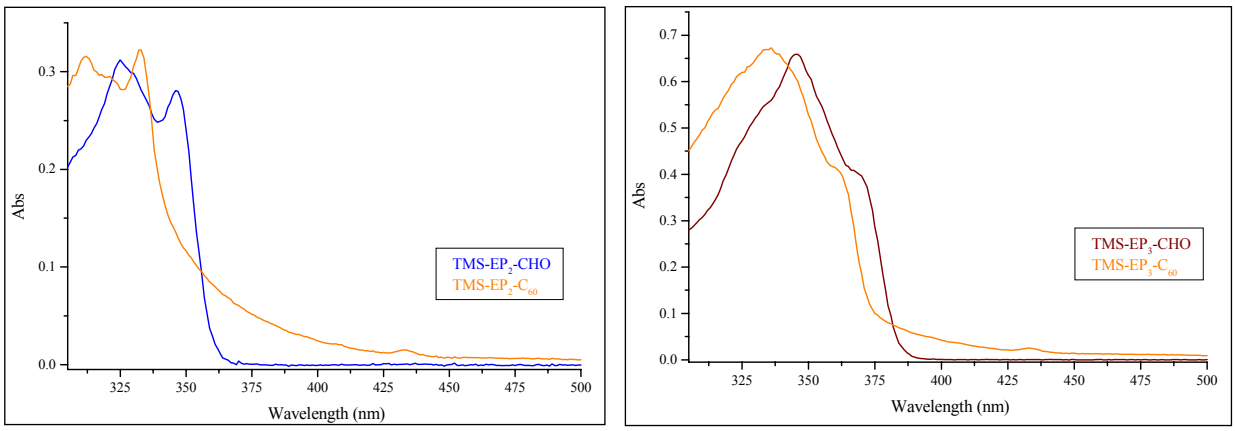

Figure 4.4. 3 *Comparison of UV-visible absorption spectra of "molecular wires" and "wire"-fullerene systems in toluene solution. Series with n = 2 on the left and with n = 3 on the right, absorbance values match at the respective maxima*

Much more important are the UV-visible spectra of porphyrin-"wire"-fullerene compounds and the porphyrin-"wire" systems. The data underline a non interacting porphyrin-fullerene

compounds, as it has been expected due to the increased distance between the two moieties, hence in the respective spectra the generic porphyrin-"wire"-fullerene absorption could be considered as given by the sum of the porphyrin-"wire" plus "wire"-fullerene absorption. The Soret band of the porphyrin moiety does not show any change upon derivatization of the system with fullerene, remaining, both for n = 2 and n = 3, at 430 nm (Figure 4.4.4).

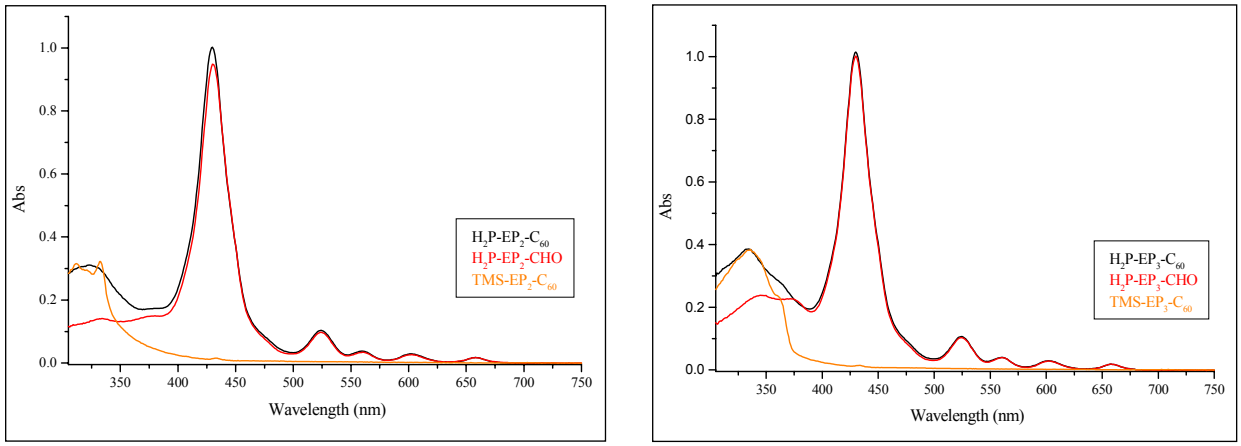

Figure 4.4. 4 *Comparison of UV-visible absorption spectra of porphyrin-"wire", "wire"-fullerene and porphyrin-"wire"-fullerene systems in toluene solution. Series with n = 2 on the left part and that with n = 3 on the right part. Absorbance values match at the respective maxima.*

If we compare the absorption spectra of only the porphyrin-"wire" systems including the similar compound with n = 1 the effect of the extension of the conjugation in the linker part is clearly visible, it determines a continuous red shift of the ultraviolet absorption part of the spectrum together with an increased absorption value, indicated by an arrow in the spectra of the Figure 4.4.5, where also the free base porphyrin-"wire"-fullerene systems are reported.

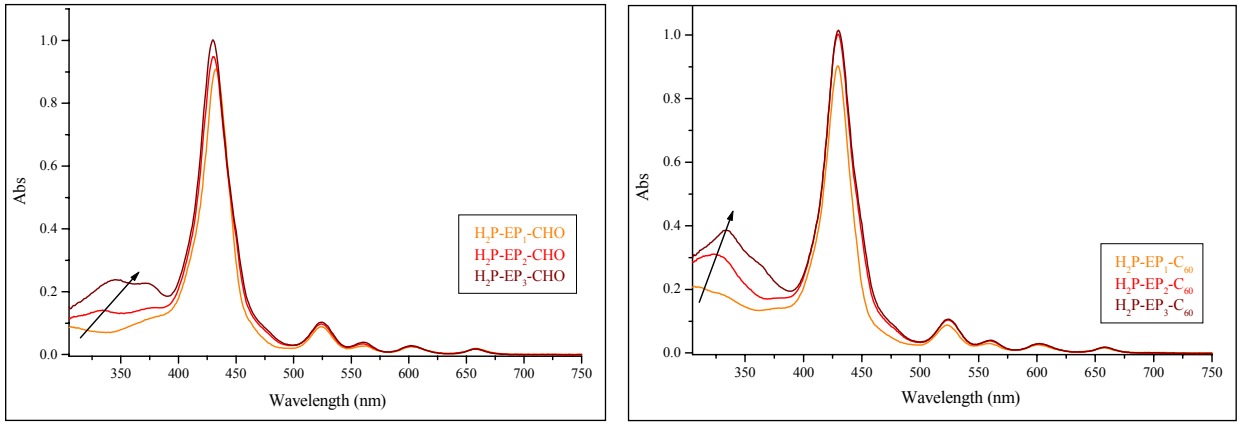

Figure 4.4. 5 *Comparison of UV-visible absorption spectra of H_2P-EP_n-CHO systems on the left part, and H_2P-EP_n-C_{60} systems on the right part, in toluene solution, n = 1, 2, 3.*

The same results have been obtained for the zinc derivatives of previous reported porphyrin-fullerene systems. It is possible to assume that no particular interactions between porphyrin and fullerene, porphyrin and linkers and finally between linkers and fullerene have been pointed out from UV-visible measurements. A much more detailed study is necessary to confirm this observation because, if we can affirm quite surely that no interaction is present between porphyrin and fullerene, essentially due to the intervening distance between them, we can not exclude some interactions between linkers and porphyrin and obviously between linkers and fullerene.

To shed light on this aspect cyclic voltammetry studies have been carried out in *ortho*-dichlorobenzene solution, adopting $TBAPF_6$ 0.05 M as supporting electrolyte. The equipment and operative condition are similar to those reported in the previous paragraph. The results obtained must be considered preliminary because of the complexity of the systems and further elucidation are necessary and most probably different operative conditions must be tested before to make definitive conclusions. The discussion will be divided in two parts; first the free base porphyrin compounds and then the respective zinc complexes will be taken into consideration. It is useful to start taking into account the cyclic voltammetries of the linkers: both TMS-EP_2-CHO and TMS-EP_3-CHO compounds do not show oxidation processes in the considered potential range, from 0 to 1.80 V; on the other hand the two linkers present one irreversible reduction process at -1.74 and -1.76 V, respectively for TMS-EP_2-CHO and for TMS-EP_3-CHO. Noteworthy this reduction process is not reproducible after the first scan, because the two molecules undergo to a side reaction at the working electrode interface producing a sort of adsorbed film on the electrode surface, which has to be removed to continue the measurements. Most probably the experimental conditions induce polymerization or activation of terminal aldehydic group, preventing the possibility to have a deeper insight in the redox properties of these two linkers. Fortunately this does not happen for the porphyrin-linker systems. Both H_2P-EP_2-CHO and H_2P-EP_3-CHO have almost identical oxidation processes: two reversible waves at 1.12 and 1.45 V for the first system and at 1.11 and 1.45 V for the second one. As in the oxidation process also in the reduction window two identical reversible reductions are present at -1.10 and -1.33 V for both porphyrins and as it has been expected, the partial reduction of the linker also appears like a third irreversible signal at 1.74 V in the H_2P-EP_2-CHO and 1.72 V in the H_2P-EP_3-CHO. Despite all these similarities between the two porphyrin-"wire" systems, a more accurate analysis show that, while in the H_2P-EP_3-CHO both the first and second reduction are completely reversible and both can be considered as one electron process, in the H_2P-EP_2-CHO system the two processes are reversible, but the second

one seems to be a two electron reduction if compared to the first reduction wave. In fact, in the system with the longest linker (H_2P-EP_3-CHO) the width of the two reduction waves, calculated taking the peaks values as extremities, have the same entity (242 mV), on the contrary in the H_2P-EP_2-CHO system there is a difference of more or less 60 mV in width between the first reduction (wave width 191 mV) and the second ones (wave width 252 mV), as it is possible to see in the Figure 4.4.6.

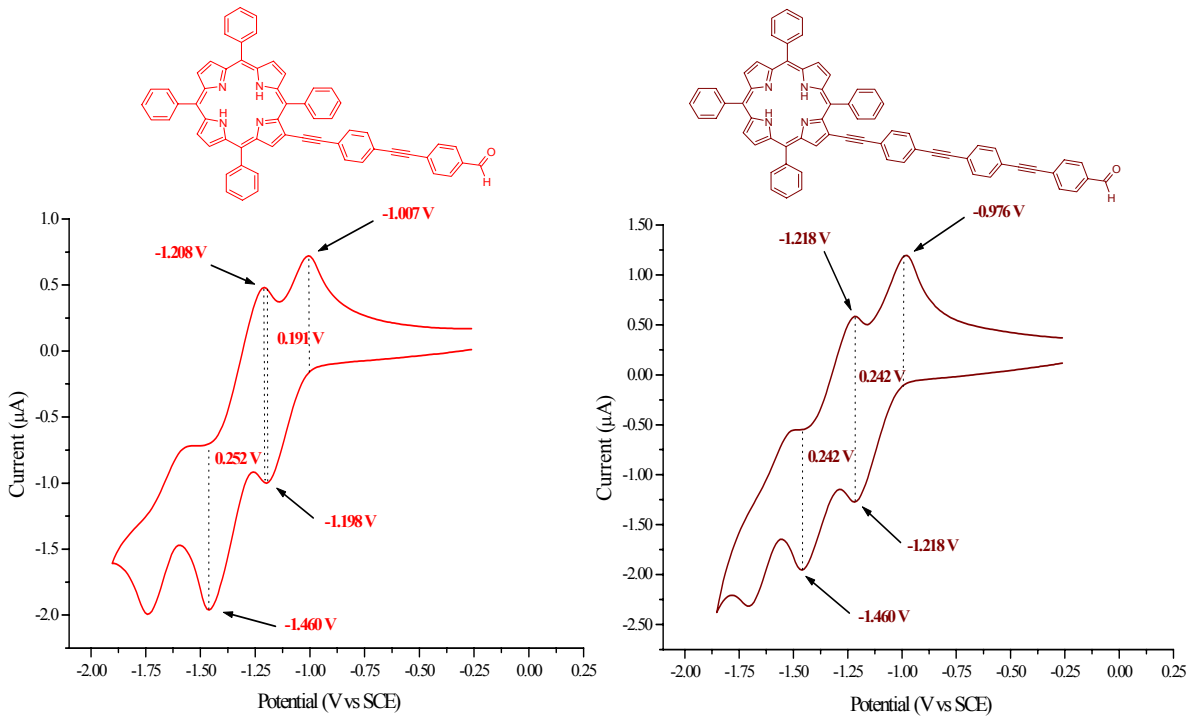

Figure 4.4. 6 *Reduction waves of H_2P-EP_2-CHO on the left and of H_2P-EP_3-CHO on the right, in DCB with 0.05 M of $TBAPF_6$, scan rate 100mV/s.*

This is an anomaly that must be clarified. Changing the scan rate or recording several cyclic voltammetry measurements no appreciable changes were found. Comparing the redox potentials of this two porphyrins with those found for the similar compound with only one ethynylenephenylene subunit (System A in the previous chapter, actually named H_2P-EP_1-CHO) it seems that no particular interactions are present between the porphyrin and the two linkers, since within a difference of 20 mV all the systems present the same values for both reduction and oxidation potentials. Hence, in conclusion the 2.20 V HOMO-LUMO gap in the free base porphyrin of the series H_2P-EP_n-CHO, where n = 1, 2, 3, remains substantially the same. The same analyses carried out on the "wire"-fullerene reference systems (TMS-EP_n-C_{60}, where n = 2, 3) have shown a classical expected behaviour of fulleropyrrolidine derivatives. No oxidation processes are present, while three reversible reduction waves are clearly discernable,

all due to the C_{60} moiety. In TMS-EP_2-C_{60}, these three reductions are at -0.64, -1.10 and at -1.70 V; in the TMS-EP_3-C_{60} the potential values remain more or less the same: being at -0.62, -1.06 and -1.65 V, but it is quite evident a sort of trend: the difference between the respective reduction potential tends to increase passing from first reduction to the third reduction, in fact between these two compounds we have a ΔV = 20, 40 and 50 mV respectively for the first, the second and the third reduction process. Noteworthy no irreversible reductions due to the linkers are clearly discernable in the potential window investigated. Considering the absence of the aldehydic group is plausible to assume that such irreversible wave, noticed at a negative potential of -1.7 V both in porphyrin systems and in TMS-EP_n-CHO systems, could arise from a side reaction of the aldehydic group itself. Further differences between the two "wire"-fullerene systems are not visible, except for a little shoulder, around -1.60 V, near the third reduction process in the TMS-EP_2-CHO reference compound (See Figure 4.4.8). Such discrepancies could be also due to the concentration or solution problems within the experimental conditions. The cyclic voltammetries of the free base porphyrin-"wire"-fullerene systems hold together the redox properties of both porphyrin and C_{60}. The H_2P-EP_2-C_{60} compound has three one electron reduction processes and one two electron reduction process, this last, that is the second wave at -1.09 V in the Figure 4.4.9, is given by the superimposition of the first porphyrin reduction and the second reduction of C_{60} moiety. The other one electron processes can be divided in the following way: the first reduction at -0.63 V is centered on the fullerene site, the third one at -1.39 V is the second reduction of the porphyrin part and the fourth reduction wave at -1.63 V corresponds to the third reduction of the fullerene residue.

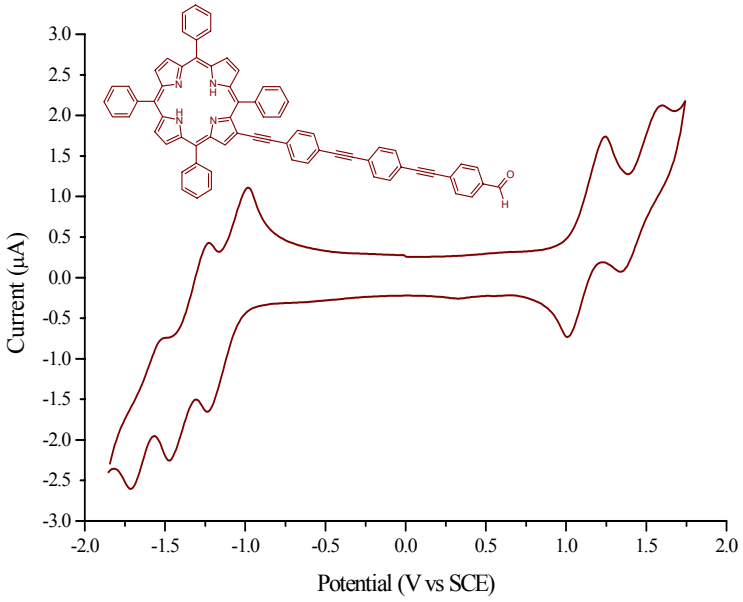

Figure 4.4. 7 *A complete scan of H_2P-EP_3-CHO in DCB solution with 0.05 M of $TBAPF_6$*

The two reversible oxidation processes are both centered on the porphyrin macrocycle and they are at 1.10 V and 1.46 V, values that are closely similar to the oxidation potential of H_2P-EP_2-CHO porphyrin-"wire" system. The porphyrin-"wire"-fullerene system with the longest linker

(H_2P-EP_3-C_{60}) shows similar behaviour for the reduction process (See Table 4.4.1 below at the end of the discussion), but it was impossible to obtain reversible oxidation. Most probably this is due to the low solubility and tendency to aggregation of the biggest porphyrin-"wire"-fullerene system. In this case a complete scan of the system, starting from positive potential and arriving at negative ones, evidences the presence of two shoulders at negative current values between 0 and -0.50 V, indicating the necessity to increase the negative potential to complete the oxidation-reduction process that takes place on the porphyrin moiety in the oxidation window (Figure 4.4.10).

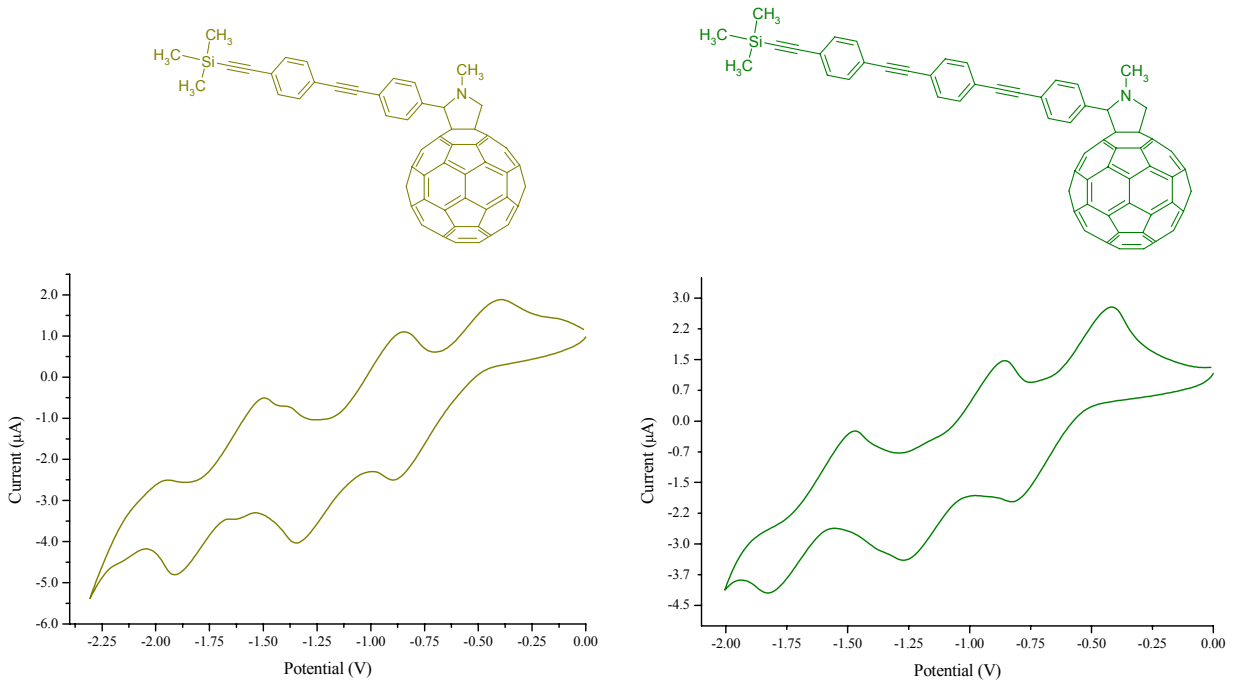

Figure 4.4. 8 *Cyclic voltammetries (reduction processes) in DCB solution of 0.05 M $TBAPF_6$ of TMS-EP_2-C_{60} on the left part and of TMS-EP_3-C_{60} on the right part of the figure.*

The study of the corresponding zinc derivatives was a little bit more difficult especially for the porphyrin-"wire" system, since these compounds show reversible oxidation processes, but it is very difficult to have a reversible reduction process. Both porphyrin systems have two reversible oxidation waves: ZnP-EP_2-CHO at 0.96 and 1.26 V, while ZnP-EP_3-CHO at 0.98 and 1.28 V. The difference of 20 mV between corresponding first and second oxidations in both compounds, could be considered quite low. On the contrary the reduction process is really difficult for the zinc porphyrins, in fact for both compounds it was not possible to isolate neither a first reversible reduction process, although half waves are evident at least at negative current values.

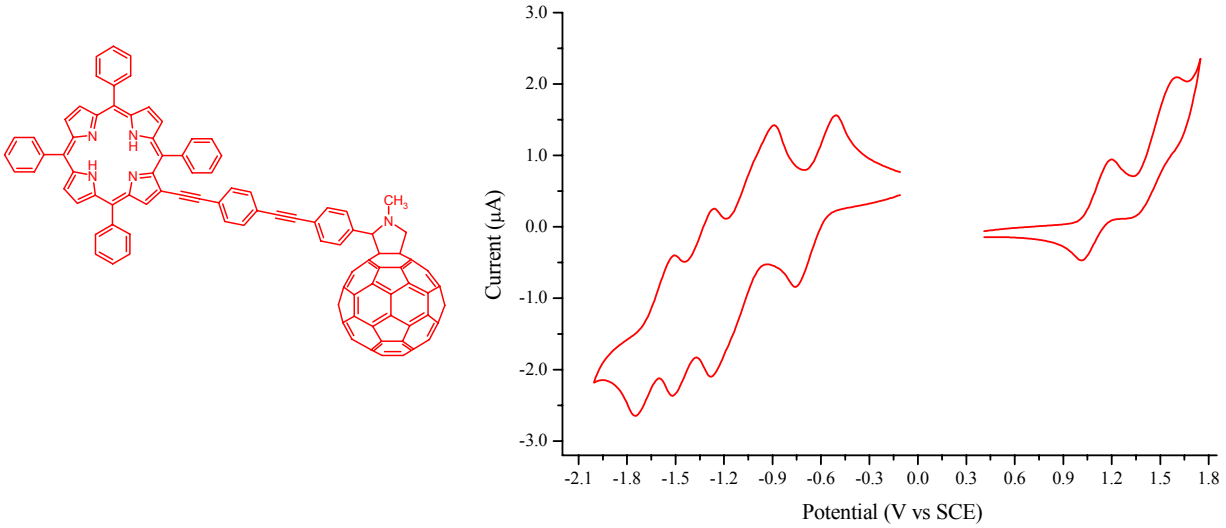

Figure 4.4. 9 *Oxidation and reduction waves in the H_2P-EP_2-C_{60} in DCB solution of 0.05 M of $TBAPF_6$. The two curves are recorded separately, but reported together in the same graph.*

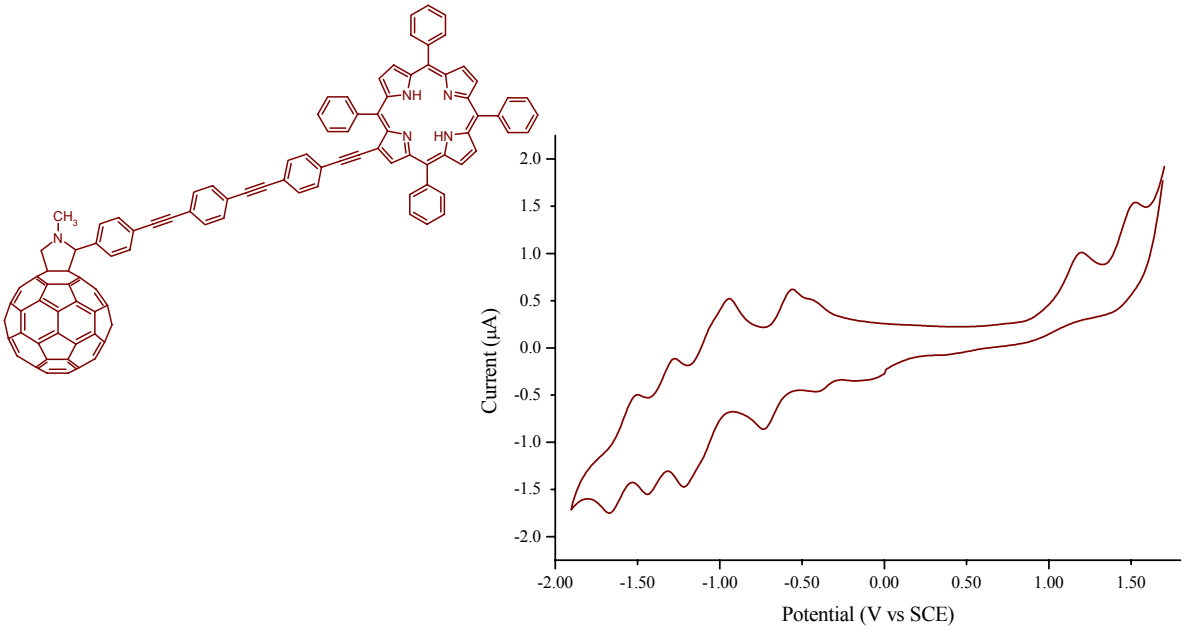

Figure 4.4. 10 *Complete cyclic voltammety of H_2P-EP_3-C_{60} in DCB solution of 0.05 M of $TBAPF_6$. Two shoulders between 0 and -0.50 V are clearly visible.*

The Square Wave technique was used to have an idea about the reduction potential values concerning the zinc derivatives (ZnP-EP_2-CHO). The measurements produce two peaks at -1.46 and -1.87 V, but the shape of such peaks did not show the same intensity and moreover the first one was flanked by a shoulder around -1.30 V, underlining one more time the irreversibility of the process. A complete scan reduction-oxidation experiment, carried out on the ZnP-EP_3-CHO

system, shows two weak shoulders between 0.35 and 0.75 V that could be considered as the residual re-oxidation processes, after the first two reductions at -1.30 and -1.59 V on the left part of the graph, this fact further evidences the necessity to use higher potential to complete the re-oxidation process coming after the first two reductions on the zinc porphyrin moiety (See Figure 4.4.11).

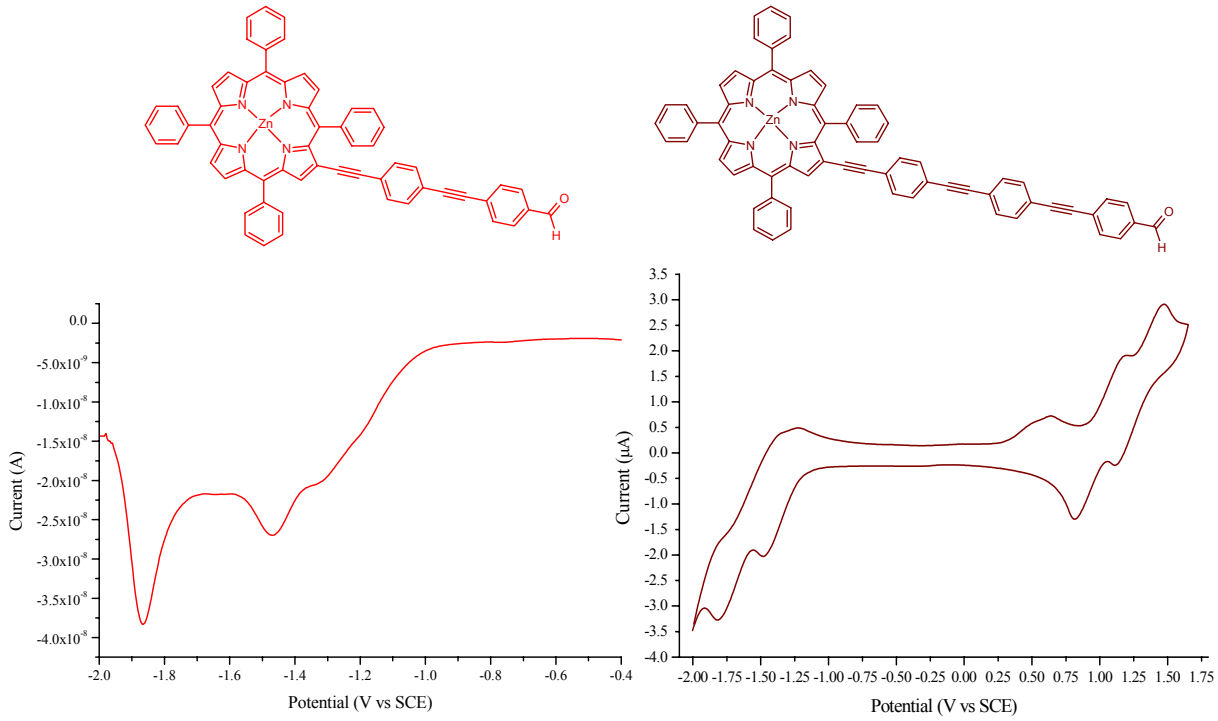

Figure 4.4. 11 *Square wave voltammetry of the ZnP-EP$_2$-C$_{60}$ in DCB solution of 0.05 M of TBAPF$_6$ on the left and a complete scan reduction-oxidation of ZnP-EP$_3$-C$_{60}$ in DCB solution of 0.05 M of TBAPF$_6$ on the right part.*

Despite the difficulties found in the zinc porphyrin systems, the measurements carried out on the zinc porphyrin-"wire"-fullerene systems were quite simple and almost all the reduction and oxidation processes were reversible. The oxidation window was characterized by the presence of two distinctive reversible oxidations due to the porphyrin moiety at 0.96 and 1.23 V for ZnP-EP$_2$-C$_{60}$ and at 0.98 and 1.24 V for ZnP-EP$_3$-C$_{60}$. Considering the substantial similarity between these values and those of the related ZnP-EP$_n$-CHO systems, where n = 2, 3, (0.96 and 1.26 V for n = 2, and 0.98 and 1.28 V for n = 3) it is possible to assume that the porphyrin moiety retains its own chemical physical properties. The reduction window is instead characterized by four reduction processes, moreover the reduction of porphyrin part seems to appear more clearly compared to those in the ZnP-EP$_n$-CHO systems.

In both systems the first two one electron reductions at -0.63 and -1.02 V for ZnP-EP$_2$-C$_{60}$, and at -0.64 and again -1.02 V for ZnP-EP$_3$-C$_{60}$ are due to the first and second reduction of fullerene

part. The third one at -1.30 and -1.31 V respectively for ZnP-EP_2-C_{60} and ZnP-EP_3-C_{60} can be attributed to the first reduction of the zinc porphyrin moiety. The last wave is a two electrons reduction process located virtually at the same potential for both systems (-1.59 V for ZnP-EP_2-C_{60} and -1.57 V for ZnP-EP_3-C_{60}) and it is given by the superimposition of the second porphyrin reduction with the third fullerene reduction (See Figure 4.4.12).

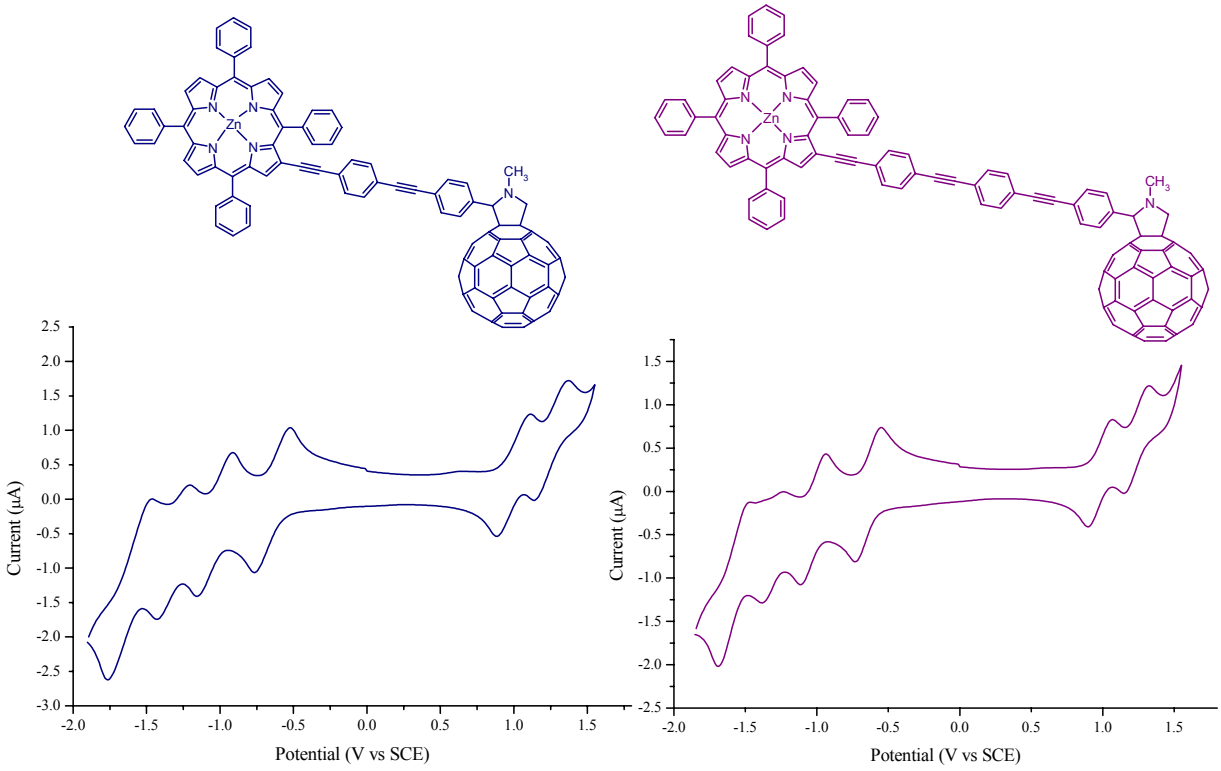

Figure 4.4. 12 *Cyclic voltammetry in DCB solution containing 0.05 M of $TBAPF_6$ of ZnP-EP_2-C_{60} on the left part and of ZnP-EP_3-C_{60} on the right part*

In conclusion cyclic voltammetry studies seem to suggest no particular interaction between the two chromophores and the linkers, assuming that the anomalies could arise from solubility problems and, as it has been outlined before, from side reaction involving the terminal aldehydic group of the spacer. Some improvements in the experimental condition must be found in order to have a better evaluation of all the anomalies found out with these experiments. Below a table with all the potential values of all investigated compounds in order to have a complete vision about the oxidation and reduction processes is reported.

Compound	Oxidation (V)		Reduction (V)			
	I	II	I	II	III	IV
H_2P-EP_2-CHO	1.12	1.45	-1.10	-1.33	-1.74 (irr.)	-
TMS-EP_2-CHO	-	-	-	-	-1.74 (irr.)	-
ZnP-EP_2-CHO	0.96	1.26	-1.31 (sw)	-1.47 (sw)	-1.87 (sw)	-
TMS-EP_2-C_{60}	-	-	-0.64	-1.10	-1.70	-
H_2P-EP_2-C_{60}	1.10	1.46	-0.63	-1.09	-1.39	-1.63
ZnP-EP_2-C_{60}	0.96	1.23	-0.63	-1.02	-1.30	-1.59
H_2P-EP_3-CHO	1.11	1.45	-1.10	-1.34	-1.60	-
TMS-EP_3-CHO	-	-	-	-	-1.76 (irr.)	-
ZnP-EP_3-CHO	0.98	1.28	-1.30	-1.59	-	-
TMS-EP_3-C_{60}	-	-	-0.62	-1.06	-1.65	-
H_2P-EP_3-C_{60}	1.20 (?)	1.52 (?)	-0.65	-1.08	-1.34	-1.59
ZnP-EP_3-C_{60}	0.98	1.24	-0.64	-1.02	-1.31	-1.58

Table 4.4. 1 *Oxidation ad reduction potentials in DCB solution, with 0.05 M of $TBAPF_6$, for the investigated compounds; sw = square wave, irr. = irreversible, ? = value corresponding to the oxidation wave vertex*

To evaluate photophysical properties of new compounds, steady state fluorescence experiments were carried out in three different solvents: toluene, THF and benzonitrile. The first evident result, both for the free base and zinc derivatives, is given by the fact that the introduction of an increasing length linker does not alter the porphyrin fluorescence quantum yield as it is visible in the Figure 4.4.13, where the emission of H_2P-EP_n-CHO and ZnP-EP_n-CHO systems in different solvent is reported. In toluene solution the new porphyrin systems present two emission bands at 664 and 731 nm for the free base derivatives, and at 605 and 660 nm for the respective zinc complexes. Obviously in coordinating solvents like THF and benzonitrile the emission bands of zinc porphyrins undergo to a red shift; the respective emission maxima are at 618 and 670 nm in THF and at 627 and 678 nm in benzonitrile. The free base porphyrins do not show particular changes in the emission bands varying the solvent, unless a 3 nm red shift in benzonitrile.

Comparing the fluorescence quantum yield of the different H_2P-EP_n-C_{60} systems in toluene solution, it is possible to see a decreasing quenching of porphyrin fluorescence as the length of the linker increases. In particular the porphyrin emission is quenched by the C_{60} moiety for 93, 47 and 20% respectively when n is equal to 1, 2, 3. A similar trend has been pointed out for the

corresponding zinc derivatives (See Figure 4.4.14) even if, in general, the quenching efficiency is higher for zinc porphyrin compounds if compared to the free base analogous compounds, for example the porphyrin emission in the ZnP-EP_2-C_{60} triad is quenched for 81% while in the ZnP-EP_3-C_{60} for 45%, even in toluene solution.

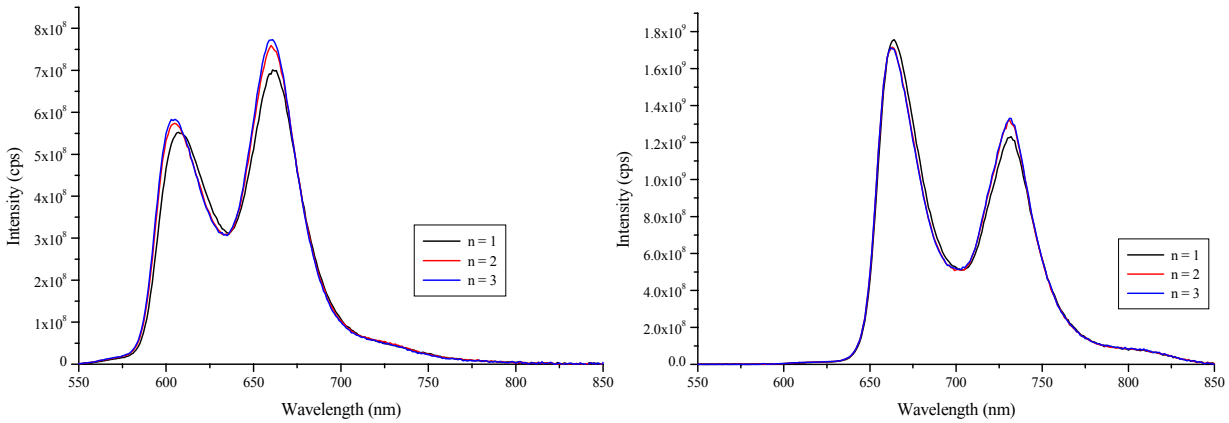

Figure 4.4. 13 *Left: fluorescence emission spectra of ZnP-EP_n-CHO system in toluene solution upon excitation at 460 nm. Right: fluorescence emission spectra of H_2P-EP_n-CHO system in THF solution upon excitation at 440 nm. In both cases the absorbance values (0.1) match at excitation wavelength.*

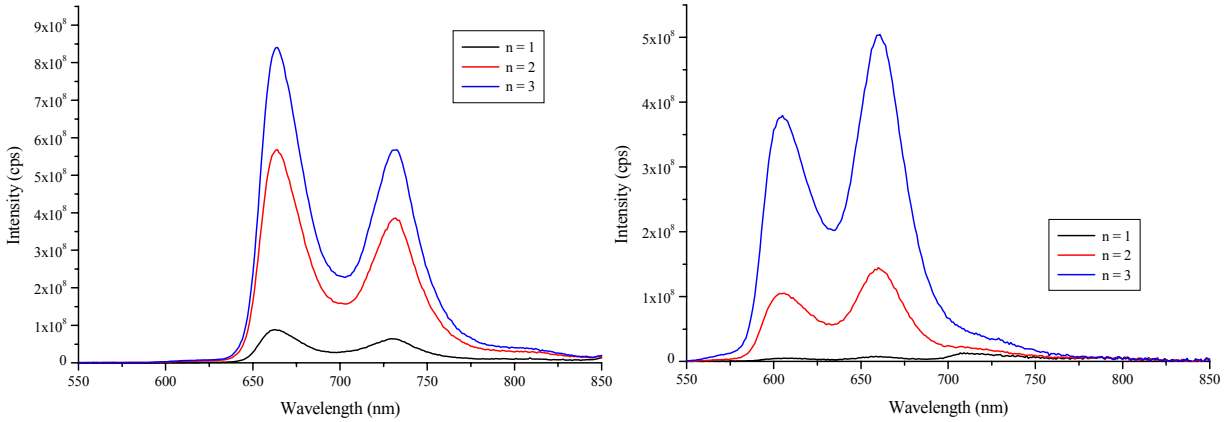

Figure 4.4. 14 *Left: fluorescence emission spectra of H_2P-EP_n-C_{60} system in toluene solution upon excitation at 440 nm. Right: fluorescence emission spectra of ZnP-EP_n-C_{60} system in toluene solution upon excitation at 460 nm. In both cases the absorbance values (0.1) match at excitation wavelength.*

This is an expected behaviour, because the increased distance between the porphyrin and fullerene moieties makes the energy and electron transfer reactions less active. Furthermore while in the ZnP-EP_1-C_{60} the strong quenching of porphyrin emission allows a direct identification of the energy transfer process, because it is clearly visible the emission of the C_{60} singlet excited state at 715 nm (See previous chapter Figure 4.3.14), in the new triads ZnP-EP_2-C_{60} and ZnP-EP_3-C_{60}, this was not observed, because the residual porphyrin emission cover this

signal. Steady state measurements carried out in THF and benzonitrile solution have confirmed the results obtained in toluene solution, with only one important difference: passing from less polar to more polar solvent the quenching efficiency of the porphyrin emission increases, suggesting a solvent dependent reaction pathway. In particular more polar solvent should shift the reaction from energy transfer to electron transfer. Figure 4.4.15 shows what we have just affirmed: the porphyrin emission in ZnP-EP$_n$-C$_{60}$ triads, where n = 2, 3, tends to decrease passing from toluene, to THF, to benzonitrile, highlighting a better quenching, most probably due to electron transfer reaction toward the C$_{60}$ moiety.

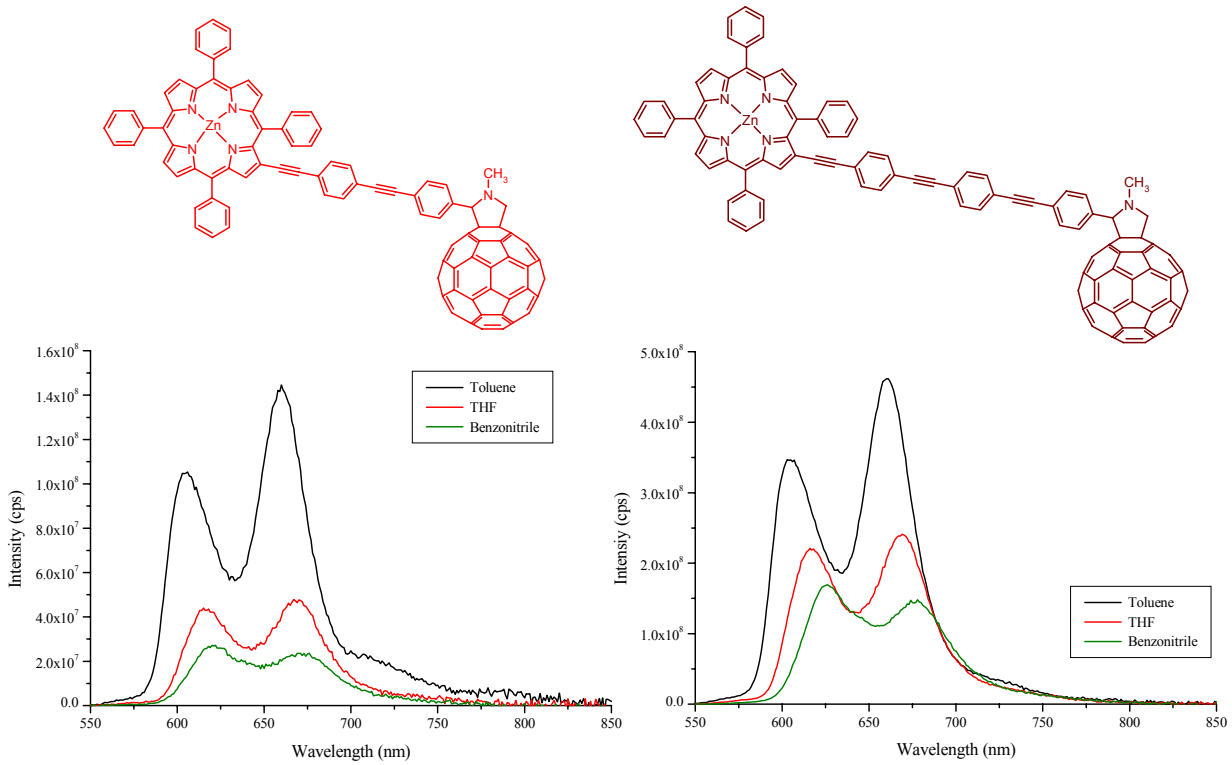

Figure 4.4. 15 *Steady state fluorescence emission spectra in different solvents of ZnP-EP$_2$-C$_{60}$ triad (on the left) and ZnP-EP$_3$-C$_{60}$ triad (on the right) upon excitation at 460 nm. In both cases the absorbance values (0.1) match at excitation wavelength.*

The table 4.4.2 summarizes the quenching percentage of the porphyrin fluorescence emission in both free base and zinc derivatives triad H$_2$P-EP$_n$-C$_{60}$ and ZnP-EP$_n$-C$_{60}$, where n = 2, 3. The results obtained from fluorescence steady state studies in different solvents are also reported in this table.

These fluorescence studies have pointed out a typical distance dependent energy or electron transfer, this last much more probable in polar solvent; but no information about the interaction between porphyrin and linkers, or between fullerene and linkers emerge. So it was decided to test the presence of eventually interaction between the single units within the triads exciting the

linker molecule at 335 nm. This study was carried out in toluene, THF and benzonitrile to evaluate a potentially solvent effect.

Compound	Quencing Efficiency		
	Toluene	THF	Benzonitrile
H_2P-EP_2-C_{60}	47%	60%	71%
ZnP-EP_2-C_{60}	81%	94%	95%
H_2P-EP_3-C_{60}	20%	23%	24%
ZnP-EP_3-C_{60}	45%	58%	66%

Table 4.4. 2 *Quencing efficiency for the porphyrin fluorescence emission in the new porphyrin-"wire"-fullerene systems in different solvents. The values are estimated from steady state fluorescence measurements.*

The linker molecules present a fluorescence emission band in the UV near visible region between 350 and 450 nm. TMS-EP_2-CHO compound shows a maximum at 380 nm, while TMS-EP_3-CHO a more broadened band with two peaks, one at 366 nm and the second at 384 nm. Considering that in this region both porphyrin and fullerene have absorption band, it is natural to expect energy transduction from the linker to porphyrin and fullerene. Exciting at 335 nm a toluene solution of H_2P-EP_n-CHO systems, no fluorescence emission originating from the linker, has been observed. This fact was observed also for zinc porphyrin derivatives and fullerene compounds, as it is possible to see in Figure 4.4.16 where the fluorescence of the linkers is completely quenched by porphyrin and fullerene moiety.

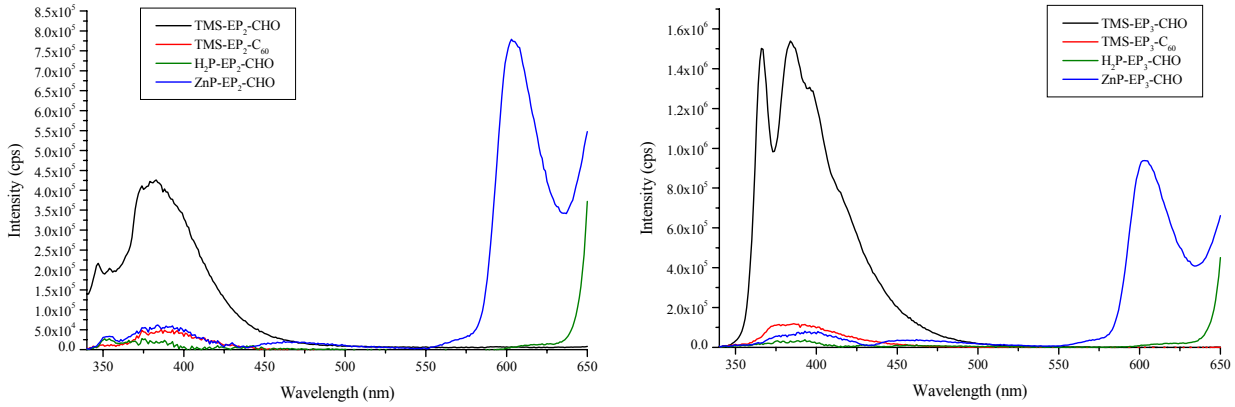

Figure 4.4. 16 *Fluorescence emission spectra of compounds H_2P-EP_n-CHO (green line), ZnP-EP_n-CHO (blue line), TMS-EP_n-C_{60} (red line) and TMS-EP_n-CHO (black line) in toluene solution upon excitation at 355 nm, the series with n = 2 is on the left and that with n = 3 on the right. It is clearly visible that the linker emission is completely quenched in all compounds of both series. Absorbance at excitation wavelength is 0.1.*

Since there is no possibility to have a complete selective excitation because also porphyrin and fullerene absorb at 335 nm, there is no possibility to evaluate if the quenching of the linker emission is due to an energy or an electron transfer. An indirect proof comes from the same measurements carried out in THF and benzonitrile: since the linker emission is completely quenched also in these two solvents, hence it is possible to affirm that no solvent effect was observed changing solvent polarity and it is plausible to assume that the meaning deactivation process for the linker excited state could be an energy transfer process.

Also time resolved fluorescence measurements were carried out on the new compounds but, although the preliminary results confirm the steady state data about the porphyrin fluorescence quenching both in H_2P-EP_n-C_{60} and ZnP-EP_n-C_{60} systems, in different solvents, other studies are necessary to have a complete description of these new porphyrin-"wire"-fullerene systems and to estimate the damping factor of the linker within these systems. For this last aim particular relevance has the possible conformation of the single unit within the bridge. In fact every ethynylenephenylene subunit can rotate around the single carbon-carbon bond which links each subunit and it has been proved[159] that in the donor-acceptor system linked by *para*-ethynylenephenylene bridge the electronic coupling between the two photoactive moieties and also the damping factor for energy and electron transfer could be dependent on the bridge conformation. In such direction could be useful some computational studies carried out on porphyrin-"wire"-fullerene systems, Figure 4.4.17 and 4.4.18 show the HOMO (orange) and LUMO (blue) orbital in the H_2P-EP_n-C_{60} and ZnP-EP_n-C_{60} systems, where n = 2, 3. Moreover it is possible to see that at this computational level (AM1 force field) the linker is tilted respect the porphyrin plane except in the ZnP-EP_2-C_{60} and the single subunits seem to be coplanar to each other. Further analyses must be carried out to complement this study.

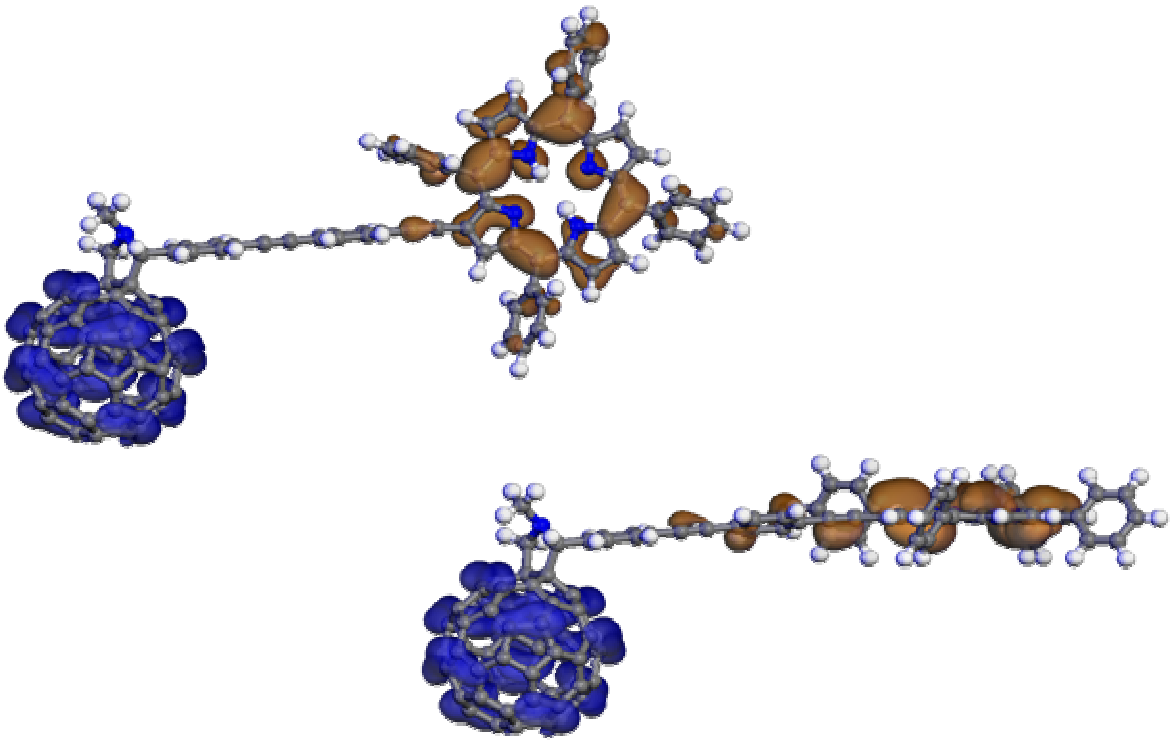

Figure 4.4. 17 *Computational study at AM1 level for H_2P-EP_2-C_{60} (left part) and ZnP-EP_2-C_{60} (right part).*

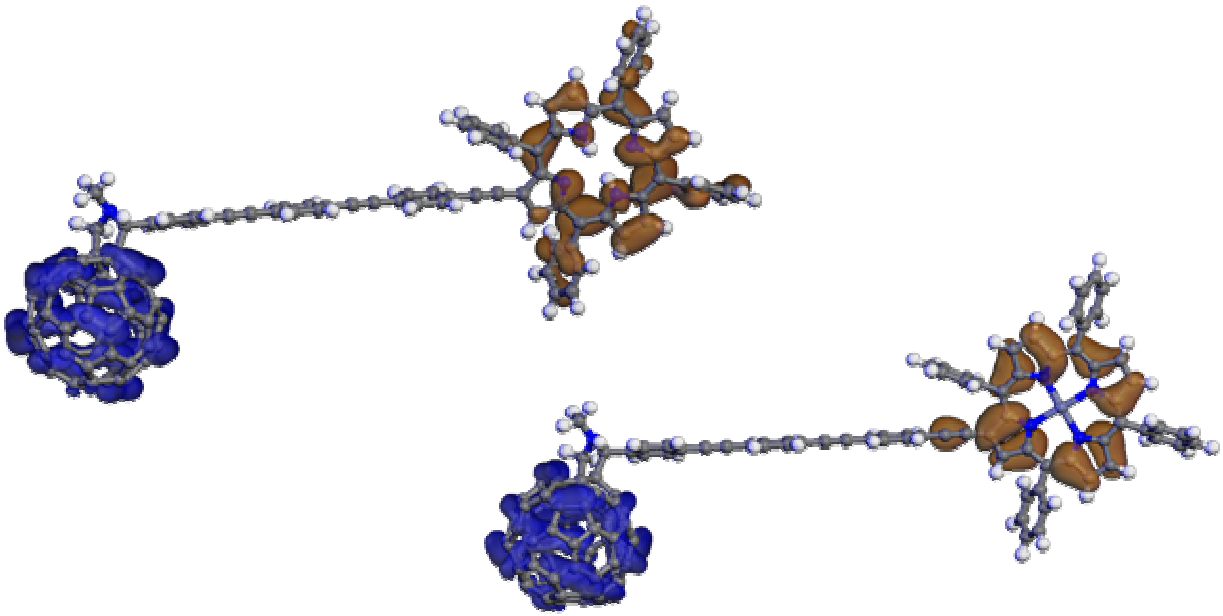

Figure 4.4. 18 19 *Computational study at AM1 level for H_2P-EP_3-C_{60} (left part) and ZnP-EP_3-C_{60} (right part).*

4.5. Preliminary UV-vis Study on Self-Assembling Zn-Porphyrin-Fullerene Dyad

The zinc porphyrin-fullerene dyad with pyridyl anchor group depicted in the Figure 4.5.1 recovers a theoretical importance: due to the presence of the pyridyl unit it undergoes to self assembling reaction in solution. Moreover since it is an already photoactive unit, offers the opportunity to study two contemporary electron transfer reactions, in fact as Figure 4.5.1 shows, once that the self assembling polymer is formed (in this case a trimer is depicted) we should notice two competitive electron transfer processes: one *intramolecular* electron transfer, where in this case *intramolecular* means that the process occurs between porphyrin and fullerene that are covalently linked, indicated by the blue arrow, and one *intermolecular* electron transfer between the porphyrin and axially coordinated fullerene moiety belonging to another dyad molecule, indicated by the red arrow.

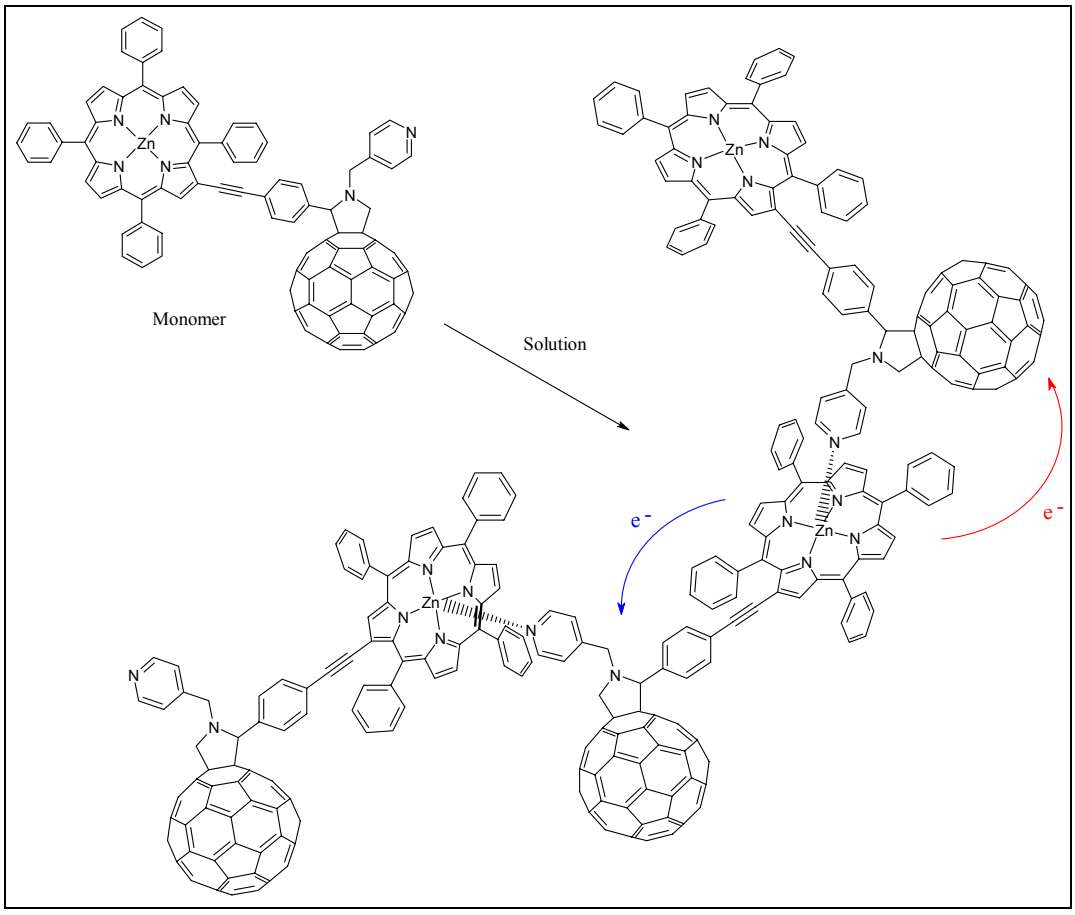

Figure 4.5. 1 *Self assembling zinc porphyrin-fullerene dyad with a pyridyl group as ligand.*

Before to complement fluorescence study it is necessary to get information on the binding process and because of the low solubility of this compound, the first step was to study the self-

assembling reaction between two reference compounds in toluene solution as reported in the Figure 4.5.2. Taking in consideration that the binding constants of several pyridyl groups toward zinc porphyrin derivative are of the order of 10^3 and the steric hindrance of substituent group of our two molecules, we have decided to carry out a preliminary titration of a zinc porphyrin solution in toluene adding a sovrastoichiometry quantity of fullerene derivative, in order to obtain an appreciable quantity of porphyrin-fullerene adduct. A 4.4 μM solution of zinc porphyrin was titrated with a 0.0126 M solution of fullerene derivative adding 2.5 μl each time.

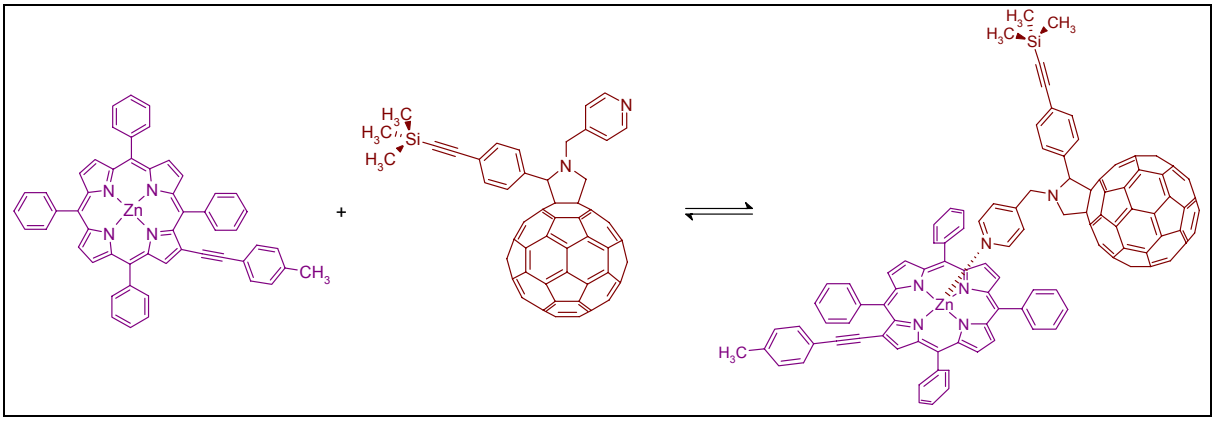

Figure 4.5. 2 *Self assembling reaction between zinc porphyrin and fullerene derivatives*

The spectral changes are reported in the Figure 4.5.3, it is possible to notice that in the condition described before, no isosbestic points are visible, only a continuous increase of the Soret band is observable. Elaborating the data, the Scatchard plot gives a binding constant of $(2.7\pm0.1)\times10^3$ M^{-1} that is in line with the values reported in literature[160].

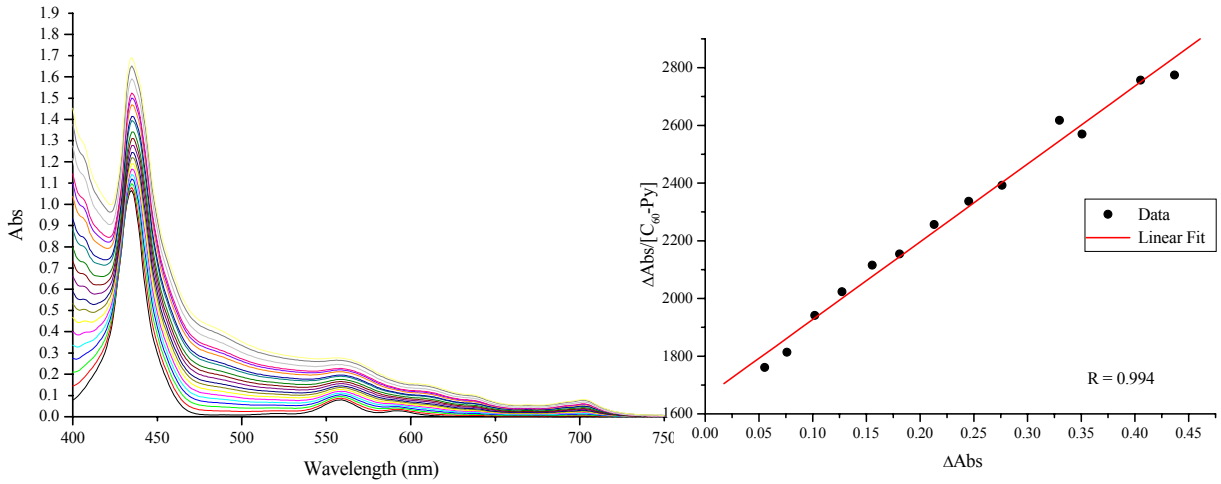

Figure 4.5. 3 *Uv-vis spectral changes of 4.4 μM toluene solution of zinc porphyrin, upon titration with C_{60} pyridyl derivative (on the left). Scatchard plot of the change of absorbance at 435 nm (on the right).*

Hence despite the restricted conformational degree of the pyridyl moiety, as it has been shown in the Chapter 1 through ^{1}H-NMR analysis, the fullerene derivatives presents the capability to give self assembling, moreover computational study (MM+ force field) carried out to optimize the self assembled porphyrin-fullerene geometry structure, do not show particular steric hindrance as it is visible in the Figure 4.5.4. This is only a preliminary study and further more accurate ones must be carried out. A series of studies have to be done to fully characterized the ZnP-C_{60}-Py system in solution. The previous reported self-assembling process between zinc porphyrin derivative and C_{60} pyridyl derivative is a starting point, in fact the self-assembling system coming from ZnP-C_{60}-Py monomer is much more complicated: the length of the self assembled olygomers must be determined, eventually concentration dependence of such length and also possible conformational effects, despite the rigidity of the system, must be considered. The first evident difference between the ZnP-C_{60}-Py system and the respective compound ZnP-C_{60} without pyridyl group, emerges from UV-vis spectra of the corresponding chloroform solutions (Figure 4.5.5).

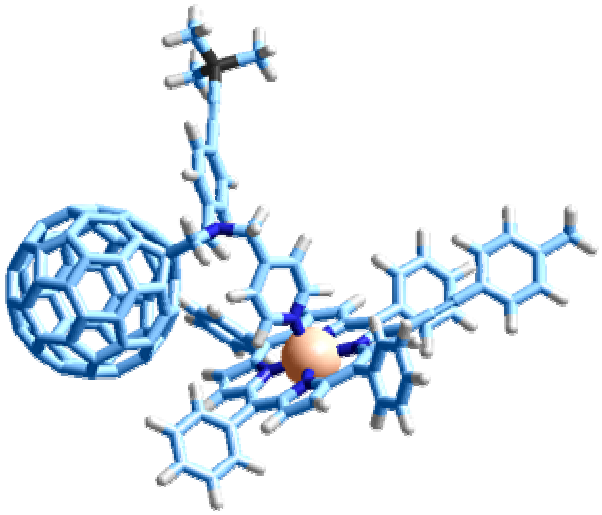

Figure 4.5. 4 *Optimized geometry (MM+ force field) of porphyrin-fullerene self assembling compounds.*

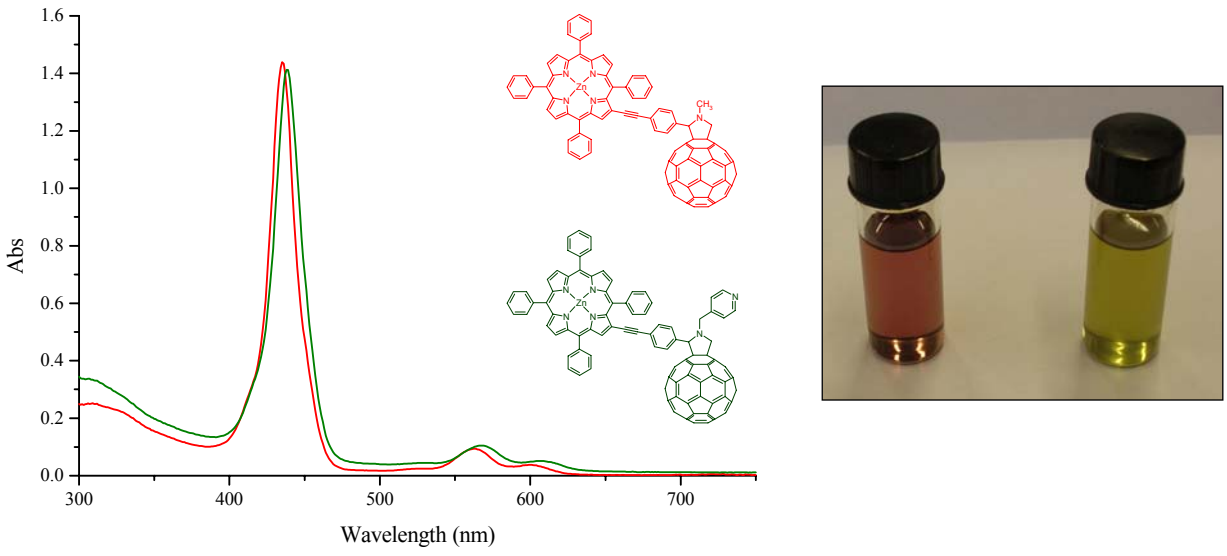

Figure 4.5. 5 *UV-vis absorption spectra of ZnP-C_{60} (red) and ZnP-C_{60}-Py (green) in chloroform solution. It is clearly visible the different colour solution.*

The ZnP-C_{60} dyad has the Soret band at 435 nm, while chloroform solution of the corresponding pyridyl derivative ZnP-C_{60}-Py, presents Soret band at 438 nm, outlining a little red shift, that is also visible for the Q bands, but much more evident is the different colour of the respective solutions: while a concentrated ZnP-C_{60} chloroform solution has a reddish colour a ZnP-C_{60}-Py chloroform solution presents a green colour, similar to that assumed by respective ZnP-C_{60} dyad in benzonitrile due to the axial coordination of the solvent.

The preliminary study of ZnP-C_{60}-Py system has evidenced interesting aspects for this new compound, that have to be fully understood and further studies are moving in such direction.

4.6. Conclusions and Potential Applications

We have focused our attention on the synthesis of new β-modified porphyrin-fullerene compounds in order to evaluate how such type of connection, altering the chemico-physical properties of the porphyrin moiety, can influence energy and electron transfer process. Ethynylenephenylene subunit was chosen as molecular spacer between porphyrin and fullerene. Due to its electronic properties these type of molecular bridges should offer quite good electronic coupling between the two chromophores. Under the light of these considerations three different porphyrin-fullerene compounds and their corresponding zinc complexes and reference compounds were synthesized, as depicted in Figure 4.6.1. Hence, starting from the simple MP-C_{60} dyad (**1** and **2** in Figure 4.6.1) we have developed MP-"wire"-C_{60} systems where the molecular wire is directly attached to the β-position of the tetrapyrrole ring.

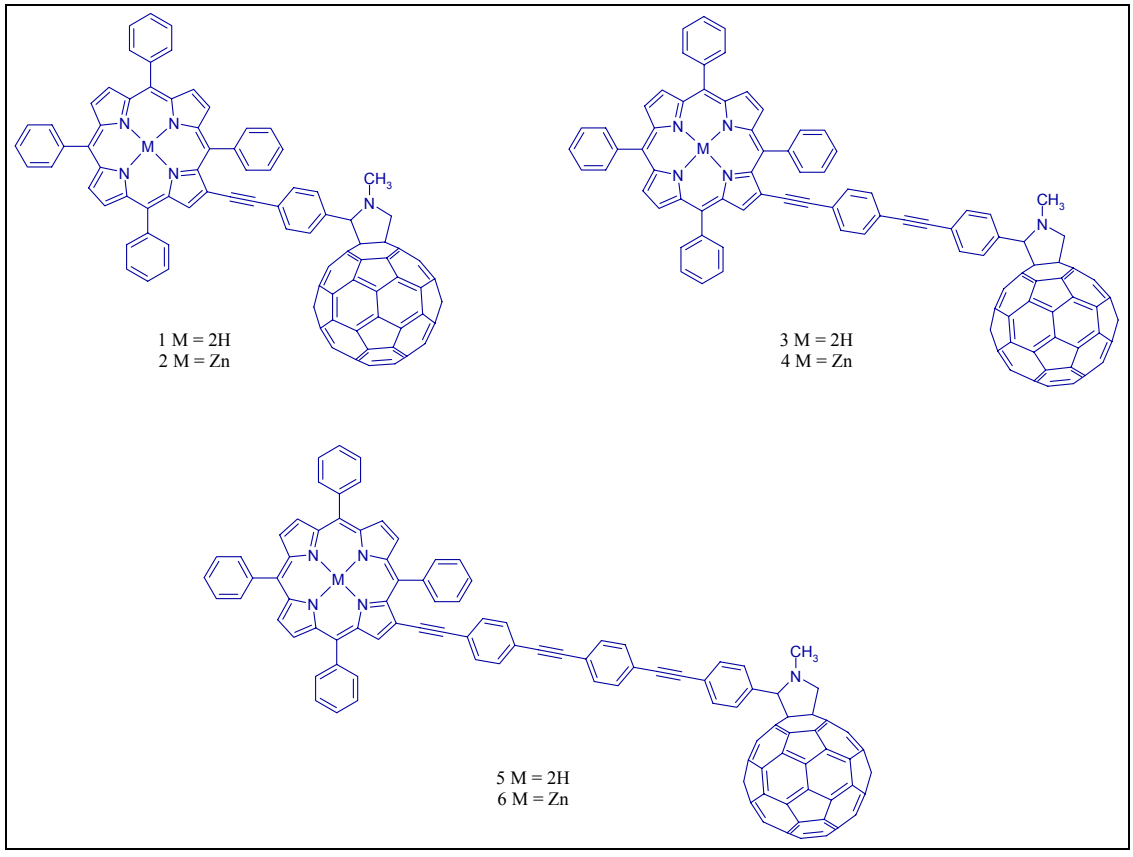

Figure 4.6. 1 *Porphyrin-"wire"-fullerene systems synthesized in our work*

The compounds indicated with number **1** and **2**, were completely characterized through Uv-visible; cyclic voltammetry, ^{1}H-NMR, ^{13}C-NMR and fluorescence analyses[152]. The study has revealed extension of conjugation along the substituent in the porphyrin system and fluorescence studies have confirmed ultrafast deactivation of the porphyrin singlet excited state,

quenched by the C_{60} moiety. In particular singlet-singlet energy transfer was found to be active in toluene solution, while in polar solvent like THF and benzonitrile the meaning deactivation pathway is electron transfer, that generates radical ion pair state that in THF solution lives for 398 ps and 1175 ps respectively for zinc porphyrin and free base porphyrin derivatives. The lifetime of the charge separated state is not so high, most probably due to the quite good electronic coupling between the two photoactive chromophores and the electronic properties of the spacer. Furthermore the increased distance between the donor and acceptor moiety in the longer analogues should increase the lifetime for the radical ion pair state. The systems indicated with number **3**, **4**, **5**, **6**, in the Figure 4.6.1 were partially investigated through UV-visible, cyclic voltammetry and steady state fluorescence studies. Essentially no interaction between porphyrin and fullerene was found in the fundamental state and it is also possible to assume that no direct interaction between the two aforementioned chromophores and linker is present in the fundamental state, while upon excitation of the spacer, an energy transfer towards both porphyrin and fullerene moiety is possible to take place. Further studies are necessary to complete the characterization and to evaluate the "wire" behaviour of the spacer.

Since many factor can influence the electron transfer reactions, we decided to synthesize also a porphyrinn-fullerene dyad where the two chromophores are frozen in a well defined geometry without having the possibility to rotate around any single carbon-carbon bond. For this aim a β-modified porphyrin was synthesized, bearing two ethynylenephenylene substituents on the same pyrrole ring. Due to the presence of two aldehydic groups it was possible to obtain three cyclic porphyrin-fulleropyrrolidine bis-adducts, whose nature must be clarified (Figure 4.6.2)

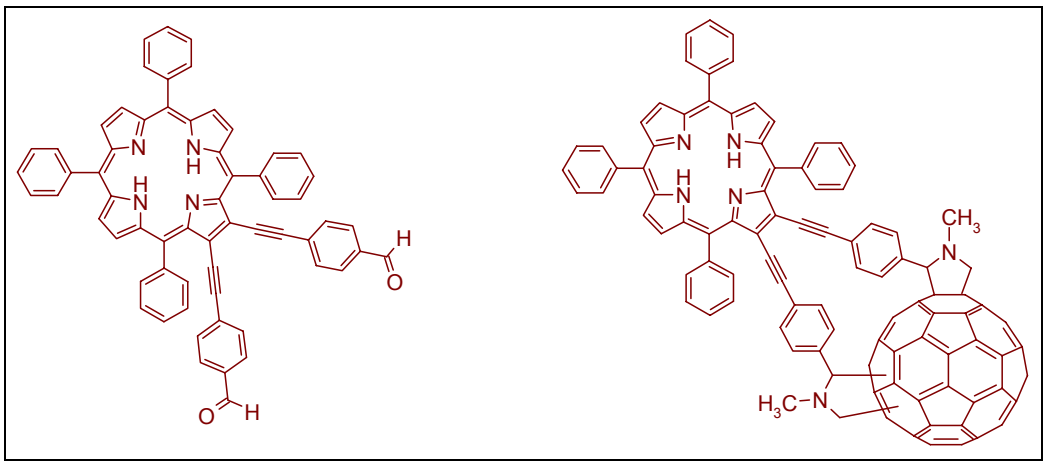

Figure 4.6. 2 *Cyclic porphyrin-fulleropyrrolidine bis-adduct (on the right) and respective β-modified porphyrin (on the left)*

From preliminary considerations and computational studies it is possible to suppose that the most probable bis adducts have a *trans*-3 and *trans*-4 configuration. This is only an hypothesis

supported by the constrained geometry of the two porphyrin branches, that should avoid the formation of *cis* or *equatorial* isomers. Further experimental evidences are necessary to confirm our hypothesis. Neverthless the new cyclic porphyrin-fullerene compounds can offer the possibility to evaluate conformational effect on electron transfer reactions.

Since not only theoretical aspect are important but it is also important to confer to these studies a practical application a synthetic route to introduce an anchor group, in particular a pyridyl group, into the porphyrin-fullerene systems previous shown, was developed. This has led to obtain the MP-C60-Py systems depicted in the Figure 4.6.3.

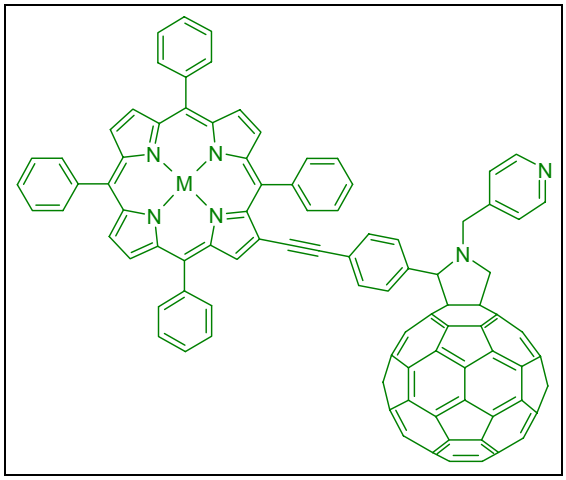

Figure 4.6. 3 *MP-C_{60}-Py system where M = 2H and Zn*

Although the study of this new self assembling porphyrin-fullerene dyad is at the beginning, interesting features are emerging. In this case the ZnP-C_{60}-Py molecule gives self assembled olygomers in non coordinating solvents and we have the opportunity to study two contemporary and competitive electron-transfer reactions: one directed toward the covalently linked fullerene and the other one toward the axial coordinated fullerene sphere. Moreover it is also possible to evaluate if a self assembling polymeric system, made of already photoactive dyads, can influence the electron transfer reaction decreasing or increasing the lifetime of the charge separated state.

The presence of the pyridyl group offers the possibility to obtain the respective methyl pyridinium salt, upon derivatization with CH_3I, a synthetic route that has been successfully proved. With a positive charged group at one terminus of the porphyrin fullerene dyad it is possible to use coulombic interactions to obtain, through a layer-by-layer deposition, ITO modified electrode as depicted in the Figure 4.6.4., so it is theoretically possible to build up organic solar cells with the new porphyrin-fullerene derivatives in order to evaluate their

photocurrent generation efficiency. The device can also be improved adding a self assembling ferrocene moiety as last electron donor.

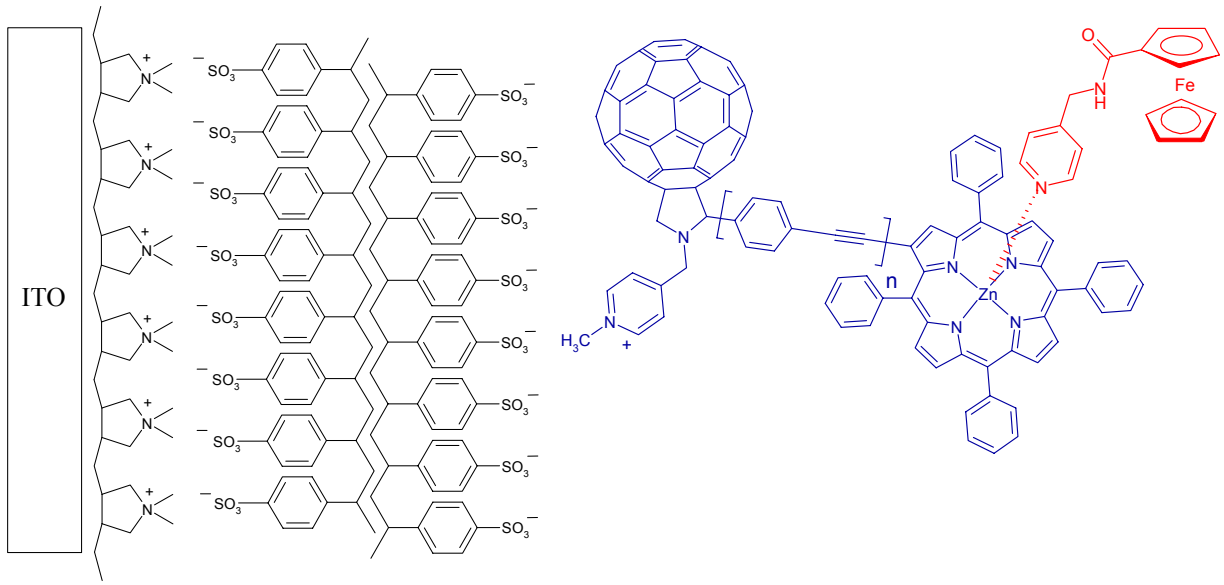

Figure 4.6. 4 *Potential application of new ZnP-EP$_n$-C$_{60}$ systems to modify ITO electrode surface for building organic solar cells; n = 1, 2, 3.*

In conclusion during this Ph.D. thesis a series of new porphyrin fullerene compounds was synthesized and fully or partially characterized. These compounds offer the possibility to have a further insight into energy and electron transfer reactions occurring between porphyrin and fullerene chromophores and it was also developed a synthetic route, which offer the opportunity to give a practical application to these new porphyrin-fullerene architectures.

Chapter 5

"Synthetic Methodologies"

In this chapter all the synthetic methodologies adopted to obtain the different compounds will be reported together with complete or partially characterization throughout mass spectrometry and NMR techniques.

5.1. General Methods

^{1}H-NMR and ^{13}C-NMR spectra were recorded as $CDCl_3$ or CD_3OD solutions on a Bruker AM-400 and Bruker AM-300 instrument using residual solvent signal as an internal standard. Chemical shifts are given as δ values. FAB mass spectra were measured on a VG-4 spectrometer using *m*-nitrobenzyl alcohol (NBA) as a matrix. GC mass spectra were recorded on a VG-4 spectrometer equipped with a 30 mt Supelco SPB-5 capillary column. MALDI mass spectra were performed with a MALDI-TOF Reflex IV (Bruker-Daltonics) in reflector mode, using a 337 nm nitrogen laser (8 Hz). A 2 mg/ml 2,5-dihydroxybenzoic acid (gentysic acid) solution in CH_3CN/TFA (0.1% solution), was used as a matrix.

UV/vis spectra were recorded on a Varian Cary 50 Scan spectrophotometer in toluene or chloroform solution. Steady state fluorescence studies were carried out on a Fluoromax 3 (Horiba) instrument and all the spectra were corrected for the instrument response. Time resolved fluorescence spectra were recorded on a Photon Technology International Company lifetime spectrofluorometer in the nanosecond time domain, with a 337 nm nitrogen laser and elaborated with Felix software. The femtosecond transient absorption studies were performed with 387 nm laser pulses (1Khz 150 fs pulse width) from an amplified Ti:Sapphire laser system (Model CPA 2101, Clark-MXR Inc.). Nanosecond laser Flash Photolysis experiments were performed with 532 nm laser pulses from a Quanta-Ray CDR Nd:YAG system (6 ns pulse width) in a front face geometry. Cyclic voltammetry was carried out with a Autolab electrochemical system, Eco Chemie equipped with PG Stat-12. Current-voltage curves were recorded using GPES, Eco Chemie software. A three electrode system was used and consisted of a platinum button working electrode, a platinum wire counter electrode and a saturated calomel reference electrode (SCE). This reference electrode was separated from the bulk of the solution by a fritted-glass bridge filled with solvent/supporting electrolyte mixture. All potentials are referenced to the SCE.

5.2. Chemicals

Silica gel 60 (70-230 and 230-400 mesh, Merck) was used for column chromatography. 1,2-dichlorobenzene (DCB) for electrochemistry was purchased from Aldrich Chemical Co. and purified by several washings with conc. H_2SO_4 and distilled over P_2O_5 under vacuum prior to use. Tetra-n-butylammonium hexafluorophosphate ($TBAPF_6$), from Aldrich Chemical Co., was recrystallized from ethyl acetate and dried under vacuum at 40 ^oC for at least one week prior to use. High-purity-grade nitrogen gas was purchased from Rivoira. C_{60} was purchased from Term-USA. All other reagents were from Fluka Chem. Co., Aldrich Chem. Co. or Carlo Erba and were used as received. Solvents used for fluorescence analyses were from Aldrich Chem. Co. and were spectrofotometric grade. When anhydrous conditions were required the solvents were freshly distilled under nitrogen atmosphere and at ambient pressure, following the literature procedures: toluene was distilled over sodium, dichloromethane and chloroform were distilled over P_2O_5 and THF over $LiAlH_4$.

5.3. Syntheses

4-(trimethylsilyl)ethynylbenzaldheyde. 16 g (86 mmol) of 4-bromobenzaldehyde and 14 g (142 mmol) of trimethylsilylacetylene were dissolved in 100 ml of dried (KOH) triethylamine. The solution was deareated using argon bubbling for 30 minutes, after that 227 mg (1 mmol) of $Pd(OAc)_2$ and 450 mg (1.7 mmol) of PPh_3 were added to the solution. The solution was then refluxed under argon, with vigorous stirring. After 4 h the crude mixture was cooled, filtered and the solid salts washed with triethylamine. The organic solution was concentrated under vacuum, diluted with dichloromethane (100 ml) and washed with water (3x100 ml). The organic layer was separated, dried over anhydrous Na_2SO_4 and filtered. The solvent was then evaporated under vacuum. The pale yellow residue was purified by column chromatography on silica gel eluting with petroleum ether (40°-70°)/diethyl ether, 98:2, giving the desired product as white crystals, 10.8 g (62% yield). MS (GC): *m/z*: 202 [M^+]; ^{1}H-NMR (400 MHz, $CDCl_3$): δ(ppm) 10.02 (s, 1H), 7.84 (d, 2H; J= 8.2 Hz), 7.63 (d, 2H; J=8.2 Hz), 0.29 (s, 9H).

4-ethynylbenzaldehyde. 4g (20 mmol) of 4-(trimethylsilyl)ethynylbenzaldehyde were dissolved under nitrogen in 50 ml of $CHCl_3$ and then a saturated solution (10 ml) of K_2CO_3 in methanol was added dropwise. After 2 h water was added to the organic solution. The organic phase was separated and the aqueous phase was extracted with chloroform. The combined organic solutions were washed with water and dried over anhydrous Na_2SO_4. The solvent was evaporated under vacuum to give 2.4 g of pure 4-ethynylbenzaldehyde (92% yield). MS (GC):

m/z: 130 [M^+]; ^{1}H-NMR (400 MHz, $CDCl_3$,): δ(ppm) 9.98 (s, 1H), 7.70 (d, 2H; J=8.2 Hz), 7.50 (d, 2H; J=8.2 Hz), 3.22 (s, 1H).

1-iodo-4-(trimethylsilyl)ethynyl-benzene. 7.6 g (23 mmol) of 1,4-diiodobenzene, 212 mg (3×10^{-4} mol) of $PdCl_2(PPh3)_2$ and 115 mg (6×10^{-4} mol) of CuI were dissolved in 50 ml of anhydrous THF, then 3 ml of anhydrous (KOH) triethylamine was added. The solution was left under nitrogen atmosphere at 40 °C and a solution of 1.40 g (14 mmol) of trimethylsilylacetylene in 10 ml of THF was added dropwise over one hour. After 6 h, the reaction was stopped and solvent evaporated under vacuum, the product was directly purified by column chromatography on silica gel eluting with petroleum ether (40°-70°). The desired product was obtained as white needles in a 62% yield. MS (GC): *m/z*: 300 [M^+]; 285 [M -15]$^+$, 158 [285-127]$^+$; ^{1}H-NMR (300 MHz, $CDCl_3$,): δ(ppm) 7.66 (d, 2H; =8.8 Hz), 7.20 (d, 2H; J=8.8 Hz), 0.26 (s, 9H).

4-[4'-(trimethylsilyl)ethynyl]phenyl-ethynylbenzaldeide, (TMS-EP$_2$-CHO). 700 mg (2.3 mmol) of 1-iodo-4-(trimethylsilyl)ethynyl-benzene and 305 mg (2.3 mmol) of 4-ethynylbenzaldehyde were dissolved in 50 ml of anhydrous THF, then 3 ml of triethylamine with 44 mg (6.3×10^{-5} mol) of $PdCl_2(PPh3)_2$ and 28 mg (1.5×10^{-4} mol) of CuI were added and the mixture was left to react under nitrogen at 40 °C. After 5 h the solvent was removed under vacuum and the product purified with silica gel column eluting with CH_2Cl_2/petroleum ether (40°-70°), 30:70 recovering 450 mg of the desired product as white powder (yield 65%). MS (GC): *m/z*: 302 [M^+];^{1}H-NMR (300 MHz, $CDCl_3$,): δ(ppm) 10.05 (s, 1H), 7.89 (d, 2H; J=8.3 Hz), 7.69 (d, 2H; J=7.5 Hz), 7.51 (m, 4H), 0.28 (s, 9H). UV/vis (Toluene): λ_{max} (nm) = 325, 347.

4-[(4'-ethynyl)phenyl]-ethynylbenzaldeide. Deprotection of terminal triple bond was carried out following the procedures reported for the 4-ethynylbenzaldehyde, the reaction is quantitative. ^{1}H-NMR (300 MHz, $CDCl_3$,): δ(ppm) 10.05 (s, 1H), 7.90 (d, 2H; J=7.8 Hz), 7.70 (d, 2H; J=7.8 Hz), 7.52 (s, 4H), 3.22 (s, 1H).

4-{4'-[4''-(trimethylsilyl)ethynylphenyl]ethynylphenyl}-ethynylbenzaldehyde, (TMS-EP$_3$-CHO). 155 mg (6.6×10^{-4} mol) of 4-[(4'-ethynyl)phenyl]-ethynylbenzaldeide, 205 mg (6.8×10^{-4} mol) of 1-iodo-4-(trimethylsilyl)ethynyl-benzene, 11,5 mg (1.6×10^{-5} mol) of $PdCl_2(PPh3)_2$ and 10 mg (4.7×10^{-5} mol) of CuI in THF/NEt_3 solution (60:3 ml) were left to react at 40 °C under nitrogen atmosphere for 6 h. Then the reaction was stopped, the solvent evaporated under vacuum and the product purified with silica gel column eluting with CH_2Cl_2/petroleum ether (40°-70°),

30:70. The desired product was obtained as pale yellow powder and it was recrystallized from $CHCl_3$/petroleum ether, affording 170 mg of pale yellow-white needles (yield 65%). MS (FAB): *m/z*: 402 [M^+];^{1}H-NMR (300 MHz, $CDCl_3$,): δ(ppm) 10.05 (s, 1H), 7.90 (d, 2H; J=7.98 Hz), 7.70 (d, 2H; J=7.98 Hz), 7.55 (s, 4H), 7.48 (s, 4H), 0.28 (s, 9H). UV/vis (Toluene): λ_{max} (nm) = 345.

4-{4'-[4''-(ethynyl)phenyl]ethynylphenyl}-ethynylbenzaldehyde. Also in this case the removal of the trimethylsilyl protecting group was carried out adopting the procedure reported for 4-ethynylbenzaldehyde, the reaction is quantitative. ^{1}H-NMR (300 MHz, $CDCl_3$,): δ(ppm) 10.05 (s, 1H), 7.90 (d, 2H; J=7.98 Hz), 7.70 (d, 2H; J=7.98 Hz), 7.55 (s, 4H), 7.50 (s, 4H), 3.20 (s, 1H).

N-methyl-2-(4'-ethynyl)phenyl-3,4-fulleropyrrolidine, (C_{60}-ref.). A mixture of 4-ethynylbenzaldheyde (10 mg, 77 μmol), C_{60} (56 mg, 77 μmol) and N-methylglicine (54 mg, 0.6 mmol) was refluxed for 24 h in anhydrous toluene under nitrogen atmosphere. After cooling to room temperature, the solvent was evaporated under vacuum and the residue was purified on silica gel column eluting with toluene/petroleum ether (40°-70°), 3:2, recovering as first band the unreacted [60]fullerene, followed by the reaction product (29 mg, yield 42%). MS (MALDI): *m/z*: 877 [M^+], 720 [M-157]$^+$; ^{1}H-NMR (400 MHz, $CDCl_3$): δ(ppm) 7.81 (d, 2H; J=7.9 Hz), 7.58 (d, 2H; J=7.9 Hz), 5.0 (d, 1H; J=8.9 Hz), 4.96 (s, 1H), 4.28 (d, 1H; J=9.9 Hz), 3.11 (s, 1H), 2.82 (s, 3H); UV/vis (Toluene): λ_{max} ($10^{-4}\varepsilon$) = 330 (5.0).

N-methyl-2-[(4'-trimethylsilylethynyl)phenyl]ethynylphenyl-3,4-fulleropyrrolidine, (TMS-EP_2-C_{60}). 16 mg (5.2×10^{-5} mol) of 4-[4'-(trimethylsilyl)ethynyl]phenyl-ethynylbenzaldeide, 55 mg (7.6×10^{-5} mol) of C_{60} and 70 mg (7.6×10^{-4} mol) of N-methylglicine were left to react under nitrogen atmosphere, in 60 ml of refluxing anhydrous toluene solution. After 24 h the solvent was removed under vacuum and the product purified by silica gel chromatography eluting with petroleum ether (40°-70°)/toluene, 3:2 obtaining 33 mg of brown powder as final product (yield 60%). MS (MALDI): *m/z*: 1049 [M^+], 720 [M-329]$^+$; ^{1}H-NMR (300 MHz, $CDCl_3$): δ(ppm) 7.82 (br d, 2H), 7.61 (d, 2H; J=7.6 Hz), 7.45 (s, 4H), 5.02 (d, 1H; J=9.8 Hz), 4.98 (s, 1H), 4.29 (d, 1H; J=9.8 Hz), 2.84 (s, 3H), 0.26 (s, 9H). UV/vis (Toluene): λ_{max} (nm) = 312, 332. MALDI-TOF mass spectrum and ^{1}H-NMR spectrum in $CDCl_3$ solution are reported below in Figure 5.3.1 and 5.3.2 respectively.

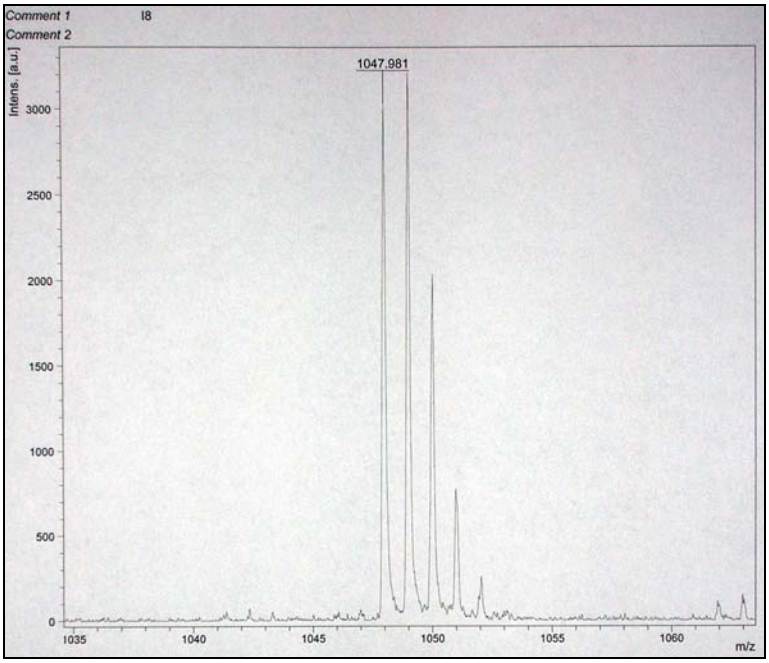

Figure 5.3. 1 *MALDI-MS spectrum of TMS-EP$_2$-C$_{60}$*

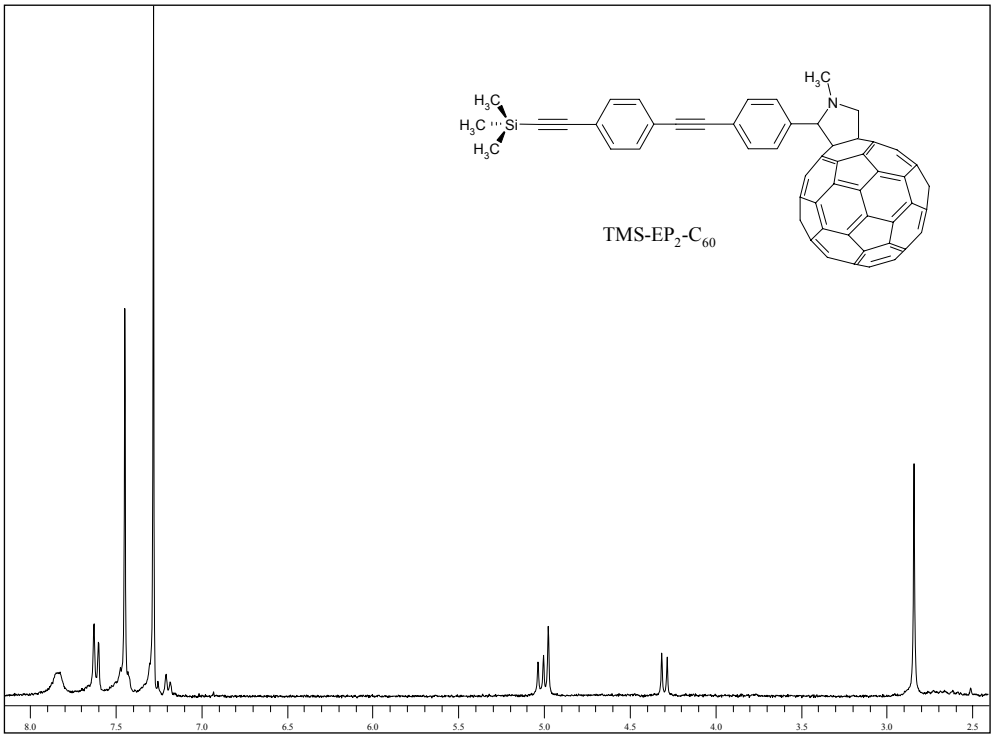

Figure 5.3. 2 *^{1}H-NMR spectrum in $CDCl_3$ solution of TMS-EP$_2$-C$_{60}$*

N-methyl-2-{4'-[4''-(trimethylsilyl)ethynylphenyl]ethynylphenyl}ethynylphenyl-3,4-fulleropyrrolidine, (TMS-EP$_3$-C$_{60}$). The desired product was synthesized following the previously reported procedures for the N-methyl-2-(4'-ethynyl)phenyl-3,4-fulleropyrrolidine and purified with silica gel chromatography eluting with petroleum ether (40°-70°)/toluene, 3:2 obtaining brown-reddish powder (yield 70%). 20 mg of TMS-EP$_3$-CHO (5×10^{-5} mol), 54 mg (7.5×10^{-5} mol) of C_{60} and 67 mg (7.5×10^{-4} mol) of N-methylglicine were used as starting reagents. MS (MALDI): *m/z*: 1149 [M^+], 720 [M-429]$^+$; ^{1}H-NMR (400 MHz, $CDCl_3$): δ(ppm) 7.85 (br d, 2H), 7.63 (d, 2H; J=8.3 Hz), 7.50 (s, 4H), 7.46 (s, 4H) 5.02 (d, 1H; J=9.1 Hz), 4.98 (s, 1H), 4.29 (d, 1H; J=9.1 Hz), 2.84 (s, 3H), 0.27 (s, 9H). UV/vis (Toluene): λ_{max} (nm) = 336. MALDI-TOF mass spectrum and ^{1}H-NMR spectrum in $CDCl_3$ solution are reported below in Figure 5.3.3 and 5.3.4 respectively.

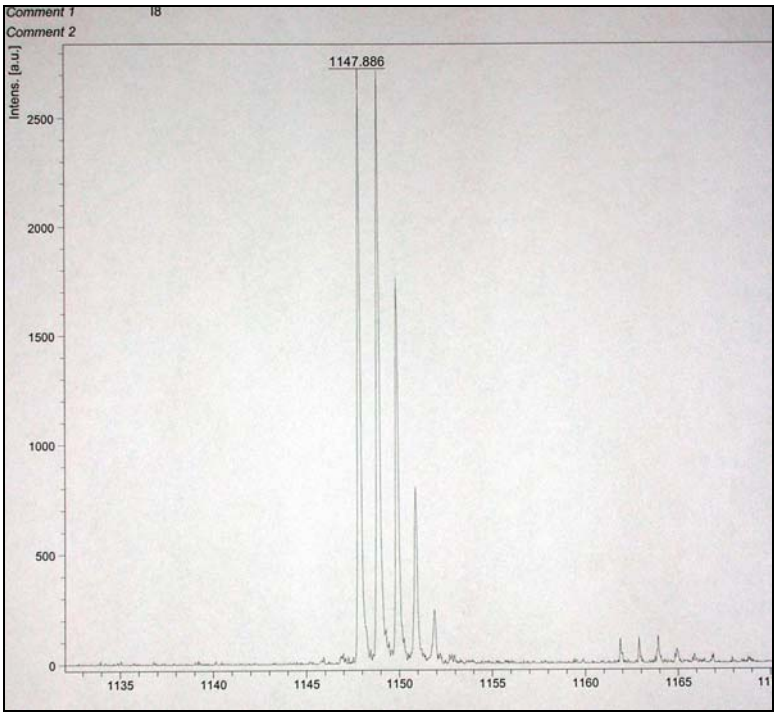

Figure 5.3. 3 *MALDI-MS spectrum of TMS-EP$_3$-C$_{60}$*

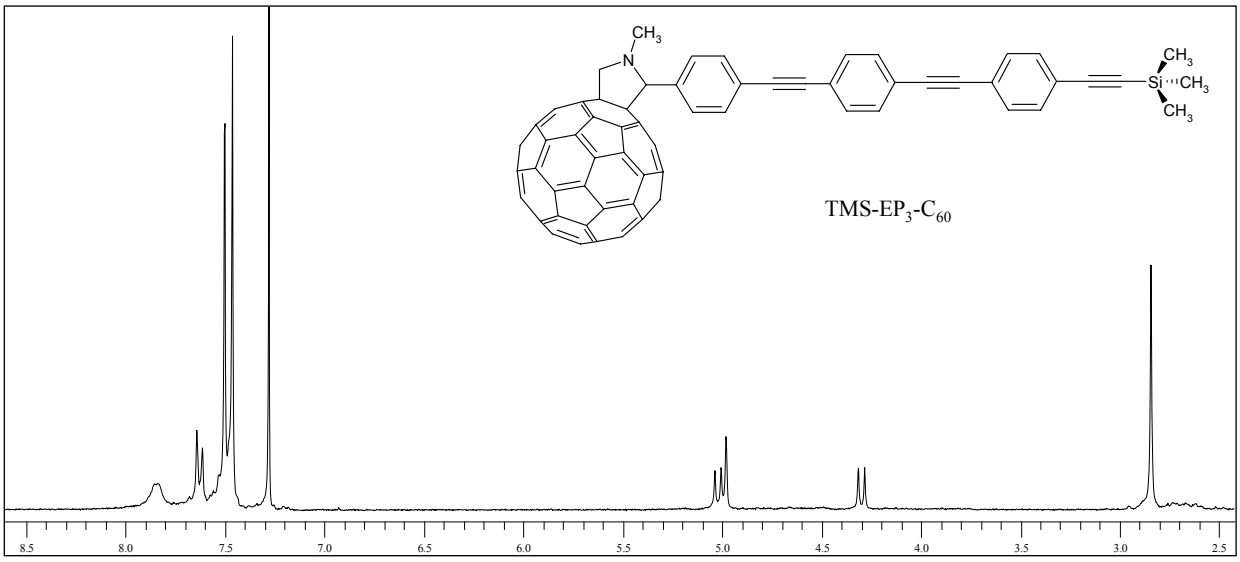

Figure 5.3. 4 *^{1}H-NMR spectrum in $CDCl_3$ solution of TMS-EP_3-C_{60}*

2-bromo-5,10,15,20-tetraphenylporphyrin. N-bromosuccinimide (251 mg, 1.4 mmol) was slowly added to a refluxing solution of *meso*-tetraphenylporphyrin (500 mg, 0.8 mmol) in $CHCl_3$ (150 ml) under nitrogen. After 2 h the crude mixture was cooled to room temperature and 2 ml of pyridine were added. The solvent was evaporated under vacuum and the crude product was purified by column chromatography on silica gel eluting with xilene/petroleum ether (40°-70°), 3:2, obtaining 260 mg of the desired porphyrin (yield 46%). MS (FAB): *m/z*: 693 [M^+], 613 [M-80]$^+$; ^{1}H-NMR (400 MHz, $CDCl_3$): δ(ppm) 8.94-8.91 (br m, 2H), 8.89 (s, 1H), 8.88-8.83 (br m, 2H), 8.79-8.77 (br m, 2H), 8.22 (br m, 6H), 8.11 (br m, 2H), 7.82-7.72 (br m, 12H), -2.82 (br s, 2H).

2-[(4'-formyl)phenyl]ethynyl-5,10,15,20-tetraphenylporphyrin (System A or H_2P-EP_1-CHO). A three necks round bottom flask, fitted with a condenser, was carefully deoxygenated with a strong stream of dry argon, after that a solution of 2-bromo-5,10,15,20-tetraphenylporphyrin (260 mg, 0.37 mmol) and 4-ethynylbenzaldehyde (70 mg, 0.54 mmol) in toluene/triethylamine, 5:1 (60 ml), was added. The solution was deareated for 30 minutes with argon bubbling and then $Pd(dba)_2$ (40 mg, 0.07 mmol) and $AsPh_3$ (170 mg, 0.55 mmol) were added. The solution was deareated for further 5 minutes, after that the argon inlet was placed 1 cm above the solution. The argon flow rate was turned up slightly and the reaction was left under nitrogen at 60 °C. After 16 h, the mixture was cooled at room temperature and the solvent evaporated. The

crude product was dissolved in dichloromethane and washed several times with water. The organic solution was dried over anhydrous Na_2SO_4 and the solvent evaporated under vacuum. The product was purified by column chromatography on silica gel eluting with CH_2Cl_2/petroleum ether (40°-70°), 2:3. The first compound eluted from the column was $AsPh_3$ after that the polarity of eluting mixture was gradually increased up to CH_2Cl_2/petroleum ether (40°-70°), 3:2. The desired porphyrin obtained from the column was recrystallized from dichloromethane/methanol to give 247 mg of purple powder (yield 90%). MS (FAB): *m/z*: 742 [M^+]; ^{1}H-NMR (400 MHz, $CDCl_3$): δ(ppm) 10.06 (s, 1H), 9.14 (s, 1H), 8.92 (s, 2H), 8.86 (d, 1H; J=5.1 Hz), 8.80 (br s, 3H), 8.25 (br m, 5H), 7.86 (d, 2H; J=8.2 Hz), 7.80-7.66 (br m, 15H), 7.52 (d, 2H; J=8.2 Hz), -2.64 (s, 2H); UV/vis (Toluene): λ_{max} ($10^{-4}\varepsilon$) = 432 (20.9), 525 (2.03), 560 (0.62), 602 (0.58), 659 (0.46). HSQC and HMBC spectra in $CDCl_3$ solution were reported below in Figure 5.3.5 and 5.3.6.

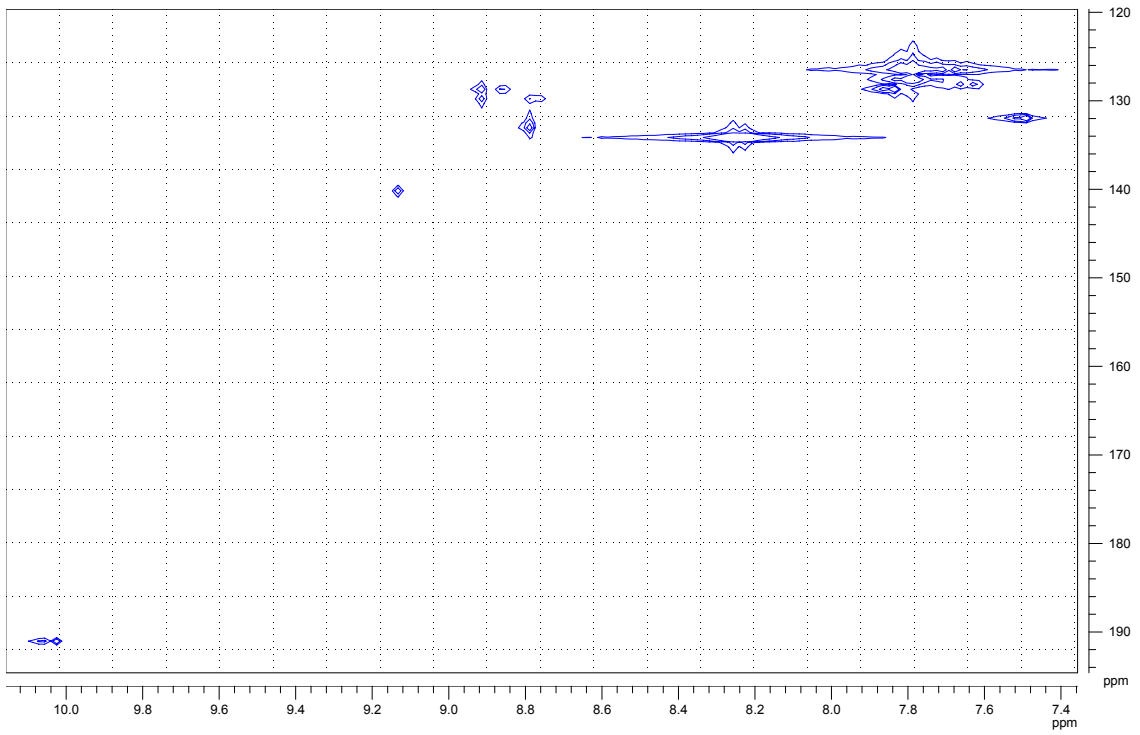

Figure 5.3. 5 *HSQC spectrum of System A (2-[(4'-formyl)phenyl]ethynyl-5,10,15,20-tetraphenylporphyrin)*

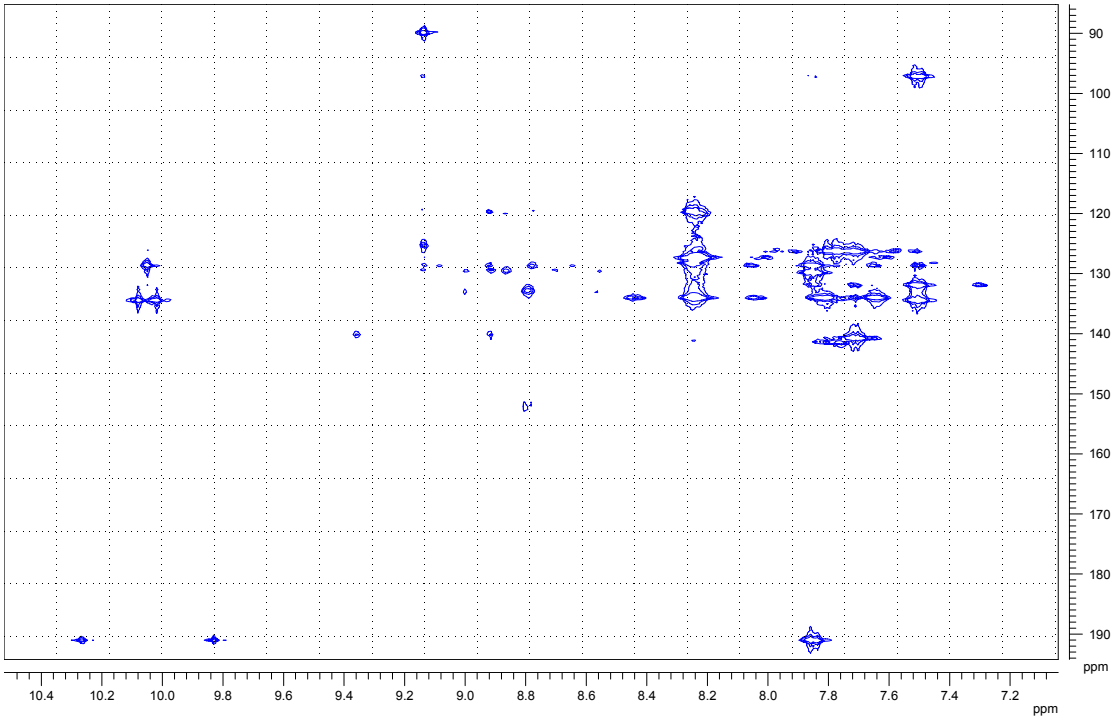

Figure 5.3. 6 *HMBC spectrum of System A (2-[(4'-formyl)phenyl]ethynyl-5,10,15,20-tetraphenylporphyrin)*

2-[(4'-methyl)phenyl]ethynyl-5,10,15,20-tetraphenylporphyrin (System B). A solution of 2-bromo-5,10,15,20-tetraphenylporphyrin (40 mg, 57 µmol) and 4-ethynyltoluene (9 mg, 77 µmol) in toluene/triethylamine,5:1 (36 ml), with $Pd(dba)_2$ (6 mg, 10 µmol) and $AsPh_3$ (24 mg, 80 µmol) was allowed to react under nitrogen atmosphere for 16 h at 60 °C. The mixture was cooled at room temperature, the solvent evaporated under vacuum and the residue redissolved in dichloromethane. The organic solution was washed with water (3x50 ml), dried over anhydrous Na_2SO_4 and evaporated under vacuum. The residue was purified on silica gel column eluting with CH_2Cl_2/petroleum ether (40°-70°), 25:75 to obtain 33 mg of porphyrin (yield 79%) which was recrystallized from dichloromethane/methanol to give the desired compound as purple powder. MS (FAB): *m/z*: 728 [M^+]; ^{1}H-NMR (400 MHz, $CDCl_3$): δ(ppm) 9.07 (s, 1H), 8.88 (s, 2H), 8.82 (d, 1H; J=5.1 Hz), 8.80 (s, 2H), 8.74 (d, 1H; J=5.1 Hz) 8.23 (br m, 5H), 7.80-7.66 (br m, 15H), 7.25 (d, 2H; J=7.3 Hz), 7.16 (d, 2H; J=7.3 Hz), 2.42 (s, 3H), -2.66 (s, 2H); UV/vis (Toluene): λ_{max} ($10^{-4}\varepsilon$) = 428 (22.5), 523 (2.15), 558 (0.609), 600 (0.59), 657 (0.36). The HSQC spectrum in $CDCl_3$ solution is reported below in Figure 5.3.7.

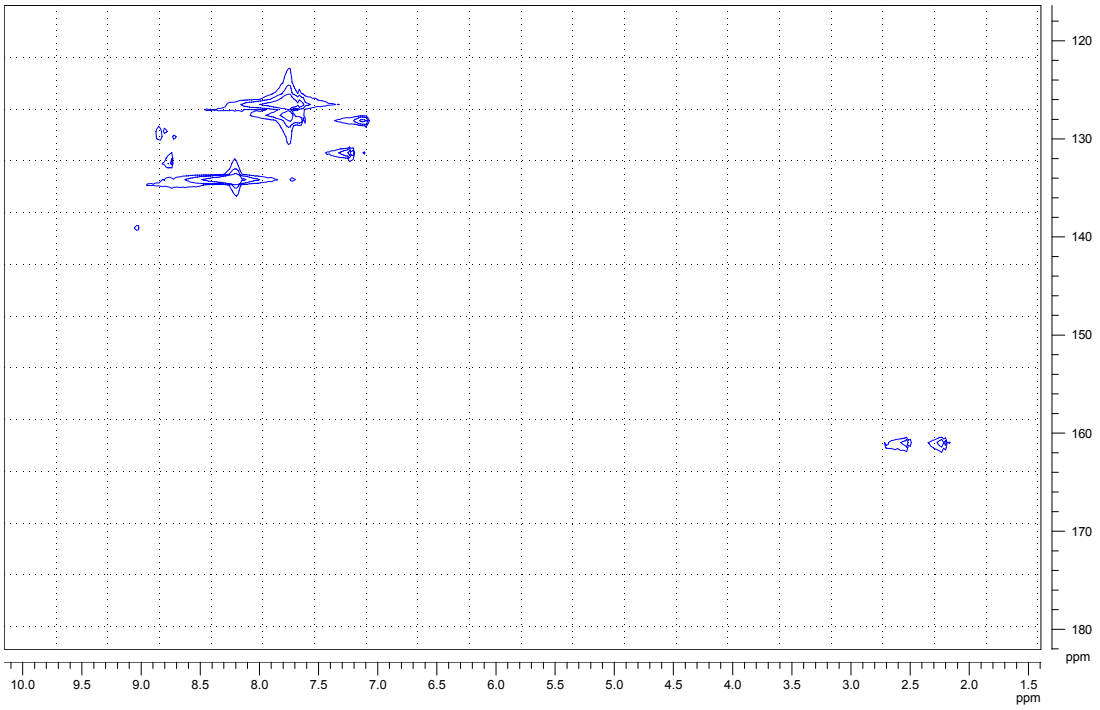

Figure 5.3. 7 *HSQC spectrum of System B (2-[(4'-methyl)phenyl]ethynyl-5,10,15,20-tetraphenylporphyrin)*

H_2P-EP_2-CHO. The synthesis of compound was carried out in the same conditions reported for 2-[(4'-formyl)phenyl]ethynyl-5,10,15,20-tetraphenylporphyrin. The desired product was purified by column chromatography on silica gel eluting with $CHCl_3$/petroleum ether (40°-70°), 1:1. The first compound eluted from the column was $AsPh_3$ after that the polarity of eluting mixture was gradually increased up to $CHCl_3$/petroleum ether (40°-70°), 70:30. The desired porphyrin obtained from the column was recrystallized from dichloromethane/methanol to give a purple powder (yield 65%). MS (FAB): *m/z*: 842 [M^+]; ^{1}H-NMR (300 MHz, $CDCl_3$): δ(ppm) 10.06 (s, 1H), 9.10 (s, 1H), 8.90 (s, 2H), 8.85 (d, 1H; J=5.9 Hz), 8.79 (s, 2H), 8.77 (d, 1H; J=5.9 Hz), 8.23 (br m, 5H), 7.91 (d, 2H; J=7.8 Hz), 7.80-7.66 (br m, 17H), 7.54 (d, 2H; J=7.8 Hz), 7.38 (d, 2H; J=7.8), -2.65 (s, 2H); UV/vis (Toluene): λ_{max} (nm) = 333, 374, 430, 524, 560, 603, 659.

H_2P-EP_3-CHO. The synthesis of compound was carried out in the same conditions reported for 2-[(4'-formyl)phenyl]ethynyl-5,10,15,20-tetraphenylporphyrin. The desired product was purified by column chromatography on silica gel eluting with $CHCl_3$/petroleum ether (40°-70°), 1:1. The first compound eluted from the column was $AsPh_3$ after that the polarity of eluting

mixture was gradually increased up to $CHCl_3$/petroleum ether (40°-70°), 3:2. The desired porphyrin obtained from the column was recrystallized from dichloromethane/methanol to give a purple powder (yield 70%). MS (FAB): *m/z*: 942 [M^+]; ^{1}H-NMR (300 MHz, $CDCl_3$): δ(ppm) 10.04 (s, 1H), 9.10 (s, 1H), 8.90 (s, 2H), 8.85 (d, 1H; J=4.5 Hz), 8.79 (br s, 3H), 8.23 (br m, 5H), 7.91 (d, 2H; J=8.3 Hz), 7.80-7.66 (br m, 15H), 7.70 (d, 2H; J=8.3 Hz), 7.58 (s, 4H), 7.53 (d, 2H; J=8.3 Hz), 7.38 (d, 2H; J=8.3), -2.67 (s, 2H); UV/vis (Toluene): λ_{max} (nm) = 344, 373, 430, 524, 560, 603, 659.

H_2P-C_{60} (or H_2P-EP_1-C_{60}). A mixture of 2-[(4'-formyl)phenyl]ethynyl-5,10,15,20-tetraphenylporphyrin (35 mg, 47 μmol), C_{60} (51 mg, 70 μmol) and N-methylglicine (63 mg, 0.7 mmol) was refluxed for 24 h in anhydrous toluene under nitrogen atmosphere. After cooling, the solvent was evaporated and the residue purified on silica gel column eluting with toluene, recovering the unreacted [60]fullerene as first fraction, the reaction product as second (42 mg, yield 59%) and the unreacted porphyrin as the third one. MS (FAB): *m/z*: 1490 [M+H]$^+$, 769 [M-720]$^+$, 720 [M-769]$^+$; ^{1}H-NMR (400 MHz, $CDCl_3$): δ(ppm) 9.07 (s, 1H), 8.89 (s, 2H), 8.82 (d, 1H; J=5.1 Hz), 8.79 (s, 2H), 8.73 (d, 1H; J=5.1 Hz), 8.22 (br m, 5H), 7.79 (br m, 15H), 7.61 (br, m, 2H), 7.43 (br, m, 2H), 4.96 (d, 1H; J=9.2 Hz), 4.89 (s, 1H), 4.22 (d, 1H; J=9.2 Hz), 2.86 (s, 3H), -2.68 (s, 2H); UV/vis (Toluene): λ_{max} ($10^{-4}\varepsilon$) = 300 (4.88), 429 (21.6), 523 (2.1), 558 (0.71), 601 (0.62), 657 (0.38). FAB-MS spectrum and ^{1}H-NMR spectrum in $CDCl_3$ solution are reported below in Figure 5.3.8 and 5.3.9.

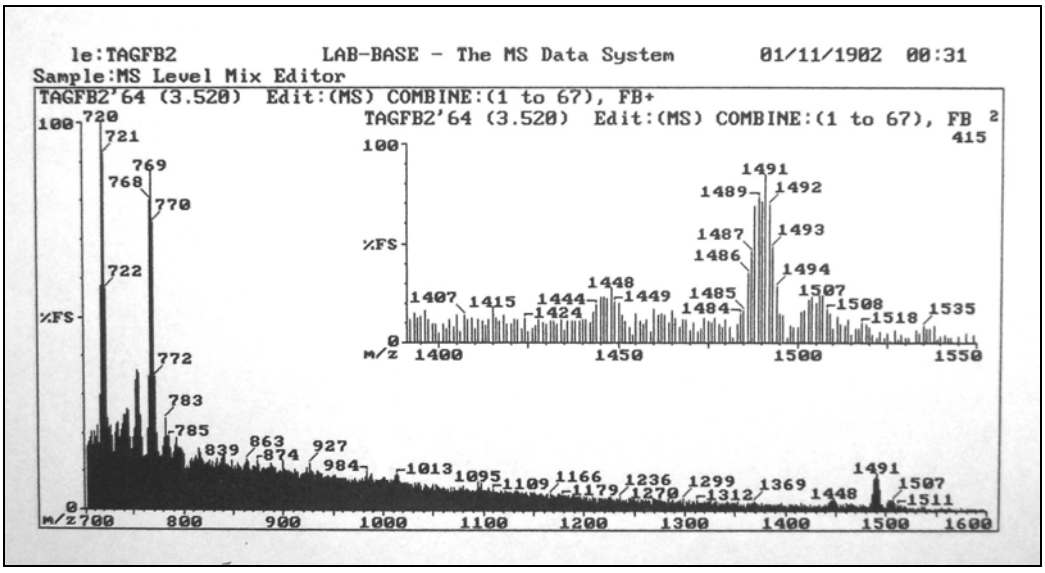

Figure 5.3. 8 *FAB-MS spectrum of H_2P-C_{60} (or H_2P-EP_1-C_{60})*

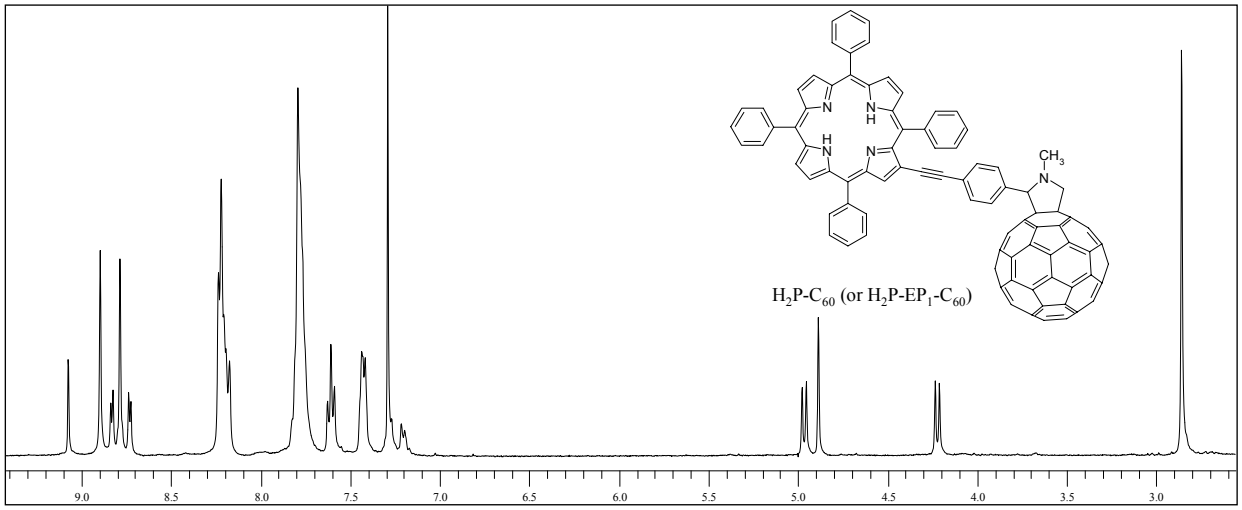

Figure 5.3. 9 *^{1}H-NMR spectrum in $CDCl_3$ solution of H_2P-C_{60} (or H_2P-EP_1-C_{60})*

H_2P-EP_2-C_{60}. Reaction conditions are equal to those reported for the synthesis of H_2P-EP_1.C_{60}. After reaction the product was purified by silica gel chromatography eluting with toluene/petroleum ether (40°-70°), 70:30 recovering a black-purple powder (yield 57%). MS (MALDI): *m/z*: 1590 $[M+H]^+$, 869 $[M-720]^+$, 720 $[M-869]^+$; ^{1}H-NMR (300 MHz, $CDCl_3$): δ(ppm) 9.09 (s, 1H), 8.89 (s, 2H), 8.83 (d, 1H; J=5.8 Hz), 8.77 (s, 2H), 8.75 (d, 1H; J=5.8 Hz), 8.21 (br m, 5H), 7.80-7.66 (br m, 19H), 7.48 (d, 2H; J=7.8 Hz), 7.34 (d, 2H; J=7.8), 4.92 (d, 1H; J=9.8), 4.84 (s, 1H), 4.16 (d, 1H; J=9.8), 2.80 (s, 3H), -2.67 (s, 2H); UV/vis (Toluene): λ_{max} (nm) = 323, 430, 524, 560, 603, 659. MALDI-MS spectrum and ^{1}H-NMR spectrum in $CDCl_3$ solution are reported below in Figure 5.3.10 and 5.3.11.

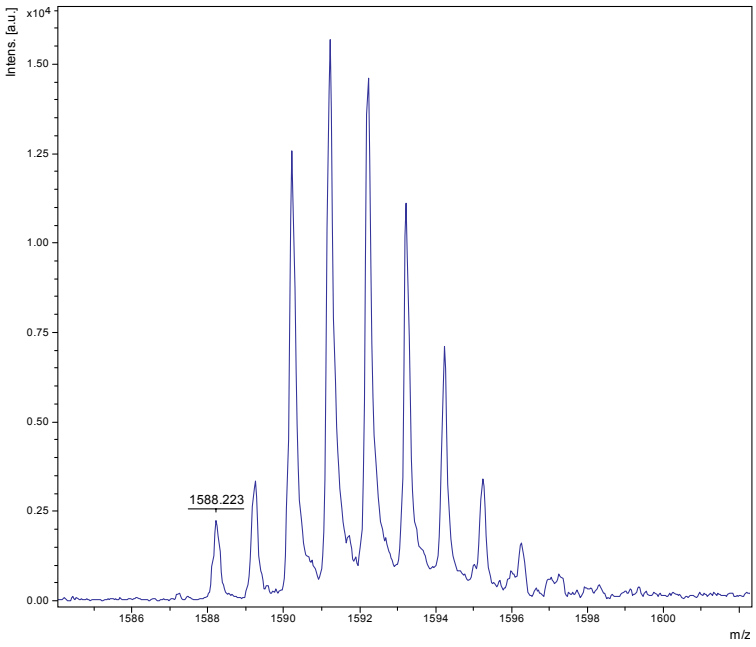

Figure 5.3. 10 *MALDI-MS spectrum of H_2P-EP_2-C_{60}*

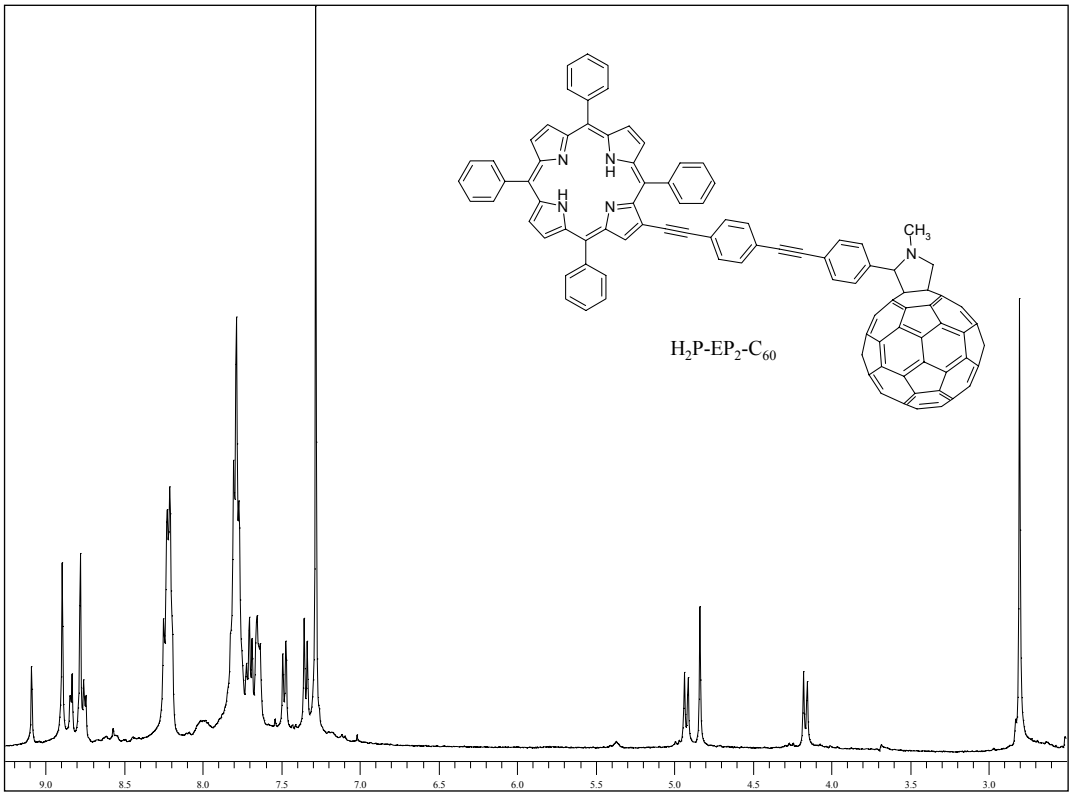

Figure 5.3. 11 *^{1}H-NMR spectrum in $CDCl_3$ solution of H_2P-EP_2-C_{60}*

H_2P-EP_3-C_{60}. Reaction conditions are equal to those reported for the synthesis of H_2P-EP_1-C_{60}. After reaction the product was purified by silica gel chromatography eluting with toluene/petroleum ether (40°-70°), 70:30 recovering a black powder (yield 52%). MS (MALDI): *m/z*: 1690 $[M+H]^+$, 969 $[M-720]^+$, 720 $[M-969]^+$; ^{1}H-NMR (300 MHz, $CDCl_3$): δ(ppm) 9.10 (s, 1H), 8.89 (s, 2H), 8.85 (d, 1H; J=5.3 Hz), 8.78 (s, 2H), 8.75 (d, 1H; J=5.3 Hz), 8.23 (br m, 5H), 7.80-7.50 (br m, several signals difficult to resolve and integrate), 7.48 (d, 2H; J=7.8 Hz), 7.34 (d, 2H; J=8.3), 4.90 (d, 1H; J=9.8), 4.79 (s, 1H), 4.13 (d, 1H; J=9.8), 2.78 (s, 3H), -2.67 (s, 2H); UV/vis (Toluene): λ_{max} (nm) = 334, 430, 524, 560, 603, 659. MALDI-MS spectrum and ^{1}H-NMR spectrum in $CDCl_3$ solution are reported below in Figure 5.3.12 and 5.3.13.

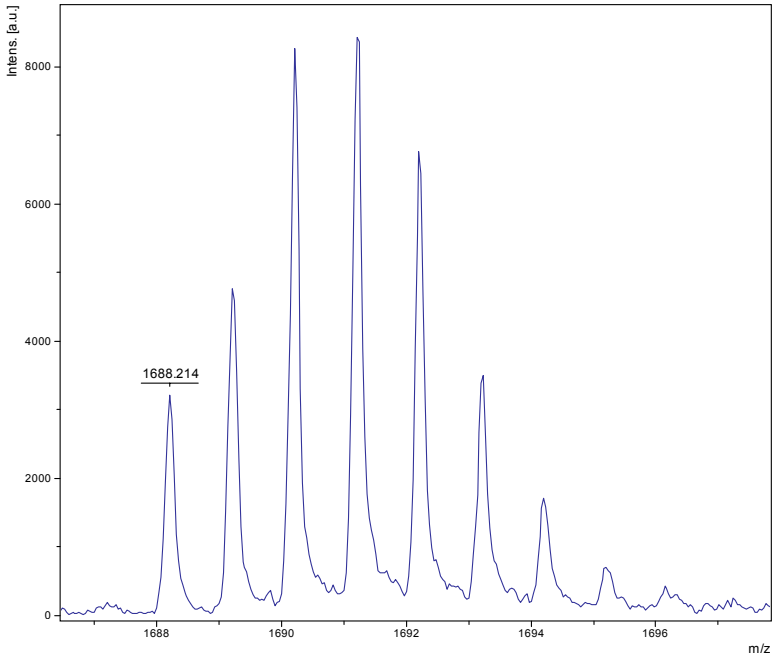

Figure 5.3. 12 *MALDI-MS spectrum of H_2P-EP_3-C_{60}*

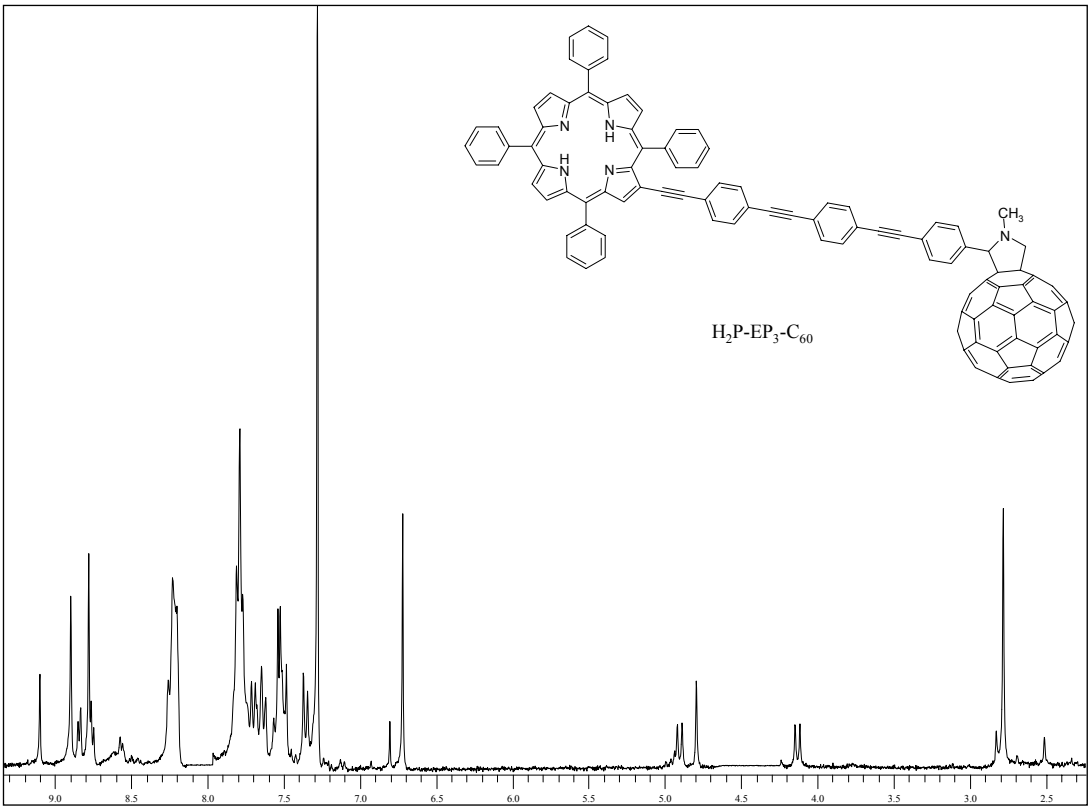

Figure 5.3. 13 *^{1}H-NMR spectrum in $CDCl_3$ solution of H_2P-EP_3-C_{60}*

General procedure for zinc insertion. To a solution of starting compound (porphyrins or dyad) in chloroform a saturated solution of $Zn(AcO)_2$ in methanol was added and the mixture was left to react at room temperature under nitrogen for 2 h. The solvent was evaporated and the product was purified using a plug of silica gel and eluting with chloroform.

2-[(4'-formyl)phenyl]ethynyl-5,10,15,20-tetraphenylporphyrin Zn(II), (Zn-System A). Zinc porphyrin was obtained following the general procedures previously described. Yield 95%. MS (FAB): *m/z*: 805 [M^+]; ^{1}H-NMR (400 MHz, $CDCl_3$): δ(ppm) 10.06 (s, 1H), 9.30 (s, 1H), 8.96 (s, 2H), 8.95 (s, 2H), 8.91 (d, 1H; J=5.1 Hz), 8.80 (d, 1H; J=5.1 Hz), 8.25 (br m, 5H), 7.88 (d, 2H; J=8.2 Hz), 7.80-7.66 (br m, 15H), 7.55 (d, 2H; J=8.2 Hz); UV/vis (Toluene): λ_{max} ($10^{-4}\varepsilon$) = 311 (2.17), 438 (23.8), 559 (1.86), 596 (0.96).

2-[(4'-methyl)phenyl]ethynyl-5,10,15,20-tetraphenylporphyrin Zn(II), (Zn-System B.) Yield: 95%. MS (FAB): *m/z*: 791 [M^+]; ^{1}H-NMR (400 MHz, $CDCl_3$): δ(ppm) 9.24 (s, 1H,), 8.95 (s, 2H), 8.93 (s, 2H), 8.90 (d, 1H; J=5.1 Hz), 8.80 (d, 1H; J=5.1 Hz), 8.23 (br m, 5H), 7.78-7.66 (br m, 15H), 7.25 (d, 2H; J=7.3 Hz), 7.16 (d, 2H; J=7.3 Hz), 2.42 (s, 3H); UV/vis (Toluene): λ_{max} ($10^{-4}\varepsilon$) = 434 (23.9), 558 (1.75), 592 (0.63).

ZnP-C_{60} or (ZnP-EP_1-C_{60}). Yield: 98%. MS (FAB): *m/z*: 1552 [M^+], 832 [M-720]$^+$, 720 [M-832]$^+$; ^{1}H-NMR (400 MHz, $CDCl_3$): δ(ppm) 9.24 (s, 1H,), 8.95 (s, 2H), 8.93 (s, 2H), 8.88 (d, 1H; J=5.1 Hz), 8.77 (d, 1H; J=5.1 Hz), 8.22 (br m, 3H), 8.16 (br d, 2H; J=7.2 Hz), 7.80 (br m, 10H), 7.60 (m, 3H), 7.45-7.40 (br m, 4H), 7.20 (d, 2H; J=7.2 Hz), 4.95 (d, 1H; J=9.2 Hz), 4.85 (s, 1H), 4.20 (d, 1H; J=9.2 Hz), 2.87 (s, 3H); UV/vis (Toluene): λ_{max} ($10^{-4}\varepsilon$) = 311 (4.8), 434 (26.1), 558 (1.94), 593 (0.82).

ZnP-EP_2-CHO. Yield: 97%. MS (MALDI): *m/z*: 905 [M^+]; UV/vis (Toluene): λ_{max} (nm) = 333, 436, 559, 594.

ZnP-EP_3-CHO. Yield: 95%. MS (MALDI): *m/z*: 1005 [M^+]; UV/vis (Toluene): λ_{max} (nm) = 345, 436, 559, 594.

ZnP-EP_2-C_{60}. Yield: 97%. MS (MALDI): *m/z*: 1652 [M^+], 932 [M-720]$^+$, 720 [M-932]$^+$; UV/vis (Toluene): λ_{max} (nm) = 324, 436, 559, 594.

ZnP-EP$_3$-C$_{60}$. Yield: 96%. MS (MALDI): *m/z*: 1752 [M$^+$], 1032 [M-720]$^+$, 720 [M-1032]$^+$; UV/vis (Toluene): λ_{max} (nm) = 333, 436, 559, 594.

N-(4'-pyridylmethyl)glicine ethyl ester. 510 mg (4.7 mmol) of 4-aminomethyl-pyridine and an excess of anhydrous K_2CO_3 were dissolved in 12 ml of anhydrous acetonitrile at 0 °C. A solution of 400 mg (1.9 mmol) of ethyliodoacetate in 3 ml of anhydrous acetonitrile was added slowly over 1 h. The reaction was left under nitrogen atmosphere for further 2 h, then the solvent was evaporated and the crude product was dissolved in chloroform and passed through a silica gel plug eluting with $CHCl_3$/CH_3OH, 99:1. The desired product was obtained as a colorless viscous oil. MS (GC): *m/z*: 194 [M$^+$]; 121 [M -73]$^+$; ^{1}H-NMR (300 MHz, $CDCl_3$): δ(ppm) 8.36 (d, 2H; J=6.0 Hz), 7.11 (d, 2H; J=6.0 Hz), 4.01 (q, 2H), 3.66 (s, 2H), 3.24 (s, 2H), 2.20 (br s, 1H), 1.10 (t, 3H). GC-MS spectrum and ^{1}H-NMR spectrum in $CDCl_3$ solution are reported below in Figure 5.3.14 and 5.3.15.

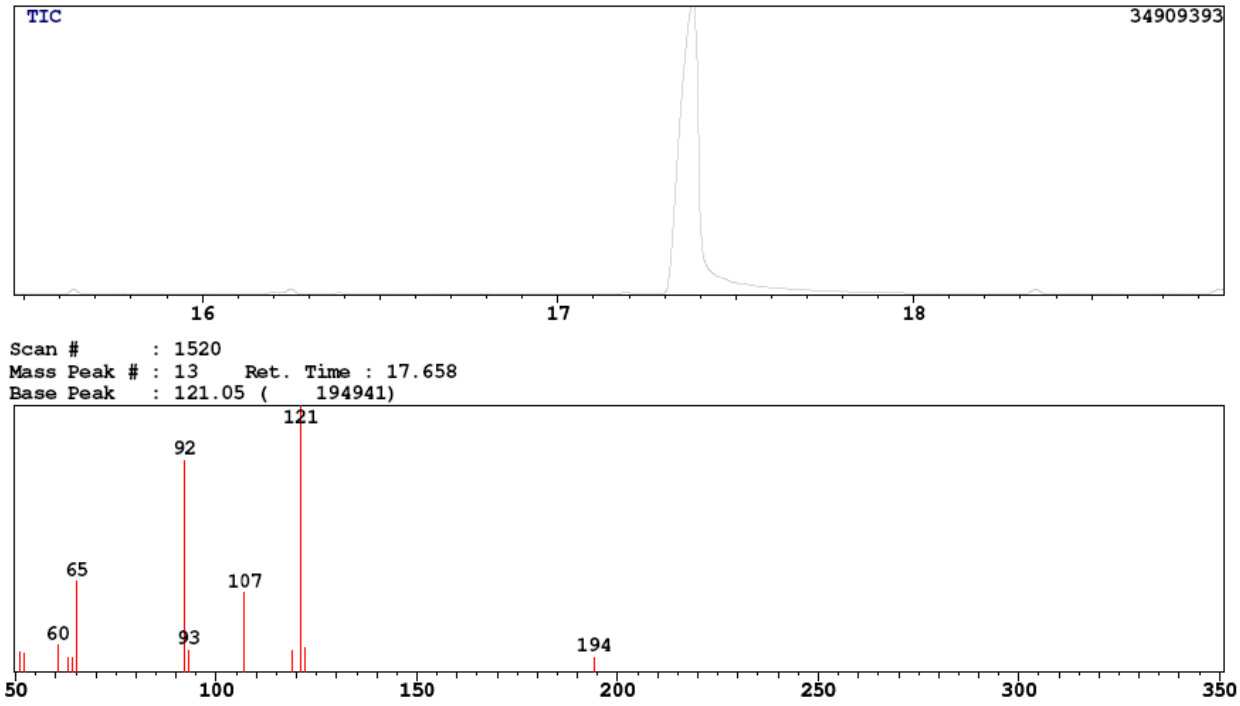

Figure 5.3. 14 *GC-MS spectrum of N-(4'-pyridylmethyl)glicine ethyl ester*

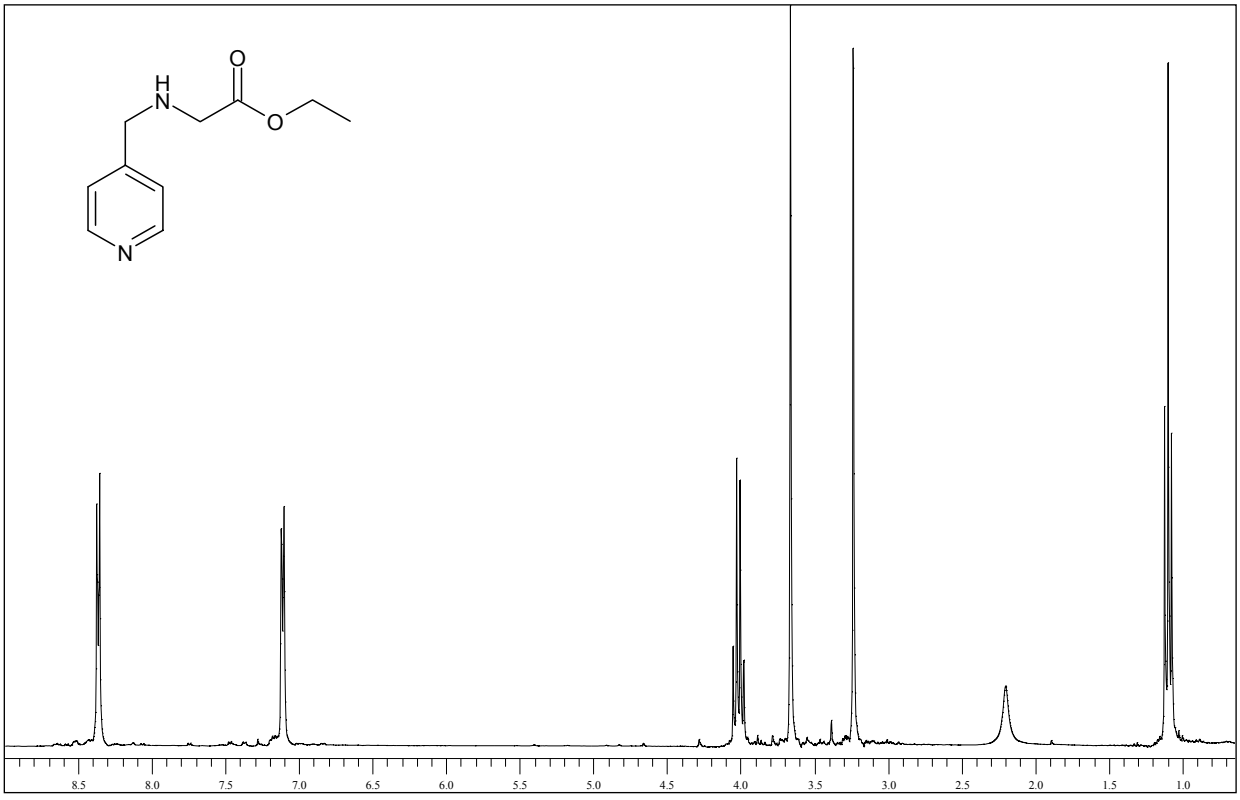

Figure 5.3. 15 *^{1}H-NMR spectrum in $CDCl_3$ solution of N-(4'-pyridylmethyl)glicine ethyl ester*

N-(4'-pyridylmethyl)glicine. The hydrolysis of N-(4'-pyridylmethyl)glicine ethyl ester was carried out dissolving the aminoacid in acetonitrile and adding a solution of KOH (slightly excess). The solution was allowed to react under a nitrogen atmosphere at room temperature for 3 h. The solvent was evaporated under vacuum and the crude product redissolved in chloroform. The organic solution was passed through a silica gel plug eluting with $CHCl_3/CH_3OH$, 4:1. The desired product was obtained as a pale yellow powder in an overall yield of 77% (calculated respect to the ethyliodoacetate). The modified amino-acid must be conserved in a dry box because it is moisture sensitive and it tends to become a sticky oil. ^{1}H-NMR (300 MHz, CD_3OD): δ(ppm) 8.57 (d, 2H; J=6.0 Hz), 7.55 (d, 2H; J=6.0 Hz), 4.12 (s, 2H) 3.44 (s 2H).

N-(4'-pyridylmethyl)-2-[(4'-trimethylsilyl)ethynyl]phenyl-3,4-fulleropyrrolidine. 9 mg (4.3×10^{-5} mol) of 4-(trimethylsilyl)ethynylbenzaldheyde, 44 mg (6.1×10^{-5} mol) of C_{60} and 100 mg (6.0×10^{-4} mol) of N-(4'-pyridylmethyl)glicine were dissolved in *ortho*-dichlorobenzene (10 ml). The solution was allowed to react at 130 °C, under a nitrogen atmosphere for 12 h. The solvent was then evaporated and the desired product was purified by silica gel chromatography eluting with toluene to recover the unreacted C_{60} and then with toluene/$CHCl_3$, 1:1 to obtain 14

mg of fullerene pyridyl derivative as brown powder (yield 32%). MS (MALDI): *m/z*: 1026 $[M^+]$, 720 $[M\text{-}306]^+$; ^{1}H-NMR (300 MHz, $CDCl_3$): δ(ppm) 8.74 (d, 2H; J=5.00 Hz), 7.68 (d, 2H; J=5.00 Hz), 7.58 (d, 2H; J=8.9 Hz), 7.39 (d, 2H; J= 5.00 Hz), 5,27 (s, 1H), 4.87 (d, 1H; J=8.9 Hz), 4.53 (d, 1H; J=13.9 Hz), 4.18 (d, 1H; J=9.9 Hz), 3.70 (d, 1H; J=14.9 Hz), 0.25 (s, 9H). MALDI-MS spectrum and ^{1}H-NMR spectrum in $CDCl_3$ solution are reported below in Figure 5.3.16 and 5.3.17.

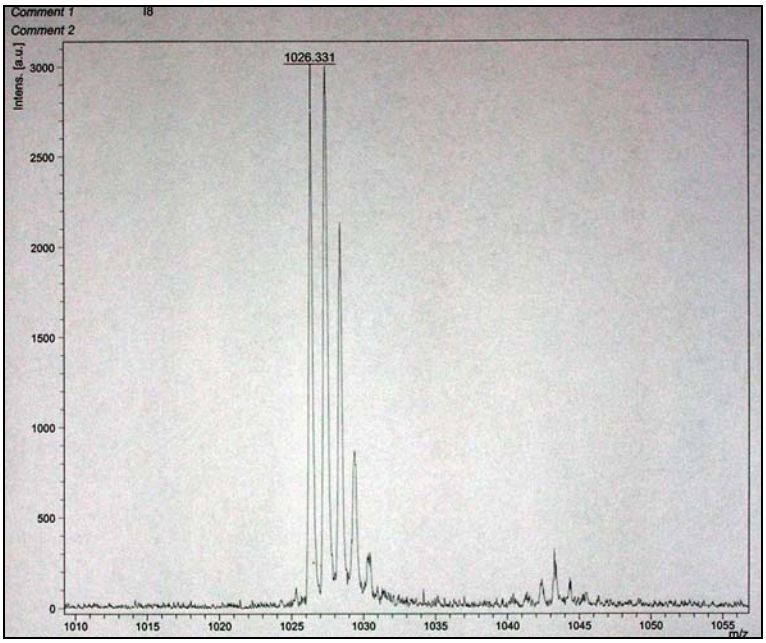

Figure 5.3. 16 *MALDI-MS spectrum of* ***N****-(4'-pyridylmethyl)-2-[(4'-trimethylsilyl)ethynyl]phenyl-3,4-fulleropyrrolidine*

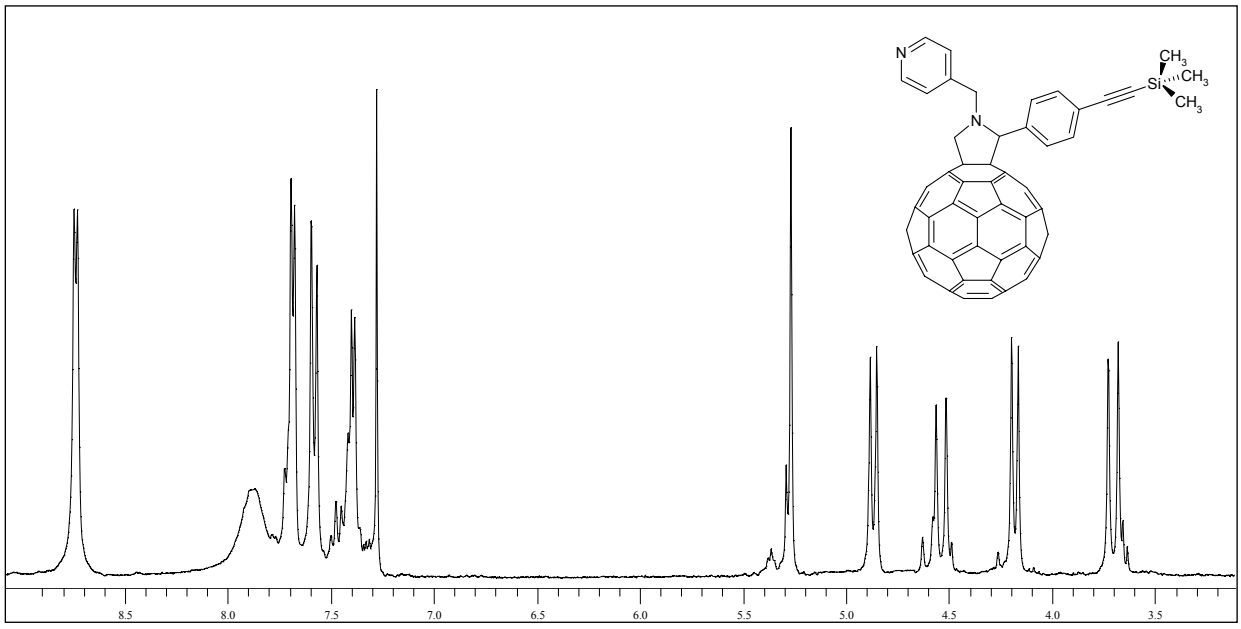

Figure 5.3. 17 *^{1}H-NMR spectrum in $CDCl_3$ solution of* ***N****-(4'-pyridylmethyl)-2-[(4'-trimethylsilyl)ethynyl]phenyl-3,4-fulleropyrrolidine*

H_2P-C_{60}-Py system. 30 mg (4.0×10^{-5} mol) of 2-[(4'-formyl)phenyl]ethynyl-5,10,15,20-tetraphenylporphyrin, 44 mg (6.0×10^{-5} mol) of C_{60} and 70 mg (6.0×10^{-4} mol) of N-(4'-pyridylmethyl)glicine, were dissolved in 70 ml of anhydrous toluene. The suspension was allowed to react under a nitrogen atmosphere at 120 °C for 18 h. The solvent was evaporated under vacuum and the product was purified by silica gel column chromatography eluting with toluene. The first two compound eluted from the column were unreacted C_{60} and unreacted porphyrin; after that, the polarity of the eluting mixture was increased up to toluene/$CHCl_3$, 1:1. the desired porphyrin-fullerene dyad was recovered as dark powder in a 50% yield (31 mg). MS (MALDI): *m/z*: 1566 [M^+]; ^{1}H-NMR (300 MHz, $CDCl_3$): δ(ppm) 9.07 (s, 1H), 8.89 (s, 2H), 8.82 (d, 1H; J=4.5 Hz), 8.77 (s, 2H), 8.72 (br m, 3H), 8.20-7.40 series of unresolved multiplets (See Figure 5.3.19), 7.38 (d, 2H; J=8.3 Hz), 4.83 (s, 1H), 4.64 (d, 1H; J=9.8 Hz), 4.40 (d, 1H; J=13.6 Hz), 3.76 (d, 1H; J=9.8 Hz), 3.39 (d, 1H; J=15 Hz), -2.70 (s, 2H); UV/vis (Toluene): λ_{max} (nm) = 300, 429, 523, 558, 601, 657. MALDI-MS spectrum and ^{1}H-NMR spectrum in $CDCl_3$ solution are reported below in Figure 5.3.18 and 5.3.19.

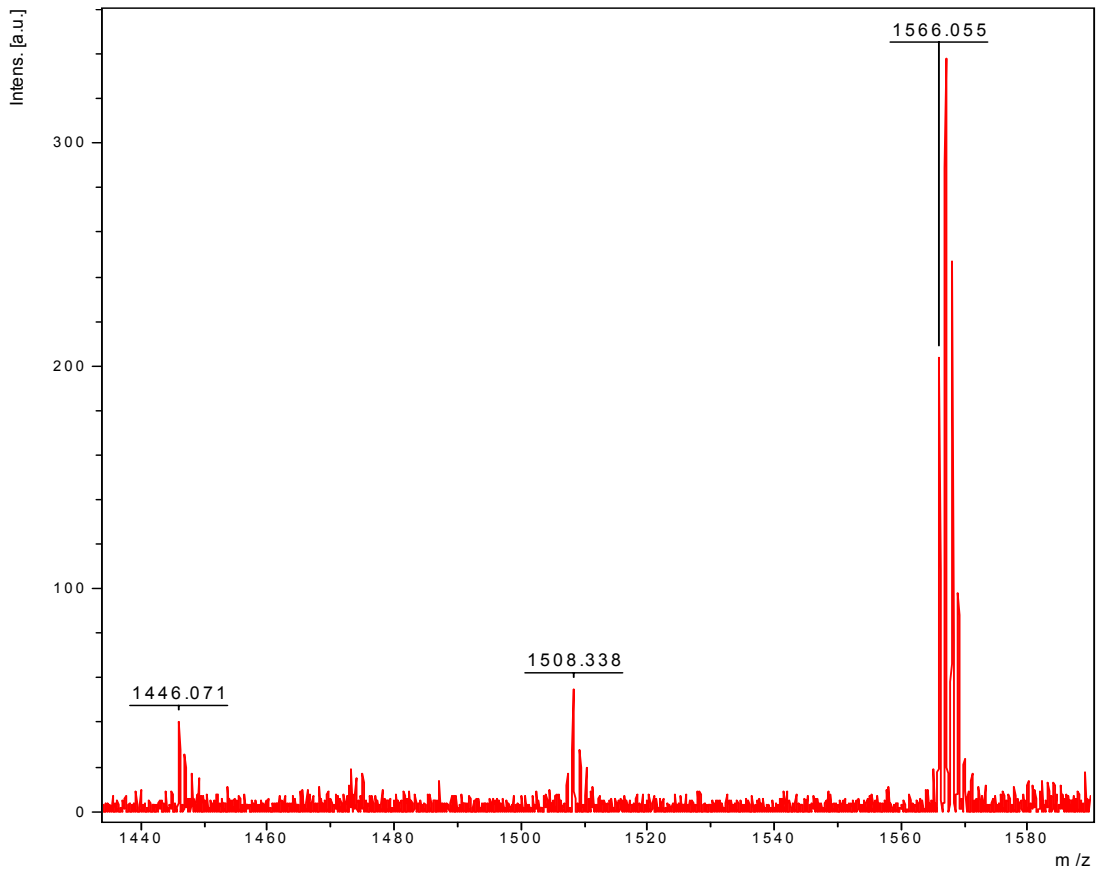

Figure 5.3. 18 *MALDI-MS spectrum of H_2P-C_{60}-Py system*

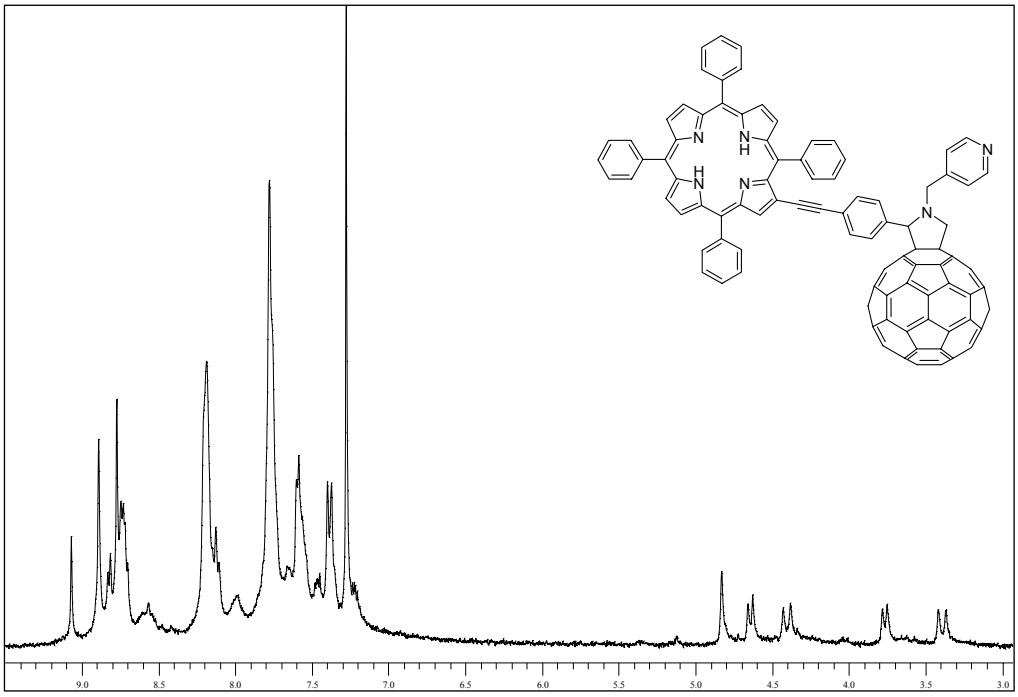

Figure 5.3. 19 *^{1}H-NMR spectrum in $CDCl_3$ solution of H_2P-C_{60}-Py system*

ZnP-C_{60}-Py system. To a chloroform solution of 10 mg (6.4×10^{-6} mol) of H_2P-C_{60}-Py system was added a slightly excess of saturated $Zn(OAc)_2$ methanol solution. The mixture was left to react under a nitrogen atmosphere for 2 h at room temperature. During the reaction a green precipitate was formed, the solvent was removed under vacuum and the crude product redissolved in 50 ml of chloroform. The organic solution was washed with 50 ml of water, the two phases were separated, the organic phase was dried over anhydrous Na_2SO_4 and filtered. The aqueous solution was back extracted with several additional 30 ml portions of chloroform, until the organic solution appeared colourless. The organic phases were combined and solvent was removed under vacuum. The product was obtained as green powder and was dried under vacuum at 80 °C. After that the powder changed colour from green to black. 9.5 mg of zinc complex was obtained (yield 91%). MS (MALDI): *m/z*: 1629 [M^+]; UV/vis ($CHCl_3$): λ_{max} (nm) = 306, 438, 568, 606. Due to the low solubility of compound in chloroform it was impossible to perform ^{1}H-NMR analysis a better condition must to be find. MS-MALDI spectrum is reported below in Figure 5.3.20.

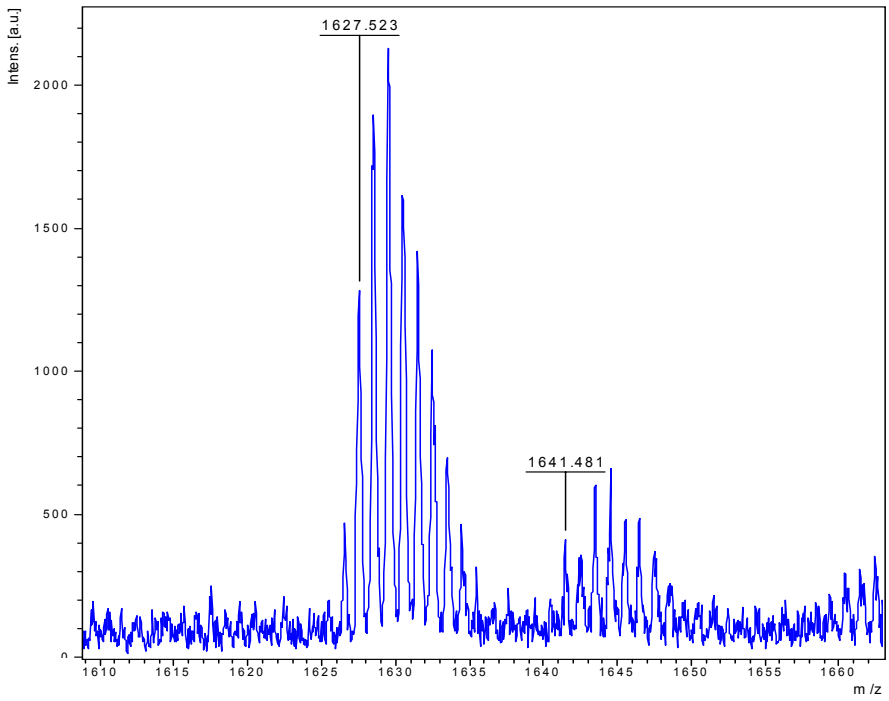

Figure 5.3. 20 *MALDI-MS spectrum of ZnP-C_{60}-Py system.*

Methylation of pyridyl moiety of ZnP-C_{60}-Py system. 5 mg of ZnP-C_{60}-Py compound were dissolved in 15 ml of anhydrous DMF and an excess of CH_3I was added. The solution was allowed to react under a nitrogen atmosphere at 60 °C for 12 h. The conversion of the product is almost quantitative, but the respective quantity is to low to allow an adequate characterization of compound.

(4'-pyridylmethyl)aminocarbonyl-ferrocene. To an anhydrous toluene solution of 100 mg (4.35×10^{-4} mol) of ferrocenylcarboxylic acid, 115 mg (5.4×10^{-4} mol) of PCl_5 and 0.5 ml of pyridine were added and the solution was allowed to react at room temperature, under a nitrogen atmosphere. Once that all the carboxylic acid was converted into respective acyl chloride a solution of 60 mg (5.4×10^{-4} mol) of 4-aminomethylpyridine was added dropwise. After 3 h the reaction was stopped and the solvent was removed under vacuum, the crude product was dissolved in 50 ml of dichloromethane and washed with two portion of 50 ml of water. The organic phase was separated, dried over anhydrous Na_2SO_4 and filtered. The solvent was evaporated under vacuum and the product was purified by column chromatography eluting with diethyl ether. The first compound eluted was the unreacted carboxylic acid, then the polarity of the eluting mixture was increased up to diethyl ether/methanol, 9:1 to recover the desired product as a red-orange powder in a 50% yield (70 mg). ^{1}H-NMR (300 MHz, $CDCl_3$):

δ(ppm) 8.51 (d, 2H; J=5.0 Hz), 7.24 (d, 2H; J=5.0 Hz), 6.88 (t, 1H), 4.74 (s, 2H), 4.51 (d, 2H; J=6.0), 4.35 (s, 2H), 4.17 (s, 5H).

Copper(II) 2-nitro-5,10,15,20-tetratphenylporphyrin. To a solution of 1 g (1.6 mmol) of tetraphenylporphyrin in 600 ml of chloroform a solution of 1.130 g (4.7 mmol) of $Cu(NO_3)_2 \cdot 3H_2O$ in 72 ml of acetic anhydride was added. The mixture was left under a nitrogen atmosphere at room temperature for 48 h. Then a 50 ml of 0.1 M solution of NaOH was added and the mixture was transferred into a separatory funnel and the two phases were separated. The organic phase was washed with three additional 400ml portions of water. The organic phase was then dried over Na_2SO_4 and filtered. The solvent was evaporated under vacuum and the desired product was purified through a silica gel plug, eluting with $CHCl_3$/petroleum ether, 4:1 and recovering 1.04 g of copper(II) 2-nitro-5,10,15,20-tetratphenylporphyrin as purple powder (yield 88%). MS (FAB): *m/z*: 720 $[M^+]$, 674 $[M- 46]^+$

H_2-2-nitro-5,10,15,20-tetraphenylporphyrin. 1 g (1.4 mmol) of Cu-2NO_2-TPP was dissolved in a 30 ml 1:2 mixture of trifluoroacetic acid and sulphuric acid (96%) and was left to react at room temperature, under a nitrogen atmosphere for 2 h. Then the solution was carefully added to a 500 ml of water and was gradually neutralized adding K_2CO_3. The aqueous suspension was extracted with chloroform, the organic phase was then dried over anhydrous Na_2SO_4 and filtered. The solvent was removed under vacuum and the compound was recrystallized from $CHCl_3$/CH_3OH obtaining 864 mg of porphyrin (yield 94%).

12,13-dibromo-2-nitro-5,10,15,20-tetraphenylporphyrin. A mixture of 805 mg (1.22 mmol) of 2-NO_2-TPP and 530 mg (3 mmol) of N-bromosuccinimide in chloroform was heated under reflux overnight. After being cooled to room temperature, the reaction mixture was filtered through an alumina plug (Grade III; eluting with CH_2Cl_2). The solvent was evaporated under vacuum and the resulting product was recrystallized from CH_2Cl_2/CH_3OH obtaining 777 mg of desired porphyrin (yield 78%). MS (FAB): *m/z*: 818 $[M^+]$; ^{1}H-NMR (300 MHz, $CDCl_3$): δ(ppm) 8.97 (s, 1H), 8.83 (m, 4H), 8.25 (m, 8H), 7.80 (m, 12H), -2.55 (s, 1H), -2.62 (s, 1H); UV/vis ($CHCl_3$): λ_{max} (nm) = 436, 538, 688.

12,13-dibromo-2,3-dihydro-2-nitro-5,10,15,20-tetraphenylporphyrin. 652 mg (7.98×10^{-4} mol) 12,13-dibromo-2-nitro-TPP and 63 mg (1.7 mmol) of $NaBH_4$ were dissolved in a cold solution (ice bath) of anhydrous THF (50 ml). The reaction was left under a nitrogen atmosphere at 0 °C for 1 h then the ice bath was removed and the solution was allowed to react for further 2 h. The

progress of reaction was monitored by UV-visible spectroscopy; after 2 h the Soret band had shifted from 436 to 424 nm. Dichloromethane (100 ml) was then added and the reaction mixture was poured into water. The organic phase was washed twice with water, then it was separated, dried over anhydrous Na_2SO_4 and filtered. The solvent was evaporated and the crude product was filtered through an alumina plug (Grade V) eluting with dichloromethane. The desired product was recrystallized from CH_2Cl_2/CH_3OH obtaining 620 mg of desired chlorine (yield 95%). MS (FAB): *m/z*: 773 $[M-48]^+$; ^{1}H-NMR (300 MHz, $CDCl_3$): δ(ppm) 8.85 (m, 2H), 8.24 (m, 2H), 8.01 (m, 4H), 7.70 (m, 14H), 7.17 (m, 1H), 4.71 (m, 1H), 4.49 (m, 1H) -1.71 (s, 1H), -1.79 (s, 1H); UV/vis ($CHCl_3$): λ_{max} (nm) = 424, 524, 555 sh, 592, 642.

2,3-dibromo-5,10,15,20 tetraphenylporphyrin. A mixture of nitrochlorine (202 mg 0.25 mmol) and 20 g of silica gel was refluxed in a chloroform solution (150 ml) for one day under argon. The reaction mixture was cooled to room temperature and the silica gel was removed by filtration and washed with dichloromethane. The desired product was purified by a silica gel chromatography eluting with $CHCl_3$/petroleum ether, 2:3 obtaining the desired product as a purple powder. The porphyrin was then recrystallized from CH_2Cl_2/CH_3OH affording 135 mg of purple crystals (yield 70%). MS (FAB): *m/z*: 773 $[M^+]$; ^{1}H-NMR (300 MHz, $CDCl_3$): δ(ppm) 8.86 (m, 4H), 8.71 (s, 2H), 8.17 (m, 8H), 7.85 (m, 12H), -2.83 (s, 2H); UV/vis ($CHCl_3$): λ_{max} (nm) = 424, 522, 560, 598, 656.

2,3-bis-[4'-(formylphenyl)ethynyl]-5,10,15,20-tetraphenylporphyrin. A three necks round bottom flask, fitted with a condenser, was carefully deoxygenated with a strong stream of dry argon, after that a solution of 2,3-dibromo-5,10,15,20 tetraphenylporphyrin (123 mg, 0.16 mmol) and 4-ethynylbenzaldehyde (55 mg, 0.43 mmol) in toluene/triethylamine, 5:1 (90 ml), was added. The solution was deareated for 30 minutes with argon bubbling and then $Pd(dba)_2$ (44 mg, 0.077 mmol) and $AsPh_3$ (121 mg, 0.40 mmol) were added. The solution was deareated for further 5 minutes, after that the argon inlet was placed 1 cm above the solution. The argon flow rate was turned up slightly and the reaction was left under nitrogen at 60 °C. After 24 h, the mixture was cooled at room temperature and the solvent evaporated. The crude product was dissolved in dichloromethane and washed several times with water. The organic solution was dried over anhydrous Na_2SO_4 and the solvent evaporated under vacuum. The product was purified by column chromatography on silica gel eluting with $CHCl_3$/petroleum ether (40°-70°), 70:30. The desired porphyrin obtained from the column was recrystallized from dichloromethane/methanol to give 30 mg of purple powder (yield 21%). MS (FAB): *m/z*: 870

[M^+]; ^{1}H-NMR (300 MHz, $CDCl_3$): δ(ppm) 10.03 (s, 2H), 8.88 (d, 2H; J=5.3), 8.83 (d, 2H; J=5.3), 8.73 (s, 2H), 8.30-8.20 (m, 8H), 7.83-7.71 (m, 18H), 7.50 (d, 2H; J=8.3), -2.55 (s, 2H); UV/vis (Toluene): λ_{max} (nm) = 448, 532, 571, 618, 673. ^{1}H-NMR spectrum in $CDCl_3$ solution is reported below in Figure 5.3.21.

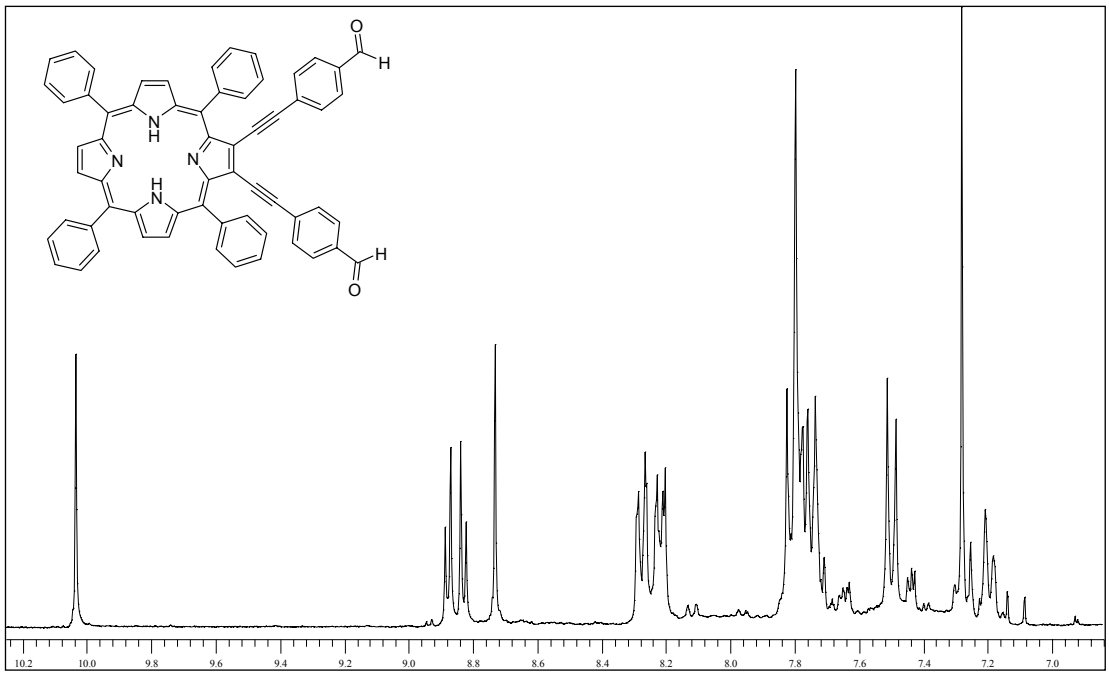

Figure 5.3. 21 *^{1}H-NMR spectrum in $CDCl_3$ solution of 2,3-bis-[4'-(formylphenyl)ethynyl]-5,10,15,20-tetraphenylporphyrin.*

Cyclic porphyrin-fulleropyrrolidine bis adducts. A mixture of 2,3-bis-[4'-(formylphenyl)ethynyl]-5,10,15,20-tetraphenylporphyrin (15 mg, 1.74×10^{-5} mol), C_{60} (19 mg, 2.64×10^{-5} mol) and N-methylglicine (23 mg, $\times10^{-4}$ mol) was refluxed for 18 h in anhydrous toluene under nitrogen atmosphere. After cooling, the solvent was evaporated and the residue purified on silica gel column eluting with toluene, recovering the unreacted [60]fullerene as first fraction and three different reaction products. The MS-MALDI analyses of reaction products confirm molecular weight equal to 1644, corresponding to the cyclic bis-adduct molecular weight, for the first two compounds. For the third one it is possible to see only characteristic fragmentation *m/z* = 924 [1644-720], corresponding to the loss of fullerene sphere and other peaks corresponding to the loss of methyl and methylene groups (Figure 5.3.22-24). Only for the compound n° 2 it was possible to carry out a ^{1}H-NMR measurement in $CDCl_3$ solution (Figure 5.3.25).

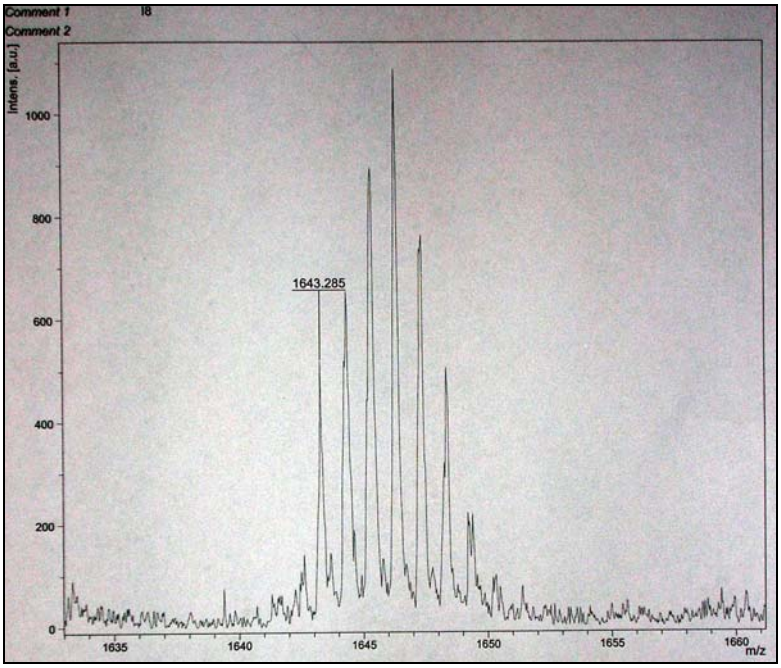

Figure 5.3. 22 *MALDI-MS spectrum of cyclic porphyrin-fulleropyrrilidine bis-adduct compound 1*

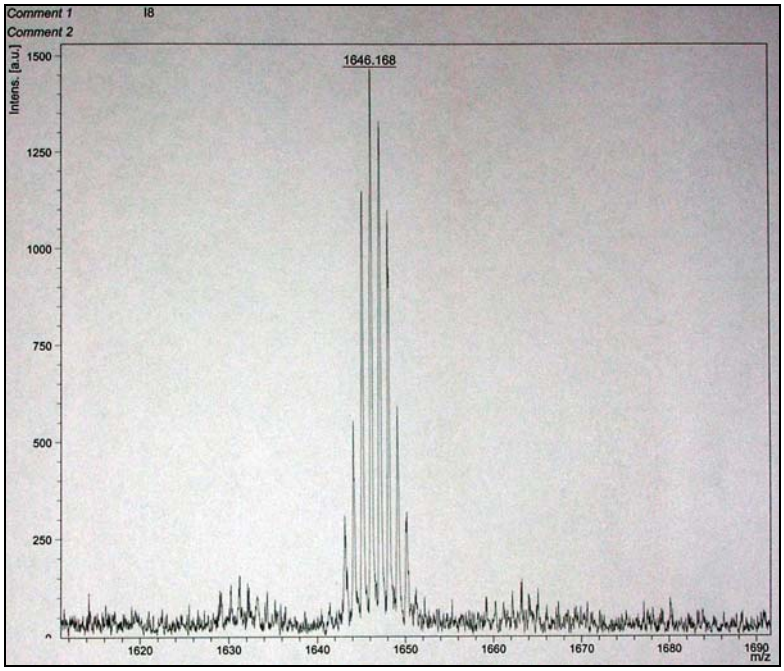

Figure 5.3. 23 *MALDI-MS spectrum of cyclic porphyrin-fulleropyrrilidine bis-adduct compound 2*

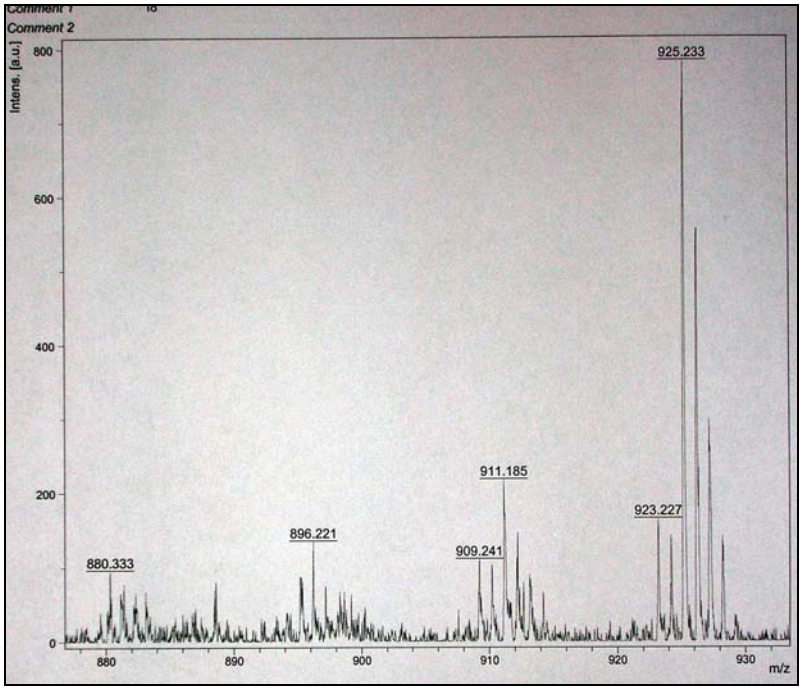

Figure 5.3. 24 *MALDI-MS spectrum of porphyrin-fulleropyrrilidine bis-adduct compound 3*

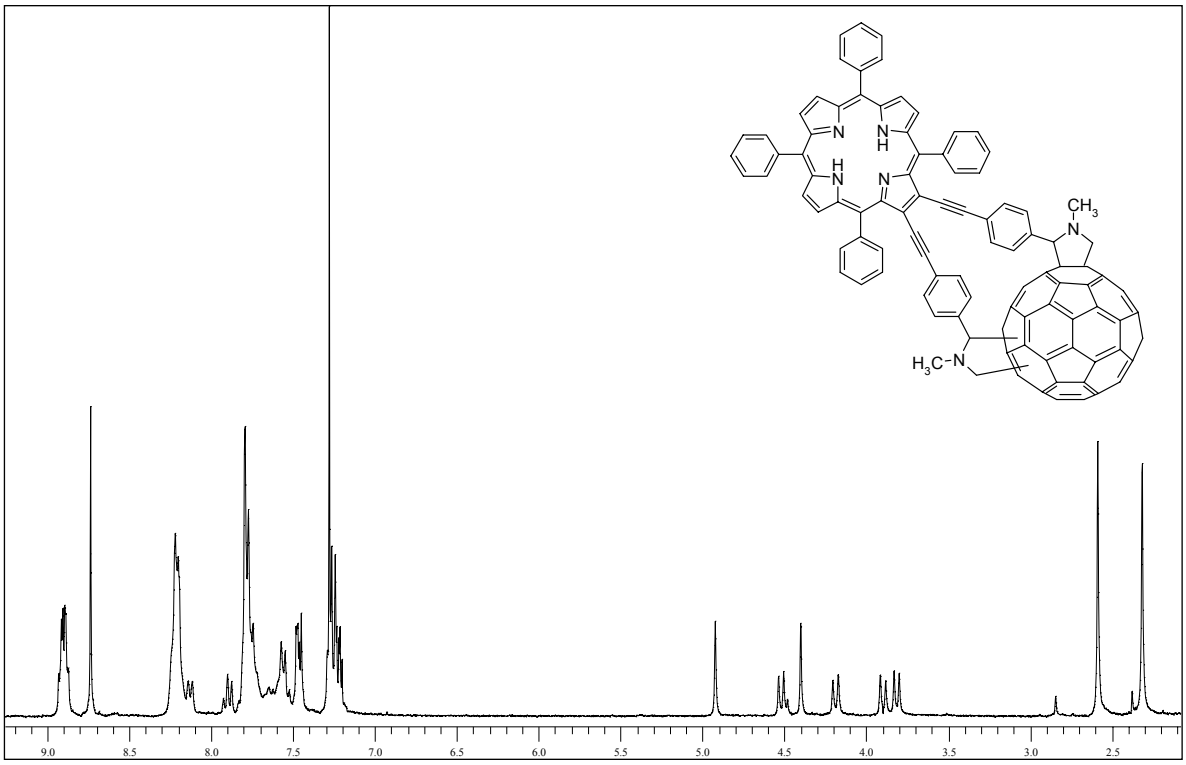

Figure 5.3. 25 *^{1}H-NMR spectrum in $CDCl_3$ solution of cyclic porphyrin-fulleropyrrilidine bis-adduct compound 2*

References.

[1] N. Nelson; A. Ben-Shem *Nature Reviews*, **2004**, *5*, 1

[2] J. P. McEvoy; G. W. Brudvig *Chem. Rev.*, **2006**, *106*, 4455

[3] V. Balzani; A. Credi; M. Venturi *"Molecular Device and Machines-A Journey into the Nanoworld"*, **2004**, Chapter 6, ed. Wiley-VCH

[4] G. Ciamician *Science*, **1912**, *36*, 385

[5] P. Jordan; P. Fromme; H. T. Witt; O. Klukas; W. Saenger; N. Krauß *Nature*, **2001**, *411*, 909

[6] A. Ben-Shem; F. Frolow; N. Nelson *Nature*, **2003**, *426*, 630

[7] Z. Liu; H. Yan; K. Wang; T. Kuang; J. Zhang; L. Gui; X. An; W. Chang *Nature*, **2004**, *428*, 287

[8] K. N. Ferriera; T. M. Iverson; K. Maghlaoui; J. Barber; S. Iwata *Science*, **2004**, *303*, 1831

[9] a) J. Deisenhofer; O. Epp; K. Miki; R.Huber; H. Michel *J. Mol. Biol.*, **1984**, *180*, 385 b) W. Zinth; W. Kaiser; H. Michel *Biochim. Biophys. Acta*, **1983**, *723*, 128 c) W. Zinth; E. W. Knapp; S. F. Fisher; W. Kaiser; J. Deisenhofer; H. Michel *Chem. Phys. Lett.*, **1985**, *119*, 1

[10] N. Ivashin; S. Larsson *J. Phys. chem. B*, **2005**, *109*, 23051

[11] C. Lunde; P. E. Jensen; A. Haldrup; J. Knoetzel; H. V. Scheller *Nature*, **2000**, *408*, 613

[12] R. C. Jennings; G. Zucchelli; R. Croce; F. M. Garlaschi *Biochim. Biophys. Acta*, **2003**, *1557*, 91

[13] a) E. J. Boekema; A. Hifney; A. E. Yakushevska; M. Piotrowski; W. Keegstra; S. Berry; K.-P. Michel; E. K. Pistorius; J. Kruip *Nature*, **2001**, *412*, 745 b) T. S. Bibby; J. Nield; J. Barber *Nature*, **2001**, *412*, 743

[14] W. Zinth; J. Wachtveitl *ChemPhysChem*, **2005**, *6*, 871

[15] a) J. L. Martin; J. Breton; A. J. Hoff; A. Migus; A. Antonetti *Proc. Natl. Acad. Sci. U.S.A.*, **1986**, *83*, 957 b) G. R. Fleming; J. L. Martin; J. Breton *Nature*, **1988**, *333*, 190

[16] C. Kirmaier; D. Holten *Biochemistry*, **1991**, *30*, 609

[17] a) C. Lauterwasser; U. Finkele; H. Scheer; W. Zinth *Chem. Phys. Lett.*, **1991**, *183*, 471 b) W. Holzapfel; U. Finkele; W. Kaiser; D. Oesterhelt; H. Scheer; H. U. Stilz; W. Zinth *Chem. Phys. Lett.*, **1989**, *160*, 1

[18] M. Ziolek; N. Pawlowicz; R. Naskrecki; A. Dobek *J. Phys. Chem. B*, **2005**, *109*, 18171

[19] C. Kirmaier; J. A. Bautista; P. D. Laible; D. K. Hanson; D. Holten *J. Phys. Chem. B*, **2005**, *109*, 24160

[20] V. Sundström; T. Pullerits; R. van Grondelle *J. Phys. Chem. B*, **1999**, *103*, 2327

[21] a) R. A. Marcus *J. Chem. Phys.* **1956**, *24*, 966; b) R. A. Marcus *J. Chem. Phys.* **1956**, *24*, 979 c) R. A. Marcus *J. Chem. Phys.* **1957**, *26*, 867 d) R. A. Marcus *J. Chem. Phys.* **1957**, *26*, 872 e) R. A. Marcus *Discussion Faraday Soc.* **1960**, *29*, 21 f) R. A. Marcus *J. Chem. Phys.* **1963**, *38*, 1858 g) R. A. Marcus *J. Chem. Phys.* **1963**, *39*, 1734 h) R. A. Marcus *J. Chem. Phys.* **1965**, 43, 679 i) R. A. Marcus *J. Phys. Chem.* **1968**, *72*, 891

[22] W. F. Libby *J. Phys. Chem.* **1952**, *56*, 863

[23] R. A. Marcus *Nobel Prize Lecture*, **1992**, available at www.nobelprize.org

[24] James R. Bolton; Noboru Mataga; George McLendon *Advances in Chemistry Series CSC Symposium Series* **1991**, Chapter 2, ed. American Chemical Society and Canadian Society for Chemistry

[25] R. A. Marcus; N. Sutin *Biochim. Biophys. Acta* **1985**, *811*, 265

[26] J. R. Miller; J. V. Beitz; R. K. Huddlestone *J. Am. Chem. Soc.* **1984**, *106*, 5057

[27] J. R. Miller; L. T. Calcaterra; G. L. Closs *J. Am. Chem. Soc.* **1984**, *106*, 3047

[28] P. Siders; R. A. Marcus *J. Am. Chem. Soc.* **1981**, *103*, 748

[29] T. Kakitani; N. Mataga *J. Phys. Chem.* **1985**, *89*, 4752

[30] R. A. Marcus *Annu. Rev. Phys. Chem.* **1964**, *15*, 155

[31] M. D. Newton; N. Sutin *Annu. Rev. Phys. Chem.* **1984**, *35*, 437

[32] James R. Bolton; Noboru Mataga; George McLendon *Advances in Chemistry Series CSC Symposium Series* **1991**, Chapter 3, ed. American Chemical Society and Canadian Society for Chemistry

[33] S. Larsson *J. Phys. Chem.* **1984**, *88*, 1321

[34] S. Larsson *J. Chem. Soc., Faraday Trans. 2* **1983**, *79*, 1375

[35] M. A. Ratner *J. Phys. Chem.* **1990**, *29*, 3686

[36] a) S. Woitellier; J. P. Launay; C. W. Spangler *Inorg. Chem.* **1989**, *28*, 758 b) J. E. Sutton; H. Taube *Inorg. Chem.* **1981**, *20*, 3125 c) J. C. Curtis; B. P. Sullivan; T. J. Meyer *Inorg. Chem.* **1983**, *22*, 224 d) J. P. Chang; E. Y. Fung; J. C. Curtis *Inorg. Chem.* **1986**, *25*, 4233 e) J. T. Hupp; M. J. Weaver *J. Phys. Chem.* **1985**, *89*, 1601

[37] Y. Kim; C. M. Lieber *Inorg.Chem.* **1989**, *28*, 399

[38] a) J. A. Schmidt; A. Siemiarczuk; A. C. Weedon; J. R. Bolton *J. Am. Chem. Soc.* **1985**, *107*, 6112 b) ; J. R. Bolton; T.-F. Ho; S. Liauw; A. Siemiarczuk; C. S. K. Wan; A. C. Weedon *J. Chem. Soc., Chem. Commun.* **1985**, 559 c) J. H. Wilford; M. D. Archer; J. R. Bolton; T.-F. Ho; J. A. Schmidt; A. C. Weedon *J. Phys. Chem.* **1985**, *89*, 5395 d) M. D. Archer; V. P. Y. Gadzekpo; J.R. Bolton; J. A. Schmidt; A. C. Weedon *J. Chem. Soc. Faraday Trans. 2*, **1986,** *82*, 2305 e) J. A. Schmidt; A. R. McIntosh; A. C. Weedon; J. R. Bolton; J. S. Connolly; J. K. Hurley; M. R. Wasielewski *J. Am. Chem. Soc.* **1988**, *110*, 1733 f) J. A. Schmidt; J.-Y. Liu; J. R. Bolton; M. D. Archer; V. P. Y. Gadzekpo *J. Chem. Soc. Faraday Trans. 2*, **1989**, *85*, 1027

[39] James R. Bolton; Noboru Mataga; George McLendon *Advances in Chemistry Series CSC Symposium Series* **1991**, Chapter 7, ed. American Chemical Society and Canadian Society for Chemistry

[40] a) H. W. Kroto *Nobel Prize Lecture* **1996** b) R. E. Smalley *Nobel Prize Lecture* **1996** both available at www.nobelprize.org

[41] a) K. M. Kadish; D. Dubois; S. Flanagan; R. E. Haufler; L. P. F. Chibante; L. J. Wilson *J. Am. Chem. Soc.*, **1991**, *113*, 4364 b) K. M. Kadish; D. Dubois; S. Flanagan; L. J. Wilson . *J. Am. Chem. Soc.*, **1991**, *113*, 7773

[42] A. Hirsch; I. Lamparth; H. R. Karfunkel *Angew. Chem. Int. Ed. Eng.*, **1994**, *33*, 437

[43] M. Prato; M. Maggini; G.Scorrano *J. Am. Chem. Soc.* **1993**, *115*, 9798

[44] reference 18 Chapter 2

[45] A. Osuka; S. Morikawa; K. Maruyama; S. Hirayama; T. Minami *J. Chem. Soc., Chem. Commun.*, **1987**, 359

[46] A. Osuka; K. Maruyama; S. Hirayama *Tetrahedron*, **1989**, *45*, 4815

[47] J. S. Lindsey; J. K. Delaney; D. C. Mauzerall; H. Linschitz *J. Am. Chem. Soc.* **1988**, *110*, 3610

[48] J. K. Delaney; D. C. Mauzerall; J. S. Lindsey *J. Am. Chem. Soc.*, **1990**, *112*, 957

[49] D. C. Mauzerall; J. Weiser; H. Staab *Tetrahedron*, **1989**, *45*, 4807

[50] J. L. Sessler; M. R. Johnson; T. Y. Lin *Tetrahedron*, **1989**, *45*, 4767

[51] J. L. Sessler; M. R. Johnson; S. E. Creager; J. C. Fettinger; J. A. Ibers *J. Am. Chem. Soc.*, **1990**, *112*, 9310

[52] J. Rodriguez; C. Kirmaier; M.R. Johnson; R. A. Friesner; D. Holten; J. L. Sessler *J. Am. Chem. Soc.*, **1991**, *113*, 1652

[53] reference on the superexchange mechanism in the Charter 1 Par.3

[54] Y. Sakata; S. Nakashima; Y. Goto; S. Misumi; T. Asahi; M. Hagihara; S. Nishikawa; T. Okada; N. Mataga *J. Am. Chem. Soc.*, **1989**, *111*, 8979

[55] Y. Sakata; H. Tsue; Y. Goto; S. Misumi; T. Asahi; S. Nishikawa; T. Okada; N. Mataga *Chem. Lett.*, **1991**, 1307

[56] M. Antolovich; P. J.Keith; A. M. Oliver; M. N. Paddon-Row; J. Kroon; J. Verhoeven; S. A. Jonker; J. M. Warman *J. Phys. Chem.*, **1991**, *95*, 1933

[57] R. A. Cormier; M. R. Posey; W. L. Bell; H. N. Fonda; J. S. Connolly *Tetrahedron*, **1989**, *45*, 4831

[58] reference on exciton coupling in the Charter 1 Par.3

[59] A. Osuka; K. Maruyama *J. Am. Chem. Soc.*, **1988**, *110*, 4454

[60] T. Nagata; A. Osuka; K. Maruyama *J. Am. Chem. Soc.*, **1990**, *112*, 3054

[61] A. Osuka; T. Nagata; K. Maruyama *Chem. Lett.*, **1991**, 481

[62] A. Osuka; K. Maruyama; N. Mataga; T. Asahi; I. Yamazaki; Y. Nishimura *Chem. Phys. Lett.*, **1991**, *181*, 413

[63] T. A. Moore; D. Gust; P. Mathis; J.-C. Mialocq; C. Chachaty; R. V. Bensasson; E. J. Land; D. Doizi, P. A. Liddel; W. R.Lehman; G.A. Nemeth; A. L. Moore *Nature*, **1984**, *307*, 630

[64] a) D. Gust; T. A. Moore; P. A. Liddel; G.A. Nemeth; L. R. Makings; A. L. Moore; D. Barrett; P. J. Pessiki; R. V. Bensasson; M. Rougee; C. Chachaty; F. C. De Schryver; M. Van der Auweraer; A. R. Holzwarth; J. S.Connolly *J. Am. Chem. Soc.*, **1987**, *109*, 846 b) D. Gust; T. A. Moore; A. L. Moore; D. Barrett; L. O. Harding; L. R. Makings; P. A. Liddel; F. C. De Schryver; M. Van der Auweraer; R. V. Bensasson *J. Am. Chem. Soc.*, **1988**, *110*, 321 c) D. Gust; T. A. Moore; A. L. Moore; L. R. Makings; G. R. Seely; X. C. Ma; T. T. Trier; F.Gao *J. Am. Chem. Soc.*, **1988**, *110*, 7567 d) D. Gust; T. A. Moore; A. L. Moore; G. R. Seely; P. A. Liddel; D. Barrett; L. O. Harding; X. C. Ma; S. J. Lee; F. Gao *Tetrahedron*, **1989**, *45*, 4867

[65] a) D. Gust; T. A. Moore; A. L. Moore; F. Gao; D.Luttrull; J. M. DeGraziano; X. C. Ma; L. R. Makings; S. J. Lee; T. T. Trier; E. Bittersmann; G. R. Seely; S. Woodward; R. V: Bensasson; M. Rougee; F. C. De Schryver; M. Van der Auweraer *J. Am. Chem. Soc.*, **1991**, *113*, 3638 b) D. Gust; T. A. Moore; A. L. Moore; C. Devadoss; P. A. Liddell; R. Hermant; R. A. Nieman; L. J. Demanche; J. M. DeGraziano; I. Gouni *J. Am. Chem. Soc.*, **1992**, *114*, 3590 c) D. Gust; T. A. Moore; A. L. Moore; A. N. Macpherson; A. Lopez; J. M. DeGraziano; I. Gouni; E. Bittersmann; G. R. Seely; F. Gao; R. A. Nieman; X. C. Ma; L. J. Demanche; S.-C. Hung; D. K. Luttrull; S.-J. Lee; P. K. Kerrigan *J. Am. Chem. Soc.*, **1993**, *115*, 11141 d) D. Gust; T. A. Moore; A. L. Moore *Acc. Chem. Rev.*, **1993**, *26*, 198

[66] D. Gust; T. A. Moore; A. L. Moore; S.-J. Lee; E. Bittersmann; D. K. Luttrull; A. A. Rehms; J. M. DeGraziano; X. C. Ma; F. Gao; R. E. Belford; T. T. Trier *Science*, **1990**, *248*, 199

[67] J. S. Lindsey; D. F. Bocian; R. J. Donohoe; J.-S. Hsiao; B. P. Krueger; R. W. Wagner; T. E. Johnson; J. K. Delaney; D. C. Mauzerall; G. R. Fleming *J. Am. Chem. Soc.*, **1996**, *118*, 11181

[68] D. F. Bocian; J. S. Lindsey; J. Seth; V. Palaniappan; R. W. Wagner; T. E. Johnson *J. Am. Chem. Soc.*, **1996**, *118*, 11194

[69] J. S. Lindsey; D. F. Bocian; D. Holten; R. W. Wagner; J. Seth; S. I. Yang; D. Kim *J. Org. Chem.*, **1998**, *63*, 5042

[70] J. S. Lindsey; D. F. Bocian; D. Holten; R. W. Wagner; R. K. Lammi; A. Ambroise; T. Balasubramanian *J. Am. Chem. Soc.*, **2000**, *122*, 7579

[71] D. Holten; D. F. Bocian; J. S. Lindsey *Acc. Chem. Res.*, **2002**, *35*, 57

[72] a) T. Förster *Ann. Phys.*, **1948**, *2*, 55 b) T. Förster *Discuss. Faraday Soc.*, **1959**, *27*, 7

[73] D. L. Dexter *J. Chem. Phys.*, **1953**, *21*, 836

[74] A. Osuka; D. Kim; H. S. Cho; D. H. Jeong; M.-C. Yoon; Y. H. Kim; Y.-R. Kim; S. C. Jeoung; S. K. Kim; N. Aratani; H. Shinmori *J. Phys. Chem. A*, **2001**, *105*, 4200

[75] J. M. Warman; A. Osuka; J. J. Piet; P. N. Taylor; H. L. Anderson *J. Am. Chem. Soc.*, **2000**, *122*, 1749

[76] A. Osuka; D. Kim; N. Aratani; Y. H. Kim; D. H. Jeong *Angew. Chem. Int. Ed.*, **2000**, *39*, 1458

[77] A. Osuka; D. Kim; T. Matsumoto; T. Kawai; N Aratani, A. Takagi; Y. Yanagawa; Z. S. Yoon *Chem. Eur. J.*, **2005**, *11*, 3389

[78] a) A. Osuka; A. Tsuda; H. Furuta *Angew. Chem. Int. Ed.*, **2000**, *39*, 2549 b) A. Osuka; A. Tsuda; H. Furuta *J. Am. Chem. Soc.*, **2001**, *123*, 10304 c) A. Osuka; D. Kim; H. S. Cho; D. H. Jeong; S. Cho; Y. Matsuzaki; K. Tanaka; A. Tsuda *J. Am. Chem. Soc.*, **2002**, *124*, 14642

[79] Y. Matsuzaki; A. Osuka; A. Nogami; Y. Iwaki; N. Ohta; N. Yoshida; N. Aratani; K. Tanaka *J. Phys. Chem. A*, **2005**, *109*, 703

[80] D. Kim; A. Osuka; H. Sumi; N. Aratani; H. S. Cho; T. K. Ahn; S. Cho *J. Am. Chem. Soc.*, **2003**, *125*, 9668

[81] T. Matsumoto; T. Kaway; D. Kim; A. Osuka; T. Hori; N. Aratani; A. Takagi; M.-C. Yoon; Z. S.Yoon; S. Cho *Chem. Eur. J.*, **2006**, *12*, 1319

[82] V. Sundström; T. Pullerits; R. van Grondelle *J. Phys. Chem. B*, **1999**, *103*, 2327

[83] A. Osuka; D. Kim; Y. Nakamura; I.-W. Hwang; N. Aratani; T. K. Ahn; D. M. Ko; A. Takagi; T. Kawai; T. Matsumoto *J. Am. Chem. Soc.*, **2005**, *127*, 236

[84] L. J. Wan; J. S. Hu; Y. G. Guo; H.P. Liang; L. Jiang *J. Am. Chem. Soc.*, **2005**, *127*, 17090

[85] a) T. Aida; M.-S. Choi; T. Yamazaki; I. Yamazaki *Angew. Chem. Int. Ed.*, **2004**, *43*, 150 b) E. Alessio; M. Macchi; S. Heath; L. G. Marzilli *Chem. Commun.*, **1996**, 1411 c) C. M. Drain; F. Nifiatis; A. Vasenko; J. D. Batteas *Angew. Chem.*, **1998**, *110*, 2478 d) C. M. Drain; F. Nifiatis; A. Vasenko; J. D. Batteas *Angew. Chem. Int. Ed.*, **1998**, *37*, 2344 e) A. Prodi; M. T. Indelli; C. J. Kleverlaan; F. Scandola; E. Alessio; T. Gianferrata; L. G. Marzilli *Chem. Eur. J.*, **1999**, *5*, 2668

[86] C. A. Hunter; R. A. Haycock; A. Yartsev; U. Michelsen; V. Sundström . *Chem. Int. Ed.*, **2000**, *39*, 3616

[87] J. A. Wytko; A. M. Albrecht Gary; J. Weiss; M. Koepf; A. Trabolsi; M. Elhabiri; D. Paul *Organic Lett.*, **2005**, *7*, 1279

[88] a) T. D. Balaban; M. Linke-Schaetzel; A. D. Bhise; N. Vanthuyne; C. Roussel; C. E. Anson; G. Buth; A. Eichöfer; K. Foster; G. Garab; H. Gliemann; R. Goddard; T. Javorfi; A. K. Powell; H. Rösner; T. Schimmel *Chem. Eur. J.*, **2005**, *11*, 2267 b) T. D. Balaban *Acc. Chem. Res.*, **2005**, *38*, 612

[89] Y. Kobuke; H. Ozeki; A. Nomoto; K. Ogawa; M. Murakami; K. Hosoda; M. Ohtani; S. Nakashima; H. Miyasaka; T. Okada *Chem. Eur. J.*, **2004**, *10*, 6393

[90] a) Y. Kobuke; R. Takahashi *J. Am. Chem. Soc.*, **2003**, *125*, 2372 b) Y. Kobuke; D. Kim; H. Miyasaka; I. W. Hwang; M. Park; T. K. Ahn; Z. S. Yoon; D. M. Ko; F. Ito; Y. Ishibashi; S. R. Khan; Y. Nagasawa; C. Ikeda; R. Takahashi; K. Ogawa; A. Satake *Chem. Eur. J.*, **2005**, *11*, 3753 c) Y. Kobuke; D. Kim; F. Hajjaja; Z. S. Yoon; M.-C. Yoon; J. Park; A. Satake *J. Am. Chem. Soc.*, **2006**, *128*, 4612

[91] a) Y. Kobuke; A. Nomoto *Chem. Commun.*, **2002**, 1104 b) Y. Kobuke; A. Nomoto; H. Mitsuoka; H. Ozeki *Chem. Commun.*, **2003**, 1074 c) Y. Kobuke; M. Morisue; N. Haruta; D. Kalita *Chem. Eur. J.*, **2006**, *12*, 8123

[92] A. Osuka; D. Kim; I.-W. Hwang; T. Kamada; T. K. Ahn; D. M. Ko; T. Nakamura; A. Tsuda *J. Am. Chem. Soc.*, **2004**, *126*, 16187

[93] T. Aida; M.-S. Choi; T. Yamazaki ; I. Yamazaki *Angew. Chem. Int. Ed.*, **2004**, *43*, 150

[94] V. Balzani; A. Credi; M. Venturi *"Molecular Device and Machine-A Journey into the Nanoworld"*, **2004**, Chapter 5 ed. Wiley-VCH

[95] J. S. Lindsey; D. Holten; D. F. Bocian; M. del Rosario Benites; T. E. Johnson; S. Weghorn; L. Yu; P. D. Rao; J. R. Diers; S. I. Yang; C. Kirmaier *J. Mater. Chem.*, **2002**, *12*, 65

[96] T. Aida; M.-S. Choi; T. Yamazaki; I. Yamazaki *Angew. Chem. Int. Ed.*, **2001**, *40*, 3194

[97] K. P. Ghigghino; J. M. Crossley; E. W. Meijer; E. K. L. Yeow; J. N. H. Reek; A. W. Bosman; A. P. H. J. Schenning *J. Phys. Chem. B*, **2000**, *104*, 2596

[98] a) D. M. Guldi; M. Prato *Acc. Chem. Res.*, **2000**, *33*, 695 b) S. Leach; M. Vervloet; A. Desprès; E. Bréheret; J. P. Hare;T. J. Dennis; H. W. Kroto; R. Taylor; D. R. M. Walton *Chem. Phys.*, **2000**, *160*, 451 c) R. V. Bensasson; T. Hill; C. Lambert; E. J. Land; S. Leach; T. G. Truscott *Chem. Phys. Lett.*, **1993**, *201*, 326 d) D. Samuels; R. Weisman *Chem. Phys. Lett.*, **1998**, *295*, 105

[99] T. D. M. Bell; T. A. Smith; K. P. Ghigghino; M. G. Ranasinghe; M. J. Shephard; M. N. Paddon-Row *Chem. Phys. Lett.*, **1997**, *268*, 223

[100] H. Imahori; K. Hagiwara; M. Aoki; T. Akiyama; S. Taniguchi; T. Okada; M. Shirakawa; Y. Sakata *J. Am. Chem. Soc.*, **1996**, *118*, 11771

[101] V. Balzani; A. Credi; M. Venturi *"Molecular Device and Machine-A Journey into the Nanoworld"*, **2004**, Chapter 3 ed. Wiley-VCH

[102] C. A. Reed; P. Boyd; T. Drovetskaya *Tetrahedron Lett.*, **1995**, *36*, 7971

[103] C. A. Reed; P. D. W. Boyd; T. Drovetskaya; T. A. Moore; A. L. Moore; D. Gust; D. Kuciauskas; S. Lin; G. R. Seely *J. Phys. Chem.*, **1996**, *100*, 15926

[104] D. M. Guldi; D. I. Schuster; B. Nuber; P. J. Brancher; C. A. Alabi; S. MacMahon; J. W. Kukol; S.R. Wilson *J. Phys. Chem. A*, **2003**, *107*, 3215

[105] a) A. Efimov; P. Vainiotalo; N. V. Tkachenko; H. Lemmetyinen *J. Porphyrins. and Phthalocyanines*, **2003**, *7*, 610 b) V. Chukharev; N. V. Tkachenko; A. Efimov; D. M. Guldi; A. Hirsch; M. Scheloske; H. Lemmetyinen *J. Phys. Chem. B*, **2004**, *108*, 16377 c) T. Galili; A. Regev; H. Levanov; D. I. Schuster; D. M. Guldi *J. Phys. Chem. A*, **2004**, *108*, 10632

[106] a) H. Imahori; D. M. Guldi; O. Ito; S. Fukuzumi; K. Tamaki; C. Luo; M. Fujitsuka; Y. Sakata *J. Am. Chem. Soc.*, **2001**, *123*, 2607 b) H. Imahori; D. M. Guldi; S. Fukuzumi; Y. Yoshida; K. Tamaki; C. Luo; Y. Sakata *J. Am. Chem. Soc.*, **2001**, *123*, 6617 c) D. M. Guldi; H. Imahori; K. Tamaki; Y. Kashiwagi; H. Yamada; Y. Sakata; S. Fukuzumi *J. Phys. Chem. A*, **2004**, *108*, 541 d) H. Imahori; Y. Sekiguchi; Y. Kashiwagi; T. Sato; Y. Araki; O. Ito; H. Yamada; S. Fukuzumi *Chem. Eur. J.*, **2004**, *10*, 3184

[107] G. Kodis; P. A. Liddell; L. de la Garza; P. C. Clausen; J. S. Lindsey; A. L. Moore; T. A. Moore; D. Gust *J. Phys. Chem. A*, **2002**, *106*, 2036

[108] a) D. Kuciauskas; P. A. Liddell; T. A. Moore; A. L. Moore; D. Gust *J. Am. Chem. Soc.*, **1998**, *120*, 10880 b) P. A. Liddell; G. Kodis; L. de la Garza; A. L. Moore; T. A. Moore; D. Gust *J. Phys. Chem. B*, **2004**, *108*, 10256

[109] A. Harriman *Angew. Chem. Int. Ed.*, **2004**, *43*, 4985

[110] K. Ohkubo; H. Kotani; J. Shao; Z. Ou; K. M. Kadish; G. Li; R. K. Pandey; M. Fujitsuka; O. Ito; H. Imahori; S. Fukuzumi *Angew. Chem. Int. Ed.*, **2004**, *43*, 853

[111] a) M. Katterle; A. R. Holzwarth; A. Jesorka *Eur. J. Org. Chem.*, **2006**, 414 b) K. Ohkubo; H. Imahori; J. Shao; Z. Ou; K. M. Kadish; Y. Chen; G. Zheng; R. K. Pandey; M. Fujitsuka; O. Ito; S. Fukuzumi *J. Phys. Chem. A*, **2002**, *106*, 10991

[112] Y. Kashiwagi; K. Ohkubo; J. A. MacDonald; I. M. Blake; M. J. Crossley; Y. Araki; O. Ito; H. Imahori; S. Fukuzumi *Org. Lett.*, **2003**, *5*, 2719

[113] A. Satake; Y. Kobuke *Tetrahedron*, **2005**, *61*, 13

[114] P. D. W. Boyd; C. A. Reed *Acc. Chem. Res.*, **2005**, *38*, 235

[115] A. L. Kieran; S. I. Pascu; T. Jarrosson; J. K. M. Sanders *Chem. Commun.*, **2005**, 1276

[116] T. da Ros; M. Prato; M. Carano; P. Ceroni; F. Paolucci; S. Roffia; L. Valli; D. M. Guldi *J. Organomet. Chem.*, **2000**, *599*, 62

[117] F. D'Souza; G. L. Deviprasad; M. E. Zandler; V. T. Hoang; A. Klykov; M. VanStipdonk; A. Perera; M. E. El-Khouly; M. Fujitsuka; O. Ito *J. Phys. Chem. A*, **2002**, *106*, 3243

[118] F. D'Souza; M. E. El-Khouly; S. Gadde; A. L. McCarty; P. A. Karr; M. E. Zandler; Y. Araki; O. Ito *J. Phys. Chem. B*, **2005**, *109*, 10107

[119] F. D'Souza; R. Chitta; S. Gadde; M. E. Zandler; A. S. D. Sandanayaka; Y. Araki; O. Ito *Chem. Commun.*, **2005**, 1279

[120] F. D'Souza; R. Chitta; S. Gadde; M. E. Zandler; A. L. McCarty; A. S. D. Sandanayaka; Y. Araki; O. Ito *Chem. Eur. J.*, **2005**, *11*, 4416

[121] F. D'Souza; R. Chitta; S. Gadde; M. E. Zandler; A. L. McCarty; A. S. D. Sandanayaka; Y. Araki; O. Ito *J. Phys. Chem. A*, **2006**, *110*, 4338

[122] F. D'Souza; P. M. Smith; M. E. Zandler; A. L. McCarty; M. Itou; Y. Araki; O. Ito *J. Am. Chem. Soc.*, **2004**, *126*, 7898

[123] D. Balbinot; S. Atalick; D. M. Guldi; M. Hatzimarinaki; A. Hirsch; N. Jux *J. Phys. Chem. B*, **2003**, *107*, 13273

[124] V. Balzani; A. Credi; M. Venturi *"Molecular Device and Machine-A Journey into the Nanoworld"*, **2004**, Chapter 2 ed. Wiley-VCH

[125] T. Nakamura; M. Fujitsuka; Y. Araki; O. Ito; J. Ikemoto; K. Takimiya; Y. Aso; T. Otsubo *J. Phys. Chem. B*, **2004**, *108*, 10700

[126] G. de la Torre; F. Giacalone; J. L. Segua; N. Martin; D. M. Guldi *Chem. Eur. J.*, **2005**, *11*, 1267

[127] S. A. Vail; P. J. Krawczuck; D. M. Guldi; A. Palkar; L. Echegoyen; J. P. C. Tomé; M. A. Fazio; D. I. Schuster *Chem. Eur. J.*, **2005**, *11*, 3375

[128] S. A. Vail; D. I. Schuster; D. M. Guldi; M. Iososomppi; N. Tkachenko; H. Lemmetyinen; A. Palkar; L. Echegoyen; X. Chen; J. Z.H. Zhang *J. Phys. Chem. B*, **2006**, *110*, 14155

[129] a) H. Imahori; H. Norieda; Y. Nishimura; I. Yamazaki; K. Higuchi; N.Kato; T. Motohiro; H. Yamada; K. Tamaki; M. Arimura; Y. Sakata *J. Phys. Chem. B*, **2000**, *104*, 1253 b) H. Imahori; H. Yamada; Y. Nishimura; I. Yamazaki; Y. Sakata *J. Phys. Chem. B*, **2000**, *104*, 2099

[130] H. Imahori; J.-C. Liu; H. Hotta; A. Kira; T. Umeyama; Y. Matano; G. Li; S. Ye; M. Iososomppi; N. Tkachenko; H. Lemmetyinen *J. Phys. Chem. B*, **2005**, *109*, 18465

[131] a) D. M. Guldi; I. Zilbermann; G. Anderson; A. Li; D. Balbinot; N. Jux; M. Hatzimarinaki; A. Hirsch; M. Prato *Chem.Commun.*, **2004**, 726 b) D. M. Guldi; M. Prato *Chem.Commun.*, **2004**, 2517

[132] a) H. Imahori *J. Phys. Chem. B*, **2004**, *108*, 6130 b) T. Hasobe; H. Imahori; P. V. Kamat; T. K. Ahn; S. K. Kim; D. Kim; A. Fujimoto; T. Hirakawa; S. Fukuzumi *J. Am. Chem. Soc.*, **2005**, *127*, 1216

[133] a) H. Imahori; D. M. Guldi; O. Ito; S. Fukuzumi; K. Tamaki; C. Luo; M. Fujitsuka; Y. Sakata *J. Am. Chem. Soc.*,

2001, *123*, 2607 b) H. Imahori; D. M. Guldi; S. Fukuzumi; Y. Yoshida; K. Tamaki; C. Luo; Y. Sakata *J. Am. Chem. Soc.*, **2001**, *123*, 6617 c) D. M. Guldi; H. Imahori; K. Tamaki; Y. Kashiwagi; H. Yamada; Y. Sakata; S. Fukuzumi *J. Phys. Chem. A*, **2004**, *108*, 541 d) H. Imahori; Y. Sekiguchi; Y. Kashiwagi; T. Sato; Y. Araki; O. Ito; H. Yamada; S. Fukuzumi *Chem. Eur. J.*, **2004**, *10*, 3184

[134] Y. Kashiwagi; K. Ohkubo; J. A. MacDonald; I. M. Blake; M. J. Crossley; Y. Araki; O. Ito; H. Imahori; S. Fukuzumi *Org. Lett.*, **2003**, *5*, 2719

[135] a) K. Ohkubo; H. Kotani; J. Shao; Z. Ou; K. M. Kadish; G. Li; R. K. Pandey; M. Fujitsuka; O. Ito; H. Imahori; S.

Fukuzumi *Angew. Chem. Int. Ed.*, **2004**, *43*, 853 b) M. Katterle; A. R. Holzwarth; A. Jesorka *Eur. J. Org. Chem.*, **2006**, 414 c) K. Ohkubo; H. Imahori; J. Shao; Z. Ou; K. M. Kadish; Y. Chen; G. Zheng; R. K. Pandey; M. Fujitsuka; O. Ito; S. Fukuzumi *J. Phys. Chem. A*, **2002**, *106*, 10991

[136] a) C. Y. Yu; Y. Chong; J. F. Kajjmen; M. Gozin *J. Org. Chem.*, **1999**, *64*, 2070 b) M. P. Stewart; F. Maya; D. V. Kosynkin; S. M. Dirk; J. J. Stapleton; C. L. McGuiness; D. L. Allara; J. M. Tour *J. Am. Chem. Soc.*, **2004**, *126*, 370 c) F.-R. F. Fan; R. Y. Lai; J. Cornil; Y. Karzazi; J.-L. Bredas; L. Cai; L. Cheng; Y. Yao; D. W. Price Jr.; S. M. Dirk; J. M. Tour; A. J. Bard *J. Am. Chem. Soc.*, **2004**, *126*, 2568 d) C. D. Zangmeister; S. W. Robey; R. D. van Zee; Y. Yao; J. M. Tour *J. Am. Chem. Soc.*, **2004**, *126*, 3420 e) H. Meier; B. Mühling; H. Kolshorn *Eur. J. org. Chem.*, **2004**, 1033

[137] a) W. B. Austin; N. Bilow; W.J. Kelleghan; K. S. Y. Lau *J. Org. Chem.*, **1981**, *46*, 2280 b) S. Thorand; N. Krause *J. Org. Chem.*, **1998**, *63*, 8551 c) A. R. Gholap; K. Venkatesan; R. Pasricha; T. Daniel; R. J. Lahoti; K. V. Srinivasan *J. Org. Chem.*, **2005**, *70*, 4869 d) Y. Liang; Y.-X. Xie; J.-H. Li *J. Org. Chem.*, **2006**, *71*, 370

[138] a) Y. Yao; J. M. Tour *J. Org. Chem.*, **1999**, *64*, 1968 b) C. Xue; F.-T. Luo *Tetrahedron*, **2004**, *60*, 6285

[139] M. Prato; M. Maggini; G. Scorrano *J. Am. Chem. Soc.*, **1993**, *115*, 9798

[140] R. Gonsalves; J. M. Varejao; M. M. Pereira *J. Heterocyclic Chem.*, **1991**, *28*, 635

[141] H. J. Callot *Bull. Soc. Chim. Fr.*, **1974**, *7-8*, 1492

[142] a) J. S. Lindsey; S. Prataphan; T. E. Johnson; R. W. Wagner *Tetrahedron*, **1994**, *50*, 8941 b) R. W. Wagner; T. E. Johnson; J. S. Lindsey *J. Am:Chem. Soc.*, **1996**, *118*, 11166 c) R. W. Wagner; T. E. Johnson; F. Li; J. S. Lindsey *J. Org. Chem.*, **1995**, *60*, 5266

[143] I. Zilbermann; G. A. Anderson; D. M. Guldi; H. Yamada; H. Imahori; S. Fukuzumi *J. of Porphyrins and Phthalocyanines*, **2003**, *7*, 357

[144] P. A. Troshin; A. S. Peregudov; D. Mühlbacher; R. N. Lyubovskaya *Eur. J. Org. Chem.*, **2005**, 3064

[145] A. Trabolsi; M. Elhabiri; M. Urbani; J. L. Delgado de la Cruz; F. Ajamaa; N. Solladié; A.-M. Albrecht-Gary; J.-F. Nierengarten *Chem.Commun.*, **2005**, 5736

[146] F. T. Tat; Z. Zhou; S. MacMahon; F. Song; A. L. Rheingold; L. Echegoyen; D. I. Schuster; S. R. Wilson *J. Org. Chem.*, **2005**, *69*, 4602

[147] a) A. Harriman *Angew. Chem. Int. Ed.*, **2004**, *43*, 4985 b) K. Ohkubo; H. Kotani; J. Shao; Z. Ou; K. M. Kadish; G. Li; R. K. Pandey; M. Fujitsuka; O. Ito; H. Imahori; S. Fukuzumi *Angew. Chem. Int. Ed.*, **2004**, *43*, 853 c) M. Katterle; A. R. Holzwarth; A. Jesorka *Eur. J. Org. Chem.*, **2006**, 414 d) K. Ohkubo; H. Imahori; J. Shao; Z. Ou; K. M. Kadish; Y. Chen; G. Zheng; R. K. Pandey; M. Fujitsuka; O. Ito; S. Fukuzumi *J. Phys. Chem. A*, **2002**, *106*, 10991 e) Y. Kashiwagi; K. Ohkubo; J. A. MacDonald; I. M. Blake; M. J. Crossley; Y. Araki; O. Ito; H. Imahori; S. Fukuzumi *Org. Lett.*, **2003**, *5*, 2719

[148] L. Jaquinod; R. G. Khoury; K. M. Shea; K. M. Smith *Tetrahedron*, **1999**, *55*, 13151

[149] a) A. Mateo-Alonso; C. Sooambar; M. Prato *Org. Biomol. Chem.*, **2006**, *4*, 1629 b) K. Kordatos; S. Bosi; T. Da Ros; A. Zambon; V. Lucchini; M. Prato *J. Org. Chem.*, **2001**, *66*, 2802 c) S. Marchesan; T. Da Ros; M. Prato *J. Org. Chem.*, **2005**, *70*, 4706 d) C. Thilgen; F. Diederich *Chem. Rev.*, **2006**, *106*, 5049

[150] Z. Zhou; D. I. Schuster; S. R. Wilson *J. Org. Chem.*, **2006**, *71*, 1545

[151] a) C. A. Reed; P. Boyd; T. Drovetskaya *Tetrahedron Lett.*, **1995**, *36*, 7971 b) C. A. Reed; P. D. W. Boyd; T. Drovetskaya; T. A. Moore; A. L. Moore; D. Gust; D. Kuciauskas; S. Lin; G. R. Seely *J. Phys. Chem.*, **1996**, *100*, 15926

[152] A. Lembo; P. Tagliatesta; D. M. Guldi *J. Phys. Chem. A*, **2006**, *110*, 11424

[153] a) K. M. Kadish; J. S. Lindsey *Handbook of Porphyrins and Phthalocyanine*; K.M. Kadish, R. Guilard, K. M. Smith, Eds.; Vol. 9. b) M. Autret; Z. Ou;A. Antonini; T. Boschi; P. Tagliatesta; K. M. Kadish *J. Chem. Soc., Dalton Trans.*, **1996**, 2793 c) K. M. Kadish; N. Guo; E. Van Caemelbecke; A. Froio; R. Paolesse; D. Monti; P. Tagliatesta; T. Boschi; L. Prodi; F. Bolletta; N. Zaccheroni *Inorg. Chem.*, **1998**, *37* (10), 2358

[154] a) F. D'Souza; M. E. Zandler; P. Tagliatesta; Z. Ou; J. Shao; E. Van Caemelbecke; K. M. Kadish *Inorg. Chem.*, **1998**, *37*, 4567 b) K. M. Kadish; F. D'Souza; A. Villard; M. Autret; E. Van Caemelbecke; P. Blanco; A. Antonini; P. Tagliatesta *Inorg. Chem.*, **1994**, *33*, 5169 c) R. A. Binstead; M. J. Crossley; N. J. Hush *Inorg. Chem.*, **1991**, *30*, 1259

[155] a) A. Bax; M. F. Summers *J. Am. Chem. Soc.*, **1986**, *108*, 2093 b)) A. Bax; L. G. Marzilli; M. F. Summers *J. Am. Chem. Soc.*, **1986**, *108*, 4285

[156] M. Crossley; M. M. Harding; S. Sternell *J. Am. Chem. Soc.*, **1986**, *108*, 3608

[157] D. M. Guldi; M. Prato *Acc. Chem. Res.*, **2000**, *33*, 695

[158] S. A. Vail; D. I. Schuster; D. M. Guldi; M. Iososomppi; N. Tkachenko; H. Lemmetyinen; A. Palkar; L. Echegoyen; X. Chen; J. Z.H. Zhang *J. Phys. Chem. B*, **2006**, *110*, 14155

[159] a) K. Petterson; A. Kyrychenko; E. Ronnow; T. Ljungdahl; J. Mårtensson; B Albinsson *J. Phys. Chem. A*, **2006**, *110*, 310 b) K. Petterson; J. Wiberg; T. Ljungdahl; J. Mårtensson; B Albinsson *J. Phys. Chem. A*, **2006**, *110*, 319

[160] a) F. D'Souza; G. L. Deviprasad; M. E. Zandler; V. T. Hoang; A. Klykov; M. VanStipdonk; A. Perera; M. E. El Khouly; M. Fujitsuka; O. Ito *J. Phys. Chem. A*, **2002**, *106*, 3243 b) F. D'Souza; M. E. El-Khouly; S. Gadde; A. L. McCarty; P. A. Karr; M. E. Zandler; Y. Araki; O. Ito *J. Phys. Chem. B*, **2005**, *109*, 10107 c) A. Satake; Y. Kobuke *Tetrahedron*, **2005**, *61*, 13